SOME FUNDAMENTAL ISSUES IN RECEIVER DESIGN AND PERFORMANCE ANALYSIS FOR WIRELESS COMMUNICATION

WU MINGWEI

NATIONAL UNIVERSITY OF SINGAPORE

2011

SOME FUNDAMENTAL ISSUES IN RECEIVER DESIGN AND PERFORMANCE ANALYSIS FOR WIRELESS COMMUNICATION

WU MINGWEI

(*B.Eng, M.Eng., National University of Singapore*)

A THESIS SUBMITTED

FOR THE DEGREE OF DOCTOR OF PHILOSOPHY

DEPARTMENT OF ELECTRICAL AND COMPUTER ENGINEERING

NATIONAL UNIVERSITY OF SINGAPORE

2011

Dedications:

To my family

who loves me always.

Acknowledgment

First and Foremost, I would like to thank my supervisor, Prof. Pooi-Yuen Kam for his invaluable guidance and support throughout the past few years. From him, I learnt not only knowledge and research skills, but also the right attitude and passion towards research. I am also very grateful for his understanding when I face difficulty in work and life.

I would like to thank Dr. Yu Changyuan, Prof. Mohan Gurusamy and Prof. Marc Andre Armand for serving as my Ph.D qualification examiners.

I grateful acknowledge the support of part of my research studies from the Singapore Ministry of Education AcRF Tier 2 Grant T206B2101.

I would like to thank fellow researchers Cao Le, Wang Peijie, Chen Qian, Kang Xin, Li Yan, Fu Hua, Zhu Yonglan, Li Rong, He Jun, Lu Yang, Yuan Haifeng, Jin Yunye, Gao Xiaofei, Gao Mingsheng, Jiang Jinhua, Cao Wei, Elisa Mo, Zhang Shaoliang, Lin Xuzheng, Pham The Hanh, Shao Xuguang, Zhang Hongyu and many others for their help in my research and other ways. I would also like to thank my best friends, Xiong Ying and Zhao Fang, for their emotional support.

Last but not least, I would like to thank my family for their love, encouragement and support that have always comforted and motivated me.

Contents

Summary

This thesis studies two fundamental issues in wireless communication, i.e. robust receiver design and performance analysis.

In wireless communication with high mobility, the channel statistics or the channel model may change over time. Applying the joint data sequence detection and (blind) channel estimation approach, we derive the robust maximum-likelihood sequence detector that does not require channel state information (CSI) or knowledge of the fading statistics. We show that its performance approaches that of coherent detection with perfect CSI when the detection block length L becomes large. To detect a very long sequence while keeping computational complexity low, we propose three pilot-based algorithms: the trellis search algorithm, pilot-symbol-assisted block detection and decision-aided block detection. We compare them with block-by-block detection algorithms and show the former's advantages in complexity and performance.

The commonly used performance measures at the physical layer are average error probabilities, obtained by averaging instantaneous error probabilities over fading distributions. For average performance of coherent receivers, we propose to use the convexity property of the exponential function and apply the Jensen's inequality to obtain a family of exponential lower bounds on the Gaussian Q-function. The tightness of the bounds can be improved by increasing the number of exponential terms. The coefficients of the exponentials are constants, allowing easy averaging over fading distribution using the moment generating function (MGF) method. This method is applicable to finite integrals of the exponential function.

It is further applied to the two-dimensional Gaussian Q-function, symbol error probability (SEP) of M-ary phase shift keying, SEP of M-ary differential phase shift keying and signals with polygonal decision regions over additive white Gaussian channel, and their averages over general fading. The tightness of the bounds is demonstrated.

For average performance of differential and noncoherent receivers, by expressing the noncentral Chi-square distribution as a Poisson-weighted mixture of central Chi-square distributions, we obtain an exact expression of the error performance of quadratic receivers. This expression is in the form of a series summation involving only rational functions and exponential functions. The bit error probability performances of optimum and suboptimum binary differential phase shift keying (DPSK) and quadrature DPSK receivers over fast Rician fading with Doppler shift are obtained. Numerical computation using our general expression is faster than existing expressions in the literature.

Moving on to the perspective of the data link layer, we propose to use the probability of instantaneous bit error outage as a performance measure of the physical layer. It is defined as the probability that the instantaneous bit error probability exceeds a certain threshold. We analyze the impact of channel estimation error on the outage performance over Rayleigh fading channels, and obtain the optimum allocation of pilot and data energy in a frame that minimizes the outage probability. We further extend the outage concept to packet transmission with automatic repeat request (ARQ) schemes over wireless channels, and propose the probability of instantaneous accepted packet error outage (IAPEO). It is observed that, in order to satisfy a system design requirement of maximum tolerable IAPEO, the system must operate above a minimum signal-to-noise ratio (SNR) value. An ARQ scheme incorporating channel gain monitoring (ARQ-CGM) is proposed, whose IAPEO requirement can be satisfied at any SNR value with the right channel gain threshold. The IAPEO performances of ARQ-CGM with different retransmission protocols are related to the conventional data link layer performance

measures, i.e. average accepted packet error probability, throughput and goodput.

List of Tables

List of Figures

List of Acronyms

AAPEP	Average Accepted Packet Error Probability
ABEP	Average Bit Error Probability
ARQ	Automatic Retransmission reQuest
AWGN	Additive White Gaussian Noise
BEP	Bit Error Probability
BPSK	Binary Phase Shift Keying
CGM	Channel Gain Monitoring
CRC	Cyclic Redundancy Check
CSI	Channel State Information
DABD	Decision-Aided Block Detection
GBN-ARQ	Go Back N Automatic Retransmission reQuest
GLRT	Generalized Likelihood Ratio Test
IAPEO	Instantaneous Accepted Packet Error Outage
IAPEP	Instantaneous Accepted Packet Error Probability
IBEO	Instantaneous Bit Error Outage
IBEP	Instantaneous Bit Error Probability
IEEE	Institute of Electrical and Electronics Engineers
IPEO	Instantaneous Packet Error Outage
IPEP	Instantaneous Packet Error Probability
LOS	Line Of Sight
MGF	Moment Generating Function
ML	Maximum Likelihood

MLSD	Maximum Likelihood Sequence Detection/Detector
MMSE	Minimum Mean Square Error
MPSK	M-ary Phase Shift Keying
MSDD	Multiple Symbol Differential Detection
MSE	Mean Square Error
NCFSK	Noncoherent Frequency Shift Keying
NCSI	No Channel State Information
PCSI	Perfect Channel State Information
PDF	Probability Density Function
PEO	Packet Error Outage
PEP	Pairwise Error Probability
PLL	Phase-Locked Loop
PSABD	Pilot-Symbol-Assisted Block Detection
PSAM	Pilot-Symbol-Assisted Modulation
QAM	Quadrature Amplitude Modulation
QoS	Quality of Service
QPSK	Quadrature Phase Shift Keying
SEP	Symbol Error Probability
SIMO	Single-Input Multiple-Output
SNR	Signal-to-Noise Ratio
SR-ARQ	Selective Repeat Automatic Retransmission reQuest
SW-ARQ	Stop and Wait Automatic Retransmission reQuest

List of Notations

a	lowercase letters are used to denote scalars
$\mathbf{a}$	boldface lowercase letters are used to denote column vectors
$\mathbf{A}$	boldface uppercase letters are used to denote matrices
$(\cdot)^T$	the transpose of a vector or a matrix
$(\cdot)^*$	the conjugate only of a scalar or a vector or a matrix
$(\cdot)^H$	the Hermitian transpose of a vector or a matrix
$\lvert \cdot \rvert$	the absolute value of a scalar
$\lVert \cdot \rVert$	the Euclidean norm of a vector
$\lVert \cdot \rVert_F$	the Frobenius norm of a matrix
$\mathrm{E}[\cdot]$	the statistical expectation operator
$\mathrm{Re}[\cdot]$	the real part of the argument
$\mathrm{Im}[\cdot]$	the imaginary part of the argument

Chapter 1

Introduction

Wireless voice and data communication has become an increasingly vital part of our modern daily life. Signals in wireless communication experience path loss, shadowing and multipath fading effects. We focus here on the small-scale multipath fading effect, which causes rapid fluctuation in the signal over a short period of time or short travel distance, where the effects of path loss and shadowing are ignored. Multipath fading causes a change in the signal amplitude and phase. In the case of moving transmitter, receiver or moving objects in the environment, the signal frequency is affected due to Doppler shift. The fading channel is classified as fast fading or slow fading accordingly. Signals with large bandwidth may experience multipath delay spread. Thus, the fading channel is classified as frequency selective. Otherwise, the channel is considered flat.

Just like in any communication, two fundamental research issues in wireless communication are receiver design and performance analysis. The objective of receiver design is to find an optimum receiver structure that minimizes the probability of detection error. Receiver design depends on the channel model and the knowledge of the channel statistics or the channel state information (CSI) at the receiver. There are many fading models, e.g. Rayleigh fading, Rician fading and Nakagami-m fading, each with one or more fading parameters. The receiver may have perfect, partial or no knowledge of the instantaneous CSI, the channel

model and the fading parameters. Different detection techniques are designed, e.g. coherent detection, differential detection, sequence detection, depending on the channel model and receiver knowledge [1–6]. As the channel model may change due to mobility, there exists the need for a robust and simple receiver that applies to all channel models and is easy to implement. As our demand on the data rate increases and so does the signal spectrum, the fading channel changes from flat or frequency nonselective to frequency selective. We are faced with the additional challenge of the frequency selectivity in receiver design. However, in general, receiver techniques developed for flat fading, e.g. diversity reception, can be extended to frequency selective fading. Therefore, we focus on the receiver design for flat fading in this thesis.

Similarly, in the performance analysis for flat fading channels, there remain many unsolved problems. We want to obtain the performance in a simple closed form, such that it is easy for system designers to specify required SNR to meet a certain level of performance. The most commonly used performance measures for fading channels are average bit error probability (ABEP) and average symbol error probability (ASEP). They are obtained by averaging the instantaneous values, i.e. instantaneous BEP (IBEP) and instantaneous SEP (ISEP), which are equivalent to BEP and SEP over additive white Gaussian noise (AWGN) channels, over the fading distribution. As receivers are classified into coherent receivers and differential/noncoherent receivers, we look into the performance of coherent receivers and differential/noncoherent receivers separately. For coherent receivers, the IBEP and ISEP usually involve the Gaussian Q-function, or integrals of exponential functions. Thus, averaging the IBEP/ISEP over fading may not result in a closed form. For example, the average BEP of M-ary phase shift keying (MPSK) and M-ary differential phase shift keying (MDPSK) over arbitrary Nakagami-m fading involves special functions [7]. In such cases, we need simple and tight closed-form bounds that can be averaged over fading. For differential/noncoherent receivers, existing general expressions on error performance involve special functions including

the Marcum Q-function and the modified Bessel function of the first kind, or integrals [8, 9]. These forms are not convenient for computation or further analysis. Expressions involving only elementary functions are desired.

We also observe that, for high data rate transmission or burst mode transmission, ABEP or ASEP does not give a full picture of the quality of service that the user experiences over time. As average metrics are obtained by averaging the instantaneous values over all possible values of the fading distribution, the use of a single average metric loses instantaneous information. Moreover, ABEP and ASEP are performance measures of the physical layer. Conventionally, data link layer protocols and higher layer protocols are often analyzed based on a two-state Markov chain model of the physical layer performance [10, 11]. The model assumes only two states of the physical layer performance, i.e. good or bad. There is no direct mapping of the physical layer performance metrics into the protocol analysis framework. This makes cross layer performance analysis and cross layer design difficult. Therefore, new physical layer performance measures are needed for higher layer performance analysis.

In this chapter, we first give an overview of receiver design in wireless communication and our research objective in robust receiver design in Section 1.1. We then give an overview of performance analysis in wireless communication and our detailed research objectives in this area in Section 1.2. In Section 1.3, we give a summary of our main contributions in the two areas. Finally, we present the organization of the thesis in Section 1.4.

1.1 Receiver Design

In a fading channel, the received signal is corrupted by channel fading as well as AWGN. To overcome the effect of the channel gain, one approach of coherent detection is to estimate the channel gain accurately and then compensate for it before symbol-by-symbol data detection. Estimation of the fading gain is referred to as channel estimation, or extraction of CSI. The decision-feedback method in

[1–3] performs channel estimation using previous data decisions. It works well at high SNR where decision errors are rare, but it suffers from error propagation at low SNR. Another widely used channel estimation method is pilot-symbol-assisted modulation (PSAM) [4]. It first estimates the fading gain using pilot symbols periodically inserted into the data sequence, and then performs symbol-by-symbol data detection. To improve the performance by obtaining more accurate channel estimation, more frequent or longer pilot sequences can be used, but this reduces bandwidth and power efficiencies. Alternatively, pilot symbols that are more distant to the symbol(s) being detection can be used, but this incurs longer detection delay. Differential encoding and differential detection is a viable alternative that does not require CSI information. However, it incurs substantial performance loss compared to coherent detection. For example, the performance of binary differential phase shift keying (BDPSK) is 3dB worse than that of coherent BPSK over Rayleigh fading [8]. The above-mentioned receivers are symbol-by-symbol receivers.

An example of sequence detectors is the multiple symbol differential detector (MSDD) over static fading in [5,6]. It does not require CSI information or knowledge of parameters of the fading channel. However, it is derived by averaging the likelihood function over Rayleigh fading before making the data decision. Therefore, knowledge of the channel model, i.e. Rayleigh fading, is required. Moreover, MSDD for different channel models, e.g. AWGN, Rayleigh and Rician fading, have different forms.

Due to mobility, the applicable channel model may change over time, e.g. when the user in a high speed vehicle moves from an urban environment to a suburban environment. The optimum receiver designed for one particular fading environment may not perform well for another fading environment. In addition, the channel statistics may change so quickly that the channel estimation method cannot produce a good channel estimate in time. Our previous experience in [1, 2] and the works of [12, 13] show that, for a receiver which requires knowledge of channel statistics, an imperfect knowledge of channel statistics causes degradation

in the performance. Therefore, there is the need for a robust receiver that does not require CSI information or knowledge of the fading statistics.

Joint data sequence detection and blind channel estimation is an alternative approach for receiver design. It is shown in [14] that this approach works well with joint data sequence detection and carrier phase estimation on a phase noncoherent AWGN channel. No knowledge of the channel statistics is required at the receiver and no explicit carrier phase estimation is required in making the data sequence decision. Being a sequence detector, the performance of the sequence detector in [14] improves monotonically as the sequence length increases, and approaches that of coherent detection with perfect CSI, in the limit as the sequence length becomes large. This work shows that the joint data sequence detection and blind channel estimation approach is a successful approach in designing robust receivers. Therefore, we can apply this approach in designing a robust receiver for the fading channel, that does not require CSI information or fading statistics.

1.2 Performance Analysis

For performance analysis, simple closed-form expressions are always preferred for efficient evaluation. In cases where closed-form expressions are not available, finite range integrals that can be computed efficiently are often resorted to. Lastly, performance can always be obtained by simulation. However, for further analysis such as parameter optimization which involves iterative algorithms, complicated expressions and simulation would incur intensive computation and are often not practical. Therefore, simple closed-form exact expressions are always desired. Alternatively, closed-form bounds and approximations can be used.

A communication system is usually divided into several layers for design and performance analysis. In this thesis, we consider the physical layer and and the data link layer.

The commonly used physical layer performance measures for fading channels are ABEP and ASEP. As the received signal strength is variable, ABEP and ASEP

are computed by averaging the IBEP conditioned on the instantaneous SNR (or the fading gain), over the distribution of the instantaneous SNR (or the fading gain).

Receivers are generally classified into two categories: coherent receivers and differential/noncoherent receivers. For coherent receivers, it is well-known that the Gaussian Q-function characterizes their error performance over the AWGN channel. The BEP and SEP performances over AWGN are equivalent to IBEP and ISEP for fading. The Gaussian Q-function is conventionally defined as the area under the tail of the probability density function (PDF) of a normalized (zero mean, unit variance) Gaussian random variable. An alternative form of the Gaussian Q-function was discovered by Craig [15], which is a finite range integral of an exponential function. Due to the two integral forms of the Gaussian Q-function, a lot of work has been done to compute it efficiently [16–24]. The tight bounds in the literature are usually in forms that cannot be averaged over fading distributions easily [16, 21, 23]. Bounds that are in very simple forms and can be averaged over fading easily are usually quite loose [24]. On the other hand, the SEP performances of a few two-dimensional modulation schemes, e.g. MPSK and MDPSK, are in the form of a finite range integral of an exponential function, which is similar to the Craig's form of the Gaussian Q-function. The averages of these SEP performances over fading do not always reduce to closed forms. For example, the SEP performances of MPSK and MDPSK over Rayleigh fading are given in closed form in [25]. Their SEP performances over Nakagami-m are found in closed form only for positive integer values of m in [7, 26], while for arbitrary m they are expressed in terms of Gauss hypergeometric function and Lauricella function [27, 28]. Their SEP performances over Rician fading are found in finite range integrals [29]. Therefore, we aim to find bounds on integrals of exponential functions that are in simple forms, such that the average performances of various coherent receivers over fading can be obtained easily. Though approximations and upper bounds are used more often, lower bounds are also useful, as the combined use of upper and lower bounds shows the tightness of the bounds, without comparing the individual bounds with numerical integration

of the exact value.

Having reviewed the average performances of coherent receivers, we now look into the performances of differential and noncoherent receivers. The performance of many differential or noncoherent receivers have been obtained individually. For example, the performances of MDPSK and FSK with single or multichannel reception over AWGN or fading are given in [8, 30–37]. The decision metrics of these differential and noncoherent receivers are in quadratic forms. Therefore, we refer to receivers with quadratic decision metrics as quadratic receivers. Ma and Lim derived the MGF of the decision metrics of DPSK and NCFSK and obtains from the cumulative density function a BEP expression involving an infinite multi-level summation [37]. It does not show, however, how to generalize this approach to a general quadratic receiver. Only a few publications obtain general expressions on the error performance of a general quadratic receiver. Using a characteristic function method, Proakis finds an expression involving the first-order Marcum Q-function and the modified Bessel functions of the first kind [8, eq. (B-21)]. Hereafter, we refer to [8, eq. (B-21)] as the Proakis' expression. The two special functions in the Proakis' expression are usually expressed as integrals or infinite series summations. Therefore, the Proakis' expression is not easy to compute. Simon and Alouini express the Proakis' expression for single channel reception over AWGN in a finite range integral form [9]. The average of the finite range integral over the fading distribution results in another finite range integral with integrand in terms of elementary functions. Numerical integration is required to compute it. As both the Proakis' expression and the Simon and Alouini's expression for general quadratic receivers are not in simple forms, we aim to derive general expressions that involve only elementary functions.

Having reviewed the average physical layer performance over fading, we now move on to the data link layer. For high data rate communication, a single fade may last over the duration of a large number of consecutive bits, and therefore, result in the loss of these data. In a network scenario, it would result in poor

upper layer performance [38]. ABEP as an average metric, does not reflect the poor instantaneous quality of service (QoS) experienced by the user over such long fades, nor do they reflect how often such poor QoS occurs. However, many upper layer protocols are analyzed as a function of a single physical layer performance measure. For example, [39, Fig. 22.4] shows the throughput of three pure ARQ schemes as a function of ABEP. These results do not give a full picture of how upper layer protocols perform with high data rates over a time-varying fading channel. Cross layer analysis provides more information by considering physical layer parameters when analyzing protocol performance. Reference [40], for example, analyzes the impact of channel estimation error and pilot energy allocation on the throughput, goodput and reliability of pure ARQ schemes. These parameters, however, do not provide a good and concise indication of the physical layer performance. References [41–43] use the packet error outage (PEO) probability as the performance measure for log-normal shadowing channels. This PEO probability is the probability that the average packet error probability (instantaneous packet error probability averaged over the fading gain distribution) exceeds an APEP threshold. Thus, this PEO probability is calculated using the statistical distribution of the shadowing parameter. Hence, [41–43] address the system outage caused by the shadowing effect which occurs over a large number of measurement locations [44], but not yet reflect the instantaneous performance affected by multipath fading. We aim to propose new physical layer performance measures suitable for higher layer protocol analysis of a practical system. We also intend to improve on existing protocols based on new performance measures.

1.3 Main Contributions

1.3.1 Receiver Design with No CSI

We want to design a robust receiver that works well in many channels without CSI information or knowledge of the channel statistics. It has been shown that the

joint data sequence detection and blind channel estimation approach works well in a phase noncoherent AWGN channel [14]. Therefore, we apply the joint data sequence detection and blind channel estimation approach to single-input-multiple-output (SIMO) fading channels here, and derive the maximum-likelihood sequence detector (MLSD) for quadrature-amplitude-modulated (QAM) signals. Similar to the detector in [14], the detector for QAM over SIMO fading channels does not require explicit channel estimation in making the data sequence decision. Therefore, we name it MLSD with no CSI (MLSD-NCSI). As an imperfect knowledge of channel statistics causes degradation in the performance of a receiver which requires knowledge of channel statistics, we make the simplifying assumption that MLSD-NCSI has no prior knowledge of channel statistics. We also assume that the fading gain remains static over the sequence duration. This assumption is valid for low fade rates and is common in the wireless communication literature [45–47].

By deriving an exact closed-form pairwise error probability expression for the detector over slowly time-varying Rayleigh fading, we show that its performance approaches that of coherent detection with perfect CSI when the detection block length L becomes large. However, the computational complexity of MLSD-NCSI increases exponentially with L. Therefore, to detect a very long sequence of S symbols over a channel which can be assumed to remain static only over L symbols, where $S \gg L$, while keeping computational complexity low, we propose three pilot-based algorithms: the trellis search algorithm, pilot-symbol-assisted block detection and decision-aided block detection. We show that the algorithms resolve phase and divisor ambiguities easily. We compare the three algorithms with block-by-block detection algorithms, and show the former's advantages in complexity and performance.

1.3.2 Performance Analysis

We first analyze the the average performance of coherent receivers over fading. Noticing that the Gaussian Q-function can be expressed as integrals of exponential

functions, we propose to use the convexity property of the exponential function and apply the Jensen's inequality. We obtain three families of exponential upper and lower bounds on the Gaussian Q-function. The tightness of the bounds can be improved by increasing the number of exponential terms. The bounds are in simple forms and they can be averaged over fading. This method is also applicable to finite integrals of the exponential function. It is further applied to the two-dimensional Gaussian Q-function, SEP of MPSK, MDPSK and signals with polygonal decision regions over AWGN channel, and their averages over general fading. The tightness of the bounds are demonstrated.

For quadratic receivers, their decision metrics are noncentral Chi-square distributed. By expressing the noncentral Chi-square distribution as a Poisson-weighted mixture of central Chi-square distributions, we obtain an exact expression of the error performance of quadratic receivers. This expression is in the form of a series summation involving only rational functions and exponential functions. The BEP performances of optimum and suboptimum BDPSK and QDPSK receivers over fast Rician fading with Doppler shift are obtained using the general expression. Numerical computation using our general expression is faster than existing expressions in the literature.

So far, the average performance analysis over fading is for the physical layer. We now move on to the data link layer and analyze the physical layer performance from the perspective of the data link layer. For high data rate or burst mode transmissions, we propose to use the probability of instantaneous bit error outage (IBEO) as a performance measure. It is defined as the probability that the IBEP exceeds an IBEP threshold. For a given modulation scheme, the IBEO probability is mathematically equivalent to the probability that the instantaneous SNR falls below an SNR threshold required for the system to operate [48, chap.1]. However, if the SNR outage probability is used as a performance measure, the SNR threshold values for different modulation schemes should be different. The IBEO probability uses the same IBEP threshold regardless of modulation scheme used, and, therefore, is a fair

performance measure for comparison. The IBEO probability is also mathematically equivalent to the capacity outage probability [49] defined as the probability that the transmission rate is above the error-free Shannon capacity [50]. In practice, even when a system transmits at a rate below the Shannon capacity using a capacity achieving code, it still makes decision errors and the error performance is not related to the capacity outage probability. We want to analyze the outage performance of a specific practical system, e.g. ARQ with BPSK with channel estimation errors. The capacity outage probability is not useful in this analysis.

The IBEO probability has been considered for BPSK over Rayleigh fading in [51] and Nakagami-m fading in [52], assuming perfect knowledge of the CSI. However, in practice, CSI is obtained using pilots that require energy. The quality of CSI, in terms of channel estimation error, depends on the pilot energy. In this thesis, we analyze the impact of channel estimation error on the outage performance over Rayleigh fading channels. Given total energy and allowable bandwidth expansion, we obtain the optimum allocation of pilot and data energy in a frame that minimizes the outage probability.

We now proceed to performance analysis of data link layer protocol and protocol design. We extend the outage concept to packet transmission with ARQ schemes over wireless channels, and propose the probability of instantaneous accepted packet error outage (IAPEO). It is observed that, in order to satisfy a system design requirement of maximum tolerable IAPEO, the system must operate above a minimum SNR value. An ARQ scheme by incorporating channel gain monitoring (ARQ-CGM) is proposed, whose IAPEO requirement can be satisfied at any SNR value with the right channel gain threshold. The IAPEO performances of ARQ-CGM with selective repeat (SR-ARQ), stop and wait (SW-ARQ) and go back N (GBN-ARQ) retransmission protocols are related to the data link layer performance measures, i.e. average accepted packet error probability, throughput and goodput.

1.4 Organization of the Thesis

The rest of the thesis is organized as follows.

In Chapter 2, we derive the robust MLSD-NCSI detector and propose three pilot-based algorithms to detect very long sequences over time-varying fading. We compare our algorithms with existing block-by-block detection algorithms, in terms of detection delay, complexity and performance.

We then go into performance analysis in the next chapters. In Chapter 3, we propose to use the Jensen's inequality to lower bound the Gaussian Q-function, and obtain two families of closed-form lower bounds.

In Chapter 4, a family of tight closed-form lower bounds on the finite range integrals of exponential functions is obtained. It is applied to the SEP of MPSK, MDPSK, signals with polygonal decision regions, and closed-form simple bounds are obtained.

In Chapter 5, a new expression of the performance of general quadratic receivers is obtained. It is applied to optimum and suboptimum BDPSK and QDPSK receivers over fast Rician fading with Doppler shift.

In Chapter 6, the outage probability is proposed as a performance measure for high data rate transmission or burst mode transmission over time-varying fading.

In Chapter 7, we propose ARQ with channel gain monitoring that has higher reliability in time-varying channel than conventional ARQ schemes.

Finally, the concluding remarks are drawn in Chapter 8 and possible extensions of the work in this thesis are recommended.

Chapter 2

Sequence Detection Receivers with No Explicit Channel Estimation

A signal transmitted over a wireless channel is perturbed by an unknown, complex, fading gain in addition to AWGN noise. PLL based coherent detection requires long acquisition times and, therefore, is not suitable for channels with significant time variations or for burst mode transmission. Differential encoding and differential detection is a viable alternative that does not require explicit CSI. However, it incurs substantial performance loss compared to coherent detection. For example, the performance of BDPSK is 3dB worse than that of coherent BPSK over Rayleigh fading or AWGN [8]. Joint data sequence detection and (blind) channel estimation is an alternative approach for receiver design. The channel is assumed to remain static over L symbol intervals. We showed in [14] that this approach works well with joint data sequence detection and carrier phase estimation on a phase noncoherent AWGN channel. We extend this approach here to single-input-multiple-output (SIMO) fading channels, and obtain the maximum-likelihood sequence detector with no CSI (MLSD-NCSI) for QAM signals with diversity reception. It is also known as the generalized likelihood ratio test (GLRT) detector [53]. MLSD-NCSI does not require explicit channel estimation or knowledge of the channel statistics in making the data sequence decision. Multiple symbol differential detection (MSDD) over static fading

in [5] has a form similar to our MLSD-NCSI, but it requires perfect knowledge of the channel statistics. The works of [54] and [6] take the same approach as [5]. Using some approximations, a detector is obtained in [6] for Rayleigh fading that does not require knowledge of the channel statistics. However, [6] does not explain why the same detector is also robust over Rician fading. We show here that the detector of [6] is equivalent to MLSD-NCSI, and that its robustness is due to joint data sequence detection and channel estimation.

The pairwise error probability (PEP) of MLSD-NCSI (GLRT) has been analyzed in [53, 55]. PEP bounds over a phase noncoherent AWGN channel are obtained in [53]. The divisor ambiguity error floor is obtained in [55]. We obtained in [14] an approximate PEP over a phase noncoherent AWGN channel. Here, we derive a new, exact, closed-form PEP expression over time-varying Rayleigh fading. For static fading or at low fade rates, the PEP performance improves with L and approaches that of coherent detection with perfect CSI (PCSI) when L becomes large. The value of L, however, is limited by the channel fade rate. In practice, we are concerned with detection of a very long sequence of S symbols while the channel remains static only over L symbol intervals, where we have $S \gg L$. One approach is to divide the S-symbol sequence into blocks of L symbols and perform block-by-block detection using MLSD-NCSI. The decision on a block of L symbols is independent of previous and subsequent blocks. This decision process is clearly not optimal for a slowly time-varying channel that has channel memory over more than one block interval. Algorithms such as sphere decoding [56, 57] and lattice decoding [58] are based on this approach, and aim to reduce the computational complexity of block-by-block detection via exhaustive search. An alternative approach for long sequence detection is to make use of the continuity of the channel fading process by using more than L adjacent symbols in each decision. Its performance is expected to be better than block-by-block detection. We consider here three algorithms based on this approach: the *trellis-search algorithm*, *pilot-symbol-assisted block detection* (*PSABD*), and *decision-aided block detection* (*DABD*). Our aim is to compare

the performance and complexity of these three algorithms with algorithms for block-by-block detection, namely, sphere decoding [56, 57] and lattice decoding [58], which are simplified approximations to block-by-block detection using exhaustive search.

The computational complexity of block-by-block detection using exhaustive search grows exponentially with L, thus, rendering detector implementation usually impractical for large values of L that are permitted by the channel fade rate. MSDD for DPSK based on sphere decoding [56, 57] and combinatorial geometry [59] over time-varying fading has a complexity still exponential in L for large L. Lattice decoding algorithms for QAM in [58] have complexities of $O(L^2 \log L)$. But, still, the average complexity per symbol of all these algorithms increases with L. Therefore, the choice of L remains a trade-off between complexity and additional performance gains. The performance of our three pilot-based algorithms can be improved by increasing L, but without an increase in the complexity.

Another key feature of our algorithms is the use of pilot symbols or the trellis-search algorithm to resolve phase and divisor ambiguities of MLSD-NCSI. In comparison, sphere decoding and lattice decoding rely on differential encoding to resolve the ambiguities [56–58]. Since they are approximations of block-by-block detection using exhaustive search, their error performance is lower bounded by that of the latter. Therefore, we need only compare our pilot-based algorithms with block-by-block detection using exhaustive search and differential encoding. We will show that the use of pilot symbols or the trellis-search algorithm is more efficient than using differential encoding in resolving the ambiguities, and leads to better performance.

This chapter is organized as follows. In Section 2.1, MLSD-NSCI on an unknown flat SIMO channel is derived and compared with MSDD. In Section 2.2, PEP performance over time-varying Rayleigh fading is analyzed. The PEP analysis result motivates the three pilot-based algorithms we introduce in Section 2.3. The detection delay, computational complexity and BEP performances of the

three algorithms are compared in Section 2.4. Conclusions are made in Section 2.5.

2.1 Maximum Likelihood Sequence Detector with No Channel State Information (MLSD-NCSI)

Assume that the channel gain remains constant over the interval of L symbols. We denote a baseband L-symbol uncoded transmitted block as $\mathbf{s} = [s(0)\ s(1)\ ...\ s(L-1)]^T$, where $s(k)$ is the transmitted symbol for the kth symbol interval $[kT, (k+1)T)$, and T is the symbol duration. The received signal over the unknown channel at the ith antennas is

$$\mathbf{r}_i = h_i\mathbf{s} + \mathbf{n}_i. \tag{2.1}$$

The gain h_i is the complex path gain between the transmitter and the ith receive antenna, i.e. the ith path, among a total of N paths. The path gains $\{h_i\}_{i=1}^N$ are mutually independent of one another. The noise vector $\mathbf{n}_i = [n_i(0)\ n_i(1)\ ...\ n_i(L-1)]^T$ is the complex AWGN in the ith path over the L-symbol interval, with $E[n_i(k)] = 0$ and $E[|n_i(k)|^2] = N_0$. The noise vectors $\{\mathbf{n}_i\}_{i=1}^N$ are all mutually independent of one another, and also independent of the path gains $\{h_i\}_{i=1}^N$. The total average received SNR per bit is defined as

$$\gamma_b = N\gamma_c = N\frac{E[|h_i|^2]E_b}{N_0} = N\frac{2\sigma^2 E_b}{N_0}, \tag{2.2}$$

where γ_c is the average SNR at each receiver branch.

We can denote the received signal at all N antennas in matrix form as

$$\mathbf{R} = \mathbf{s}\mathbf{h}^T + \mathbf{N}, \tag{2.3}$$

where $\mathbf{R}_{L\times N} = [\mathbf{r}_1, ..., \mathbf{r}_N]$, $\mathbf{h}_{N\times 1} = [h_1\ ...\ h_N]^T$, and $\mathbf{N}_{L\times N} = [\mathbf{n}_1, ..., \mathbf{n}_N]$.

Under the i.i.d. complex AWGN assumption on the noise matrix $\mathbf{N}$, we have

$$p(\mathbf{R}|\mathbf{s}, \mathbf{h}) = \frac{1}{(\pi N_0)^{NL}} \exp\left(-\frac{\|\mathbf{R} - \mathbf{s}\mathbf{h}^T\|_F^2}{N_0}\right), \tag{2.4}$$

where $\| \ \|_F$ denotes the Frobenius norm of a matrix [60]. We want to design an ML receiver which decides on the sequence $\mathbf{s}$ and channel gain $\mathbf{h}$ that jointly maximize $p(\mathbf{R}|\mathbf{s}, \mathbf{h})$, i.e.

$$(\hat{\mathbf{s}}, \hat{\mathbf{h}}) = \arg\max_{\mathbf{s},\mathbf{h}} p(\mathbf{R}|\mathbf{s}, \mathbf{h}). \tag{2.5}$$

It is clear from (2.4) that (2.5) is equivalent to

$$\begin{aligned}(\hat{\mathbf{s}}, \hat{\mathbf{h}}) &= \arg\min_{\mathbf{s},\mathbf{h}} \|\mathbf{R} - \mathbf{s}\mathbf{h}^T\|_F^2 \\ &= \arg\min_{\mathbf{s},\mathbf{h}} \sum_{i=1}^{N} \|\mathbf{r}_i - h_i\mathbf{s}\|^2. \end{aligned} \tag{2.6}$$

Conditioned on a sequence hypothesis $\mathbf{s}$, we first minimize $\sum_{i=1}^{N} \|\mathbf{r}_i - h_i\mathbf{s}\|^2$ with respect to the channel gain $\mathbf{h}$. Due to the independence of $\{h_i\}_{i=1}^{N}$, this is equivalent to minimizing each term

$$\|\mathbf{r}_i - h_i\mathbf{s}\|^2 \tag{2.7}$$

with respect to h_i individually. Using the orthogonal projection theorem, the quantity in (2.7) is minimized when the error vector $\mathbf{r}_i - h_i\mathbf{s}$ is orthogonal to the signal vector $\mathbf{s}$, i.e.

$$(\mathbf{r}_i - h_i\mathbf{s}) \cdot \mathbf{s} = 0, \tag{2.8}$$

where the inner product of two complex vectors is defined as $\mathbf{x} \cdot \mathbf{y} = \sum_i x_i y_i^* = \mathbf{y}^H\mathbf{x}$. Solving (2.8) gives the ML estimate $\hat{h}_i(\mathbf{s})$ that minimizes the error term in (2.7) and, hence, that in (2.6), corresponding to the sequence hypothesis $\mathbf{s}$, i.e.

$$\hat{h}_i(\mathbf{s}) = \frac{\mathbf{s}^H\mathbf{r}_i}{\|\mathbf{s}\|^2}. \tag{2.9}$$

Substituting (2.9), (2.6) becomes

$$\hat{\mathbf{s}} = \arg\min_{\mathbf{s}} \sum_{i=1}^{N} \left\| \mathbf{r}_i - \frac{\mathbf{s}^H\mathbf{r}_i}{\|\mathbf{s}\|^2}\mathbf{s} \right\|^2. \tag{2.10}$$

Expanding the metric in (2.10) and dropping terms independent of $\mathbf{s}$, the MLSD detection rule simplifies to

$$\hat{\mathbf{s}} = \arg\max_{\mathbf{s}} \lambda(\mathbf{s}) = \arg\max_{\mathbf{s}} \frac{\sum_{i=1}^{N} |\mathbf{s}^H\mathbf{r}_i|^2}{\|\mathbf{s}\|^2}. \tag{2.11}$$

The detector (2.11) does not require explicit channel estimation or knowledge of the statistics of $\mathbf{h}$ in making its data sequence decision $\hat{\mathbf{s}}$. It is applicable to any flat channel model, e.g. phase noncoherent AWGN, Rayleigh/Rician and Nakagami fading. Our MLSD-NCSI is commonly known as the GLRT detector [53]. In comparison, MSDD maximizes the probability $p(\mathbf{r}_1, ..., \mathbf{r}_N|\mathbf{s})$, which is obtained by averaging (2.4) over $\mathbf{h}$ [5] (and θ [6]). Therefore, knowledge of the channel statistics is required. Moreover, MSDD detectors for different channel models, e.g. AWGN, Rayleigh and Rician fading, have different forms [5, 6]. By assuming high SNR, we can easily simplify the MSDD detector for Rayleigh fading to the MLSD-NCSI in (2.11) [6]. Simulation results show that the performance of MLSD-NCSI [6, eq. (23)] with differential encoding over Rayleigh fading is almost equal to that of MSDD with perfect knowledge of the channel statistics [6, eq. (22)]. In addition, it is observed in [6] that the performance of MLSD-NCSI with differential encoding over Rician fading [6, eq. (23)] is almost equal to that of MSDD with perfect knowledge of the channel statistics [6, eq. (18)], although no explanation is given. The derivation of (2.11) in this section gives the mathematical proof of the optimality and robustness of MLSD-NCSI regardless of SNR value, while its equivalence to MSDD in performance has been shown in [6].

2.2 PEP Performance Analysis

In this section, we use two methods in the two subsections to show that the PEP performance of MLSD-NCSI with arbitrary QAM signals approaches that of the coherent MLSD detector with perfect CSI, when the sequence length L becomes large. As the PEP probability is equivalent to the node error probability of two paths merging in a trellis structure, which will be discussed in full details in Section 2.3, it motivates us to propose the algorithms in Section 2.3.

2.2.1 PEP Performance over General Blockwise Static Fading

We first analyze the PEP performance of MLSD-NCSI with arbitrary QAM signals over a blockwise static fading channel with arbitrary fading statistics. Suppose that the actual transmitted sequence is $\mathbf{s}_0 = [s_0(0)\ s_0(1)\ ...\ s_0(L-1)]^T$ and $\mathbf{s}_1 = [s_1(0)\ s_1(1)\ ...\ s_1(L-1)]^T$ is an alternative sequence. We will show that, for a fixed fading gain $\|\mathbf{h}\|$ (which is not known to the detector (2.11)), the probability of the event that the detector (2.11) decides in favor of $\mathbf{s}_1$ given that $\mathbf{s}_0$ is sent and $\mathbf{s}_1$ is the only other alternative, approaches the value

$$P_c(\varepsilon\big|\mathbf{s}=\mathbf{s}_0) = Q\left(\sqrt{\frac{\|\mathbf{s}_0-\mathbf{s}_1\|^2}{2N_0}\|\mathbf{h}\|^2}\right), \tag{2.12}$$

as the sequence length L becomes large. The PEP for detector (2.11) is given by

$$\begin{aligned} P(\varepsilon\big|\mathbf{s}=\mathbf{s}_0) &= P\left(\frac{\|\mathbf{s}_0^H\mathbf{R}\|^2}{\|\mathbf{s}_0\|^2} < \frac{\|\mathbf{s}_1^H\mathbf{R}\|^2}{\|\mathbf{s}_1\|^2}\big|\mathbf{s}=\mathbf{s}_0\right) \\ &= P\left(\left\|\|\mathbf{s}_1\|(\|\mathbf{s}_0\|^2\mathbf{h}+\mathbf{N}^T\mathbf{s}_0^*)\right\|^2 < \left\|\|\mathbf{s}_0\|(\mathbf{s}_1^H\mathbf{s}_0\mathbf{h}+\mathbf{N}^T\mathbf{s}_1^*)\right\|^2\big|\mathbf{s}=\mathbf{s}_0\right). \end{aligned} \tag{2.13}$$

Using the identity: $\|\mathbf{x}\|^2 - \|\mathbf{y}\|^2 = \mathrm{Re}[(\mathbf{x}+\mathbf{y})\cdot(\mathbf{x}-\mathbf{y})]$, (2.13) simplifies to

$$\begin{aligned} P(\varepsilon\big|\mathbf{s}=\mathbf{s}_0) &= P\left(\mathrm{Re}\{\left[\|\mathbf{s}_0\|^3(c_0\mathbf{h}+\mathbf{v}_0)\right]\cdot\left[\|\mathbf{s}_0\|^3(c_1\mathbf{h}+\mathbf{v}_1)\right]\} < 0\Big|\mathbf{s}=\mathbf{s}_0\right) \\ &= P\left(\mathrm{Re}\left[c_1^*c_0\|\mathbf{h}\|^2 + c_0\mathbf{v}_1^H\mathbf{h} + c_1^*\mathbf{h}^H\mathbf{v}_0 + \mathbf{v}_1^H\mathbf{v}_0\right] < 0\big|\mathbf{s}=\mathbf{s}_0\right). \end{aligned} \tag{2.14}$$

Here,

$$\begin{aligned} c_0 &= (\|\mathbf{s}_0\|\|\mathbf{s}_1\| + a + jb)/\|\mathbf{s}_0\|^2, \\ c_1 &= (\|\mathbf{s}_0\|\|\mathbf{s}_1\| - a - jb)/\|\mathbf{s}_0\|^2, \\ \mathbf{v}_0 &= \mathbf{N}^T(\|\mathbf{s}_1\|\mathbf{s}_0^* + \|\mathbf{s}_0\|\mathbf{s}_1^*)/\|\mathbf{s}_0\|^3, \\ \mathbf{v}_1 &= \mathbf{N}^T(\|\mathbf{s}_1\|\mathbf{s}_0^* - \|\mathbf{s}_0\|\mathbf{s}_1^*)/\|\mathbf{s}_0\|^3, \end{aligned} \tag{2.15}$$

where

$$\begin{aligned} a &= \mathrm{Re}[\mathbf{s}_1^H \mathbf{s}_0], \\ b &= \mathrm{Im}[\mathbf{s}_1^H \mathbf{s}_0]. \end{aligned} \tag{2.16}$$

The elements of $\mathbf{v}_0$ are i.i.d. circularly symmetric Gaussian random variables, each with variance $2(\frac{\|\mathbf{s}_1\|^2}{\|\mathbf{s}_0\|^2} + \frac{\|\mathbf{s}_1\|}{\|\mathbf{s}_0\|}\frac{a}{\|\mathbf{s}_0\|^2})N_0/\|\mathbf{s}_0\|^2$, while the elements of $\mathbf{v}_1$ are i.i.d. circularly symmetric Gaussian random variables, each with variance $2(\frac{\|\mathbf{s}_1\|^2}{\|\mathbf{s}_0\|^2} - \frac{\|\mathbf{s}_1\|}{\|\mathbf{s}_0\|}\frac{a}{\|\mathbf{s}_0\|^2})N_0/\|\mathbf{s}_0\|^2$. It is easy to show that

$$\begin{aligned} x_0 &= c_1^* \mathbf{h}^H \mathbf{v}_0 \\ x_1 &= c_0 \mathbf{v}_1^H \mathbf{h} \end{aligned} \tag{2.17}$$

are independent circularly symmetric Gaussian random variables. Thus,

$$x = \mathrm{Re}[x_0 + x_1] \tag{2.18}$$

is a zero-mean Gaussian random variable with variance $2\frac{\|\mathbf{s}_1\|^2}{\|\mathbf{s}_0\|^2}(\frac{\|\mathbf{s}_1\|^2}{\|\mathbf{s}_0\|^2} - \frac{a^2-b^2}{\|\mathbf{s}_0\|^4})\|\mathbf{h}\|^2 N_0/\|\mathbf{s}_0\|^2$. As L becomes large so that $\|\mathbf{s}_0\|$ and $\|\mathbf{s}_1\|$ also become large, the variance of x decays as $1/\|\mathbf{s}_0\|^2$, while

$$y = \mathrm{Re}\left[c_1^* c_0\right] \|\mathbf{h}\|^2 \tag{2.19}$$

does not decay with $1/\|\mathbf{s}_0\|^2$ nor with $1/\|\mathbf{s}_1\|^2$. Finally, it is easily to show that

$$\mathrm{Re}\left[\mathbf{v}_1^H \mathbf{v}_0\right] = \mathrm{Re}\left[\sum_{i=1}^{N} v_1^*(i) v_0(i)\right] \tag{2.20}$$

is zero-mean with variance proportional to $1/\|\mathbf{s}_0\|^4$. Thus, when L is large, $\mathrm{Re}[\mathbf{v}_1^H \mathbf{v}_0]$ in (2.14) can be neglected in comparison with x and y, and (2.14) simplifies to

$$P(\varepsilon \big| \mathbf{s} = \mathbf{s}_0) \approx P\left(x < -y \big| \mathbf{s} = \mathbf{s}_0\right). \tag{2.21}$$

We finally arrive at the sequence PEP of

$$P(\varepsilon \big| \mathbf{s} = \mathbf{s}_0) \approx Q\left(\sqrt{\frac{\left(\|\mathbf{s}_0\|^2\|\mathbf{s}_1\|^2 - a^2 - b^2\right)^2}{2\|\mathbf{s}_1\|^2\left(\|\mathbf{s}_0\|^2\|\mathbf{s}_1\|^2 - a^2 + b^2\right)N_0}\|\mathbf{h}\|^2}\right). \tag{2.22}$$

Reorder elements of the sequences such that $\mathbf{s}_0 = [\mathbf{d}_0^T, \mathbf{c}^T]^T$ and $\mathbf{s}_1 = [\mathbf{d}_1^T, \mathbf{c}^T]^T$, where $\mathbf{d}_0$ and $\mathbf{d}_1$ contain all the elements in which $\mathbf{s}_0$ and $\mathbf{s}_1$ differ. It is easy to show that

$$\mathbf{s}_1^H \mathbf{s}_0 = \mathbf{d}_1^H \mathbf{d}_0 + \|\mathbf{c}\|^2. \tag{2.23}$$

As L becomes large while $\mathbf{d}_0$ and $\mathbf{d}_1$ remain the same, $\|\mathbf{c}\|^2$ also becomes large. We obtain from (2.22) that:

$$P(\varepsilon \big| \mathbf{s} = \mathbf{s}_0) \xrightarrow[L\to\infty]{} Q\left(\sqrt{\frac{\|\mathbf{d}_0 - \mathbf{d}_1\|^2}{2N_0}\|\mathbf{h}\|^2}\right). \tag{2.24}$$

The quantity on the right hand side of (2.24) is the PEP $P_c(\varepsilon|\mathbf{s} = \mathbf{s}_0)$ in (2.12) of the coherent MLSD detector with perfect CSI, under the assumption that the difference between $\mathbf{s}_0$ and $\mathbf{s}_1$ remains fixed.

2.2.2 PEP Performance over Time-varying Rayleigh Fading

We now analyze the PEP performance of MLSD-NCSI over slowly time-varying Rayleigh fading, where the fading gain remains constant over one symbol interval. Let $h_i(k)$ denote the fading gain at the ith path over the kth symbol interval. The received symbol in the ith path at the kth symbol interval over time-varying Rayleigh fading is given by

$$r_i(k) = h_i(k)s(k) + n_i(k). \tag{2.25}$$

The fading processes in different paths are assumed mutually independent, i.e. $\{h_i(k)\}_k$ and $\{h_j(l)\}_l$ are independent for $i \neq j, \forall k, l$. The autocorrelation of the fading process in any path is given by

$$\mathrm{E}[h_i(k+n)h_i^*(k)] = 2\sigma^2\rho(n). \tag{2.26}$$

Note that even in the presence of uniformly distributed phase offset θ, $h_i e^{j\theta}$ and h_i are statistically identical.

From the decision rule (2.11), the probability of the event that the detector decides in favor of $\mathbf{s}_1$ given that $\mathbf{s}_0$ is sent and $\mathbf{s}_1$ is the only other alternative, is given by

$$\begin{aligned} P(\varepsilon|\mathbf{s}=\mathbf{s}_0) &= P\left(\frac{\sum_{i=1}^{N}|\mathbf{s}_0^H\mathbf{r}_i|^2}{\|\mathbf{s}_0\|^2} < \frac{\sum_{i=1}^{N}|\mathbf{s}_1^H\mathbf{r}_i|^2}{\|\mathbf{s}_1\|^2}\middle|\mathbf{s}=\mathbf{s}_0\right) \\ &= P\left(\sum_{i=1}^{N}\|\mathbf{s}_1\|^2|\mathbf{s}_0^H\mathbf{r}_i|^2 < \sum_{i=1}^{N}\|\mathbf{s}_0\|^2|\mathbf{s}_1^H\mathbf{r}_i|^2\middle|\mathbf{s}=\mathbf{s}_0\right) \end{aligned} \tag{2.27}$$

Using the identity:$|x|^2-|y|^2=\mathrm{Re}[(x-y)(x+y)^*]$, (2.27) simplifies to

$$P(\varepsilon|\mathbf{s}=\mathbf{s}_0) = P\left(\sum_{i=1}^{N}\mathrm{Re}\left[\left(\mathbf{s}_-^H\mathbf{r}_i\right)\left(\mathbf{s}_+^H\mathbf{r}_i\right)^*\right] < 0\middle|\mathbf{s}=\mathbf{s}_0\right), \tag{2.28}$$

where we have defined

$$\begin{aligned} \mathbf{s}_+ &= \|\mathbf{s}_1\|\mathbf{s}_0 + \|\mathbf{s}_0\|\mathbf{s}_1 \\ \mathbf{s}_- &= \|\mathbf{s}_1\|\mathbf{s}_0 - \|\mathbf{s}_0\|\mathbf{s}_1. \end{aligned} \tag{2.29}$$

Letting

$$\begin{aligned} X_{1i} &= \mathbf{s}_-^H\mathbf{r}_i = x_i + jy_i \\ X_{2i} &= \mathbf{s}_+^H\mathbf{r}_i = u_i + jv_i \end{aligned} \tag{2.30}$$

(2.28) simplifies to

$$\begin{aligned} P(\varepsilon|\mathbf{s}=\mathbf{s}_0) &= P\left(\mathrm{Re}\left[\sum_{i=1}^{N}X_{1i}X_{2i}^*\right] < 0\middle|\mathbf{s}=\mathbf{s}_0\right) \\ &= P\left(\sum_{i=1}^{N}x_iu_i + y_iv_i < 0\middle|\mathbf{s}=\mathbf{s}_0\right). \end{aligned} \tag{2.31}$$

We now examine the statistics of $\{x_i\}_{i=1}^N$, $\{y_i\}_{i=1}^N$, $\{u_i\}_{i=1}^N$ and $\{v_i\}_{i=1}^N$. It is easy to show that $\{x_i\}_{i=1}^N$ are i.i.d. zero-mean Gaussian random variables with variance

$$\sigma_x^2 = \sigma^2\sum_{k=0}^{L-1}\sum_{l=0}^{L-1}s_-^*(k)s_-(l)s_0(k)s_0^*(l)\rho(k-l) + \frac{N_0}{2}\|\mathbf{s}_-\|^2. \tag{2.32}$$

Similarly, $\{y_i\}_{i=1}^N$ are i.i.d. zero-mean Gaussian random variables with variance $\sigma_y^2=\sigma_x^2$. The sequences $\{x_i\}_{i=1}^N$ and $\{y_i\}_{i=1}^N$ are independent of each other. Similarly,

$\{u_i\}_{i=1}^N$ are i.i.d. zero-mean Gaussian random variables with variance

$$\sigma_u^2 = \sigma^2 \sum_{k=0}^{L-1}\sum_{l=0}^{L-1} s_+^*(k)s_+(l)s_0(k)s_0^*(l)\rho(k-l) + \frac{N_0}{2}\|\mathbf{s}_+\|^2, \tag{2.33}$$

and $\{v_i\}_{i=1}^N$ are i.i.d. zero-mean Gaussian random variables with variance $\sigma_v^2 = \sigma_u^2$. The sequences $\{u_i\}_{i=1}^N$ and $\{v_i\}_{i=1}^N$ are independent of each other. It can easily be shown that x_i, y_i, u_i and v_i have cross-covariances

$$\begin{aligned}
\mu_{xu} &= \mathrm{E}\big[(x_i - \mathrm{E}[x_i])(u_i - \mathrm{E}[u_i])\big] \\
\mu_{yv} &= \mathrm{E}\big[(y_i - \mathrm{E}[y_i])(v_i - \mathrm{E}[v_i])\big] \\
\mu_{xv} &= \mathrm{E}\big[(x_i - \mathrm{E}[x_i])(v_i - \mathrm{E}[v_i])\big] \\
\mu_{yu} &= \mathrm{E}\big[(y_i - \mathrm{E}[y_i])(u_i - \mathrm{E}[u_i])\big]
\end{aligned} \tag{2.34}$$

where

$$\begin{aligned}
\mu_{xu} = \mu_{yv} &= \sigma^2 \sum_{k=0}^{L-1}\sum_{l=0}^{L-1} \mathrm{Re}[s_-^*(k)s_+(l)s_0(k)s_0^*(l)]\rho(k-l) \\
&\quad + \frac{N_0}{2}\|\mathbf{s}_0\|\|\mathbf{s}_1\|(\|\mathbf{s}_1\| - \|\mathbf{s}_0\|), \\
\mu_{xv} = -\mu_{yu} &= \sigma^2 \sum_{k=0}^{L-1}\sum_{l=0}^{L-1} \mathrm{Im}[s_-^*(k)s_+(l)s_0(k)s_0^*(l)]\rho(k-l).
\end{aligned} \tag{2.35}$$

We next evaluate (2.31) conditioned on $\{u_i\}_{i=1}^N$ and $\{v_i\}_{i=1}^N$, i.e. $P\big(\varepsilon|\mathbf{s} = \mathbf{s}_0, \{u_i\}_{i=1}^N, \{v_i\}_{i=1}^N\big)$, where x_i and y_i remain independent Gaussian random variables with means and variances

$$\begin{aligned}
\eta_{x|uv} &= \mathrm{E}[x_i\big|u_i, v_i] = \frac{\mu_{xu}}{\sigma_u^2}u_i + \frac{\mu_{xv}}{\sigma_u^2}v_i, \\
\eta_{y|uv} &= \mathrm{E}[y_i\big|u_i, v_i] = \frac{\mu_{xu}}{\sigma_u^2}u_i - \frac{\mu_{xv}}{\sigma_u^2}v_i, \\
\sigma_{x|uv}^2 &= \sigma_{y|uv}^2 = \frac{\sigma_x^2\sigma_u^2 - \mu_{xu}^2 - \mu_{xv}^2}{\sigma_u^2}.
\end{aligned} \tag{2.36}$$

Hence, conditioned on $\{u_i\}_{i=1}^N$ and $\{v_i\}_{i=1}^N$,

$$Z = \sum_{i=1}^{N} x_i u_i + y_i v_i \tag{2.37}$$

is Gaussian distributed with mean and variance

$$\begin{aligned}\eta_{Z|uv} &= \mathrm{E}\big[Z\big|\{u_i\}_{i=1}^N, \{v_i\}_{i=1}^N\big] = \frac{\mu_{xu}}{\sigma_u^2}q,\\ \sigma_{Z|uv}^2 &= \frac{\sigma_x^2\sigma_u^2 - \mu_{xu}^2 - \mu_{xv}^2}{\sigma_u^2}q,\end{aligned} \tag{2.38}$$

where

$$q = \sum_{i=1}^{N}(u_i^2 + v_i^2) \tag{2.39}$$

is χ_{2N}^2 distributed with $2N$ degrees of freedom and PDF [8, eq. (2-1-110)]

$$p_q(q) = \frac{q^{N-1}\exp(-\frac{q}{2\sigma_u^2})}{(N-1)!(2\sigma_u^2)^N}. \tag{2.40}$$

Thus, we have

$$P\left(Z<0\big|\mathbf{s}=\mathbf{s}_0, \{u_i\}_{i=1}^N, \{v_i\}_{i=1}^N\right) = Q\big(\eta_{z|uv}/\sigma_{z|uv}\big). \tag{2.41}$$

Since

$$P\big(\varepsilon\big|\mathbf{s}=\mathbf{s}_0, \{u_i\}_{i=1}^N, \{v_i\}_{i=1}^N\big) = P\left(Z<0\big|\mathbf{s}=\mathbf{s}_0, \{u_i\}_{i=1}^N, \{v_i\}_{i=1}^N\right), \tag{2.42}$$

we have

$$P\big(\varepsilon\big|\mathbf{s}=\mathbf{s}_0, \{u_i\}_{i=1}^N, \{v_i\}_{i=1}^N\big) = Q\left(\sqrt{\frac{\mu_{xu}^2}{\sigma_u^2(\sigma_x^2\sigma_u^2 - \mu_{xu}^2 - \mu_{xv}^2)}q}\right). \tag{2.43}$$

As (2.43) turns out to be only a function of q, we can evaluate (2.31) by integrating (2.43) over the χ_{2N}^2 distribution of q. This gives us [61, eq. (A13)]

$$\begin{aligned}P(\varepsilon\big|\mathbf{s}=\mathbf{s}_0) &= \int_{q=0}^{\infty} P\left(Z<0\big|\mathbf{s}=\mathbf{s}_0, q\right) f_q(q)dq\\ &= \frac{1}{2}\left[1 - \mu\sum_{i=0}^{N-1}\binom{2i}{i}\left(\frac{1-\mu^2}{4}\right)^i\right],\end{aligned} \tag{2.44}$$

where

$$\mu = \sqrt{\frac{\mu_{xu}^2}{\sigma_x^2\sigma_u^2 - \mu_{xv}^2}}. \tag{2.45}$$

This PEP performance expression holds for arbitrary QAM signals.

In order to show that the PEP of MLSD-NCSI over blockwise static Rayleigh fading approaches that of coherent detection in the limit as L becomes large, we examine the case of BPSK as an example for simplicity. Since we assume static fading, we have $\rho(n) = 1, \forall n$. For PSK signals, we have $s(k) = \sqrt{E_s}e^{j\phi(k)}$, where E_s is the energy per symbol, and $\phi(k)$ is the data modulated phase. We have $\|\mathbf{s}_0\|^2 = \|\mathbf{s}_1\|^2 = LE_s$. Assuming that $\mathbf{s}_0$ and $\mathbf{s}_1$ differ only in l positions, we have for BPSK that $\|\mathbf{s}_0 + \mathbf{s}_1\|^2 = 4(L-l)E_s$, and $\|\mathbf{s}_0 - \mathbf{s}_1\|^2 = 4lE_s$. Substituting these and $\rho(n) = 1$ into (2.32)-(2.35) and (2.45), and after simplification, we obtain

$$\mu = \sqrt{\frac{l\gamma_c^2}{l\gamma_c^2 + (1 + \frac{l}{L-l})\gamma_c + \frac{1}{L-l}}}. \tag{2.46}$$

As L increases while l is fixed, we obtain

$$\mu \xrightarrow[L\to\infty]{} \sqrt{\frac{l\gamma_c}{l\gamma_c + 1}}. \tag{2.47}$$

The PEP of coherent detection with PCSI over static fading is given by [62, eq. (2.35)]

$$\begin{aligned} P_c(\varepsilon\big|\mathbf{s} = \mathbf{s}_0, \mathbf{h}) &= Q\left(\sqrt{\frac{\|\mathbf{s}_0 - \mathbf{s}_1\|^2}{2N_0}\|\mathbf{h}\|^2}\right) \\ &= Q\left(\sqrt{\frac{2lE_b}{N_0}\|\mathbf{h}\|^2}\right). \end{aligned} \tag{2.48}$$

Letting $q' = \|\mathbf{h}\|^2$, which is χ^2_{2N} distributed with PDF

$$p_{q'}(q') = \frac{q'^{N-1}\exp(-\frac{q'}{2\sigma^2})}{(N-1)!(2\sigma^2)^N}, \tag{2.49}$$

the average coherent PEP is given by

$$\begin{aligned} P_c(\varepsilon|\mathbf{s} = \mathbf{s}_0) &= \int_{q'=0}^{\infty} P_c(\varepsilon\big|\mathbf{s} = \mathbf{s}_0, q' = \|\mathbf{h}\|^2) p_{q'}(q') dq' \\ &= \frac{1}{2}\left[1 - \mu_c \sum_{i=0}^{N-1} \binom{2i}{i}\left(\frac{1-\mu_c^2}{4}\right)^i\right], \end{aligned} \tag{2.50}$$

where

$$\mu_c = \sqrt{\frac{l2\sigma^2 E_b}{l2\sigma^2 E_b + N_0}} = \sqrt{\frac{l\gamma_c}{l\gamma_c + 1}}. \tag{2.51}$$

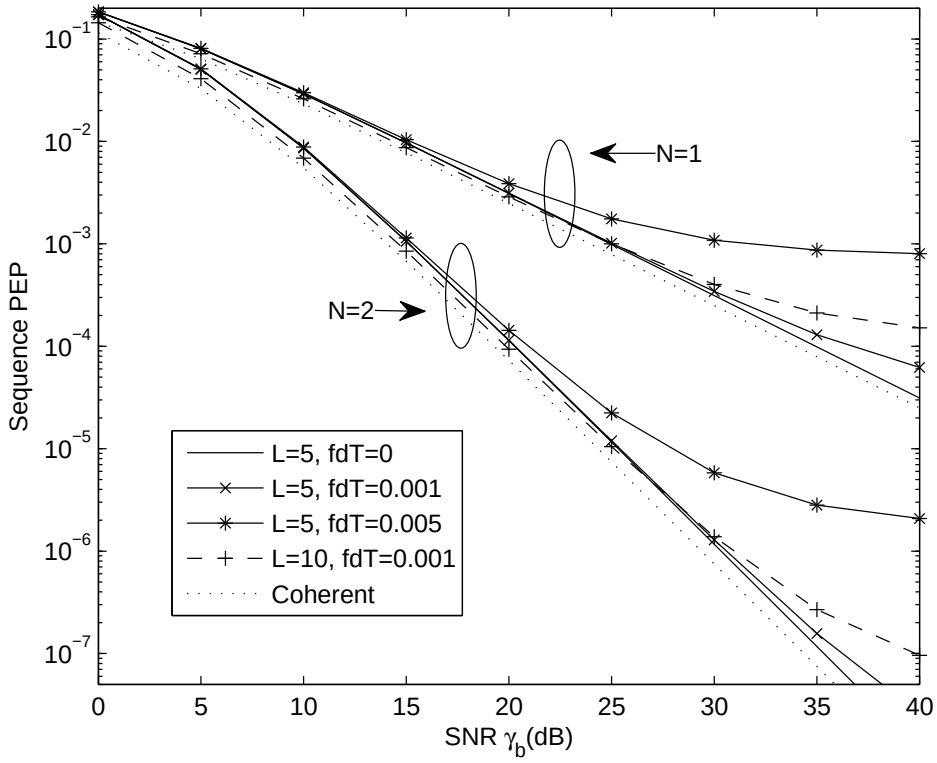

Figure 2.1: Analytical PEP performance of sequence detection with BPSK over Rayleigh fading, where $\mathbf{s}_0 = \sqrt{E_s}[1, ..., 1]^T$, $\mathbf{s}_1 = \sqrt{E_s}[1, ..., 1, -1]^T$.

Comparing (2.51) and (2.47), we can rewrite (2.47) as $\mu \xrightarrow[L\to\infty]{} \mu_c$. As (2.44) and (2.50) are identical when $\mu = \mu_c$, it is proven that $P(\varepsilon|\mathbf{s} = \mathbf{s}_0) \xrightarrow[L\to\infty]{} P_c(\varepsilon|\mathbf{s} = \mathbf{s}_0)$. This shows that MLSD-NCSI with BPSK can achieve coherent detection performance without explicit CSI or knowledge of the channel statistics. The detector only has to increase the detection block length L, while the number of positions l where the alternative sequences differ remains fixed.

The analytical PEPs of MLSD-NCSI with BPSK, QPSK and 16QAM over Rayleigh fading with various fade rates are obtained using (2.44) and (2.45) by numerical calculation, and are shown in Fig. 2.1, Fig. 2.2 and Fig. 2.3 respectively. We assume Clarke's isotropic scattering model, where we have [63]

$$\rho(n) = J_0(2\pi n f_d T) \tag{2.52}$$

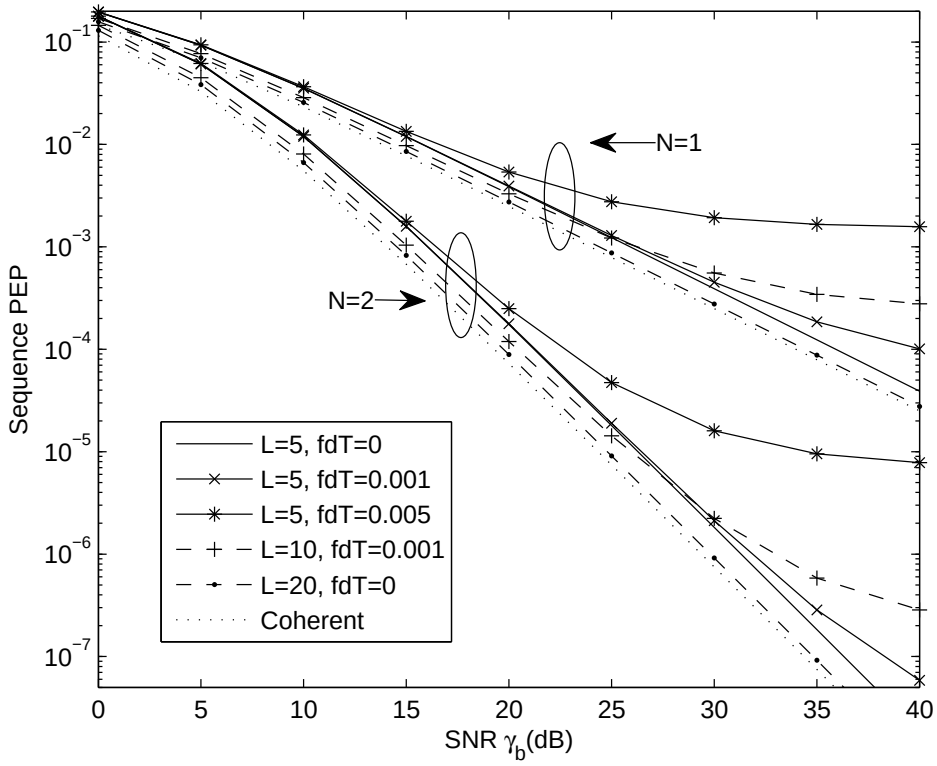

Figure 2.2: Analytical PEP performance of sequence detection with QPSK over Rayleigh fading, where $\mathbf{s}_0 = \sqrt{E_s}[1, ..., 1]^T$, $\mathbf{s}_1 = \sqrt{E_s}[1, ..., 1, j]^T$.

and i.i.d. paths. Here, f_dT is the normalized Doppler frequency. As expected, Fig. 2.2 and 2.3 show that the PEP performances of MLSD-NCSI with QPSK and 16QAM over static fading also approach that of coherent detection with PCSI, when L becomes large. The additional performance gain by increasing L gets smaller when L is already large.

The effect of time selectivity of the channel exhibits itself as an error floor, as expected. This is due to the blockwise static fading assumption used in the derivation of MLSD-NCSI, whereas the channel it is applied to is time-varying. For low fade rates, the PEP results are close to those of static fading, as expected. When the fade rate is high, error floors appear at high SNR. As MLSD-NCSI is based on the blockwise static fading assumption, its application to the time-varying

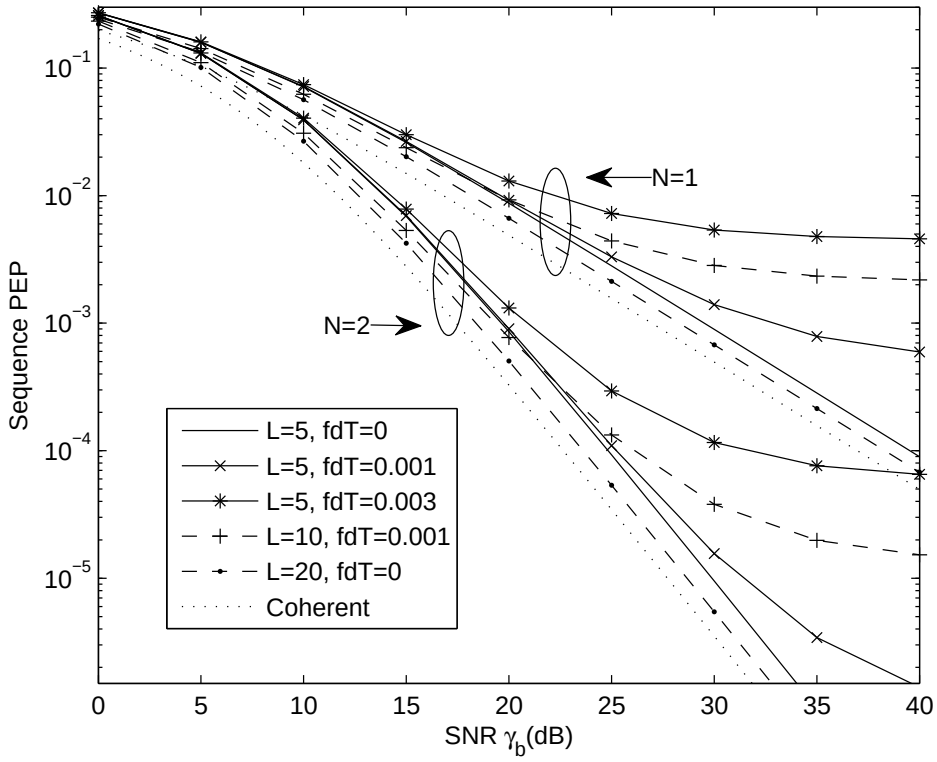

Figure 2.3: Analytical PEP performance of sequence detection with 16QAM over Rayleigh fading, where $\mathbf{s}_0 = \sqrt{E_s}[3+3j, ..., 3+3j]^T$, $\mathbf{s}_1 = \sqrt{E_s}[3+3j, ..., 3+3j, 3+j]^T$.

fading case even in the absence of noise may cause decision errors, resulting in the irreducible error floor at high SNR. As the fade rate increases or L increases, the channel varies more significantly within a detection block length, and the error floor is higher and begins to appear at lower SNR. At low SNR however, the MLSD-NCSI is robust, as its PEP performance is always close to that of static fading, because the AWGN noise is dominant in causing decision errors.

Having obtained that the PEP performance of MLSD-NCSI approaches that of coherent detection with PCSI when L increases if two sequences differ only in a few positions, we aim to design algorithms to implement MLSD-NCSI where the error probability in making each sequence decision is given by the PEP probability and

where the possible sequences when making each decision share common segments.

2.3 Three Pilot-Based Algorithms

Analytical performance results in Section 2.2 show that, to improve sequence detection performance, we need to increase the detection block length L. This, however, increases computational complexity. The complexity of the MLSD-NCSI detector in (2.11), when implemented by using exhaustive search, is exponential in L, as the metric of M^L sequences must be evaluated before a decision is made. The algorithms proposed in [56, 58, 64–66] attempt to reduce complexity, but they still require an average complexity per symbol that increases with L.

In addition, the MLSD-NCSI detector exhibits a detection ambiguity if one possible sequence is a complex scalar multiple of another. References [5, 6, 53–59] all resort to differential encoding with PSK or quadrant differential encoding with QAM to overcome the phase ambiguity. However, this limits the asymptotic performance of any sequence detector to that of coherent detection of differentially encoded PSK/quadrant differentially encoded QAM [5, 54], which has 1-2dB performance loss compared to coherent PSK/QAM. Divisor ambiguity results in an irreducible error floor even in the absence of channel variation [55, 58].

To implement the MLSD-NCSI on detection of very long sequences and to avoid a complexity increasing with L, and also to resolve detection ambiguity, we propose here three pilot-based algorithms: the trellis search algorithm, pilot-symbol-assisted block detection and decision-aided block detection. The three pilot-based algorithms adopt the general frame structure in Fig. 2.4 with $P = 1$ periodically inserted pilot symbol and D consecutive data symbols per frame. The algorithms are used to detect a long sequence of $S = N_F(P + D) + P$ symbols, where N_F denotes the number of frames in the sequence. The channel can be assumed static only over L symbol intervals. In general, we have $1 \ll L \ll S$.

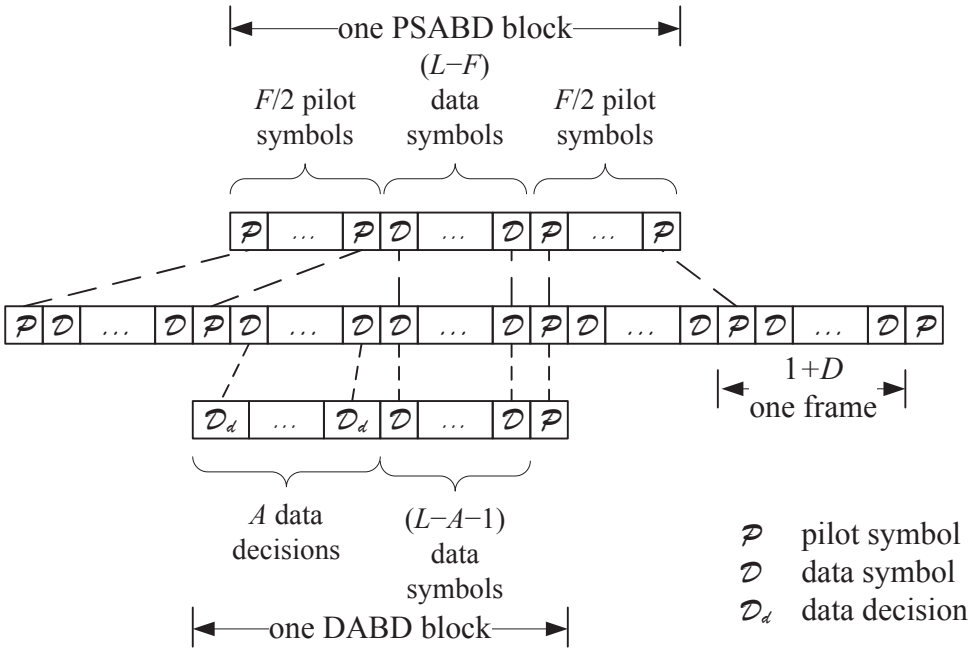

Figure 2.4: Transmitted sequence structure and detection blocks of PSABD and DABD.

2.3.1 The Trellis Search Algorithm and Performance

It is well known that a convolutional/trellis-coded sequence can be decoded by doing a trellis search. An uncoded sequence can also be decoded in a similar way. The trellis search algorithm with uncoded M-PSK, for example, constructs a trellis with M nodes at each time point k [67], each node labeled with the values assumed by the data modulated phase $\phi(k)$, as in Fig. 2.5. All the branches leading into the same node represent transmission of the symbol corresponding to that node at time point k. At a time point when a known pilot symbol is sent, there exists only one node corresponding to that pilot symbol, and all the branches leading to that node represent the same pilot symbol. The trellis for general uncoded M-QAM can be constructed in a similar manner.

Let $\mathbf{s}(k) = [s(0) \ ... \ s(k)]^T$ denote the subsequence of the hypothesized transmitted sequence $\mathbf{s}$ up to time k, and $\mathbf{r}_i(k) = [r_i(0) \ ... \ r_i(k)]^T$ denote the

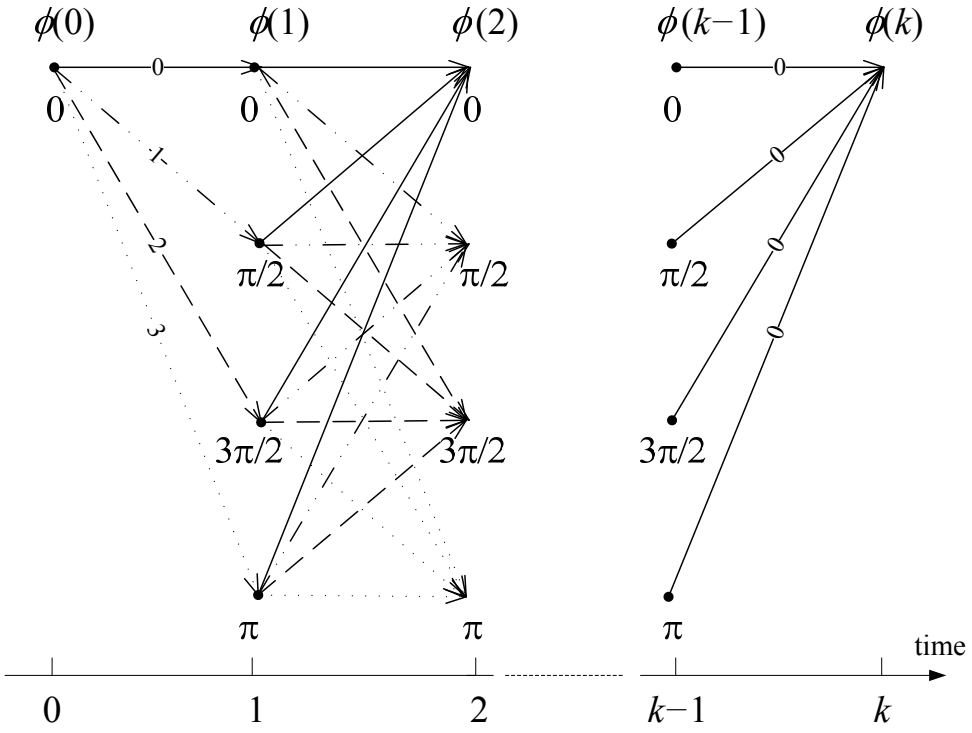

Figure 2.5: Trellis diagram of uncoded QPSK.

subsequence of the received sequence $\mathbf{r}_i$ at the ith receive antenna up to time k. The metric of the path $\mathbf{s}(k)$ at time k is computed based on (2.11) with only the L most recent symbols $\bar{\mathbf{s}}(k,L) = [s(k-L+1) \ ... \ s(k)]^T$ and the L most recent received symbols $\bar{\mathbf{r}}_i(k,L) = [r_i(k-L+1) \ ... \ r_i(k)]^T$ in all antennas $i = 1, ..., N$, as

$$\lambda(\bar{\mathbf{s}}(k,L)) = \frac{\sum_{i=1}^{N} |\bar{\mathbf{s}}(k,L)^H \bar{\mathbf{r}}_i(k,L)|^2}{\|\bar{\mathbf{s}}(k,L)\|^2}. \tag{2.53}$$

Initially when there are fewer than L received symbols, i.e. $0 \leq k \leq L-1$, the metric $\lambda_T(\mathbf{s}(k))$ is formed with all the available received signals $\mathbf{s}(k)$ instead of $\bar{\mathbf{s}}(k,L)$.

In searching through the trellis for the sequence that maximizes the $\lambda_T(\mathbf{s}(k))$, we do not need to compute the metric of all hypothesized transmitted sequences. Assume that two paths in the trellis, representing subsequences $\mathbf{s}_0(k)$ and $\mathbf{s}_1(k)$ of the sequences $\mathbf{s}_0$ and $\mathbf{s}_1$, respectively, enter the same node at time k. The algorithm compares the two metrics and discards the path representing $\mathbf{s}_1(k)$ if $\lambda(\bar{\mathbf{s}}_0(k,L)) >$

$\lambda(\bar{\mathbf{s}}_1(k,L))$, and vice versa. The same is repeated for all paths entering the same node, and the path with the largest metric is saved as the survivor. Decision on a data symbol is only made when the tails of all survivors have merged at the symbol. It is clear that the same algorithm works for coded modulations in a similar manner.

Assume that $\mathbf{s}_0$ is the transmitted sequence and $\mathbf{s}_1$ is an alternative sequence. Their subsequences $\mathbf{s}_0(k)$ and $\mathbf{s}_1(k)$ enter the same node at time k. The probability that the algorithm chooses the path representing $\mathbf{s}_1(k)$ at the node over $\mathbf{s}_0(k)$, is the PEP $P(\varepsilon|\mathbf{s} = \bar{\mathbf{s}}_0(k,L))$ given by (2.44) and (2.45) based on the subsequence $\bar{\mathbf{s}}(k,L)$. Although the metric $\lambda(\bar{\mathbf{s}}(k,L))$, as in [67] also, is not additive, it ensures that the node error event probability, i.e. PEP $P(\varepsilon|\mathbf{s} = \bar{\mathbf{s}}_0(k,L))$, and therefore the bit error probability, approaches that of PCSI as L becomes large, i.e. the additivity of the metric is not crucial. The trellis search algorithm in [6, eq. (23)] is similar, but its branch metric, although additive, is approximate – it is taken to be $\lambda(\bar{\mathbf{s}}(k,L)) - \lambda(\bar{\mathbf{s}}(k-1,L-1))$ for each branch. It is clear that the two trellis search algorithms have the same order of complexity and detection delay. Our simulations also show that they have similar performance with the same pilot-based structure. Both algorithms can be simplified using reduced state sequence detection [68].

The per-survivor processing MLSD algorithm in [69] uses a similar trellis structure. However, it first performs explicit channel estimation using the survivor data symbols. It uses the Euclidean distance metric assuming PCSI to make decision at each node. It is not shown analytically whether its error performance improves with the sequence length. The application of the algorithm is ad hoc. In comparison, the node error probability of our trellis-search algorithm is the PEP and has been shown to improve with L. It is the theoretical foundation of the trellis-search algorithm.

The BEP performance of the trellis-search algorithm over a phase noncoherent AWGN channel is simulated and found to be consistent with results in [67]. The BEP performances of the trellis-search algorithm with uncoded QPSK and 16QAM over Rayleigh fading are shown in Fig.2.6 and Fig. 2.7, respectively. Similar to

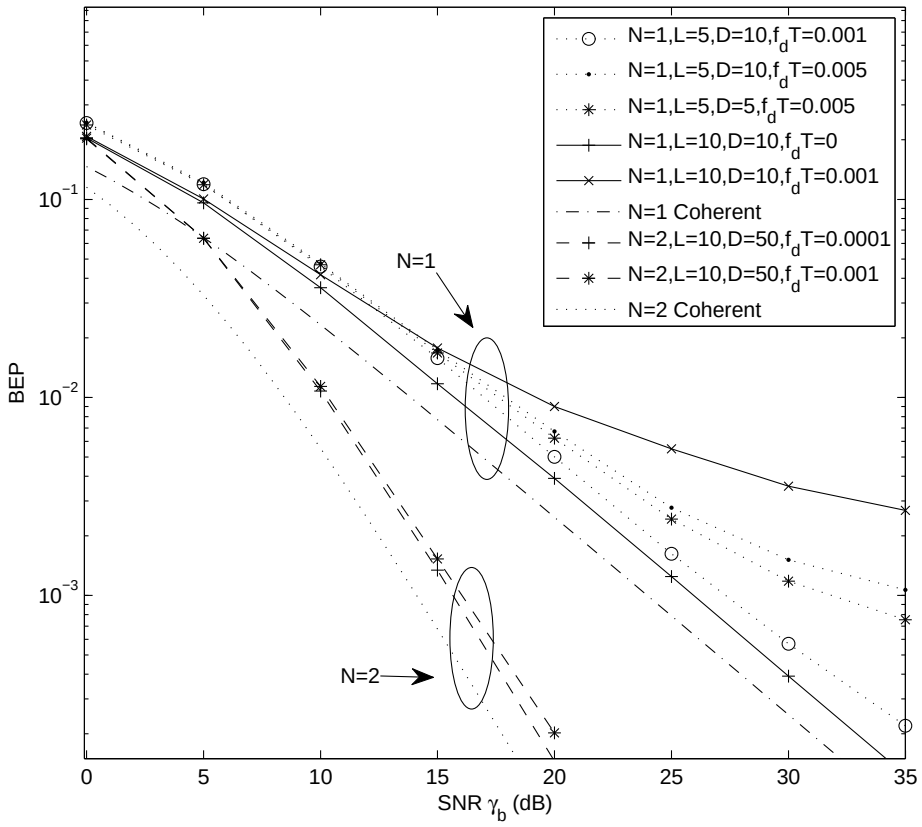

Figure 2.6: BEP performance of the trellis-search algorithm with QPSK over Rayleigh fading.

PEP observations in Section 2.2.2, its BEP over static fading and also its BEP over time-varying fading with very low fade rates improve with increasing L and approaches coherent performance. This is achieved without an increase in the computational complexity. However, if L is too large, an irreducible error floor appears at high SNR with nonzero fade rates. With a larger fade rate, the error floor is higher and begins to appear at lower SNR, as expected. On the other hand, when the window size L increases while the fade rate remains fixed, the channel varies more within a window length, and leads to a higher error floor at lower SNR. Therefore, the choice of L depends on both the fade rate and the operating SNR range. Any L thus chosen can be applied with the trellis-search algorithm as it does

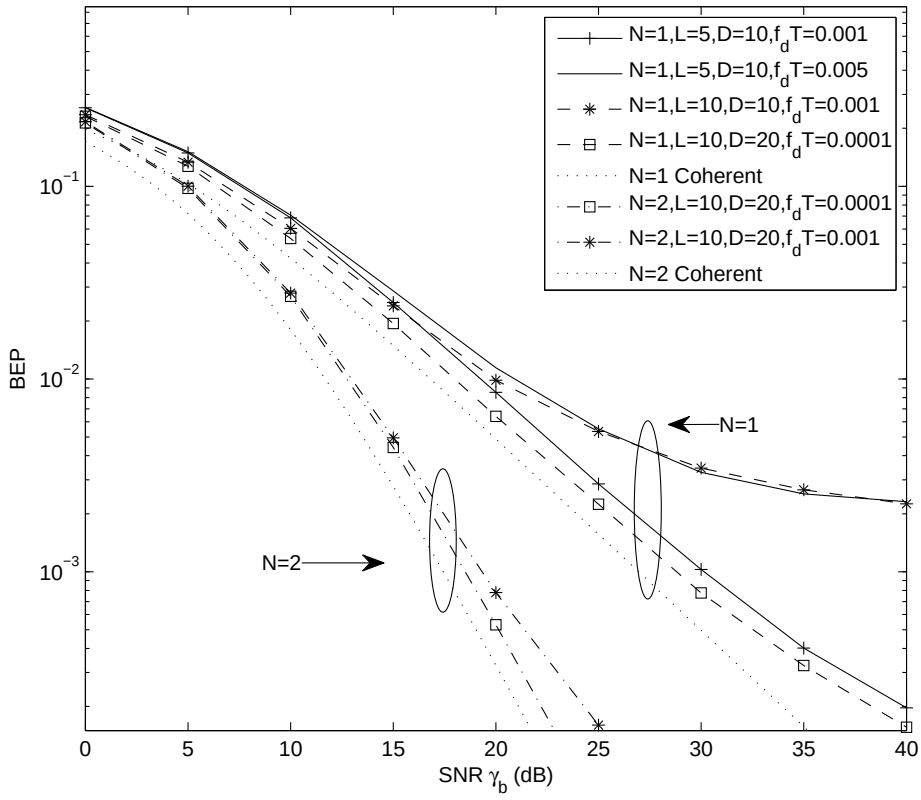

Figure 2.7: BEP performance of the trellis-search algorithm with 16QAM over Rayleigh fading.

not affect the complexity at all. For $N = 2$ diversity reception, the error floor is much lower as expected and therefore is not observed in the SNR range simulated for $f_dT = 0.0001$. Therefore, we can use larger L values than those in the single diversity case.

2.3.2 Pilot-symbol-assisted Block Detection and Performance

We propose here an alternative algorithm to implement the MLSD-NCSI by introduction of pilot symbols into sequence detection. A sequence even with a large L can be detected with a significantly reduced complexity if a sufficient number of

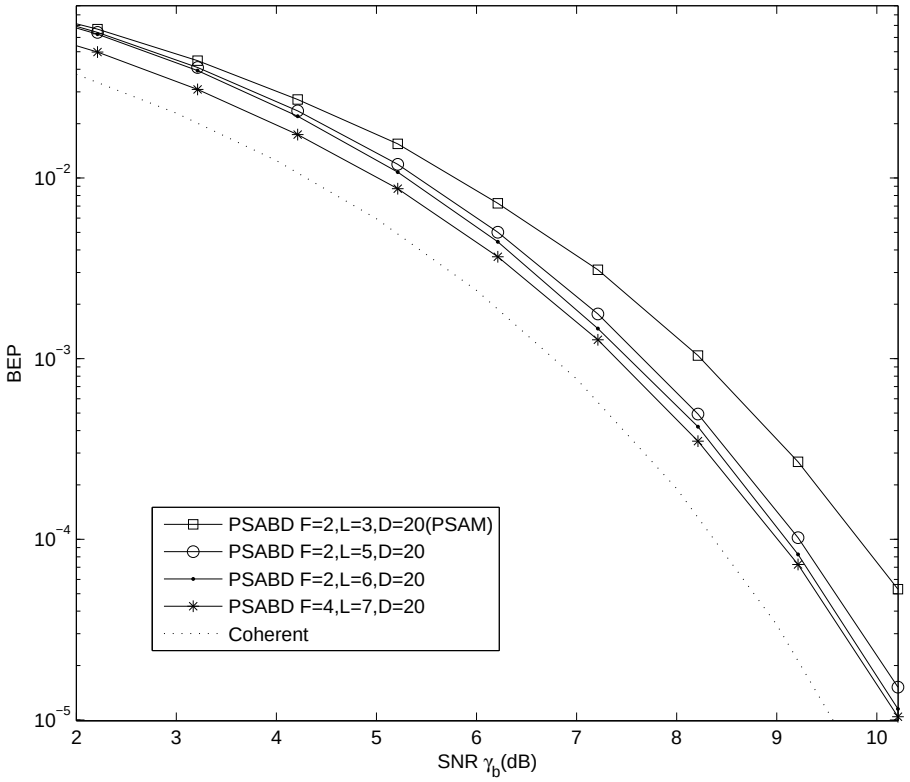

Figure 2.8: BEP performance of PSABD with QPSK over static phase noncoherent AWGN.

pilot symbols are included in each L-symbol detection.

Suppose that the channel gain remains static over F frame intervals. A subsequence $\overline{\mathbf{s}}_P$ of length L is formed with $(L-F)$ consecutive data symbols and the $F/2$ nearest pilot symbols on each sides, as shown in Fig. 2.4. The PSABD receiver decides on $\hat{\mathbf{s}}_P$ where

$$\hat{\mathbf{s}}_P = \arg\max_{\mathbf{s}_P} \lambda_P(\overline{\mathbf{s}}_P) = \arg\max_{\mathbf{s}_P} \frac{\sum_{i=1}^{N} |\overline{\mathbf{s}}_P^H \mathbf{r}_i|^2}{\|\overline{\mathbf{s}}_P\|^2}. \tag{2.54}$$

The PSABD detector in (2.54) decides on only $(L-F)$ consecutive data symbols in the block detection of $\overline{\mathbf{s}}_P$. Note that when only $(L-F)=1$ data symbol is detected each time, PSABD is equivalent to PSAM [4] with the GLRT estimator in (2.9).

The BEP performances of PSABD with QPSK and 16QAM over a static phase

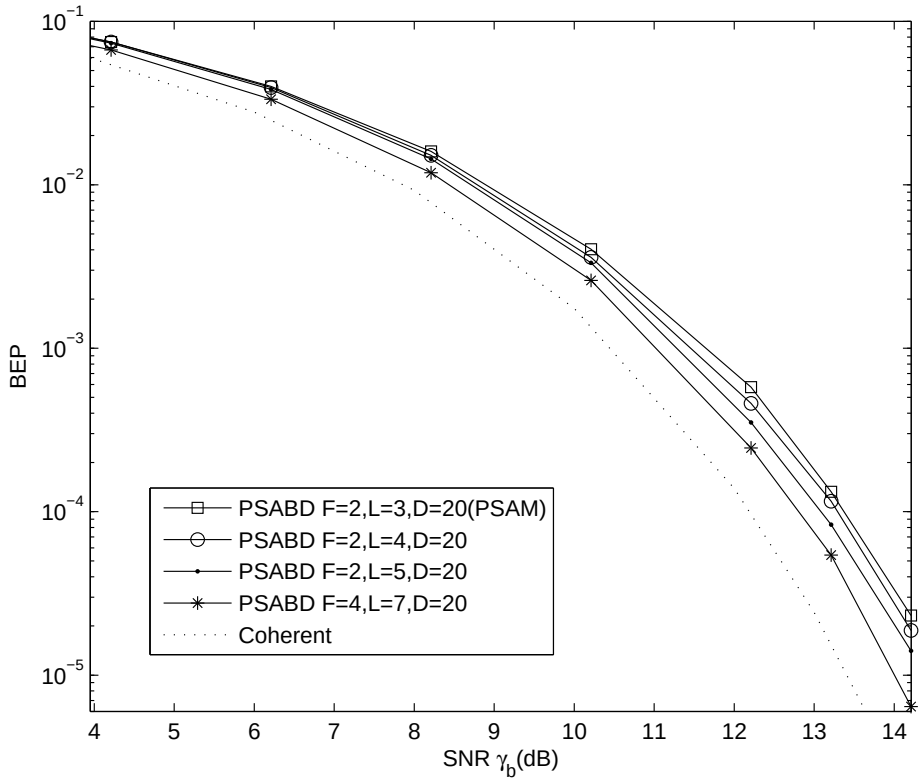

Figure 2.9: BEP performance of PSABD with 16QAM over static phase noncoherent AWGN.

noncoherent AWGN channel are shown in Fig. 2.8 and 2.9, respectively. The value of D data symbols per frame does not affect error performance of PSABD, if the channel is assumed static over F frames. Thus, we can use any D value with an L, provided there are at least $(L - F)$ data symbols in F frames for at least 1 block detection, i.e. $L - F \geq FD$. All schemes with different L values but the same D share the same sequence structure, and hence, the same bandwidth and power efficiencies, and therefore, can be compared fairly. Fig. 2.8 and 2.9 show that PSABD in both cases outperforms PSAM with the same sequence structure, and improves with increasing L, at the cost of computation complexity increasing with $(L-F)$. For the same $(L-F)$ data symbols per block detection, performance improves with F but without an increase in the complexity, which is similar to the

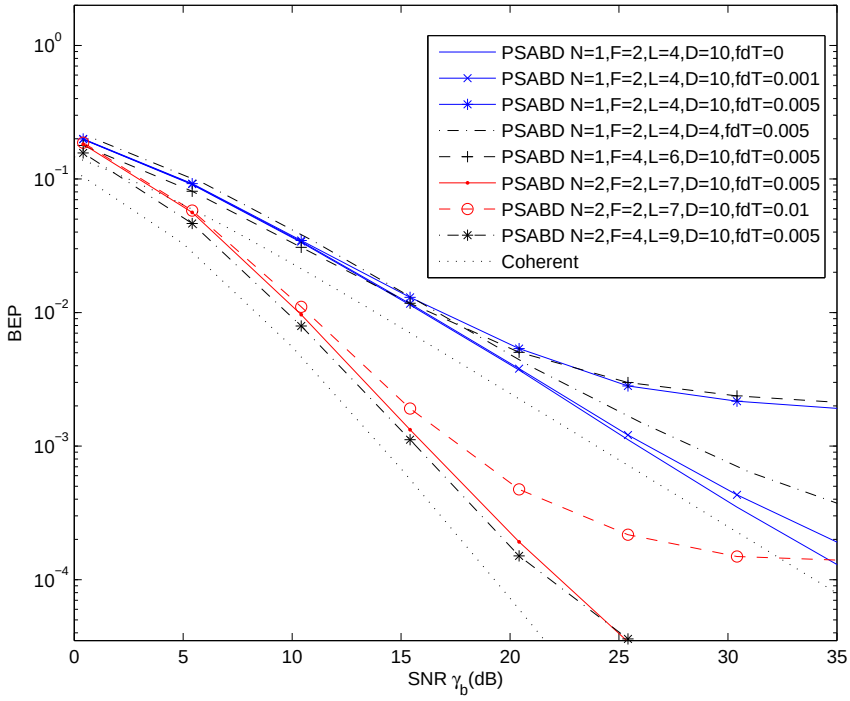

Figure 2.10: BEP performance of PSABD with QPSK over Rayleigh fading.

case of PSAM. Therefore, given a design criterion of complexity, we can fix $(L-F)$ and further improve performance by increasing L and F at the same time. A larger F can be realized, not by inserting more pilot symbols into the data sequence, but by using more distant pilot symbols in block detection. This, however, results in a longer detection delay, as in the case of PSAM.

Similar observations are made with PSABD over blockwise static Rayleigh fading. The BEP of PSABD with QPSK and receive diversity $N = 1, 2$ are shown in Fig. 2.10. The performance gain by increasing L is more significant with multiple receive diversity at high SNR, whereas the performance gain by increasing F while fixing $(L-F)$ is obvious in all diversity cases. Over time-varying fading, an irreducible error floor appears at high SNR. As expected, the higher the fade rate, the higher the error floor appearing at lower SNR. On the other hand, in the case of the same fade rate and same $(L-F)$, the error floor increases not only with F,

but also with D. This is due to the fact that the L symbols involved in each block detection span over $F(D+1)$ symbol duration. The larger $F(D+1)$ is, the more significantly the channel varies within the duration, resulting in a higher error floor. Therefore, the choice of P is a compromise between performance gain at low SNR and the error floor at high SNR. Any choice of F does not affect complexity or the increase in energy and bandwidth due to pilot symbols. The choice of D, however, affects pilot overhead and hence, effective SNR. A large D results in a small increase in SNR but a high error floor. Therefore, the choice of D is a compromise between pilot overhead and the error floor at high SNR.

2.3.3 Decision-aided Block Detection and Performance

DABD uses previous data decisions and a pilot symbol in block detection. As shown in Fig. 2.4, a subsequence $\overline{\mathbf{s}}_D$ of length L is formed with A most recent data decisions, $(L-A-1)$ consecutive data symbols and one pilot symbol in the future. DABD decides on the $(L-A-1)$ data symbols using the MLSD-NCSI metric of $\overline{\mathbf{s}}_D$, i.e.

$$\hat{\mathbf{s}}_D = \arg\max_{\mathbf{s}_D} \lambda_D(\overline{\mathbf{s}}_D) = \arg\max_{\mathbf{s}_D} \frac{\sum_{i=1}^{N} |\overline{\mathbf{s}}_D^H \mathbf{r}_i|^2}{\|\overline{\mathbf{s}}_D\|^2}. \tag{2.55}$$

The BEP performance of DABD with QPSK over a static phase noncoherent AWGN channel is shown in Fig. 2.11. The BEP performance over Rayleigh fading with receive diversity $N = 1, 2$ is shown in Fig. 2.12. Both figures show that the performance of DABD improves with the number of data symbols in each block detection, i.e. $L-A-1$. In other words, given an L value, the performance degrades with the number of previous decisions A. This is caused by error propagation when previous data symbol decisions are used in decision making. This effect is more significant when the fade rate f_dT increases. The advantage of DABD, however, is reduced computational complexity, which is determined by the value of $L-A-1$. Therefore, the choice of A is a compromise between complexity and performance.

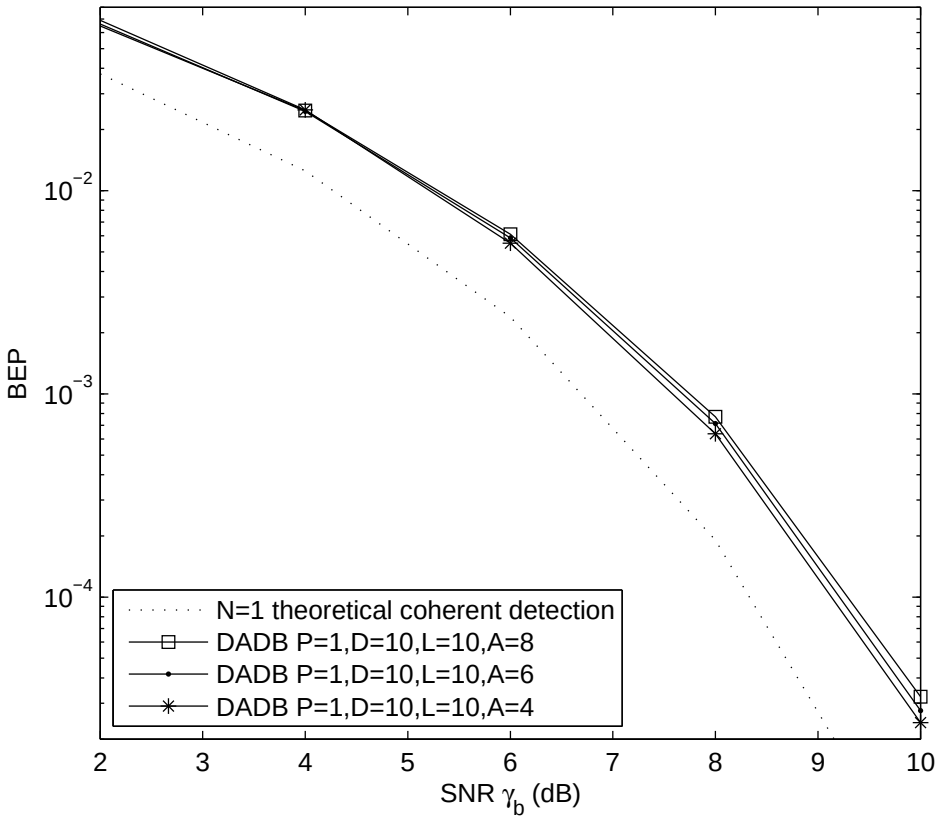

Figure 2.11: BEP performance of DABD with QPSK over static phase noncoherent AWGN.

2.4 Comparison of the Three Pilot-Based Algorithms with Existing Algorithms

2.4.1 Computational Complexity

For the trellis search algorithm, at each time point, $(M-1)$ comparisons are performed at each node to choose one survivor from the M paths that lead to that node. Hence, a total of $(M-1)M$ comparisons are performed at any time point with M nodes. Computation of the MLSD-NCSI metric can be calculated additively for both the numerator and the denominator, by adding the kth term

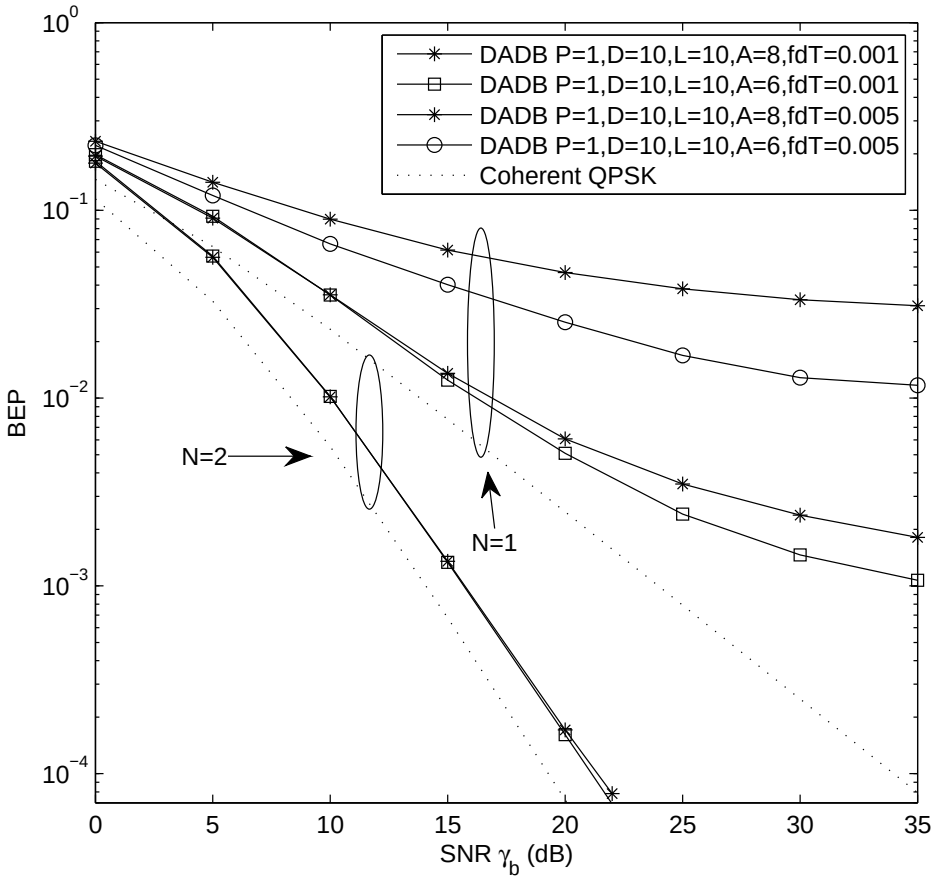

Figure 2.12: BEP performance of DABD with QPSK over Rayleigh fading.

and subtracting the $(k-L)$th term in $\bar{\mathbf{s}}(k,L)^H\bar{\mathbf{r}}_i(k,L)$ and $\|\bar{\mathbf{s}}(k,L)\|^2$. Thus, the complexity per symbol of the trellis-search algorithm is independent of L and S, and dependent only on M. Therefore, we can improve the performance by increasing L without an increase in the complexity.

With the presence of pilot symbols and data decisions in block detection, PSABD and DABD detect only $(L-F)$ and $(L-A-1)$ data symbols, respectively, in each block decision. Therefore, the computational complexity per symbol is now reduced from M^L/L to $M^{L-F}/(L-F)$ and $M^{L-A-1}/(L-A-1)$, respectively. Performance of PSABD can be improved by increasing L and F at the same time, by using more distant pilot symbols, while complexity remains fixed. Similarly,

Table 2.1: Comparison of Computational Complexity and Detection Delay

Non-pilot-based Algorithms	Computational Complexity Per Symbol	Average Detection Delay per Symbol T_d
Exhaustive search	$O(M^L/L)$	$T_d = (L-1)/2$
Sphere decoding	$O(2^L/L)$	$T_d = (L-1)/2$
Lattice decoding	$O(L \log L)$	$T_d = (L-1)/2$
Pilot-based Algorithms	**Computational Complexity Per Symbol**	**Average Detection Delay per Symbol T_d**
Trellis search	$O((M-1)M)$	$T_d \leq (D+1)/2$
PSABD	$O(M^{L-F}/(L-F))$	$T_d = (F-1)(D+1)/2$
DABD	$O(M^{L-A-1}/(L-A-1))$	$T_d = (D+1)/2$

performance of DABD can be improved by increasing L and A at the same time, by using more data decisions, while complexity remains fixed.

2.4.2 Phase and Divisor Ambiguities

Phase and divisor ambiguities are common to sequence detectors. The decision metric $\lambda(\mathbf{s})$ in (2.11) exhibits a detection ambiguity if one possible sequence is a complex scalar multiple of another. First, there is phase ambiguity between two sequences $\mathbf{s}_0$ and $\mathbf{s}_1$ if one is a phase rotation of the other, i.e. $\mathbf{s}_0 = \mathbf{s}_1 e^{j\theta}$. Second, there exists divisor ambiguity if one sequence is an amplitude amplification of the other, i.e. $\mathbf{s}_0 = |\alpha|\mathbf{s}_1$. A factor of $|\alpha|^2$ appears in both the numerator and the denominator of the metric $\lambda(\mathbf{s}_0)$ and cancel out, resulting in $\lambda(\mathbf{s}_0) = \lambda(\mathbf{s}_1)$ and hence, a decision ambiguity.

Phase and divisor ambiguities can be avoided when hypothesized sequences share common symbols, as in the three pilot-based algorithms. In the trellis-search algorithm, common symbols exist among paths that merge at a node. When two paths merge at a node, they would normally share a common segment in the tail,

when L is sufficiently large. In addition, uncoded sequences that merge at a node share the same symbol where they merge. Periodic pilot symbols are also symbols common to all sequences. All these common symbols prevent decision ambiguities. In PSABD and DABD, phase and divisor ambiguities are avoided by common pilot symbols and prior data decisions (for DABD) among all hypotheses.

2.4.3 Detection Delay

In the trellis search algorithm, decision on a data symbol is made only when the tails of all the survivors merge. Merging of survivors depends not only on signals before the data symbol concerned, but also on signals after that symbol. Therefore, detection delay of the symbol is random. However, due to the existence of only one node at time points where pilot symbols are transmitted, only one path will survive at a time point with a pilot symbol, and hence, decisions on all data symbols prior to that pilot symbol can be made latest at the pilot symbol. Therefore, the maximum detection delay of a data symbol is in the range $[1, D]$, depending on the spacing between the data symbol and the pilot symbol. Thus, the mean symbol detection delay T_d is less than the maximum of $(D+1)/2$.

For PSABD, decision on a data symbol can only be made when all transmitted pilot symbols of the corresponding detection block have been received. Depending on the position of the data symbol in a frame, detection delay of a data symbol is in the range $[(F/2-1)(D+1)+1, F/2\cdot(D+1)-1]$. Thus, the mean symbol detection delay is $T_d = (F-1)(D+1)/2$.

Similarly, for DABD, decision on a data symbol is made when the transmitted pilot symbol of the corresponding detection block has been received. Detection delay of a data symbol is in the range $[1, D]$, resulting in an average delay of $T_d = (D+1)/2$. Comparing the mean symbol detection delay of the algorithms in Table 2.1, PSABD with a large F requires a longer detection delay than the trellis search and DABD.

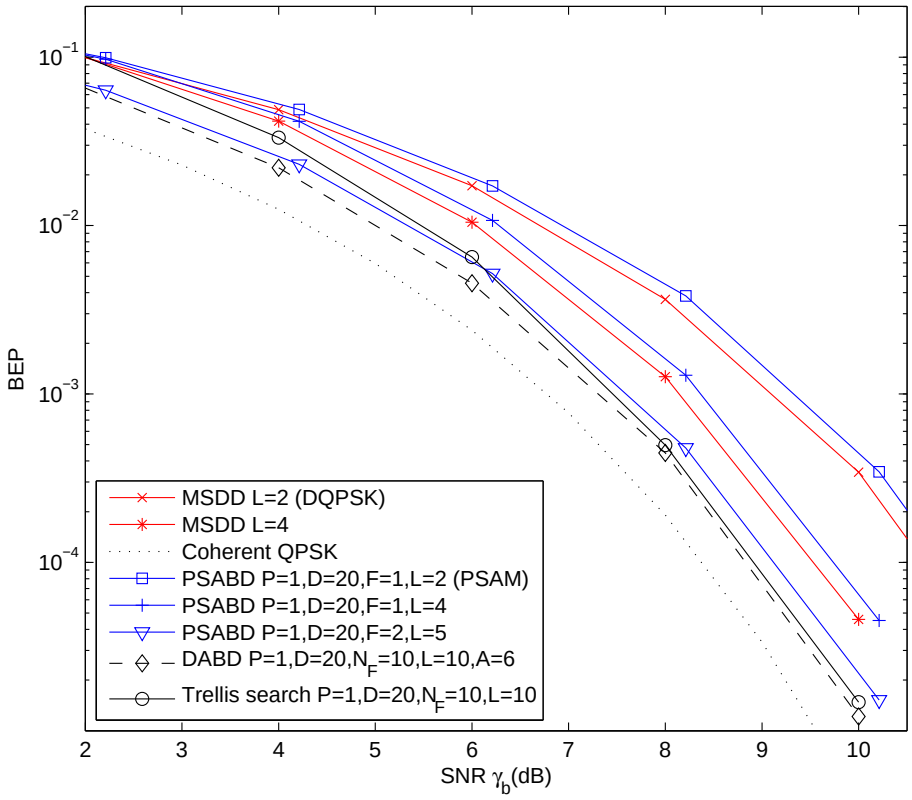

Figure 2.13: BEP performance comparison of QPSK over static phase noncoherent AWGN.

2.4.4 Performance

The increase in SNR caused by insertion of pilot symbols is accounted for in simulations, i.e.

$$\gamma_b = (1 + P/D)N\frac{2\sigma^2 E_b}{N_0}. \tag{2.56}$$

We use the three pilot-based algorithms to detect long sequences with $P = 1$ and $N_F = 10$. The performances of coherent detection with PCSI and MSDD are obtained without the use of pilot symbols.

Simulation results with QPSK over the phase noncoherent AWGN channel in Fig. 2.13 show that the performance of PSABD with $F = 1$ is close to that of

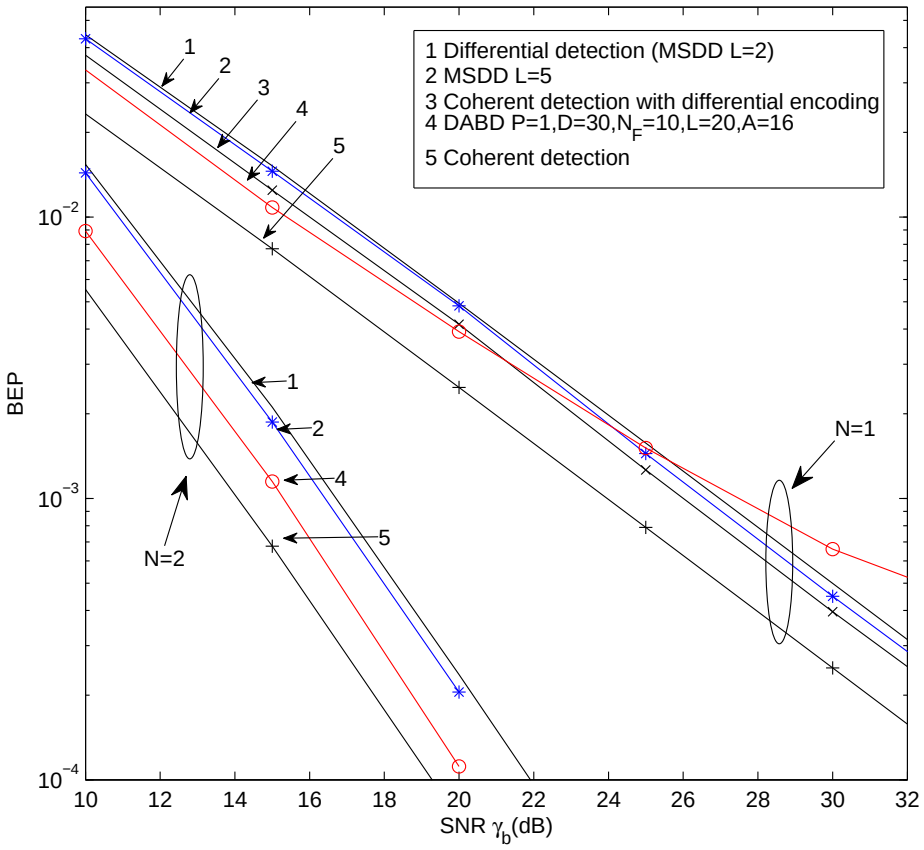

Figure 2.14: BEP performance comparison of QPSK over time-varying Rayleigh fading with $f_dT = 0.0001$.

MSDD with the same L value. When we increase F and L at the same time while maintaining a constant $(L - F)$, its performance improves. Hence, PSABD with $F > 1$ performs better than MSDD. However, a large F value results in a longer detection delay. Therefore, for a fair comparison with the trellis search algorithm and DABD, we will use a value of $F = 2$ in PSABD such that the three algorithms have similar detection delays. Further improvement in PSABD performance with $F = 2$ requires larger $(L - F)$ and hence higher complexity. The performance of the trellis search algorithm and DABD, however, can be improved with increasing L and A, respectively, without increasing the complexity.

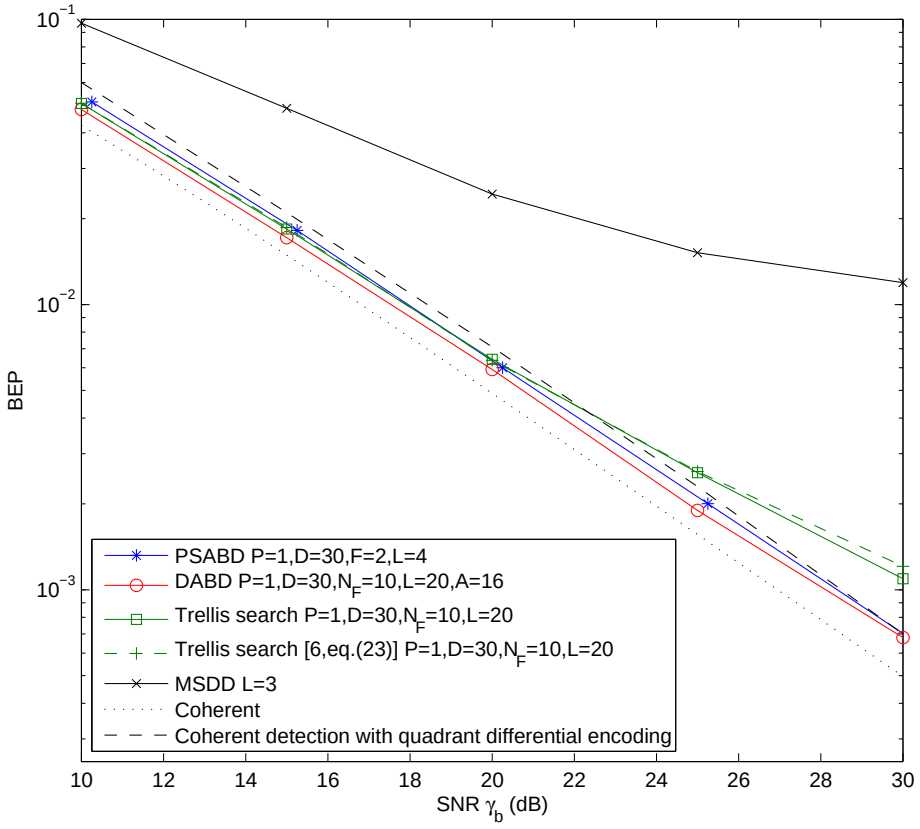

Figure 2.15: BEP performance comparison of 16QAM over time-varying Rayleigh fading with $N = 1$, $f_dT = 0.0001$.

Simulations of MSDD and the three pilot-based algorithms with QPSK and 16QAM over Rayleigh fading are shown in Fig. 2.14 and Fig. 2.15. We observe that, in order to achieve noticeable performance improvement over Rayleigh fading, L must be increased significantly. For example, MSDD with $L = 5$ in Fig. 2.14 shows slight improvement over differential encoding and differential detection (i.e. MSDD with $L = 2$). A very large L is required for MSDD to achieve a performance approaching that of coherent detection with differential encoding. In comparison, our three pilot-based algorithms at low SNR outperform coherent detection with (quadrant) differential encoding. Therefore, they outperform the algorithms in [5, 6, 53–59] that adopt (quadrant) differential encoding, because the performances

of these latter algorithms can improve to that of coherent detection only as L becomes very large. In addition, divisor ambiguity is not resolved by quadrant differential encoding and exhibits itself as an error floor in MSDD performance. Our three pilot-based algorithms do not suffer from divisor ambiguity. Observations of simulation results over Rician fading are similar but omitted by space limitation. Comparison in Fig. 2.15 shows that our trellis search algorithm performs slightly better than that of [6] over Rayleigh fading, as the branch metric in [6, eq. (23)] involves an approximation.

We do not find divisor ambiguity error floor with 16QAM in Fig. 2.13. The trellis-search algorithm with $L = 5$ over Rayleigh fading with the fade rate $f_dT = 0.001$ can reach a BEP of 2×10^{-4}, which is much lower than the divisor ambiguity error floor over static fading in [55, 58] (the error floor of block error rate 3×10^{-3} corresponds to an approximate BEP of 7.5×10^{-4}). Therefore, ambiguities are effectively resolved by the trellis-search algorithm.

2.5 Conclusions

We derive the MLSD-NCSI receiver and compare it with the MSDD receiver on the basis of the assumptions made in their derivations. It is proven that the PEP of the MLSD-NCSI detector approaches that of coherent detection when L increases. An exact closed-form PEP expression is obtained for MLSD-NCSI over time-varying Rayleigh fading. To detect a long sequence without incurring an exponential receiver complexity, we proposed three pilot-based algorithms. Their advantages in better performance and lower complexity than the existing lattice and sphere decoding block-by-block detection algorithms are demonstrated.

Chapter 3

The Gaussian Q-function

For performance analysis, simple closed-form expressions are always preferred for efficient evaluation. In cases where closed-form expressions are not available, finite range integrals that can be computed efficiently are often resorted to. Lastly, performance can always be obtained by simulation. However, for further analysis such as parameter optimization which involves iterative algorithms, complicated expressions and simulation would incur intensive computation and are often not practical. Therefore, simple closed-form exact expressions are always desired. Alternatively, closed-form bounds and approximations can be used. Hence, the rest of the thesis aims at obtaining simple expressions, whether exact expressions or bounds, that facilitate further analysis.

The Gaussian Q-function is of great importance in the performance analysis of communication systems with coherent detection over AWGN. For example, the BEP of BPSK over AWGN is expressed in a Gaussian Q-function [8, eq.(5-2-5)]. The Gaussian Q-function is conventionally defined as the area under the tail of the normalized (zero mean, unit variance) Gaussian random variable, i.e. [8, eq.(2-1-97)]

$$Q(x) = \frac{1}{\sqrt{2\pi}} \int_x^\infty \exp\left(-\frac{t^2}{2}\right) dt. \tag{3.1}$$

In order to compute it efficiently, closed-form bounds and approximations are obtained [16, 20, 23]. Moreover, as the argument appears only in the lower limit of the integral, further analysis using the definition, e.g. averaging the Gaussian

Q-function over fading distribution, very often does not reduce to a closed form. Therefore, for applications where closed-form results are not available, closed-form approximations and bounds of the Gaussian Q-function are still useful to facilitate analysis.

An alternative form of the Gaussian Q-function was discovered by Craig, as [15, eq.(9)]

$$Q(x) = \frac{1}{\pi} \int_0^{\pi/2} \exp\left(-\frac{x^2}{2\sin^2\theta}\right) d\theta, \tag{3.2}$$

which involves integration over a finite range. The Craig's form not only makes numerical evaluation easier, it also makes averaging over fading easier using the MGF method, i.e.

$$\begin{aligned} I(\bar{\gamma}) &= \int_0^{\infty} Q(\sqrt{\gamma}) p_\gamma(\gamma) d\gamma \\ &= \int_0^{\infty} \frac{1}{\pi} \int_0^{\pi/2} \exp\left(-\frac{\gamma}{2\sin^2\theta}\right) d\theta p_\gamma(\gamma) d\gamma \\ &= \frac{1}{\pi} \int_0^{\pi/2} M_\gamma\left(-\frac{1}{2\sin^2\theta}\right) d\theta. \end{aligned} \tag{3.3}$$

The MGF $M_\gamma(s)$ associated with $p_\gamma(\gamma)$ and defined as [48, eq.(2.4)]

$$M_\gamma(s) = \int_0^{\infty} \exp(s\gamma)\, p_\gamma(\gamma) d\gamma, \tag{3.4}$$

depends only on the fading model assumed [48, 1.1.3]. The use of the Craig's form leads to a closed-form expression for averaging the Gaussian Q-function over Rayleigh fading [48, eq.(5.6)]. However, the average of the Craig's form over other fading distributions, e.g. Rician and Nakagami-m fading, involve a finite range integral or the Gauss hypergeometric function. In such cases, we may resorts to approximations and bounds. New approximations and bounds of the Gaussian Q-function are derived based on the Craig's form [21, 24].

However, many well-known tight bounds are in the form of a product of an exponential function with a complex rational or irrational function, or a sum of such products. The average of these bounds over the distribution of fading very often does not reduce to closed forms. Therefore, our objective in this chapter is

to look for bounds in simple forms that can be averaged over fading distributions. Although approximations and upper bounds are used more often than lower bounds in performance analysis, lower bounds are still useful, as the combined use of upper and lower bounds shows the tightness of the bounds, without comparing the individual bounds with numerical integration of the exact value. The accuracy of approximations, in contrast, can only be obtained by comparing with numerical integration of the exact value.

Noticing that the definition and the Craig's form of the Gaussian Q-function are both integrals of the exponential function, we propose to apply the Jensen's inequality and obtain three families of exponential bounds. The tightness of our bounds can be improved by increasing the number of exponential terms.

This chapter is organized as follows. We first summarize existing well-known bounds in Section 3.1. In Section 3.2, We look into the Jensen's inequality and its application in deriving the Abreu bounds. The type 1 lower bounds are derived in Section 3.3 by applying the Jensen's inequality on the definition of the Gaussian Q-function. The type 2 lower bounds are derived in Section 3.4 by applying the Jensen's inequality on the Craig's form of the Gaussian Q-function. Our lower bounds are averaged over fading in Section 3.5 and closed-form expressions are derived. In Section 3.6, a family of lower bounds on the two-dimensional Gaussian Q-function is derived using the Jensen's inequality. Conclusions are made in Section 3.7.

3.1 Existing Bounds

Below are a few well-known closed form bounds based on the definition of the Gaussian Q-function. By integration by parts, it is show that [23, eq.(2.121)]

$$Q(x) = \frac{1}{\sqrt{2\pi}x}\exp\left(-\frac{x^2}{2}\right) - \frac{1}{\sqrt{2\pi}}\int_x^\infty \frac{1}{t^2}\exp\left(-\frac{t^2}{2}\right)dt. \tag{3.5}$$

Upper and lower bounding the second term in (3.5), upper bound $Q_{UB-WJ-1}$ [1] and lower bound $Q_{LB-WJ-2}$ are obtained [23, eq.(2.121)]

$$\begin{aligned} Q(x) &\leq Q_{UB-WJ-1}(x) = \frac{1}{\sqrt{2\pi}x}\exp\left(-\frac{x^2}{2}\right) \\ Q(x) &\geq Q_{LB-WJ-2}(x) = \left(1-\frac{1}{x^2}\right)\frac{1}{\sqrt{2\pi}x}\exp\left(-\frac{x^2}{2}\right). \end{aligned} \tag{3.6}$$

A tighter lower bound is obtained by improving the bound on the second term in (3.5) as [16, eq.(8)]

$$Q(x) \geq Q_{LB-BS-1}(x) = \frac{1}{\sqrt{2\pi}}\frac{x}{1+x^2}\exp\left(-\frac{x^2}{2}\right). \tag{3.7}$$

Tighter upper and lower bounds are obtained in [16, eq.(11-12)]

$$\begin{aligned} Q(x) &\leq Q_{UB-BS-1}(x) = \frac{1}{\frac{1}{2}x+\frac{1}{2}\sqrt{x^2+\frac{8}{\pi}}}\frac{1}{\sqrt{2\pi}}\exp\left(-\frac{x^2}{2}\right) \\ Q(x) &\geq Q_{LB-BS2-1}(x) = \frac{1}{\frac{1}{2}x+\frac{1}{2}\sqrt{x^2+4}}\frac{1}{\sqrt{2\pi}}\exp\left(-\frac{x^2}{2}\right). \end{aligned} \tag{3.8}$$

Among the bounds in (3.6)–(3.8), Q_{UB-WJ} in (3.6) is in the simplest form, and can be averaged over Rayleigh and Nakagami-m fading. Though lower bound $Q_{LB-WJ-2}(x)$ can also be averaged over Rayleigh and Nakagami-m fading, it is negative below 0dB. Therefore, it is not suitable for averaging over fading and will not be considered in this chapter. The tighter bounds in (3.7)–(3.8), are in the form of a product of an exponential function with a complex rational or irrational function. The average of these bounds over the distribution of fading is, in general, difficult to evaluate.

Since the discovery of the Craig's form of the Gaussian Q-function, more bounds have been obtained based on the Craig's form. Abreu partitions the integration range of $[0, \pi/2]$ into two subranges where the integrand is purely convex or concave [21]. The convex range is further partitioned, and the subintegral is upper bounded using the Cotes trapezoidal rule and lower bounded using the Jensen's Inequality. Similarly, the concave range is partitioned, and the subintegral is upper bounded

[1] WJ are initials of the two authors and 1 is the number of exponential terms

using the Jensen's Inequality and lower bounded using the Cotes trapezoidal rule. More detailed derivation will be shown in Section 3.23. Compact-form upper and lower bounds are obtained in [21, eq.(34)]

$$\begin{aligned} Q(x) \leq & Q_{UB-A-2}(x) = \frac{f_1(x)}{8+2(\pi-2)f_2(x)} \exp\left(-\frac{2x^2}{f_1^2(x)}\right) \\ & + \frac{4\pi + f_2(x)\pi - 6f_1(x)}{8\pi + 2\pi f_2(x)} \exp\left(-\frac{2x^2}{2+f_1(x)}\right) \end{aligned} \tag{3.9}$$

and [21, eq.(33)]

$$\begin{aligned} Q(x) \geq & Q_{LB-A-3}(x) = \frac{3f_1(x)}{4\pi + \pi f_2(x)} \exp\left(-\frac{2x^2}{2-f_2(x)}\right) \\ & + \frac{4+(\pi-2)f_2(x)-2f_1(x)}{16+4(\pi-2)f_2(x)} \left[\exp\left(-\frac{x^2}{2}\right) + \exp\left(-\frac{2x^2}{f_1^2(x)}\right)\right], \end{aligned} \tag{3.10}$$

where [21, eq.(30-31)]

$$\begin{aligned} f_1 &= \sqrt{x^2+3-\sqrt{(x^2-1)^2+8}}, \\ f_2 &= \sqrt{\sqrt{(x^2-1)^2+8}-(x^2-1)} = \sqrt{4-f_1^2}. \end{aligned} \tag{3.11}$$

Similar to the bounds in (3.7)–(3.8), the Abreu bounds are sums of a product of an exponential function with a complex rational or irrational function. The average of these bounds over the distribution of fading is, in general, difficult to evaluate.

Using the Craig's form, Chiani obtains bounds in the simplest form as far as we are aware of [24]. We summarize the derivation and results in our own notations here. Splitting the integration range of $[0, \pi/2]$ into $n+1$ subranges, by arbitrarily choosing $n+2$ values of θ_k such that $0 = \theta_0 < \theta_1 < ... < \theta_{n+1} = \pi/2$, Chiani upper bounds the integrand in (3.2) in the range $[\theta_{k-1}, \theta_k)$ by its maximum values, i.e. [24, eq.(7)]

$$\exp\left(-\frac{x^2}{2\sin^2\theta}\right) \leq \exp\left(-\frac{x^2}{2\sin^2\theta_k}\right). \tag{3.12}$$

This results in the Chiani upper bound [24, eq.(8)]

$$Q(x) \leq Q_{UB-CDS}(x) = \sum_{k=1}^{n+1} a_k \exp\left(-b_k x^2\right), \tag{3.13}$$

where

$$\begin{aligned} a_k &= \frac{\theta_k - \theta_{k-1}}{\pi}, \\ b_k &= \frac{1}{2\sin^2\theta_k}. \end{aligned} \tag{3.14}$$

Special compact-form upper bounds from (3.13) are given by

$$Q_{UB-CDS-1}(x) = \frac{1}{2}\exp\left(-\frac{x^2}{2}\right), \tag{3.15}$$

[24, eq.(10)]

$$Q_{UB-CDS-2}(x) = \frac{1}{4}\exp\left(-\frac{x^2}{2}\right) + \frac{1}{4}\exp\left(-x^2\right), \tag{3.16}$$

and [24, eq.(11)]

$$Q_{UB-CDS-3}(x) = \frac{1}{4}\exp\left(-\frac{x^2}{2}\right) + \frac{1}{12}\exp\left(-x^2\right) + \frac{1}{6}\exp\left(-2x^2\right). \tag{3.17}$$

Though not shown in [24], we can also lower bound the integrand in (3.2) in the range $[\theta_{k-1}, \theta_k)$ by its minimum values, i.e.

$$\exp\left(-\frac{x^2}{2\sin^2\theta}\right) \geq \exp\left(-\frac{x^2}{2\sin^2(\theta_{k-1})}\right) \tag{3.18}$$

and obtain the lower bound

$$Q(x) \geq Q_{LB-CDS}(x) = \sum_{k=1}^{n+1} a_k \exp\left(-b_{k-1}x^2\right), \tag{3.19}$$

where a_k and b_k are given in (3.14). With $n = 1$ and $\theta_1 = \pi/3$, we obtain

$$Q_{LB-CDS-1}(x) = \frac{1}{6}\exp\left(-\frac{2}{3}x^2\right). \tag{3.20}$$

With $n = 2$ and $\theta_1 = \pi/6, \theta_2 = \pi/3$, we obtain

$$Q_{LB-CDS-2}(x) = \frac{1}{6}\exp\left(-\frac{2}{3}x^2\right) + \frac{1}{6}\exp\left(-2x^2\right). \tag{3.21}$$

With $n = 3$ and $\theta_1 = \pi/6, \theta_2 = \pi/4, \theta_3 = \pi/3$, we obtain

$$Q_{LB-CDS-3}(x) = \frac{1}{6}\exp\left(-\frac{2}{3}x^2\right) + \frac{1}{12}\exp\left(-x^2\right) + \frac{1}{12}\exp\left(-2x^2\right). \tag{3.22}$$

We refer to the lower bounds in (3.19)–(3.22) as the Chiani lower bounds in this thesis, though they are not given in [24].

The Chiani bounds in (3.13)–(3.22) are a sum of exponentials with constant coefficients. The simple form is suitable for manipulation of the Gaussian Q-function. For example, averaging exponential bounds over any fading distribution using the MGF method reduces to a closed form, as long as the fading MGF is given in exact closed form. However, the Chiani bounds, especially the lower bounds, are in general much looser than the Abreu bounds with the same number of exponential terms.

3.2 Jensen's Inequality

We look into the Jensen's inequality here and examine how it is applied in [21] to derive the Abreu bounds on the Gaussian Q-function. We will use the Jensen's inequality in a different way to derive new bounds in Section 3.3 and Section 3.4.

Jensen's inequality [70, eq.(12.411)]: Let $f(\theta)$ and $p(\theta)$ be two functions defined for $a \leq \theta \leq b$ such that $\alpha \leq f(\theta) \leq \beta$ and $p(\theta) \geq 0$, with $p(\theta) \not\equiv 0$. Let $\phi(u)$ be a convex function defined on the interval $\alpha \leq u \leq \beta$, then

$$\phi\left(\frac{\int_a^b f(\theta)p(\theta)d\theta}{\int_a^b p(\theta)d\theta}\right) \leq \frac{\int_a^b \phi(f)p(\theta)d\theta}{\int_a^b p(\theta)d\theta}. \tag{3.23}$$

In order to bound the the Craig's form of the Gaussian Q-function in (3.2), Abreu lets [21]

$$\begin{aligned} \phi(u) &= \exp\left(-\frac{x^2}{2\sin^2 u}\right), \\ f(\theta) &= \theta, \\ p(\theta) &= 1. \end{aligned} \tag{3.24}$$

However, in order to apply the Jensen's inequality, $\phi(f)$ must be a convex function. It is shown that $\phi(f)$ is convex in $[0, \bar{\theta}_x]$ and concave in $[\bar{\theta}_x, \pi]$, where

$$\bar{\theta}_x = \sin^{-1}\left(\frac{1}{2}\sqrt{x^2+3-\sqrt{(x^2-1)^2+8}}\right). \tag{3.25}$$

Therefore, the Jensen's inequality can be applied in the interval $[0, \bar{\theta}_x]$ or $[\bar{\theta}_x, \pi]$, which can be further partitioned. If $\phi(f)$ is convex in $[a, b]$, the Jensen's inequality results in a lower bound as

$$\frac{1}{\pi}\int_a^b \exp\left(-\frac{x^2}{2\sin^2\theta}\right) d\theta \geq \frac{b-a}{\pi}\exp\left[-\frac{x^2}{2\sin^2\left(\frac{a+b}{2}\right)}\right]. \tag{3.26}$$

If $\phi(f)$ is concave in $[a, b]$, we have

$$\frac{1}{\pi}\int_a^b \exp\left(-\frac{x^2}{2\sin^2\theta}\right) d\theta \leq \frac{b-a}{\pi}\exp\left[-\frac{x^2}{2\sin^2\left(\frac{a+b}{2}\right)}\right]. \tag{3.27}$$

In order to lower bound $\phi(f)$ in concave intervals and to upper bound it in convex intervals, Cotes trapezoidal rule is applied.

In summary, to apply the Abreu method to derive a lower bound, first, the integration range is partitioned into subranges where the integrand is purely convex or concave. Second, integral in the convex subrange(s) is lower bounded using the Jensen's inequality. Third, integral in the concave subrange(s) is lower bounded using the Cotes trapezoidal rule. Last, by summing the lower bound in the convex subrange(s) and the lower bound in the concave subrange(s), the lower bound on the Gaussian Q-function is obtained.

3.3 Bounds Based on Definition

3.3.1 Lower Bounds Based on Definition

Let us look at the definition of the Gaussian Q-function in (3.1). We first split the integration range of $[x, \infty]$ into $n+1$ subranges, by arbitrarily choosing $n+2$ values of α_k such that $x = \alpha_0 x < \alpha_1 x < ... < \alpha_{n+1} x = \infty$. Thus, (3.1) becomes

$$Q(x) = \sum_{k=1}^{n+1} \frac{1}{\sqrt{2\pi}} \int_{\alpha_{k-1}x}^{\alpha_k x} \exp\left(-\frac{t^2}{2}\right) dt. \tag{3.28}$$

Due to convexity of the exponential function in the entire real domain, we can apply the Jensen's inequality for each summation term in (3.28).

Letting

$$\begin{aligned} \phi(u) &= \exp(u), \\ f(t) &= -\frac{t^2}{2}, \\ p(t) &= 1, \\ a &= \alpha_{k-1}x, \\ b &= \alpha_k x, \end{aligned} \tag{3.29}$$

we obtain a lower bound on (3.28) using the Jensen's inequality as

$$Q_{LB-KW1}(x) = \sum_{k=1}^{n+1} a_k x \exp\left(-b_k x^2\right), \tag{3.30}$$

where

$$\begin{aligned} a_k &= \frac{\alpha_k - \alpha_{k-1}}{\sqrt{2\pi}} \geq 0 \\ b_k &= \frac{\alpha_k^2 + \alpha_{k-1}^2 + \alpha_k^2\alpha_{k-1}}{6} \geq 0 \end{aligned} \tag{3.31}$$

The last summation term in (3.30) is zero for any n. Therefore, the lower bound $Q_{LB-KW1}(x)$ is a sum of n terms. The form of $Q_{LB-KW1}(x)$ is simpler than that of the Abreu bound in (3.10).

When $n \to \infty$, we have

$$\begin{aligned} \lim_{n\to\infty} Q_{LB-KW1}(x) &= \sum_{k=1}^{\infty} \frac{dt}{\sqrt{2\pi}} \exp\left(-\frac{1}{6}\frac{dt^3}{dt}\right) \\ &= \sum_{k=1}^{\infty} \int_{\alpha_{k-1}x}^{\alpha_k x} \frac{1}{\sqrt{2\pi}} \exp\left(-\frac{t^2}{2}\right) dt, \end{aligned} \tag{3.32}$$

which is equal to the Craig's form in (3.1). As expected, simply by increasing n, the lower bound $Q_{LB-KW1}(x)$ approaches the exact value for all argument values.

As the values of $\{\alpha_k\}$ can be chosen arbitrarily, they can be optimized to minimize error in the region of interest $[0, R)$, i.e.

$$\{\alpha_k\}_o = \arg\min_{\{\alpha_k\}} \int_0^R \left|Q(x) - Q_{LB-KW1}(x, \{\alpha_k\})\right| C(x)dx, \tag{3.33}$$

where $C(x)$ is the cost of error. For example, to minimize relative error, we have $C(x) = 1/Q(x)$. To minimize average error in fading, $C(x)$ given by the fading distribution. Alternatively, we can strategically select $\{\alpha_k\}$ values to obtain bounds in neat compact expressions. With $n = 1$ and $\alpha_1 = 3/2$, we have

$$Q_{LB-KW1-1}(x) = \frac{x}{2\sqrt{2\pi}} \exp\left(-\frac{19}{24}x^2\right). \tag{3.34}$$

It is tighter than the single-term Chiani lower bound $Q_{LB-CDS-1}(x)$ in (3.20) between 0dB and 10dB. With $n = 2$ and $\alpha_1 = 4/3$, $\alpha_2 = 3$, we have

$$Q_{LB-KW1-2}(x) = \frac{x}{3\sqrt{2\pi}} \exp\left(-\frac{37}{54}x^2\right) + \frac{5x}{3\sqrt{2\pi}} \exp\left(-\frac{665}{270}x^2\right). \tag{3.35}$$

This two-term bound is tighter than the two-term Chiani lower bound $Q_{LB-CDS-2}(x)$ in (3.21) between -5dB and 20dB. With $n = 3$ and $\alpha_1 = 4/3$, $\alpha_2 = 2$, $\alpha_3 = 4$ we have

$$\begin{aligned} &Q_{LB-KW1-3}(x) \\ &= \frac{x}{3\sqrt{2\pi}} \exp\left(-\frac{37}{54}x^2\right) + \frac{2x}{3\sqrt{2\pi}} \exp\left(-\frac{38}{27}x^2\right) + \sqrt{\frac{2}{\pi}}x \exp\left(-\frac{14}{3}x^2\right). \end{aligned} \tag{3.36}$$

It is tighter than the three-term Chiani bound $Q_{LB-CDS-3}(x)$ in (3.22) between -5dB and 20dB. We can find bounds in neat compact form with arbitrary number of exponential terms, as long as the values of α_k chosen are in neat compact form, e.g. integers and fractions.

Fig. 3.1 and Fig. 3.2 show that the lower bounds $Q_{LB-KW1}(x)$ increase with the number of exponential terms for any argument value and approach the exact Gaussian Q-function. However, when $n > 2$, improvement is only observed for small arguments values. The figures show the argument in log scale in order to display a wide range of argument values.

The new three-term lower bound $Q_{LB-CDS-3}(x)$ is compared with existing bounds in Fig. 3.3 and Fig. 3.4. As our interest is to obtain bounds on the Gaussian Q-function that can be averaged over fading, only bounds that can be averaged over fading are compared. It is shown that our three-term $Q_{LB-KW1-3}(x)$ is much tighter

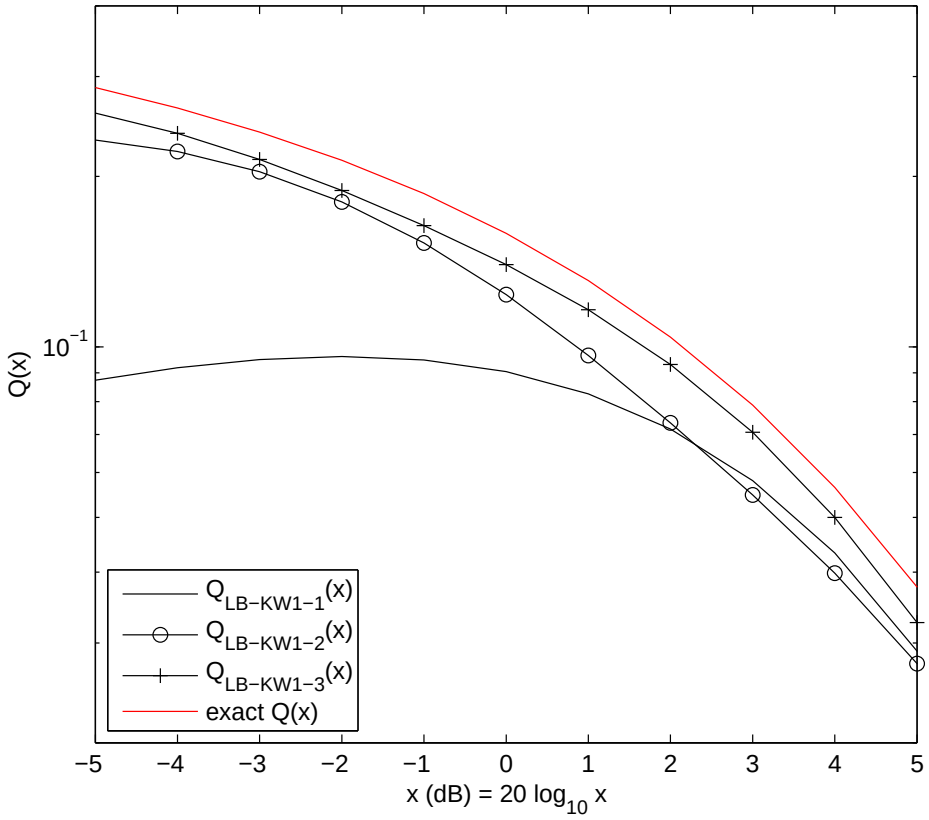

Figure 3.1: Lower bounds $Q_{LB-KW1}(x)$ for small argument values.

than the three-term $Q_{LB-CDS-3}(x)$ for all argument values. The combined use of the our three-term $Q_{LB-KW1-3}(x)$ and the Chiani upper bound $Q_{UB-CDS-3}(x)$ or $Q_{UB-WJ-1}(x)$ shows the tightness of the bounds, if the exact value is not available.

One shortcoming of lower bounds $Q_{LB-KW1}(x)$ is that they all approach zero when x approaches zero, while $Q(0) = 1/2$. Hence, lower bounds $Q_{LB-KW1}(x)$ are loose for very small argument values. Therefore, we must take care of the argument value in the application of $Q_{LB-KW1}(x)$. It is not advised to average $Q_{LB-KW1}(x)$ over a fading distribution where the PDF is concentrated at small values, e.g. for average error performance at very low average SNR.

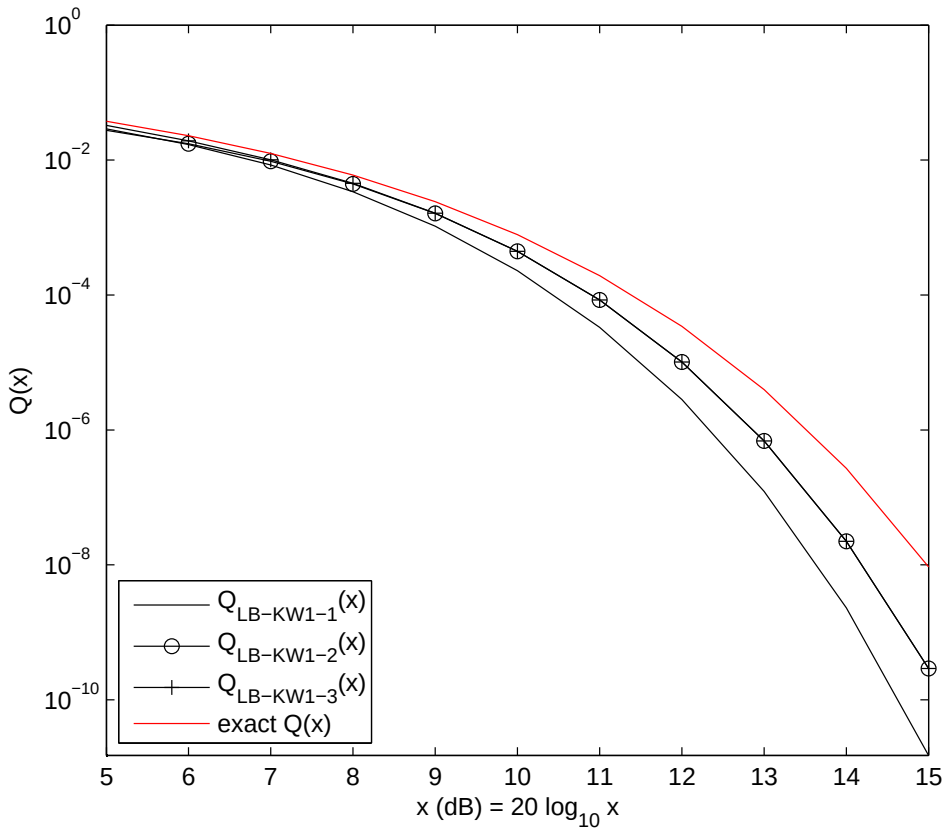

Figure 3.2: Lower bounds $Q_{LB-KW1}(x)$ for large argument values.

3.3.2 Upper Bounds Based on Definition

Now let us look at the Wozencraft's expression of the Gaussian Q-function in (3.5). We denote the second term in (3.5) as $G(x)$, i.e.

$$G(x) = \frac{1}{\sqrt{2\pi}} \int_x^\infty \frac{1}{t^2} \exp\left(-\frac{t^2}{2}\right) dt. \tag{3.37}$$

We first split the integration range of $[x, \infty]$ into $n+1$ subranges, by arbitrarily choosing $n+2$ values of β_k such that $x = \beta_0 x < \beta_1 x < ... < \beta_{n+1} x = \infty$. Thus, (3.37) becomes

$$G(x) = \sum_{k=1}^{n} \frac{1}{\sqrt{2\pi}} \int_{\beta_{k-1}x}^{\beta_k x} \frac{1}{t^2} \exp\left(-\frac{t^2}{2}\right) dt. \tag{3.38}$$

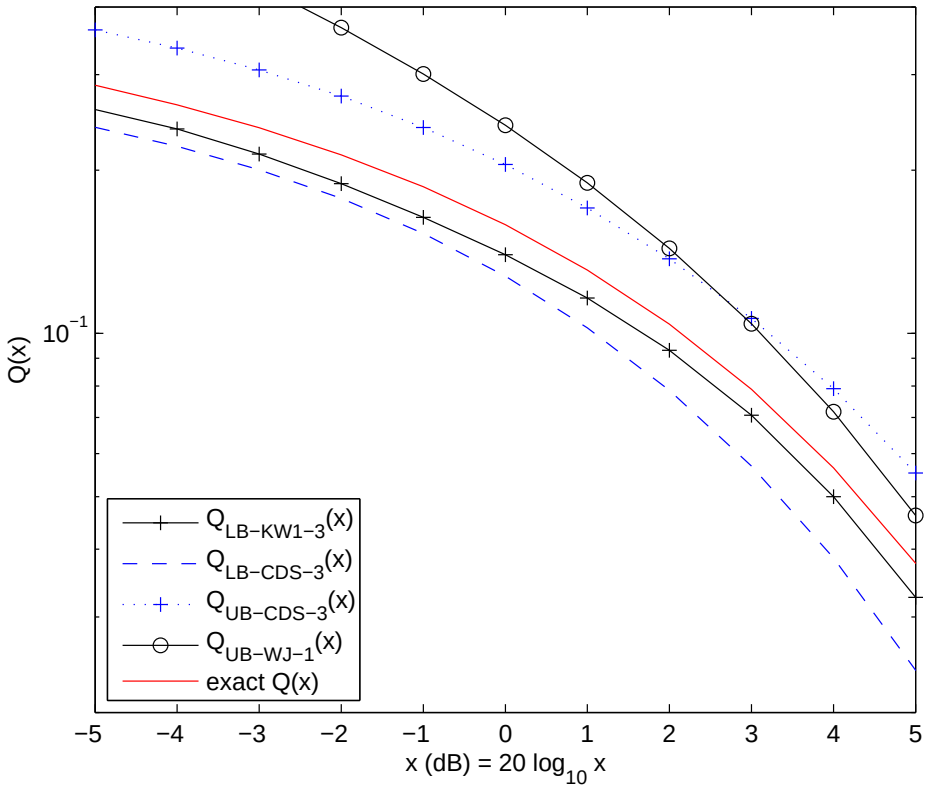

Figure 3.3: Comparison of lower bound $Q_{LB-KW1-3}(x)$ with existing bounds for small argument values.

Due to convexity of the exponential function in the entire real domain, we can apply the Jensen's inequality for each summation term in (3.38).

Letting

$$\begin{aligned} \phi(u) &= \exp(u), \\ f(t) &= -\frac{t^2}{2}, \\ p(t) &= \frac{1}{t^2}, \\ a &= \beta_{k-1}x, \\ b &= \beta_k x, \end{aligned} \tag{3.39}$$

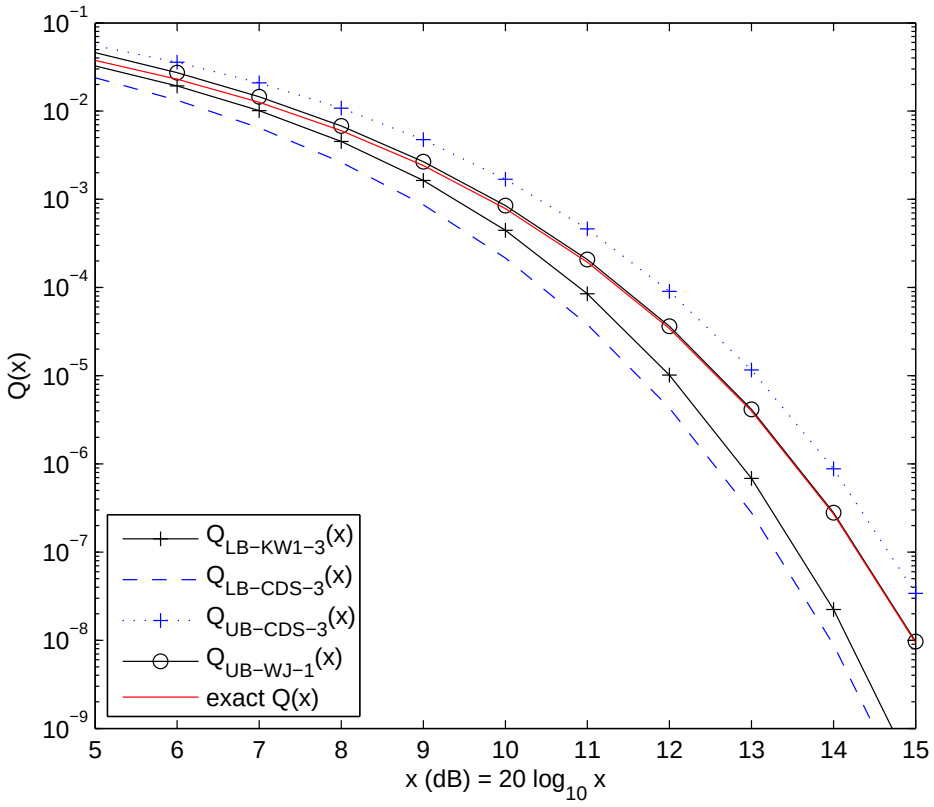

Figure 3.4: Comparison of lower bound $Q_{LB-KW1-3}(x)$ with existing bounds for large argument values.

we obtain a lower bound on (3.38) using the Jensen's inequality as

$$G_{LB}(x) = \sum_{k=1}^{n} \frac{\frac{1}{\beta_{k-1}} - \frac{1}{\beta_k}}{\sqrt{2\pi}x} \exp\left(-\frac{\beta_k \beta_{k-1}}{2} x^2\right). \tag{3.40}$$

Substituting (3.40) into (3.5), we obtain an upper bound on the Gaussian Q-function as

$$Q_{UB-KW}(x) = \sum_{k=0}^{n} \frac{a_k}{x} \exp\left(-b_k x^2\right), \tag{3.41}$$

where

$$a_k = \begin{cases} \frac{1}{\sqrt{2\pi}}, & k = 0 \\ -\frac{\beta_k - \beta_{k-1}}{\sqrt{2\pi}}, & k \geq 1 \end{cases}$$
$$b_k = \begin{cases} \frac{1}{2}, & k = 0 \\ \frac{\beta_k \beta_{k-1}}{2}, & k \geq 1 \end{cases} \tag{3.42}$$

are constant coefficients that are independent of x. This form can be averaged over Rayleigh or Nakagami-m fading.

When $n \to \infty$, we have

$$\begin{aligned} \lim_{n\to\infty} Q_{UB-KW}(x) &= \frac{1}{\sqrt{2\pi}x} \exp\left(-\frac{x^2}{2}\right) - \sum_{k=1}^{\infty} \frac{d\left(\frac{-1}{t}\right)}{\sqrt{2\pi}} \exp\left(-\frac{1}{2}\frac{dt}{d\left(\frac{-1}{t}\right)}\right) \\ &= \frac{1}{\sqrt{2\pi}x} \exp\left(-\frac{x^2}{2}\right) - \frac{1}{\sqrt{2\pi}} \sum_{k=1}^{\infty} \int_{\beta_{k-1}x}^{\beta_k x} \frac{dt}{t^2} \exp\left(-\frac{dt}{2dt/t^2}\right), \end{aligned} \tag{3.43}$$

which is equal to (3.5). As expected, simply by increasing n, the upper bound $Q_{UB-KW}(x)$ approaches the exact value for all argument values.

As the values of $\{\beta_k\}$ can be chosen arbitrarily, they can be optimized to minimize error in the region of interest. Alternatively, we strategically select $\{\beta_k\}$ values to obtain bounds in neat compact expressions. With $n = 1$, $Q_{UB-KW-1}(x)$ reduces to the upper bound $Q_{UB-WJ-1}(x)$ in (3.6). With $n = 2$ and $\beta_1 = 2$, we obtain

$$Q_{UB-KW-2}(x) = \frac{1}{\sqrt{2\pi}x} \exp\left(-\frac{x^2}{2}\right) - \frac{1}{2\sqrt{2\pi}x} \exp\left(-x^2\right). \tag{3.44}$$

With $n = 2$ and $\beta_1 = 2$, $\beta_2 = 3$, we obtain

$$Q_{UB-KW-3}(x) = \frac{1}{\sqrt{2\pi}x} \exp\left(-\frac{x^2}{2}\right) - \frac{1}{2\sqrt{2\pi}x} \exp\left(-x^2\right) - \frac{1}{6\sqrt{2\pi}x} \exp\left(-3x^2\right). \tag{3.45}$$

We can find bounds in neat compact forms with arbitrary number of exponential terms, as long as the values of β_k chosen are in neat compact form, e.g. integers and fractions.

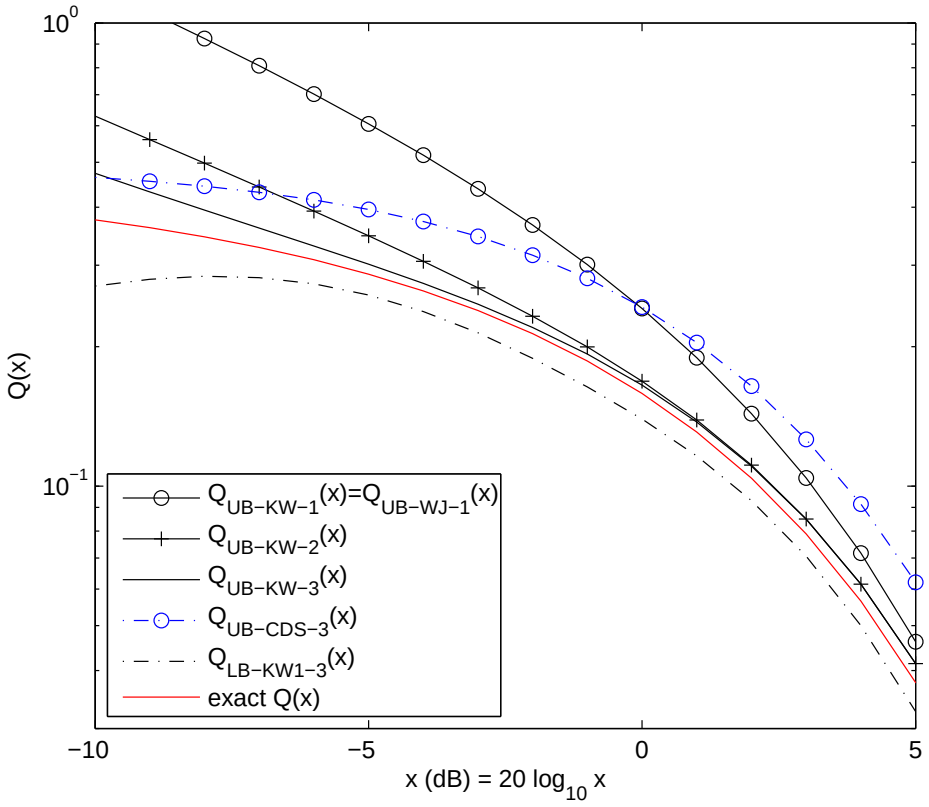

Figure 3.5: Upper bounds $Q_{UB-KW}(x)$ and comparison with existing bounds for small argument values.

The upper bounds $Q_{UB-KW}(x)$ with different numbers of exponential terms with small and large argument values are shown Fig. 3.5 and Fig. 3.6, respectively. For large argument values, our bounds are very tight even for one exponential term. They are much tighter than the Chiani three-term upper bound $Q_{UB-CDS-3}(x)$. For small argument values, it is obvious that the bounds become tighter with the number of exponential terms. Our three-term bound $Q_{UB-KW-3}(x)$ is tighter than the Chiani three-term bound $Q_{UB-CDS-3}(x)$ above 10dB. The combined use of $Q_{LB-KW1}(x)$ and the Chiani upper bound $Q_{UB-CDS-3}(x)$ shows the tightness of the bounds, if the exact value is not available.

One shortcoming of $Q_{UB-KW}(x)$ is that it approaches infinity when x approaches zero, while $Q(0) = 1/2$. Hence, $Q_{UB-KW}(x)$ is loose for very small

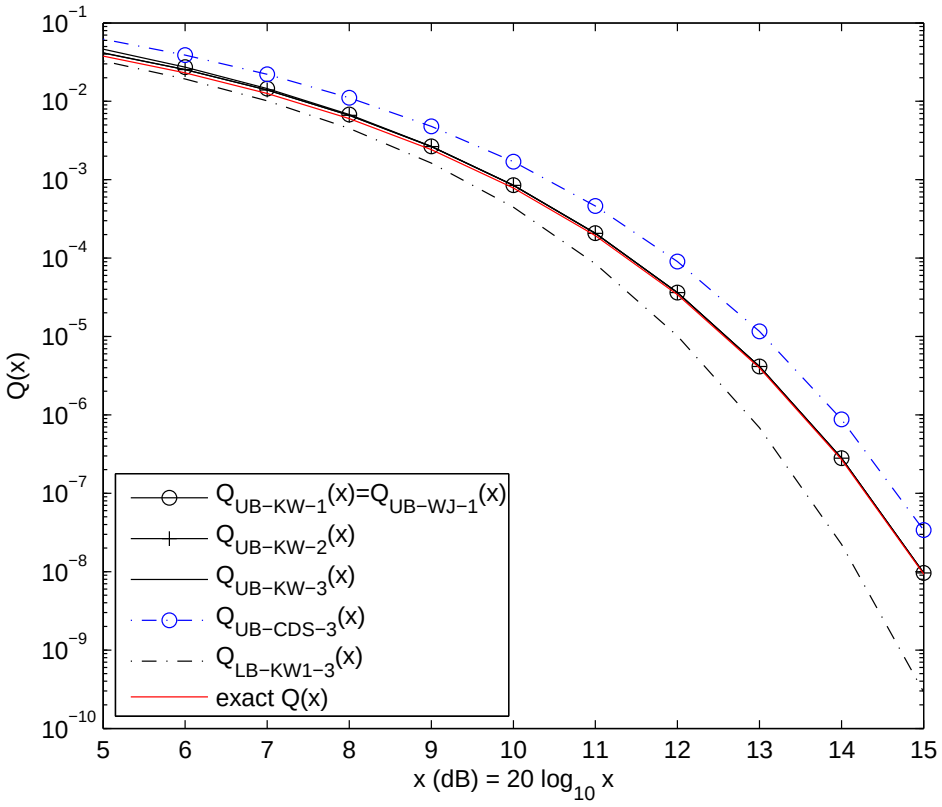

Figure 3.6: Upper bounds $Q_{UB-KW}(x)$ and comparison with existing bounds for large argument values.

argument values. Therefore, we must take care of the argument value when applying the upper bound $Q_{UB-KW}(x)$. It is not advised to average $Q_{UB-KW}(x)$ over a fading distribution where the PDF is concentrated at small values, e.g. at very low average SNR.

3.4 Lower Bounds Based on Craig's Form

We now look at the Craig's form of the Gaussian Q-function in (3.2). We first split the integration range of $[0, \pi/2]$ into $n+1$ subranges, by arbitrarily choosing $n+2$

values of θ_k such that $0 = \theta_0 < \theta_1 < ... < \theta_{n+1} = \pi/2$. Thus, (3.2) becomes

$$Q(x) = \sum_{k=1}^{n+1} \frac{1}{\pi} \int_{\theta_{k-1}}^{\theta_k} \exp\left(-\frac{x^2}{2\sin^2\theta}\right) d\theta. \tag{3.46}$$

Due to convexity of the exponential function in the entire real domain, we can apply the Jensen's inequality for each summation term in (3.46).

Applying the Jensen's inequality in (3.2) with

$$\begin{aligned} \phi(u) &= \exp(u), \\ f(\theta) &= -\frac{x^2}{2\sin^2\theta}, \\ p(\theta) &= 1, \\ a &= \theta_{k-1}, \\ b &= \theta_k, \end{aligned} \tag{3.47}$$

we obtain a lower bound on (3.46) as

$$Q_{LB-KW2}(x) = \sum_{k=1}^{n+1} a_k \exp\left(-b_k x^2\right), \tag{3.48}$$

where

$$\begin{aligned} a_k &= \frac{\theta_k - \theta_{k-1}}{\pi} \geq 0 \\ b_k &= \frac{1}{2}\frac{\cot(\theta_{k-1}) - \cot(\theta_k)}{\theta_k - \theta_{k-1}} \geq \frac{1}{2} \end{aligned} \tag{3.49}$$

are constant coefficients that are independent of x. The first summation term in (3.48) is zero for any n, given that $\cot(0) = \infty$. Therefore, $Q(x)$ is lower bounded by a sum of n exponentials. Our new lower bound has exactly the same simple form as that of the Chiani bounds in (3.19). This makes manipulation of the Gaussian Q-function simple, which will be shown in Section 3.5.

When $n \to \infty$, we have

$$\begin{aligned} \lim_{n\to\infty} Q_{LB-KW2}(x) &= \sum_{k=1}^{\infty} \frac{d\theta}{\pi} \exp\left(\frac{d\cot(\theta)}{d\theta}\frac{x^2}{2}\right) \\ &= \int_{\theta=0}^{\pi/2} \frac{1}{\pi} \exp\left(-\frac{1}{\sin^2\theta}\frac{x^2}{2}\right) d\theta, \end{aligned} \tag{3.50}$$

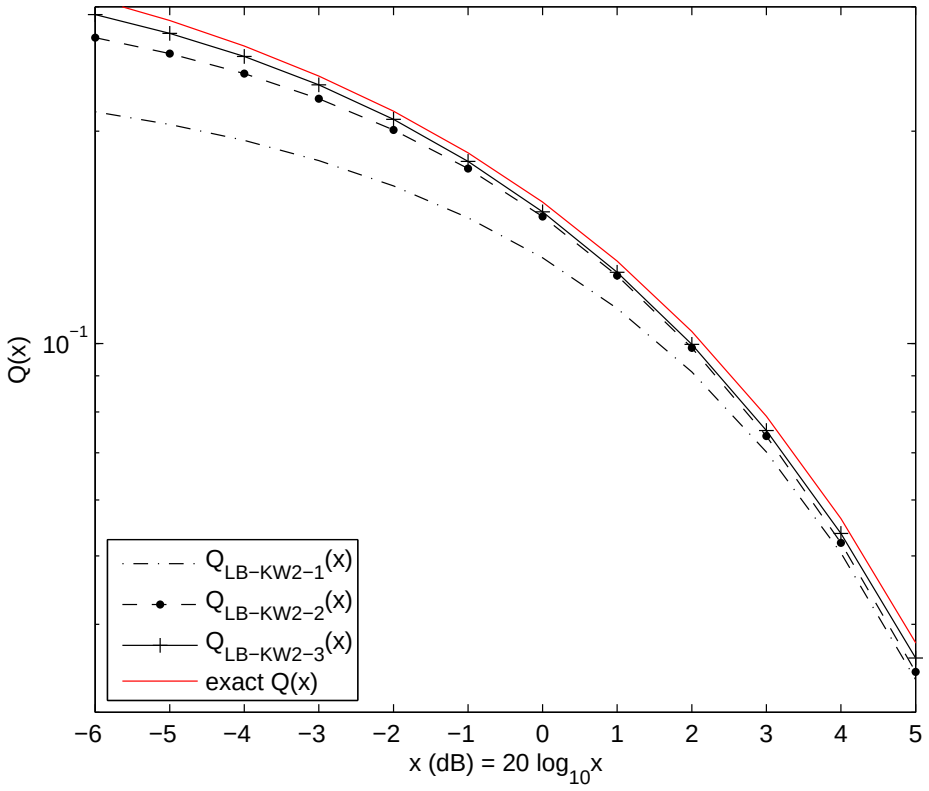

Figure 3.7: Lower bounds $Q_{LB-KW2}(x)$ for small argument values.

which is the same as (3.2). As expected, simply by increasing n, the lower bound approaches the exact value for all argument values, as shown in Fig. 3.7 and Fig. 3.8.

As the values of $\{\theta_k\}$ can be chosen arbitrarily, they can be optimized to minimize error in the region of interest. Alternatively, the values of $\{\theta_k\}$ can be chosen as equi-spaced for simplicity. However, the coefficients $\{a_k\}$ and $\{b_k\}$ are, in general, irrational numbers that are not in a compact form. Hence, the bounds using the above-mentioned two choices of $\{\theta_k\}$ are generally not in desirable form for further analysis. Therefore, we strategically select $\{\theta_k\}$ values to obtain bounds in neat compact expressions. With $n = 1$ and $\theta_1 = \pi/4$, we obtain

$$Q_{LB-KW2-1}(x) = \frac{1}{4}\exp\left(-\frac{2}{\pi}x^2\right). \tag{3.51}$$

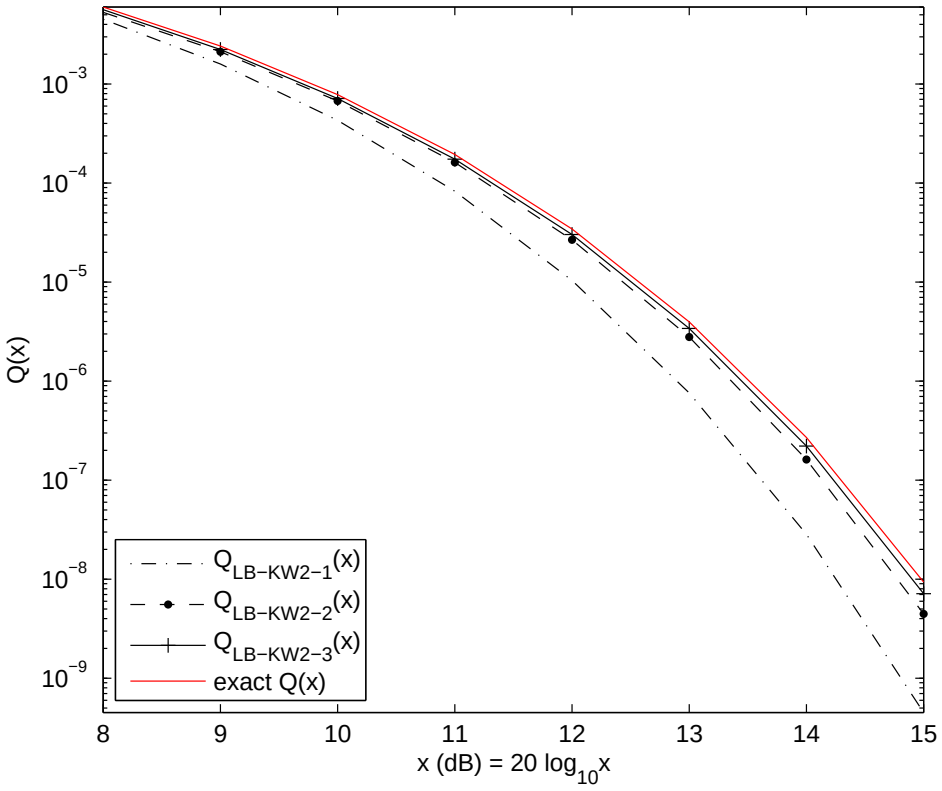

Figure 3.8: Lower bounds $Q_{LB-KW2}(x)$ for large argument values.

This bound is much tighter than the single-term Chiani lower bound $Q_{LB-CDS-1}(x)$ in (3.20) for all argument values. It is also tighter than our single-term bound $Q_{LB-KW1}(x)$ in (3.34). With $n = 2$ and $\theta_1 = \pi/6, \theta_2 = \pi/3$, we obtain

$$Q_{LB-KW2-2}(x) = \frac{1}{6}\exp\left(-\frac{\sqrt{3}}{\pi}x^2\right) + \frac{1}{6}\exp\left(-\frac{2\sqrt{3}}{\pi}x^2\right). \tag{3.52}$$

This two-term bound is much tighter than the two-term Chiani lower bound $Q_{LB-CDS-2}(x)$ in (3.21) for all argument values. It is also tighter than the two-term bound $Q_{LB-KW1-2}(x)$ in (3.35). With $n = 3$ and $\theta_1 = \pi/6, \theta_2 = \pi/4, \theta_3 = \pi/3$, we

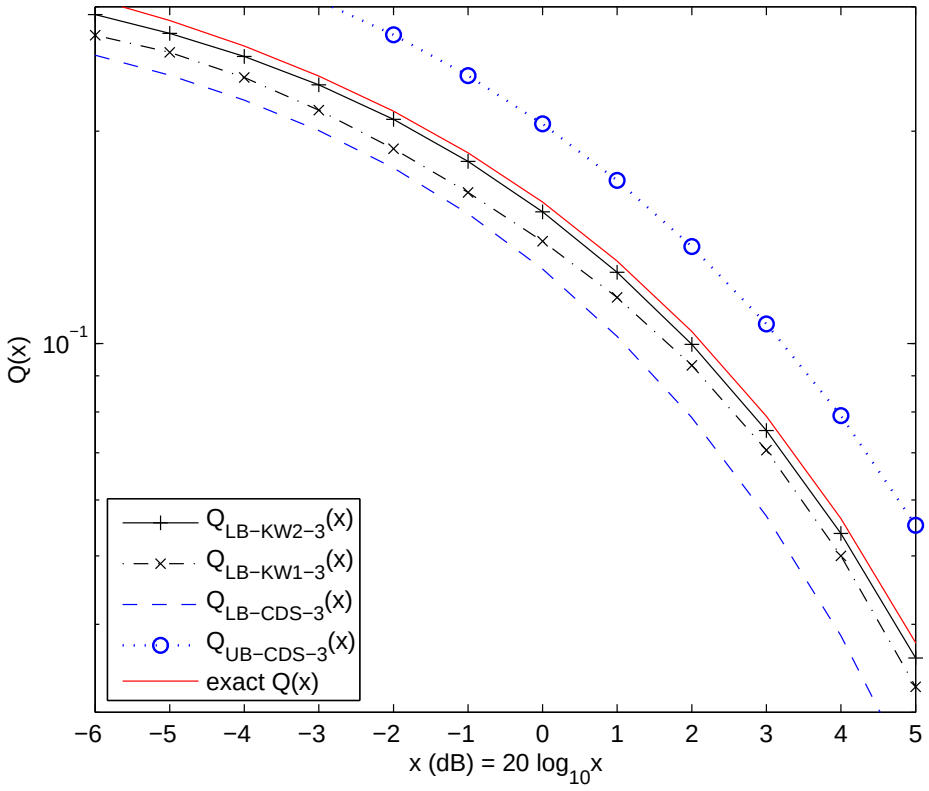

Figure 3.9: Comparison of lower bound $Q_{LB-KW2-3}(x)$ with existing bounds for small argument.

obtain

$$\begin{aligned} & Q_{LB-KW2-3}(x) \\ =& \frac{1}{6}\exp\left(-\frac{\sqrt{3}}{\pi}x^2\right) + \frac{1}{12}\exp\left(-\frac{2(3-\sqrt{3})}{\pi}x^2\right) + \frac{1}{12}\exp\left(-\frac{6(\sqrt{3}-1)}{\pi}x^2\right). \end{aligned} \tag{3.53}$$

This is the only three-term bound that has a neat compact form. It is much tighter than the three-term Chiani bound $Q_{LB-CDS-3}(x)$ in (3.22) and the three-term bound $Q_{LB-KW1-3}(x)$ in (3.36) for all argument values. No bound with a neat compact form is found with $n > 3$. Note that the values of $\{\theta_k\}$ for the bounds in (3.51) and (3.52) happen to be equi-spaced, while those for (3.53) do not.

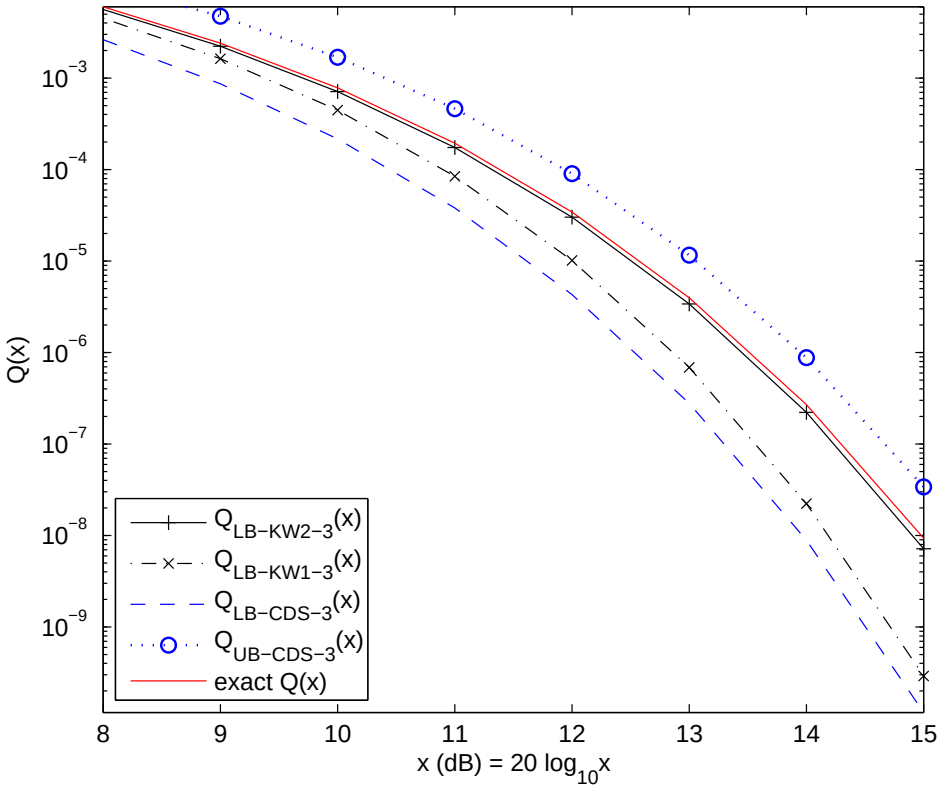

Figure 3.10: Comparison of lower bound $Q_{LB-KW2-3}(x)$ with existing bounds for large argument.

Fig. 3.9 and Fig. 3.10 show that our three-term lower bound $Q_{LB-KW2}(x)$ is tightest among three-term lower bounds. The combined use of the Chiani 3-term upper bound $Q_{UB-CDS-3}(x)$ and $Q_{LB-KW1}(x)$ shows the tightness of the bounds, when the exact value is not available.

In summary, $Q_{LB-KW2}(x)$ has a much simpler form than $Q_{LB-KW1}(x)$ and the lower bounds in the literature as far as we are aware of. It has the same simple form of Chiani lower bound $Q_{UB-CDS}(x)$. Moreover, it is tighter than the above-mentioned lower bounds with the same number of terms.

3.5 Averaging Gaussian Q-Function over Fading

The analysis of error probabilities over fading often involves averaging the Gaussian Q-function over fading distribution, i.e.

$$I(\bar{\gamma}) = \int_0^\infty Q(\sqrt{c_{sig}\gamma}) p_\gamma(\gamma) d\gamma, \tag{3.54}$$

where c_{sig} is a constant depending on the modulation scheme. For example, $c_{sig} = 2$ for BPSK and $c_{sig} = 1$ for binary orthogonal signals. Here, γ is the instantaneous SNR. The commonly used statistical characteristic of the multipath fading channel is the PDF of γ, i.e. $p_\gamma(\gamma)$. There are several models describing the statistical characteristics of the multipath fading channel. The Rayleigh distribution is used to model multipath fading with a large number of scatterers and no direct line-of-sight (LOS) path. The PDF of the instantaneous SNR is given by

$$p_\gamma(\gamma) = \frac{1}{\bar{\gamma}} \exp\left(-\frac{\gamma}{\bar{\gamma}}\right). \tag{3.55}$$

The MGF corresponding to this fading model is given by

$$M_\gamma(s) = (1 - s\bar{\gamma})^{-1}. \tag{3.56}$$

The Rice distribution is used to model a fading channel with one strong direct LOS path and many random weaker scattered paths. The instantaneous SNR is non-central Chi-square distributed with PDF

$$p_\gamma(\gamma) = \frac{(1+K)e^{-K}}{\bar{\gamma}} \exp\left(-\frac{(1+K)\gamma}{\bar{\gamma}}\right) I_0\left(2\sqrt{\frac{K(1+K)\gamma}{\bar{\gamma}}}\right). \tag{3.57}$$

The K factor is the ratio between the power in the direct LOS path and the power in the scattered paths. Its value is in the range $[0, \infty)$. The MGF of Rician fading is given by

$$M_\gamma(s) = \frac{1+K}{1+K-s\bar{\gamma}} \exp\left(\frac{Ks\bar{\gamma}}{1+K-s\bar{\gamma}}\right). \tag{3.58}$$

Rayleigh fading is a special case of Rician fading by letting $K = 0$. A more general fading model is the Nakagami-m fading. The instantaneous SNR is gamma

distribution with PDF

$$p_\gamma(\gamma) = \frac{m^m \gamma^{m-1}}{\bar{\gamma}^m \Gamma(m)} \exp\left(-\frac{m\gamma}{\bar{\gamma}}\right), \tag{3.59}$$

where m is the Nakagami-m fading parameter, with value in the range $[1/2, \infty)$. Its MGF is given by

$$M_\gamma(s) = \left(1 - \frac{s\bar{\gamma}}{m}\right)^{-m}. \tag{3.60}$$

Depending on the channel fading model, (3.54) does not always result in a closed-form expression. For example, for Nakagami-m fading with non-integer values of m, (3.54) involves the Gauss hypergeometric function [7, 27], which is defined as an infinite series. This complicates the computation of (3.54). Having obtained new lower bounds $Q_{LB-KW1}(x)$ and $Q_{LB-KW2}(x)$ in simple form, we can lower bound the average of Gaussian Q-function over fading using new lower bounds.

3.5.1 Averaging Lower Bound $Q_{LB-KW1}(x)$ over Nakagami-m Fading

The lower bound $Q_{LB-KW1}(x)$ obtained in Section 3.3 has a form simpler than that of the Abreu bound in (3.10). Due to the simple form, the average of $Q_{LB-KW1}(x)$ over Nakagami-m fading results in a closed-form expression.

By substituting $Q_{LB-KW1}(x)$ in (3.30) and $p_\gamma(\gamma)$ of Nakagami-m fading in (3.59) into (3.54) and changing order of summation and integration, we have

$$I(\bar{\gamma}) \geq \sum_{k=0}^{n} a_k \sqrt{c_{sig}} \frac{m^m}{\bar{\gamma}^m \Gamma(m)} \int_0^\infty \gamma^{m-\frac{1}{2}} \exp\left[-\left(b_k c_{sig} + \frac{m}{\bar{\gamma}}\right)\gamma\right] d\gamma. \tag{3.61}$$

Using the integration rule in [70, eq.(3.326-2)],

$$\int_0^\infty x^m \exp(-\beta x^n) dx = \frac{\Gamma(\frac{m+1}{n})}{n\beta^{\frac{m+1}{n}}}, \tag{3.62}$$

(3.61) reduces to

$$I_{LB-KW1}(\bar{\gamma}) = \sum_{k=1}^{n} \frac{a_k \sqrt{c_{sig}} m^m \Gamma(m+\frac{1}{2})}{\bar{\gamma}^m \Gamma(m)} \left(b_k c_{sig} + \frac{m}{\bar{\gamma}}\right)^{-(m+\frac{1}{2})}, \tag{3.63}$$

which is a closed-form expression. Computation of the n-term summation in (3.63) is simpler and faster than computation of expressions involving Gauss hypergeometric functions.

3.5.2 Averaging Upper Bound $Q_{UB-KW}(x)$ over Nakagami-m Fading

The simple form of the upper bound $Q_{UB-KW}(x)$ in (3.41) allows it to be averaged over Rayleigh and Nakagami-m fading in a closed-form expression. As the exact closed-form expression of the Gaussian Q-function averaged over Rayleigh fading has been obtained, we only analyze here the average of the upper bound $Q_{UB-KW}(x)$ over Nakagami-m fading.

By substituting $Q_{UB-KW}(x)$ in (3.41) and $p_\gamma(\gamma)$ of Nakagami-m fading in (3.59) into (3.54) and changing order of summation and integration, we have

$$I(\bar{\gamma}) \leq \sum_{k=1}^{n} \frac{a_k m^m}{\sqrt{c_{sig}}\bar{\gamma}^m \Gamma(m)} \int_0^\infty \gamma^{m-\frac{3}{2}} \exp\left[-\left(b_k c_{sig} + \frac{m}{\bar{\gamma}}\right)\gamma\right] d\gamma. \tag{3.64}$$

Using the integration rule in [70, eq.(3.326-2)],

$$\int_0^\infty x^m \exp(-\beta x^n) dx = \frac{\Gamma(\frac{m+1}{n})}{n\beta^{\frac{m+1}{n}}}, \tag{3.65}$$

(3.64) reduces to

$$I_{UB-KW}(\bar{\gamma}) = \sum_{k=1}^{n} \frac{a_k \sqrt{c_{sig}} m^m \Gamma(m-\frac{1}{2})}{\bar{\gamma}^m \Gamma(m)} \left(b_k c_{sig} + \frac{m}{\bar{\gamma}}\right)^{-(m-\frac{1}{2})}, \tag{3.66}$$

which is a closed-form expression. Computation of the n-term summation in (3.66) is simpler and faster than computation of expressions involving Gauss hypergeometric functions.

3.5.3 Averaging Lower Bound $Q_{LB-KW2}(x)$ over Fading

As the coefficients of our exponential lower bound $Q_{LB-KW2}(x)$, i.e. $\{a_k\}$ and $\{b_k\}$ in (3.49), are constants, manipulation of the Gaussian Q-function becomes simple

using the MGF method. By substituting the lower bound $Q_{LB-KW2}(x)$ in (3.48) into (3.54), we have

$$I(\bar{\gamma}) \geq \sum_{k=2}^{n+1} a_k \int_0^{\infty} \exp\left(-b_k c_{sig}\gamma\right) p_{\gamma}(\gamma) d\gamma. \tag{3.67}$$

Using the MGF defined in (3.4), (3.67) reduces to a closed-form lower bound, as

$$I_{LB-KW2}(\bar{\gamma}) \geq \sum_{k=2}^{n+1} a_k M_{\gamma}(-b_k c_{sig}), \tag{3.68}$$

where the coefficients $\{a_k\}$ and $\{b_k\}$ are given in (3.49). Being able to bound the Gaussian Q-function with a sum of exponentials with constant coefficients allows us to apply the MGF method conveniently. The advantage of the MGF method is that the MGF of various fading models have already been obtained in closed-form expressions and summarized in [48, 2.2]. Therefore, computation of (3.68) is simple and straightforward.

For Nakagami-m fading, for example, computation of (3.68) is simpler than the computation of the Gaussian hypergeometric function. The bound in (3.68) for fading also applies to the Chiani upper and lower bounds but with the coefficients in (3.14). Fig. 3.11 and Fig. 3.12 show that (3.68) for Nakagami-m fading is tight even with only two terms. As we have shown that the bound $Q_{LB-KW2}(x)$ is tighter than the bound $Q_{LB-KW1}(x)$ and the Chiani lower bound $Q_{LB-CDS}(x)$ with the same number of terms, as expected, the average of $Q_{LB-KW2}(x)$ over fading, i.e. $I_{LB-KW2}(\bar{\gamma})$, is tighter than the averages of $Q_{LB-KW1}(x)$ and the Chiani lower bound $Q_{LB-CDS}(x)$, i.e. $I_{LB-KW1}(\bar{\gamma})$ and $I_{LB-CDS}(\bar{\gamma})$. Similarly, $I_{UB-KW}(\bar{\gamma})$ is expected to be tighter than $I_{UB-CDS}(\bar{\gamma})$ with the same number of exponential terms. If the exact value by numerical integration is not available, the combined use of upper bound $I_{UB-KW}(\bar{\gamma})$ and lower bound $I_{LB-KW2}(\bar{\gamma})$ shows tightness of the bounds, without comparing the individual bounds with the exact value.

Although lower bound $Q_{LB-KW2-2}(x)$ diverge from $Q(x)$ for very large argument values in the log scale in Fig. 3.8, the absolute difference between the bound and the exact value is very small compared to the value for small argument

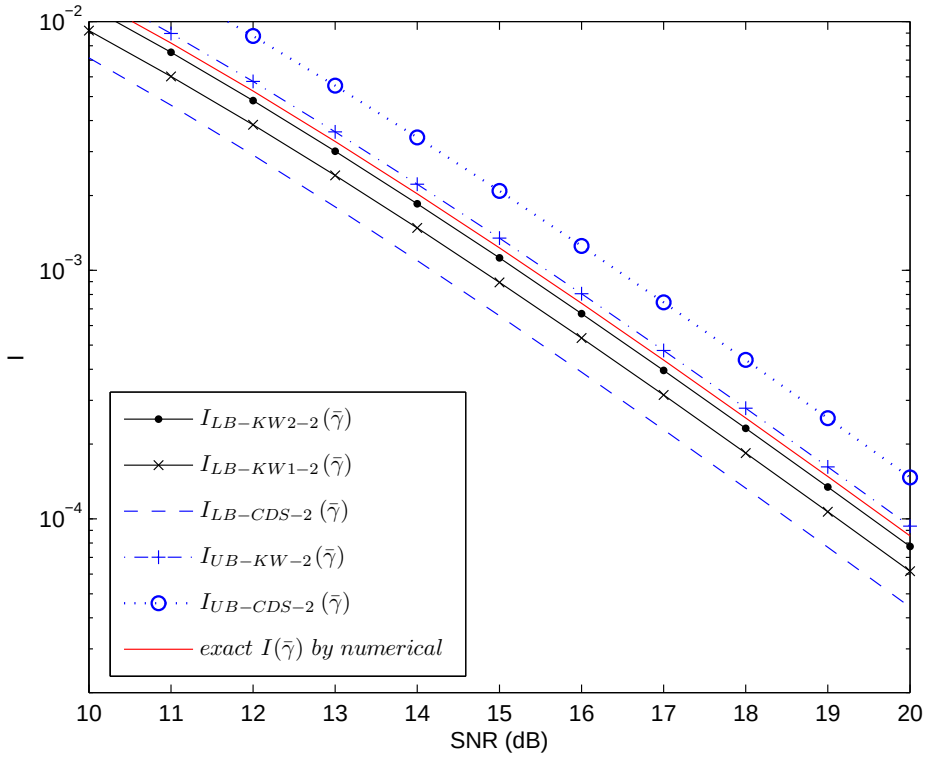

Figure 3.11: Bounds on the average of the Gaussian Q-function over Nakagami-m fading at low SNR.

values. Thus, the difference averaged over the entire argument range weighted by the fading distribution is dominated by the difference for small argument values. Therefore, the average of the bounds over fading is a constant offset from the exact average curve and do not diverge at high SNR.

3.6 Bounds on 2D Joint Gaussian Q-function

The two-dimensional joint Gaussian Q-function can also be lower bounded by a sum of exponentials using the Jensen's inequality.

The two-dimensional joint Gaussian Q-function is defined as [48, eq.(4.3)]

$$Q(x,y;\rho) = \frac{1}{2\pi\sqrt{1-\rho^2}} \int_x^\infty \int_y^\infty \exp\left[-\frac{x_1^2+y_1^2-2\rho x_1 y_1}{2(1-\rho^2)}\right] dx_1 dy_1. \tag{3.69}$$

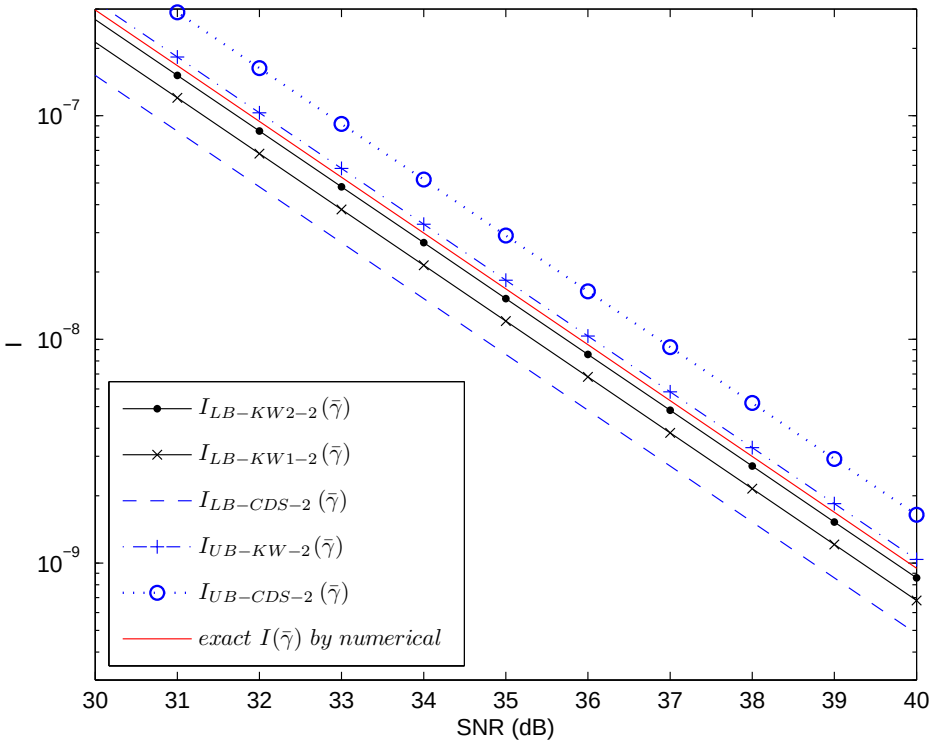

Figure 3.12: Bounds on the Gaussian Q-function over Nakagami-m fading at high SNR.

It can also be expressed as the sum of two single integrals as [71, eq.(10)]

$$Q(x,y;\rho) = \frac{1}{2\pi}\int_0^{\theta_x^*} \exp\left(-\frac{x^2}{2\sin^2\theta}\right) d\theta + \frac{1}{2\pi}\int_0^{\theta_y^*} \exp\left(-\frac{y^2}{2\sin^2\theta}\right) d\theta, \tag{3.70}$$

where

$$\begin{aligned} \theta_x^* &= \tan^{-1}\left(\frac{\frac{x}{y}\sqrt{1-\rho^2}}{1-\rho\frac{x}{y}}\right) \in [0,\pi), \\ \theta_y^* &= \tan^{-1}\left(\frac{\frac{y}{x}\sqrt{1-\rho^2}}{1-\rho\frac{y}{x}}\right) \in [0,\pi). \end{aligned} \tag{3.71}$$

Applying the Jensen's inequality as in Section 3.4, we obtain the exponential lower

bound on (3.70) as

$$\begin{aligned} Q(x,y;\rho) &\geq Q_{LB-KW}(x,y;\rho) \\ &= \sum_{k=2}^{n+1} a_{x_k} \exp\left(-b_{x_k} x^2\right) + \sum_{k=2}^{n+1} a_{y_k} \exp\left(-b_{y_k} x^2\right), \end{aligned} \tag{3.72}$$

where

$$\begin{aligned} a_{x_k} &= \frac{\theta_{x_k} - \theta_{x_{k-1}}}{2\pi}, \quad b_{x_k} = \frac{1}{2} \frac{\cot(\theta_{x_{k-1}}) - \cot(\theta_{x_k})}{\theta_{x_k} - \theta_{x_{k-1}}}, \\ a_{y_k} &= \frac{\theta_{y_k} - \theta_{y_{k-1}}}{2\pi}, \quad b_{y_k} = \frac{1}{2} \frac{\cot(\theta_{x_{y-1}}) - \cot(\theta_{y_k})}{\theta_{y_k} - \theta_{y_{k-1}}}, \end{aligned} \tag{3.73}$$

and $\theta_{x_k}, \theta_{y_k}$ are chosen such that $0 = \theta_{x_0} < \theta_{x_1} < ... < \theta_{x_{n+1}} = \theta_x^*$, $0 = \theta_{y_0} < \theta_{y_1} < ... < \theta_{y_{n+1}} = \theta_y^*$.

The product of two Gaussian Q-functions, i.e. $Q(x)Q(y)$, is a special case of (3.70) by letting $\rho = 0$. Thus, it is also lower bounded by (3.72) with (3.73) and

$$\begin{aligned} \theta_x^* &= \frac{\pi}{2} - \tan^{-1}\left(\frac{y}{x}\right) \in [0, \pi), \\ \theta_y^* &= \tan^{-1}\left(\frac{y}{x}\right) \in [0, \pi). \end{aligned} \tag{3.74}$$

In applications where the ratio y/x is constant, the integration limits θ_x^* and θ_y^* are constants. Thus, the coefficients $\{a_{x_k}\}$, $\{b_{x_k}\}$, $\{a_{y_k}\}$ and $\{b_{y_k}\}$ of our bound in (3.72) are constants which do not depend on the values of x or y. Therefore, our bound in (3.72) can be easily manipulated.

To apply the Abreu method in [21], depending on the values of x and y, the convexity of the integrands $\exp[-x^2/(2\sin^2\theta)]$ and $\exp[-y^2/(2\sin^2\theta)]$ changes over their integration ranges $[0, \theta_x^*)$ and $[0, \theta_y^*)$, respectively. In [21, eq.(50)], for each integral, there are three cases to consider. Hence, the Abreu method is more difficult to apply than our method in Section 3.4. In addition, θ_x^* and θ_y^* are functions of x and y. Thus, the coefficients of the Abreu bounds are functions of x or y. Hence, the Abreu bound, denoted as $Q_{LB-A}(x,y;\rho)$, in general, cannot be averaged over fading using the MGF method, even if the ratio y/x is constant. To apply the Chiani method in [24], if $\theta_x^* > \pi/2$, the integration range of the first integral in (3.70) must be partitioned into $[0, \pi/2)$ and $[\pi/2, \theta_x^*)$, where the integrand increases or decreases

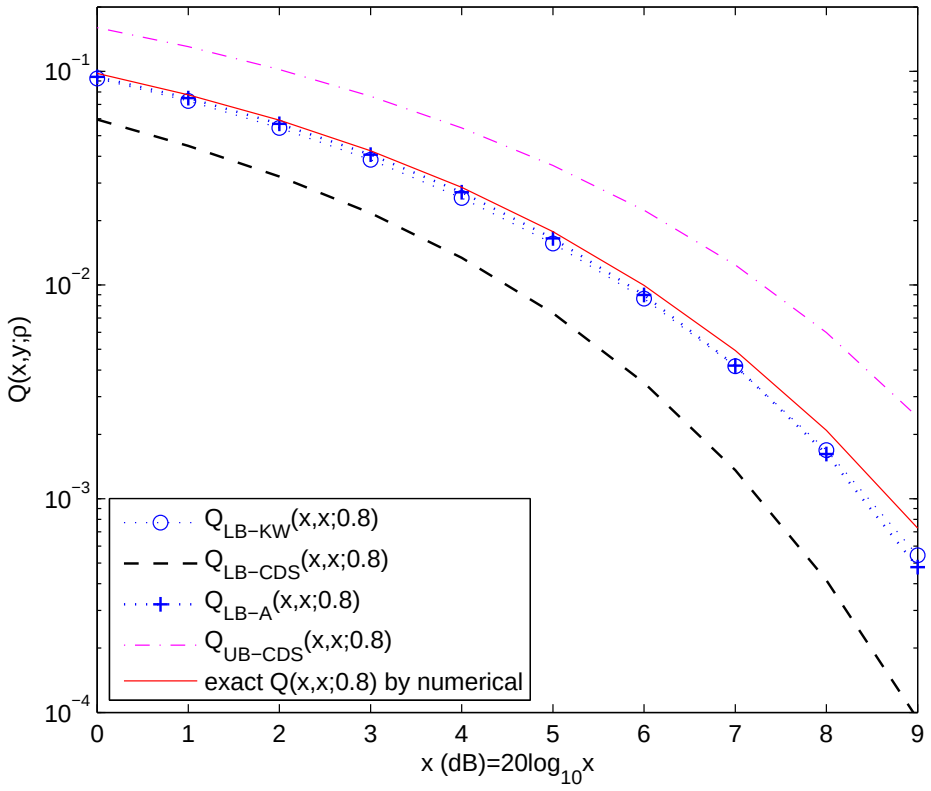

Figure 3.13: Lower bounds on 2D joint Gaussian Q-function $Q(x, x; 0.8)$ with 4 exponentials.

monotonically. The second integral is treated likewise. For constant y/x values, the Chiani bound $Q_{LB-CDS}(x, y; \rho)$ has the same form as our lower bound and can be averaged over fading. Fig. 3.13 shows that our bound $Q_{LB-KW}(x, y; \rho)$ in (3.72) is much tighter than the equally-simple Chiani lower bound $Q_{LB-CDS}(x, y; \rho)$, and has similar tightness as the Abreu bound $Q_{LB-A}(x, y; \rho)$. In comparison, both the Chiani upper bound $Q_{UB-CDS}(x, y; \rho)$ and the Chiani lower bound $Q_{LB-CDS}(x, y; \rho)$ are quite loose. For fair comparison, the bounds in Fig. 3.13 have equal numbers of exponential terms.

3.7 Conclusions

Using the Jensen's inequality on the definition and the Craig's form of the Gaussian Q-function, we obtain two families of exponential lower bounds on the Gaussian Q-function. The tightness of the lower bounds can be improved by increasing the number of exponential terms. The lower bound $Q_{LB-KW2}(x)$ has constant coefficients, which allows for easy manipulation on the Q function. A closed-form lower bound on the Gaussian Q-function averaged over fading is obtained by averaging $Q_{LB-KW2}(x)$ over fading as a function of the MGF of the fading model. Using the same method to derive $Q_{LB-KW2}(x)$, a family of lower bounds on the two-dimensional Gaussian Q-function is obtained.

Chapter 4

Error Performance of Coherent Receivers

The error performances of many two-dimensional modulation schemes with coherent detection are not in closed forms. Similar to the Craig's form of the Gaussian Q-function, the SEP performances of many modulation schemes over AWGN involve finite range integrals of exponential functions, e.g. MPSK [15], MDPSK [72] and signals with polygonal decision region [15]. In order to compute SEP values, numerical integration is usually resorted to. Alternatively, simple closed-form approximations and bounds are derived to compute it more efficiently. Though approximations and upper bounds are used more often than lower bounds in performance analysis, lower bounds are useful, as the combined use of upper and lower bounds shows the tightness of the bounds, without comparing the individual bounds with numerical integration of the exact value. The accuracy of approximations, however, can only be obtained by comparing with numerical integration of the exact value.

In [21], Abreu bounds the Craig's form of the Gaussian Q-function by making use of the convex/concave property of the integrand. This method can be applied to finite range integrals of an arbitrary exponential function. When the integrand is not purely convex or concave over the entire integration range, the integration range is

divided into several subranges where the integrand is purely convex or concave. The integrand in the convex subrange(s) is lower bounded using the Jensen's inequality and upper bounded using the Cotes trapezoidal rule. Similarly, the integrand in the concave subrange(s) is upper bounded using the Jensen's inequality and lower bounded using the Cotes trapezoidal rule. The bounds obtained using the Abreu method usually have coefficients which are functions of the SNR. Thus, in general, the Abreu bounds cannot be averaged over fading distribution easily.

Chiani [24] divides the integration range into a few subranges and bounds the integrand with its maximum and minimum values in each subrange. For applications where the integrand is not monotonic over the entire integration range, the integration range is first divided into subranges where the integrand increases or decreases monotonically. Each monotonic subrange can be further divided and the integrand is upper and lower bounded with its maximum and minimum values in each subrange. Similar to the Chiani bounds on the Gaussian Q-function, the upper and lower bounds obtained by the Chiani method has constant coefficients. Therefore, the Chiani bounds can be averaged over fading using the MGF method easily. However, the Chiani bounds are usually looser than the Abreu bounds with the same number of exponential terms.

We propose to apply the Jensen's inequality on the exponential function (instead of the integrand) in an SEP expression. A family of exponential lower bounds are obtained. The tightness of our bounds can be improved by increasing the number of exponential terms. The bounds have the same simple form of the Chiani bounds in and, therefore, can be easily averaged over the fading distribution using the MGF method. This method is applied to the SEP of MPSK, MDPSK and signals with polygonal decision regions. We show that our bounds are tighter than the Chiani bounds and the Abreu bounds with similar numbers of exponential terms. To apply the Chiani method and the Abreu method, a good analysis of the integrand is necessary to divide the integration range. Our method does not depend on the monotonicity or convexity property of the integrand. Hence, this method is

easier to apply than the Chiani method and the Abreu method.

This chapter is organized as follows. In Section 4.1, lower bounds on the SEP performances of MPSK, MDPSK and signals with polygonal decision region over AWGN are obtained using the Jensen's inequality. In Section 4.2, lower bounds on the average SEP performances over fading are obtained using the MGF method. Conclusions are made in Section 4.3.

4.1 Lower Bounds on SEP over AWGN

For an error probability that can be expressed in the following form

$$P = \sum_{k=1}^{n+1} \int_{\theta_{k-1}}^{\theta_k} \exp\left(g(\theta)\gamma\right) d\theta, \tag{4.1}$$

where $g(\theta)$ is integrable, the Jensen's inequality in (3.23) can be applied. Letting

$$\begin{aligned} \phi(u) &= \exp(u), \\ f(\theta) &= g(\theta)\gamma, \\ p(\theta) &= 1, \\ a &= \theta_{k-1}, \\ b &= \theta_k, \end{aligned} \tag{4.2}$$

we obtain the lower bound

$$P_L = \sum_k a_k \exp\left(-b_k\gamma\right), \tag{4.3}$$

where

$$\begin{aligned} a_k &= \theta_k - \theta_{k-1}, \\ b_k &= \frac{\int_{\theta_{k-1}}^{\theta_k} g(\theta) d\theta}{\theta_k - \theta_{k-1}}, \end{aligned} \tag{4.4}$$

are constant coefficients independent of γ. This lower bound can be averaged over the distribution of γ using the MGF as in (3.68). It will be shown in detail in Section 4.2.

When $n \to \infty$, we have

$$\lim_{n\to\infty} P_L = \sum_{k=1}^{\infty} d\theta \exp\left(-\frac{g(\theta)d\theta}{d\theta}\gamma\right) = \int_{\theta_0}^{\theta_{n+1}} \exp\left(-g(\theta)\gamma\right) d\theta, \tag{4.5}$$

which is equal to (4.1). As expected, simply by increasing n, the lower bound approaches the exact value for all argument values

4.1.1 SEP of MPSK over AWGN

The SEP of coherent MPSK is given by [15, eq.(5)]

$$P(e_s|\gamma) = \frac{1}{\pi}\int_0^{\pi-\pi/M} \exp\left(-\frac{\gamma \sin^2(\pi/M)}{\sin^2\theta}\right) d\theta. \tag{4.6}$$

We first split the integration range of $[0, \pi-\pi/M]$ into $n+1$ subranges, by arbitrarily choosing $n+2$ values of θ_k such that $0 = \theta_0 < \theta_1 < ... < \theta_{n+1} = \pi - \pi/M$. Thus, (4.6) becomes

$$P(e_s|\gamma) = \sum_{k=1}^{n+1} \frac{1}{\pi}\int_{\theta_{k-1}}^{\theta_k} \exp\left(-\frac{\gamma \sin^2(\pi/M)}{\sin^2\theta}\right) d\theta. \tag{4.7}$$

Applying the Jensen's inequality in (3.2) with

$$\begin{aligned} \phi(u) &= \exp(u), \\ f(\theta) &= -\frac{\gamma \sin^2(\pi/M)}{\sin^2\theta}, \\ p(\theta) &= 1, \\ a &= \theta_{k-1}, \\ b &= \theta_k, \end{aligned} \tag{4.8}$$

on each summation term in (4.7), we obtain an exponential lower bound as

$$P(e_s|\gamma) \geq \sum_{k=2}^{n+1} a_k \exp\left(-b_k\gamma\right), \tag{4.9}$$

where

$$\begin{aligned} a_k &= \frac{\theta_k - \theta_{k-1}}{\pi}, \\ b_k &= \sin^2\left(\frac{\pi}{M}\right) \frac{\cot(\theta_{k-1}) - \cot(\theta_k)}{\theta_k - \theta_{k-1}}, \end{aligned} \tag{4.10}$$

are constant coefficients that are independent of γ. Therefore, the lower bound can be averaged over fading using the MGF method easily. Note that the $k = 1$ term is 0. Hence, the lower bound is a sum of n exponentials.

When $n \to \infty$, we have

$$\begin{aligned} \lim_{n\to\infty} P(e_s|\gamma) &= \sum_{k=1}^{\infty} \frac{d\theta}{\pi} \exp\left(\sin^2\left(\frac{\pi}{M}\right) \frac{d\cot(\theta)}{d\theta}\gamma\right) \\ &= \int_{\theta=0}^{\pi-\pi/M} \frac{1}{\pi} \exp\left(-\frac{\sin^2(\pi/M)}{\sin^2\theta}\gamma\right) d\theta, \end{aligned} \tag{4.11}$$

which is equal to (4.6). As expected, simply by increasing n, the lower bound approaches the exact value for all argument values, as shown in Fig. 4.1.

The integrand in (4.6) is not monotonic over the entire integration range of $[0, \pi - \pi/M)$. Hence, the Chiani method requires partitioning the entire integration into monotonic subranges, i.e. $[0, \pi/2)$ and $[\pi/2, \pi - \pi/M)$. Bounds in the two subranges are derived separately. Choosing θ_k such that $0 = \theta_0 < \theta_1 < ... < \theta_{n_1} = \pi/2 < \theta_{n_1+1} < ... < \theta_{n+1} = \pi - \pi/M$, the Chiani bounds on the SEP of MPSK are given by

$$\begin{aligned} P(e_s|\gamma) &\le \sum_{k=1}^{n_1} a_k \exp\left(-b_k\gamma\right) + \sum_{k=n_1+1}^{n} a_k \exp\left(-b_{k-1}\gamma\right) \\ P(e_s|\gamma) &\ge \sum_{k=2}^{n_1} a_k \exp\left(-b_{k-1}\gamma\right) + \sum_{k=n_1+1}^{n} a_k \exp\left(-b_k\gamma\right) \end{aligned} \tag{4.12}$$

where

$$\begin{aligned} a_k &= \frac{\theta_k - \theta_{k-1}}{\pi}, \\ b_k &= \frac{\sin^2(\pi/M)}{\sin^2\theta}. \end{aligned} \tag{4.13}$$

The Chiani bounds have the same simple form as our lower bound.

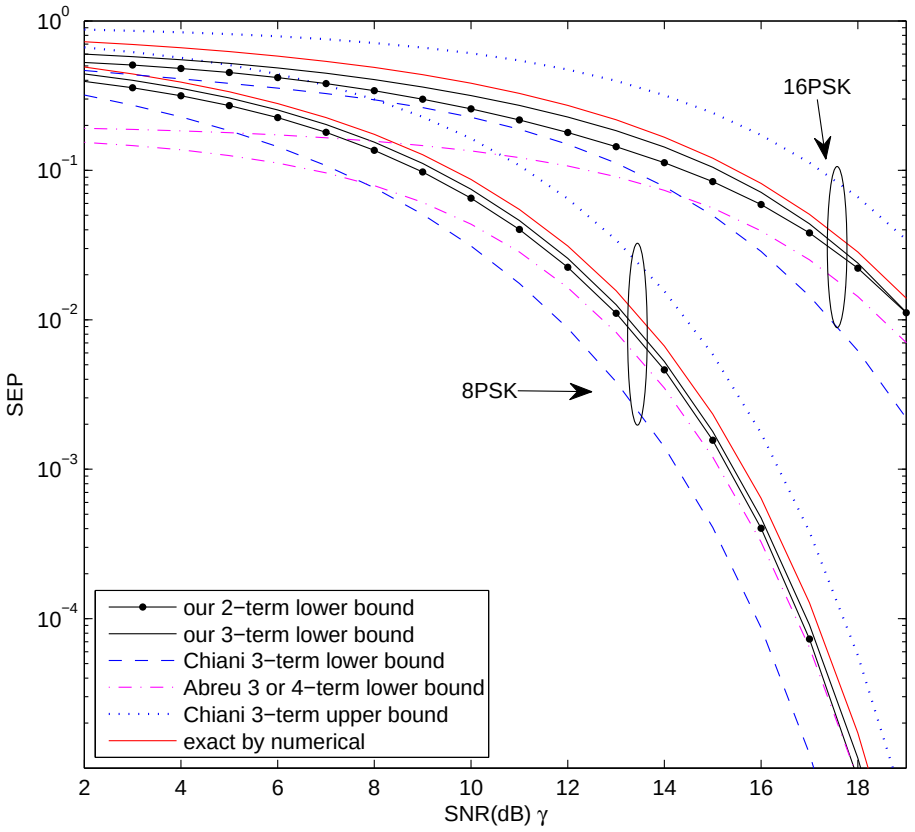

Figure 4.1: Lower bounds on the SEP of MPSK over AWGN.

The integrand is neither convex nor concave over the entire integration range. Therefore, the Abreu method in [21] requires partitioning the integration range into $[0, \bar{\theta}_\gamma)$, $[\bar{\theta}_\gamma, \pi - \bar{\theta}_\gamma)$ and $[\pi - \bar{\theta}_\gamma, \pi - \pi/M)$, in which the integrand is purely convex or concave. This partitioning results in a bound with a minimum of 4 exponential terms. The value of $\bar{\theta}_\gamma$ is obtained by solving

$$\frac{\partial^2}{\partial \theta^2} \exp\left(-\frac{\gamma \sin^2(\pi/M)}{\sin^2 \theta}\right) = 0 \tag{4.14}$$

and is given by

$$\bar{\theta}_\gamma = \sin^{-1}\left(\frac{1}{2}\sqrt{2\sin^2\left(\frac{\pi}{M}\right)\gamma + 3 - \sqrt{\left[2\sin^2\left(\frac{\pi}{M}\right)\gamma - 1\right]^2 + 8}}\right). \tag{4.15}$$

If $\bar{\theta}_\gamma < \pi/M$, the integration range is partitioned into $[0, \bar{\theta}_\gamma)$, $[\bar{\theta}_\gamma, \pi - \pi/M)$, which corresponds to a bound with three exponential terms. As $\bar{\theta}_\gamma$ is a function of γ, the coefficients of the Abreu bounds are

Our method, in comparison, does not depend on monotonicity or convexity of the integrand. Hence, partitioning is not required and implementation of the method is straightforward. Fig. 4.1 shows that our bound is much tighter than the Chiani bound and the Abreu method with similar numbers of exponential terms.

4.1.2 SEP of MDPSK over AWGN

The SEP of MDPSK is given by [72, eq.(3)]

$$P(e_s|\gamma) = \frac{1}{\pi}\int_0^{\pi-\pi/M} \exp\left(-\frac{\gamma \sin^2(\pi/M)}{1+\cos(\pi/M)\cos\theta}\right) d\theta. \tag{4.16}$$

We first split the integration range of $[0, \pi-\pi/M]$ into $n+1$ subranges, by arbitrarily choosing $n+2$ values of θ_k such that $0 = \theta_0 < \theta_1 < ... < \theta_{n+1} = \pi - \pi/M$. Thus, (4.16) becomes

$$P(e_s|\gamma) = \sum_{k=1}^{n+1} \frac{1}{\pi}\int_{\theta_{k-1}}^{\theta_k} \exp\left(-\frac{\gamma \sin^2(\pi/M)}{1+\cos(\pi/M)\cos\theta}\right) d\theta. \tag{4.17}$$

Applying the Jensen's inequality in (3.2) with

$$\begin{aligned} \phi(u) &= \exp(u), \\ f(\theta) &= -\frac{\gamma \sin^2(\pi/M)}{1+\cos(\pi/M)\cos\theta}, \\ p(\theta) &= 1, \\ a &= \theta_{k-1}, \\ b &= \theta_k, \end{aligned} \tag{4.18}$$

on each summation term in (4.17), we obtain an exponential lower bound on the SEP of MDPSK as

$$P(e_s|\gamma) \geq \sum_{k=1}^{n+1} a_k \exp\left(-b_k\gamma\right), \tag{4.19}$$

with

$$\begin{aligned} a_k &= \frac{\theta_k - \theta_{k-1}}{\pi}, \\ b_k &= 2\sin\left(\frac{\pi}{M}\right) \frac{\tan^{-1}(\beta_k) - \tan^{-1}(\beta_{k-1})}{\theta_k - \theta_{k-1}}, \end{aligned} \tag{4.20}$$

where

$$\beta_k = \tan\left(\frac{\theta_k}{2}\right) \sqrt{\frac{1-\cos(\pi/M)}{1+\cos(\pi/M)}}. \tag{4.21}$$

Note that the lower bound is a sum of $n+1$ exponentials.

As the integrand in (4.16) decreases monotonically over the entire integration range, partitioning is not required to derive the Chiani bounds [24, eq.(29)]

$$\sum_{k=1}^{n} a_k \exp\left(-b_k\gamma\right) \le P(e_s|\gamma) \le \sum_{k=1}^{n} a_k \exp\left(-b_{k-1}\gamma\right), \tag{4.22}$$

where

$$\begin{aligned} a_k &= \frac{\theta_k - \theta_{k-1}}{\pi}, \\ b_k &= \frac{\sin^2(\pi/M)}{1+\cos(\pi/M)\cos\theta_k}. \end{aligned} \tag{4.23}$$

For the Abreu method, similar to the case of MPSK, $\bar{\theta}_\gamma$ where convexity of the integrand changes is obtained by solving

$$\frac{\partial^2}{\partial\theta^2} \exp\left(-\frac{\gamma\sin^2(\pi/M)}{1+\cos(\pi/M)\cos\theta}\right) = 0 \tag{4.24}$$

and equivalently

$$\begin{aligned} &\cos^2\left(\frac{\pi}{M}\right)\cos^3\theta - \gamma\sin^2\left(\frac{\pi}{M}\right)\cos\left(\frac{\pi}{M}\right)\cos^2\theta \\ &- \left[2\cos^2\left(\frac{\pi}{M}\right)+1\right]\cos\theta + \left[\gamma\sin^2\left(\frac{\pi}{M}\right)-2\right]\cos\left(\frac{\pi}{M}\right) = 0. \end{aligned}$$

The solution of $\bar{\theta}_\gamma$ is a complex function of γ and M. If $\bar{\theta}_\gamma > \pi - \pi/M$, the integrand is concave over the entire integration range. The Abreu lower bound consists of a minimum of two exponentials. If $\bar{\theta}_\gamma < \pi - \pi/M$, the integrand is concave over $[0, \bar{\theta}_\gamma)$ and convex over $[\bar{\theta}_\gamma, \pi - \pi/M)$. The Abreu lower bound consists of a minimum of three exponential term.

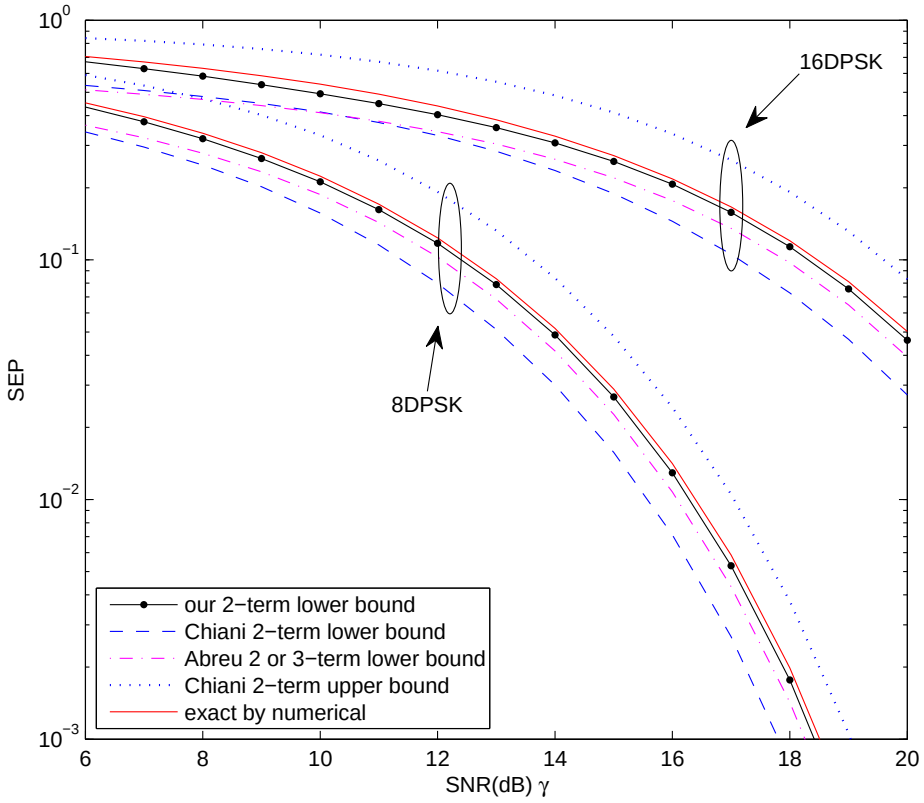

Figure 4.2: Lower bounds on the SEP of MDPSK over AWGN.

Our bound in (4.19) does not require analysis of the integrand. Fig. 4.2 shows that our two-term lower bound is already very tight. It is much tighter than the Chiani lower bound and the Abreu lower bound with similar numbers of exponentials.

4.1.3 SEP of Signals with Polygonal Decision Region over AWGN

The SEP of a two-dimensional constellation point with polygonal decision region is given by [15, eq.(13)]

$$P(e_s|\gamma) = \frac{1}{2\pi}\sum_{i=1}^{N}\int_0^{\alpha_i} \exp\left(-\frac{x_i^2\sin^2(\phi_i)}{N_o\sin^2(\theta+\phi_i)}\right)d\theta, \tag{4.25}$$

where N is the number of triangles the decision region consists of, and $x_i^2 = c_{sig}E_b$ depends on the signal decision region. Thus, (4.25) is a function of $\gamma = E_b/N_o$. Using change of variable $\theta' = \theta + \phi_i$, (4.25) becomes

$$P(e_s|\gamma) = \frac{1}{2\pi}\sum_{i=1}^{N}\int_{\phi_i}^{\phi_i+\alpha_i} \exp\left(-\frac{c_{sig}\sin^2(\phi_i)}{\sin^2(\theta')}\gamma\right)d\theta'. \tag{4.26}$$

We split the integration range of $[\phi_i, \phi_i+\alpha_i]$ into $n+1$ subranges, by arbitrarily choosing $n+2$ values of θ_k such that $\phi_i = \theta_0 < \theta_1 < ... < \theta_{n+1} = \phi_i + \alpha_i$. Applying the Jensen's inequality in each subrange, we obtain the exponential lower bound on (4.25)

$$P(e_s|\gamma) \geq \sum_{i=1}^{N}\sum_{k=1}^{n+1} a_{i_k}\exp\left(-b_{i_k}\gamma\right), \tag{4.27}$$

where

$$\begin{aligned} a_{i_k} &= \frac{\theta_{i_k} - \theta_{i_{k-1}}}{2\pi}, \\ b_{i_k} &= c_{sig}\sin^2(\phi_i)\frac{\cot(\theta_{i_{k-1}}) - \cot(\theta_{i_k})}{\theta_{i_k} - \theta_{i_{k-1}}}. \end{aligned} \tag{4.28}$$

Note that (4.27) contains $N(n+1)$ exponential terms. By choosing 0 as a θ_{i_m} for all i's, (4.27) can be reduced to Nn terms.

When $n \to \infty$, we have

$$\begin{aligned} \lim_{n\to\infty} P(e_s|\gamma) &= \sum_{i=1}^{N}\sum_{k=1}^{\infty}\frac{d\theta}{2\pi}\exp\left(c_{sig}\sin^2(\phi_i)\frac{d\cot(\theta)}{d\theta}\gamma\right) \\ &= \sum_{i=1}^{N}\int_{\phi_i}^{\phi_i+\alpha_i}\frac{1}{2\pi}\exp\left(-\frac{c_{sig}\sin^2(\phi_i)}{\sin^2\theta}\gamma\right)d\theta, \end{aligned} \tag{4.29}$$

which is equal to (4.6). As expected, simply by increasing n, the lower bound approaches the exact value for all argument values.

To apply the Chiani method, we need to determine if the integrand is monotonic in $[\phi_i, \phi_i + \alpha_i]$. It depends on the values of ϕ_i and α_i. Therefore, for each triangle of the polygonal decision region, we need to determine monotonic subranges and divide arbitrarily before applying the Jensen's inequality.

To apply the Abreu method, for each triangle of the polygonal decision region, we need to solve for the point that separates convex and concave intervals in $[\phi_i, \phi_i + \alpha_i]$. The value of the point is a function of γ and may not be obtained analytically. Numerical root-finding algorithms may be used to determine the value. Then, the convex or concave subranges are divided arbitrarily before applying the Jensen's inequality.

Our method is much simpler than the above-mentioned two methods, as the integration range can be arbitrarily divided. No analysis of the integrand or the integration range is required.

4.2 Lower Bounds on Average SEP over Fading

If an error probability can be bounded by a sum of exponentials with constant coefficients, bounds on the average probability over fading can be easily obtained by using the MGF method.

4.2.1 SEP of Signals with 2D Decision Regions over Fading

The average error probability over fading is obtained by averaging the instantaneous error probability conditioned on the instantaneous SNR γ, over the distribution of γ, i.e.

$$P(e_s) = \int_0^\infty P(e_s|\gamma) p_\gamma(\gamma) d\gamma. \tag{4.30}$$

If $P(e_s|\gamma)$ can be expressed in the following general form:

$$P(e_s|\gamma) = c \int_a^b \exp\left(f(\theta)\gamma\right) d\theta, \tag{4.31}$$

by changing the order of integration, (4.30) simplifies to

$$P(e_s) = c \int_a^b M\left(f(\theta)\right) d\theta, \tag{4.32}$$

where $M(\gamma)$ is the MGF function defined in (3.4). But still, the exact average probability in (4.32) involves a finite range integral and very often does not reduce to a closed form. For example, the SEP performances of MPSK and MDPSK over Rayleigh fading are given in closed form in [25, eq.(7-8)]. Their SEP performances over Nakagami-m are found in closed form only for positive integer values of m in [7, eq.(18)(20)], [26], while for arbitrary m they are expressed in terms of Gauss hypergeometric function and Lauricella function [27, 28], respectively. Their SEP performances over Rician fading are found in finite range integrals [29]. Numerical integration is resorted to in such cases.

If $P(e_s|\gamma)$ can be lower bounded by a sum of exponentials, i.e.

$$P(e_s|\gamma) \geq \sum_k a_k \exp\left(-b_k\gamma\right), \tag{4.33}$$

substituting (4.33) into (4.30), (4.32) is lower bounded as

$$P(e_s) \geq \sum_k a_k M_\gamma(-b_k). \tag{4.34}$$

Being able to bound the instantaneous error probability with a sum of exponentials with constant coefficients allows us to apply the MGF method conveniently.

Lower bounds on the SEP performances of MPSK and MDPSK over fading are given by (4.34) with $\{a_k\}$ and $\{b_k\}$ in (4.10) and (4.20), respectively. The SEP lower bounds for MPSK and MDPSK over Rician fading are shown in Fig. 4.3, Fig. 4.4 and Fig. 4.5, respectively. The SEP lower bounds for MPSK and MDPSK over Nakagami-m fading are shown in Fig. 4.5 and Fig. 4.6, respectively. The four figures show that our bounds are much tighter than the Chiani bounds in [24, eq.(39)(41)] with the same $\{\theta_k\}$ values. Both our bounds and the Chiani bounds become tighter with increasing n.

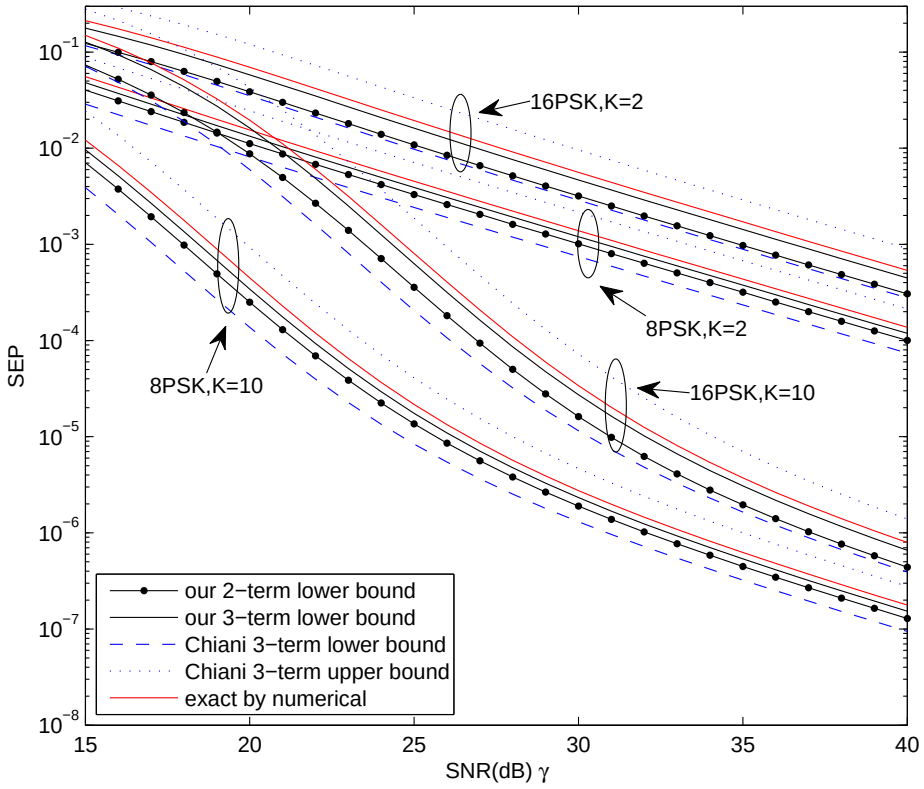

Figure 4.3: Lower bounds on the SEP of MPSK over Rician fading.

4.2.2 Product of Two Gaussian Q-functions over Fading

The average of the product of two Gaussian Q-functions over fading is given by [73, eq.(1)]

$$I = \int_0^\infty Q(A_1\sqrt{\gamma})Q(A_2\sqrt{\gamma})p_\gamma(\gamma)d\gamma, A_1 \geq 0, A_2 \geq 0. \tag{4.35}$$

It is used in obtaining the SEP of general rectangular M-ary quadrature amplitude modulation over fading. Exact closed-form expressions have been obtained for Rayleigh fading [74, eq.(5)] and Nakagami-m fading [73, eq.(6)] [75, eq.(20)(35)] but not for Rician fading.

The product of two Gaussian Q-functions is a special case of the two-dimensional Gaussian Q-functions. Using the exponential lower bound on the

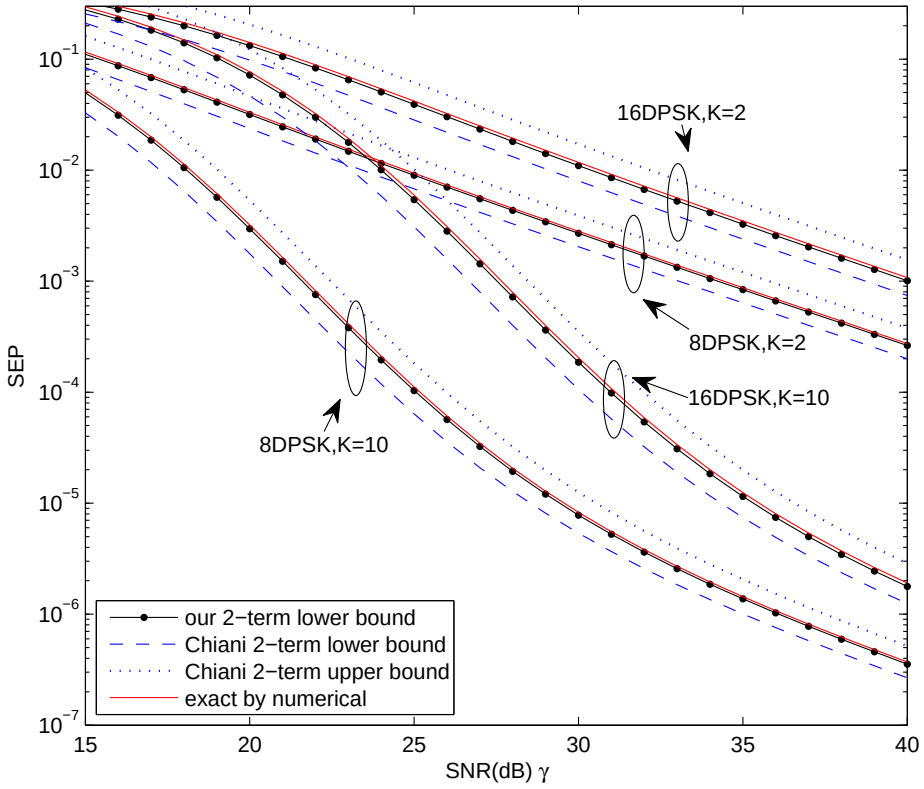

Figure 4.4: Lower bounds on the SEP of MDPSK over Rician fading.

two-dimensional Gaussian Q-functions in (3.72), the MGF of Rician fading in (3.58) and the MGF method in (4.32), (4.35) for Rician fading is lower bounded by

$$\begin{aligned} I \geq & \sum_{k=2}^{n+1} a_{x_k} \frac{1+K}{1+K-b_{x_k}A_1^2\bar{\gamma}} \exp\left(\frac{Kb_{x_k}A_1^2\bar{\gamma}}{1+K-b_{x_k}A_1^2\bar{\gamma}}\right) \\ & + \sum_{k=2}^{n+1} a_{y_k} \frac{1+K}{1+K-b_{y_k}A_2^2\bar{\gamma}} \exp\left(\frac{Kb_{y_k}A_2^2\bar{\gamma}}{1+K-b_{y_k}A_2^2\bar{\gamma}}\right), \end{aligned} \tag{4.36}$$

which is a sum of $2n$ exponential terms. Here, $\bar{\gamma}$ is the average SNR, $a_{x_k}, a_{y_k}, b_{x_k}$, and b_{y_k} are given in (3.73) and

$$\begin{aligned} \theta_x^* &= \frac{\pi}{2} - \tan^{-1}\left(\frac{A_2}{A_1}\right) \in [0,\pi), \\ \theta_y^* &= \tan^{-1}\left(\frac{A_2}{A_1}\right) \in [0,\pi). \end{aligned} \tag{4.37}$$

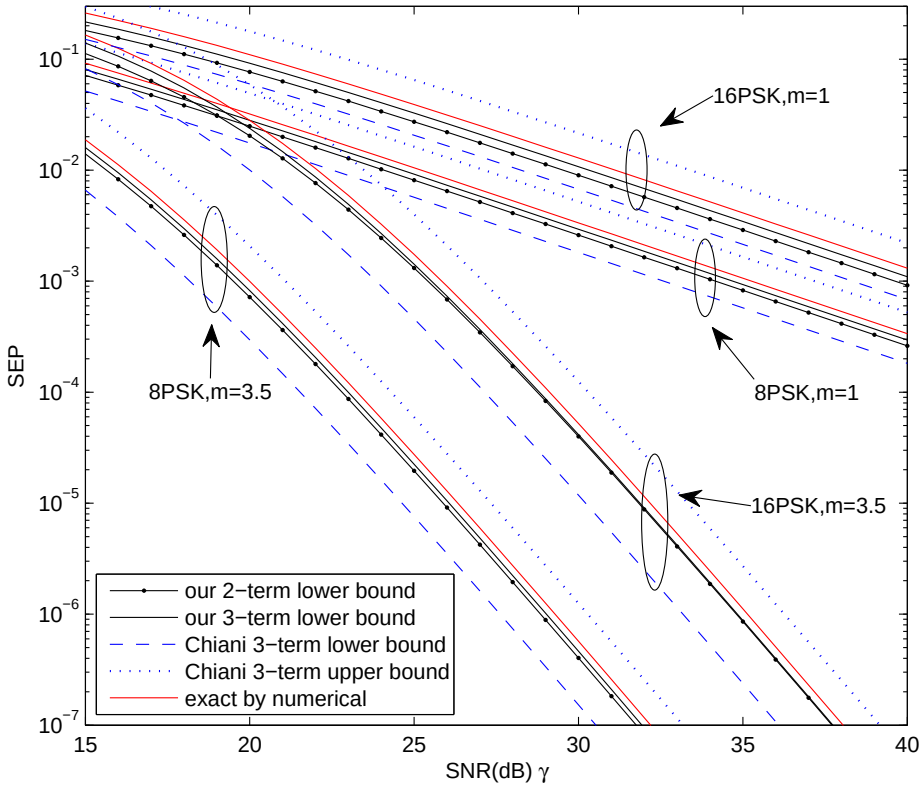

Figure 4.5: Lower bounds on the SEP of MPSK over Nakagami-m fading.

Fig. 4.7 shows that our lower bound in (4.36) becomes tighter with increasing n. It is much tighter than the Li lower bound in [73, eq.(12)] at low SNR for all the four cases.

4.3 Conclusions

We propose to apply the Jensen's inequality to lower bound integrals of exponential functions. Using this method, we obtain exponential lower bounds on the SEP of MPSK, MDPSK, and signals with polygonal decision regions over an AWGN channel. The tightness of the bounds can be improved by increasing the number of exponential terms. The coefficients of the exponential bounds are constants. Hence,

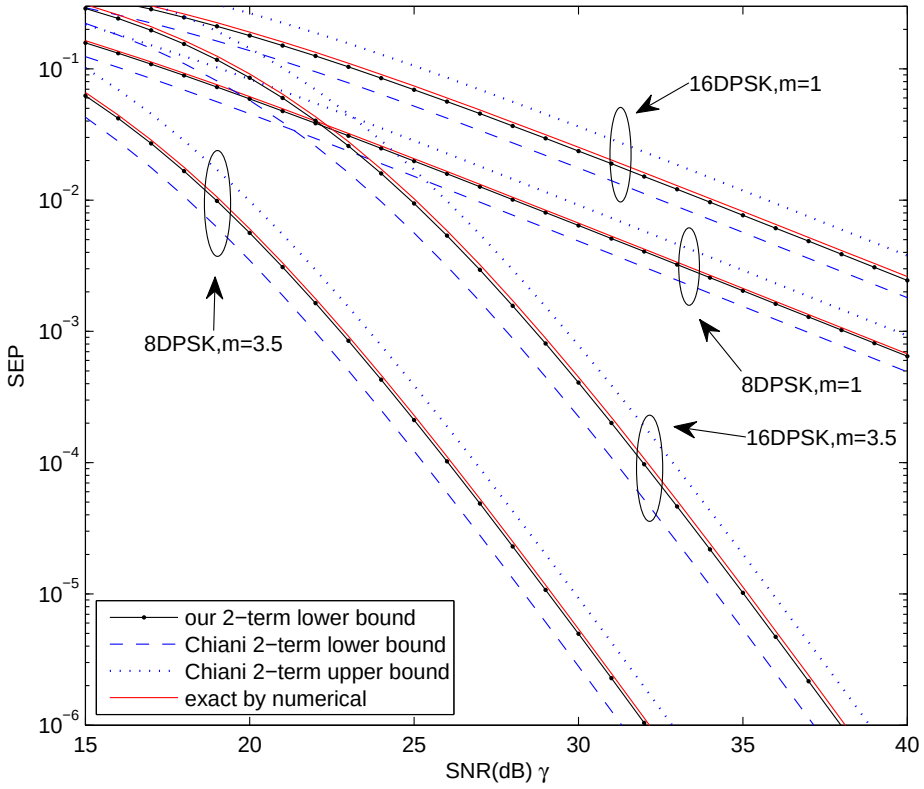

Figure 4.6: Lower bounds on the SEP of MDPSK over Nakagami-m fading.

the lower bounds on the average SEP performances over fading are easily obtained by averaging lower bounds on the SEP performances over fading distribution using the MGF method. Numerical results show that our bounds are tighter than the Chiani bounds and the Abreu bounds with similar numbers of exponential terms.

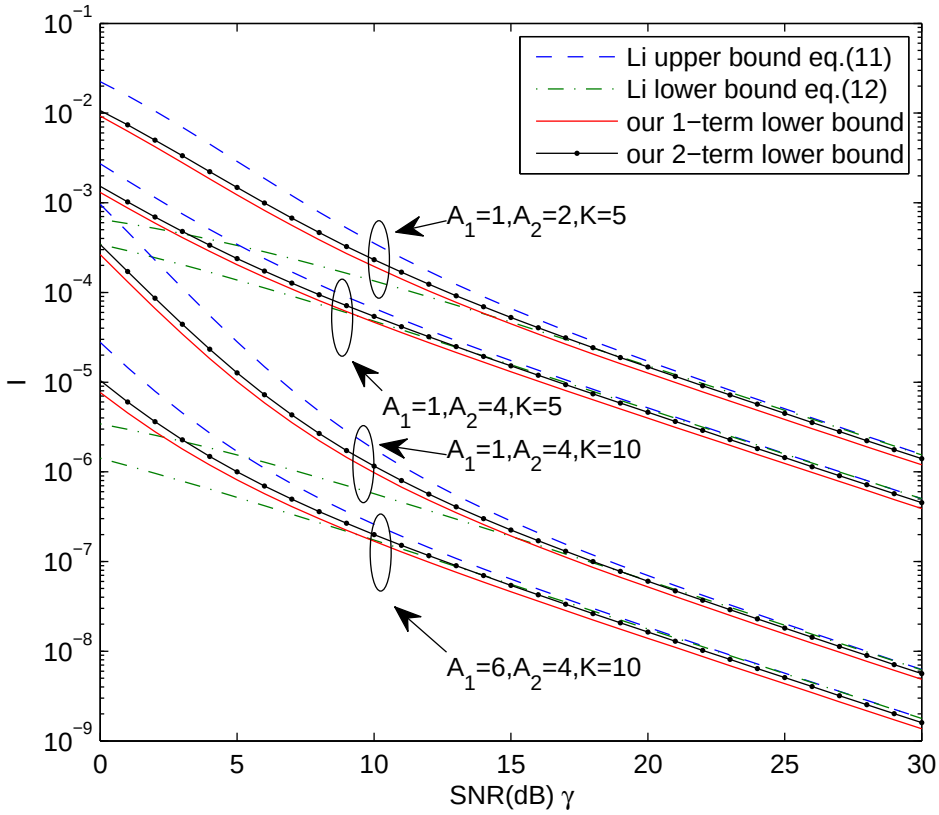

Figure 4.7: Bounds on the product of two Gaussian Q-functions over Rician fading.

Chapter 5

Error Performance of Quadratic Receivers

In Chapter 4, we looked into coherent detection. When estimation of the carrier phase is difficult, e.g. over fading channels, coherent detection is not possible. In such cases, differential and noncoherent detection techniques are used instead. For example, differentially coherent detectors are used to detect DPSK signals. The square law detector of frequency shift keying (FSK) signals, and the MLSD-NCSI detector in Chapter 2 are examples of noncoherent detectors that do not require an explicit channel estimate. A lot of work has been published on the error performance of individual differential or noncoherent detectors over AWGN or fading channels. For example, the BEP of BDPSK and binary orthogonal signals with multichannel reception over AWGN are obtained in [8, eq.(12-1-13)] and [8, eq.(12-1-24)], respectively. The average BEP of BDPSK and binary orthogonal square-law detected FSK signals over slow Rayleigh fading are given in [8, eq.(14-3-10)] and [8, eq.(14-3-11)], respectively. The average BEP of QDPSK over slow Rayleigh, Rician and Nakagami-m fading are given in [30–32], respectively. The average BEP of BDPSK and QDPSK over slow Rayleigh and Rician fading channels with diversity reception are obtained in [33, 34]. The average BEP of BDPSK over slow Nakagami-m fading channels with diversity reception is obtained in [35]. The

average BEP of BDPSK over fast Rician fading with diversity reception is obtained in [36]. The average BEP of BDPSK, QDPSK and noncoherent frequency shift keying (NCFSK) with diversity reception over arbitrarily correlated Rician fading is obtained in [37].

The decision metrics of differential and noncoherent detectors are usually in quadratic forms, for both single and multichannel reception over AWGN and fading channels. Only a few publications obtain general expressions on the error performance of a general quadratic receiver. Using a characteristic function method, Proakis finds an error probability expression for general quadratic receivers with complex Gaussian distributed signals, in terms of the first-order Marcum Q-function and the modified Bessel functions of the first kind with order $0, 1, ..., L-1$, where L is the diversity order, and other elementary functions [8, eq. (B-21)]. The first-order Marcum Q-function and the modified Bessel function of the first kind are defined as infinite range integrals. Therefore, evaluation of the Proakis' expression involves numerical integration over an infinite range due to the special functions involved.

Using alternative integral forms of the Marcum Q-function and the zeroth-order modified Bessel function of the first kind, Simon and Alouini express the Proakis' expression for single channel reception over AWGN in a finite range integral form [9]. When this integral is averaged over the fading distribution, the integration order of the double integral can be interchanged. This often results in a closed form expression or a single integral. For multichannel reception over AWGN, the Proakis' expression can be written in terms of the generalized Marcum Q-function. Again, by using the integral form of the generalized Marcum Q-function, the Proakis' expression is expressed in a finite range integral. Averaging the expression over the joint PDF of multichannel fading, by interchanging the order of integration, the performance of diversity reception over fading results in a finite range integral with integrand in terms of elementary functions. However, in general, the integral does not reduce to a closed-form expression and, hence, numerical integration is required.

By performing eigendecomposition of the decision metrics of DPSK and

NCFSK, Ma and Lim derived the MGF of the decision statistics and obtains from the cumulative density function a BEP expression involving an infinite multi-level summation [37]. It does not show, however, how to generalize this approach to a general quadratic receiver whose decision metric is of a more general form than that of DPSK and NCFSK.

Our target here is to find a general expression for a general quadratic receiver, which involves only elementary functions, such that its computation is simpler than the existing expressions. The decision metric of a quadratic receiver is noncentral Chi-square distributed. Its PDF can be expressed as a Poisson-weighted mixture of central Chi-square PDF. Thus, the error probability of a quadratic receiver results in a triple sum involving only elementary functions. Using this expression, we obtain exact BEP performances of of optimum and suboptimum BDPSK and QDPSK receivers over fast Rician fading with Doppler shift. Computation using our expressions are more efficient than the existing expressions involving confluent hypergeometric functions. We also obtain alternative BEP expressions of BDPSK over slow Rayleigh and Rician fading.

This chapter is organized as follows. In Section 5.1, we obtain a new exact expression of the error probability of general quadratic receivers which involves only elementary functions (rational functions and exponential functions) . In Section 5.2, we apply the expression to the BEP performance analysis of BDPSK over fast Rician fading with Doppler shift. New exact expressions involving only elementary functions are obtained for both the optimum receiver and the suboptimum receiver. Similarly, in Section 5.3, exact BEP expressions involving only elementary functions are obtained for the optimum and suboptimum receivers of QDPSK. Conclusions are made in Section 5.4.

5.1 New Expression for Performance of Quadratic Receivers

The error probability of quadratic receivers are usually in the following form

$$P(\varepsilon) = P(R_0 < R_1). \tag{5.1}$$

Here, the random variable R_i is the sum of squares of L independent random variables, i.e.

$$R_i = \|\mathbf{x}_i\|^2, \tag{5.2}$$

where the elements of $\mathbf{x}_i = [x_{i1}, ..., x_{iL}]^T$ are complex Gaussian distributed with nonidentical means m_{ik} and identical variances $2\sigma_i^2$. Therefore, R_i is noncentral Chi-square distributed with $2L$ degrees of freedom and noncentrality parameter

$$s_i^2 = \sum_{k=1}^{L} |m_{ik}|^2. \tag{5.3}$$

The PDF of R_i is given by [8, eq. (2-1-118)]

$$p_i(r) = \frac{1}{2\sigma_i^2}\left(\frac{r}{s_i^2}\right)^{\frac{L-1}{2}} \exp\left(-\frac{r+s_i^2}{2\sigma_i^2}\right) I_{L-1}\left(\frac{s_i\sqrt{r}}{\sigma_i^2}\right). \tag{5.4}$$

Here, $I_m(x)$ is the mth-order modified Bessel function of the first kind, usually defined as [70, eq. (8.431-3)]

$$I_m(x) = \frac{(x/2)^m}{\Gamma(m+\frac{1}{2})\Gamma(\frac{1}{2})}\int_0^{\pi} e^{\pm x\cos\theta}\sin^{2x}\theta d\theta, \qquad [\mathrm{Re}(m+\frac{1}{2}) > 0]. \tag{5.5}$$

Alternatively, it can also be represented by the infinite series [70, eq. (8.445)]

$$I_m(x) = \sum_{k=0}^{\infty} \frac{(x/2)^{m+2k}}{k!\Gamma(m+k+1)}. \tag{5.6}$$

Substituting (5.6) into (5.4), (5.4) can also be expressed as

$$p_i(r) = \sum_{k=0}^{\infty} \exp\left(-\frac{s_i^2}{2\sigma_i^2}\right)\frac{(\frac{s_i^2}{2\sigma_i^2})^k}{k!} p'_{i,L+k}(r), \tag{5.7}$$

where

$$p'_{i,k}(r) = \frac{r^{k-1}\exp\left(-\frac{r}{2\sigma_i^2}\right)}{(2\sigma_i^2)^k\Gamma(k)} \tag{5.8}$$

is the normalized central Chi-square distribution with $2k$ degrees of freedom. From the representation in (5.7), the noncentral Chi-square distribution can be seen as a Poisson-weighted mixture of central Chi-square distributions, each with $2(L+k)$ degrees of freedom.

Having obtained the PDF of R_0 and R_1, (5.1) depends on whether R_0 and R_1 are independent of each other.

5.1.1 Independent R_0 and R_1

If R_0 and R_1 are independent, we can evaluate (5.1) by averaging $P(R_1 > c|R_0 = c)$ over the statistics of R_0, i.e.

$$P(\varepsilon) = \int_{c=0}^{\infty} P(R_1 > c|R_0 = c)p_0(c)dc. \tag{5.9}$$

As R_0 and R_1 are independent of each other, we have

$$P(R_1 > c|R_0 = c) = P(R_1 > c) = \int_c^{\infty} p_1(r)dr. \tag{5.10}$$

Substituting the PDF of R_1 in (5.7), (5.10) is given by

$$P(R_1 > c|R_0 = c) = \sum_{k=0}^{\infty} \exp\left(-\frac{s_1^2}{2\sigma_1^2}\right) \frac{(\frac{s_1^2}{2\sigma_1^2})^k}{k!} \frac{1}{(2\sigma_1^2)^k\Gamma(k)} \int_c^{\infty} r^{k-1}\exp\left(-\frac{r}{2\sigma_1^2}\right) dr. \tag{5.11}$$

Using the integration rule [70, eq.(3.351-2)]

$$\int_u^{\infty} x^n \exp(-\mu x)dx = \exp(-\mu u)\sum_{k=0}^{n} \frac{n!}{k!}\frac{u^k}{\mu^{n-k+1}}, \quad [u > 0, \mathrm{Re}[\mu] > 0, n = 0, 1, 2...] \tag{5.12}$$

(5.11) reduces to

$$P(R_1 > c|R_0 = c) = \exp\left(-\frac{s_1^2 + c}{2\sigma_1^2}\right) \sum_{k=0}^{\infty} \frac{(s_1^2/2\sigma_1^2)^k}{k!} \sum_{j=0}^{k+L-1} \frac{(c/2\sigma_1^2)^j}{j!}. \tag{5.13}$$

Substituting (5.13) and the PDF of R_0 in (5.7), (5.9) can be evaluated by

$$P(\varepsilon) = \int_{c=0}^{\infty} \sum_{k=0}^{\infty} \exp\left(-\frac{s_1^2}{2\sigma_1^2}\right) \frac{\left(\frac{s_1^2}{2\sigma_1^2}\right)^k}{k!} \sum_{j=0}^{k+L-1} \exp\left(-\frac{c}{2\sigma_1^2}\right) \frac{\left(\frac{c}{2\sigma_1^2}\right)^j}{j!} \cdot \sum_{l=0}^{\infty} \exp\left(-\frac{s_0^2}{2\sigma_1^2}\right) \frac{(\frac{s_0^2}{2\sigma_0^2})^l}{l!} \frac{c^{l+L-1} \exp\left(-\frac{c}{2\sigma_0^2}\right)}{(2\sigma_0^2)^{l+L}\Gamma(l+L)} dc. \tag{5.14}$$

By changing the order of integration and summation, and using the integration rule [70, eq. (2.321 2)]

$$\int \exp(ax) x^n dx = \exp(ax) \sum_{i=0}^{n} \frac{(-1)^{n-i} n! x^i}{i! a^{n-i+1}}, \tag{5.15}$$

(5.14) can be simplified to

$$\begin{aligned} P(\varepsilon) =& \frac{\exp\left(-\frac{s_0^2}{2\sigma_0^2} - \frac{s_1^2}{2\sigma_1^2}\right)}{(1+\frac{\sigma_0^2}{\sigma_1^2})^L} \sum_{k=0}^{\infty} \frac{\left(\frac{s_1^2}{2\sigma_1^2}\right)^k}{k!} \sum_{j=0}^{L-1+k} \frac{1}{j!\ (1+\frac{\sigma_1^2}{\sigma_0^2})^j} \\ & \cdot \sum_{l=0}^{\infty} \frac{(L-1+j+l)! \left(\frac{s_0^2}{2\sigma_0^2(1+\frac{\sigma_0^2}{\sigma_1^2})}\right)^l}{(L-1+l)!\ l!} \\ =& \frac{\exp\left(-A_0 - A_1\right)}{S_0^L} \sum_{k=0}^{\infty} \frac{A_1^k}{k!} \sum_{j=0}^{L-1+k} \frac{1}{j! S_1^j} \sum_{l=0}^{\infty} \frac{(L-1+j+l)!(A_0/S_0)^l}{(L-1+l)!, l!} \end{aligned} \tag{5.16}$$

where

$$\begin{aligned} A_0 &= \frac{s_0^2}{2\sigma_0^2}, \\ A_1 &= \frac{s_1^2}{2\sigma_1^2}, \\ S_0 &= 1 + \frac{\sigma_0^2}{\sigma_1^2}, \\ S_1 &= 1 + \frac{\sigma_1^2}{\sigma_0^2}. \end{aligned} \tag{5.17}$$

By using the following formula [70, eq. (9.212-1)]

$${}_1F_1(L+j, L; x) = e^x\ {}_1F_1(-j, L; -x), \tag{5.18}$$

where ${}_1F_1(a,b;x)$ is the confluent hypergeometric function defined as

$$ {}_1F_1(a,b;x) == \sum_{k=0}^{\infty} \frac{a(a+1)\cdots(a+k-1)}{b(b+1)\cdots(b+k-1)} \frac{x^k}{k!}, \tag{5.19} $$

(5.16) further simplifies to

$$ P(\varepsilon) = \frac{e^{-A_1-A_0+\frac{A_0}{S_0}}}{S_0^L} \sum_{k=0}^{\infty} \frac{A_1^k}{k!} \cdot \sum_{j=0}^{L-1+k} \frac{(L-1+j)!}{S_1^j} \sum_{l=0}^{j} \frac{(A_0/S_0)^l}{(L-1+l)!\ l!\ (j-l)!}. \tag{5.20} $$

where the parameters are given in (5.17). The error probability expression in (5.20) is an exact expression involving only rational functions and exponential functions. It is much simpler than the Proakis' expression which involves special functions including the Marcum Q-function and the modified Bessel function of the first kind. It is also much simpler than Simon and Alouini's expression while involves integrals.

Although (5.20) involves infinite series summation, it converges fast with k and therefore, the infinite series summation indexed by k can be truncated for numerical calculation.

An alternative method to calculate the error probability in (5.1) is to use Proakis' expression for the probability [8, Appendix B]

$$ P(D < 0), \tag{5.21} $$

where

$$ D = A\|\mathbf{x}_0\|^2 + B\|\mathbf{x}_1\|^2 + C\mathbf{x}_1^H\mathbf{x}_0 + C^*\mathbf{x}_0^H\mathbf{x}_1 \tag{5.22} $$

by letting

$$ \begin{aligned} A &= 1, \\ B &= -1, \\ C &= 0, \\ \mu_{xx} &= \sigma_0^2, \\ \mu_{yy} &= \sigma_1^2, \\ \mu_{xy} &= 0. \end{aligned} \tag{5.23} $$

The error probability expression is given by [8, eq. (B-21)]

$$\begin{aligned} P(\varepsilon) = Q_1(a,b) - I_0(ab)e^{-(a^2+b^2)/2} + \frac{I_0(ab)e^{-(a^2+b^2)/2}}{(1+v_2/v_1)^{2L-1}} \sum_{k=0}^{L-1} \binom{2L-1}{k} \left(\frac{v_2}{v_1}\right)^k \\ + \frac{e^{-(a^2+b^2)/2}}{(1+v_2/v_1)^{2L-1}} \sum_{n=1}^{L-1} I_n(ab) \sum_{k=0}^{L-1-n} \binom{2L-1}{k} \\ \cdot \left[\left(\frac{b}{a}\right)^n \left(\frac{v_2}{v_1}\right)^k - \left(\frac{a}{b}\right)^n \left(\frac{v_2}{v_1}\right)^{2L-1-k} \right], \end{aligned} \tag{5.24}$$

where

$$\begin{aligned} v_1 &= \frac{1}{2\sigma_0^2}, \\ v_2 &= \frac{1}{2\sigma_1^2}, \\ a &= \sqrt{\frac{s_1^2}{\sigma_0^2+\sigma_1^2}}, \\ b &= \sqrt{\frac{s_0^2}{\sigma_0^2+\sigma_1^2}}. \end{aligned} \tag{5.25}$$

Comparing with (5.20), (5.24) involves special functions including the Marcum Q-function and the modified Bessel function of the first kind, and therefore, is more complex than our expression in (5.20). The Proakis' expression will be used to verify our expression in (5.20) numerically.

5.1.2 Correlated R_0 and R_1

Assume that the L elements of $\mathbf{x}_i$ are i.i.d. complex Gaussian random variables with mean m_i and variance $2\sigma_i^2$. The cross-covariance of x_{0l} and x_{1l} for all l is given by

$$\mu_{01} = \mathrm{E}[(x_{0l} - m_0)(x_{1l} - m_1)^*], \tag{5.26}$$

whereas x_{0l} and x_{1j} are uncorrelated for $i \neq j$. Thus, $\mathbf{x}_0$ and $\mathbf{x}_1$ can be decorrelated by linear transformation. Let

$$\begin{aligned} \mathbf{y}_0 &= \mu\mathbf{x}_0 + \mathbf{x}_1, \\ \mathbf{y}_1 &= \mathbf{x}_0 + \mu^*\mathbf{x}_1. \end{aligned} \tag{5.27}$$

By showing that

$$\begin{aligned}\mathbf{x}_0 &= \frac{\mu^*\mathbf{y}_0 - \mathbf{y}_1}{|\mu|^2 - 1},\\ \mathbf{x}_1 &= \frac{\mu\mathbf{y}_0 - \mathbf{y}_1}{|\mu|^2 - 1},\end{aligned} \tag{5.28}$$

we can prove that

$$P(\|\mathbf{x}_0\|^2 < \|\mathbf{x}_1\|^2) = P(\|\mathbf{y}_0\|^2 < \|\mathbf{y}_1\|^2). \tag{5.29}$$

We want to solve for the value of μ such that y_{0l} and y_{1l} for all l are uncorrelated, i.e.

$$\mathrm{E}\left[(y_{0l} - \mathrm{E}[y_{0l}])\,(y_{1l} - \mathrm{E}[y_{1l}])^*\right] = 0, \tag{5.30}$$

and hence,

$$\mu_{01}\mu^2 + (2\sigma_0^2 + 2\sigma_0^2) + \mu_{01}^* = 0. \tag{5.31}$$

The solution to (5.31), i.e.

$$\mu = -\frac{2\sigma_0^2 + 2\sigma_1^2 + \sqrt{(2\sigma_0^2 + 2\sigma_1^2)^2 - 4|\mu_{01}|^2}}{2\mu_{10}}, \tag{5.32}$$

ensures that $\mathbf{y}_0$ and $\mathbf{y}_1$ are independent. The means and variances of the elements of $\mathbf{y}_0$ and $\mathbf{y}_1$ are given by

$$\begin{aligned}m_0' &= \mu m_0 + m_1,\\ 2\sigma_0'^2 &= |\mu|^2 2\sigma_0^2 + 2\sigma_1^2 + 2\mathrm{Re}[\mu\mu_{01}],\\ m_1' &= m_0 + \mu^* m_1,\\ 2\sigma_1'^2 &= 2\sigma_0^2 + |\mu|^2 2\sigma_1^2 + 2\mathrm{Re}[\mu\mu_{01}].\end{aligned} \tag{5.33}$$

Hence, we have

$$\begin{aligned}s_0'^2 &= L\left(|\mu|^2|m_0|^2 + |m_1|^2 + 2\mathrm{Re}[\mu m_0 m_1^*]\right),\\ s_1'^2 &= L\left(|m_0|^2 + |\mu|^2|m_1|^2 + 2\mathrm{Re}[\mu m_0 m_1^*]\right).\end{aligned} \tag{5.34}$$

Thus, (5.29) can be computed by (5.20) with

$$\begin{aligned} A_0 &= \frac{L\left(|\mu|^2|m_0|^2 + |m_1|^2 + 2\mathrm{Re}[\mu m_0 m_1^*]\right)}{|\mu|^2 2\sigma_0^2 + 2\sigma_1^2 + 2\mathrm{Re}[\mu\mu_{01}]}, \\ A_1 &= \frac{L\left(|m_0|^2 + |\mu|^2|m_1|^2 + 2\mathrm{Re}[\mu m_0 m_1^*]\right)}{2\sigma_0^2 + |\mu|^2 2\sigma_1^2 + 2\mathrm{Re}[\mu\mu_{01}]}, \\ S_0 &= \frac{(|\mu|^2+1)(2\sigma_0^2 + 2\sigma_1^2) + 4\mathrm{Re}[\mu\mu_{01}]}{2\sigma_0^2 + |\mu|^2 2\sigma_1^2 + 2\mathrm{Re}[\mu\mu_{01}]}, \\ S_1 &= \frac{(|\mu|^2+1)(2\sigma_0^2 + 2\sigma_1^2) + 4\mathrm{Re}[\mu\mu_{01}]}{2\sigma_0^2 + |\mu|^2 2\sigma_1^2 + 2\mathrm{Re}[\mu\mu_{01}]}. \end{aligned} \tag{5.35}$$

Computation of (5.20) with (5.35) involving only elementary functions is simpler than computation using the Proakis' expression involving special functions.

An alternative method to calculate the error probability in (5.1) is to use Proakis' expression for the probability in (5.21) [8, Appendix B] by letting

$$\begin{aligned} A &= 1, \\ B &= -1, \\ C &= 0, \\ \mu_{xx} &= \sigma_0^2, \\ \mu_{yy} &= \sigma_1^2, \\ \mu_{xy} &= \frac{1}{2}\mu_{01}. \end{aligned} \tag{5.36}$$

The error probability expression is given by (5.24) [8, eq. (B-21)] with

$$\begin{aligned} v_1 &= \frac{\sqrt{(\sigma_0^2+\sigma_1^2)^2 - |\mu_{01}|^2} - \sigma_0^2 + \sigma_1^2}{4\sigma_1 0^2\sigma_1^2 - |\mu_{01}|^2}, \\ v_2 &= \frac{\sqrt{(\sigma_0^2+\sigma_1^2)^2 - |\mu_{01}|^2} + \sigma_0^2 - \sigma_1^2}{4\sigma_1 0^2\sigma_1^2 - |\mu_{01}|^2}, \\ a &= \sqrt{\frac{2v_1^2 v_2(\alpha_1 v_1 - v_2)}{(v_1+v_2)^2}}, \\ b &= \sqrt{\frac{2v_1 v_2^2(\alpha_1 v_1 + v_2)}{(v_1+v_2)^2}}, \end{aligned} \tag{5.37}$$

where

$$\begin{aligned} \alpha_1 &= 2L\left(|m_0|^2\sigma_1^2 + |m_1|^2\sigma_2^2 - \mathrm{Re}[m_0 m_1^* \mu_{01}^*]\right), \\ \alpha_1 &= L\left(|m_0|^2 - |m_1|^2\right). \end{aligned} \tag{5.38}$$

The Proakis' expression will be used to verify our expression in (5.20) with (5.35) numerically.

5.2 BEP of BDPSK over Fast Rician Fading with Doppler Shift and Diversity Reception

The BEP performances of BDPSK over fast Rician fading channels with Doppler shift and MRC using optimum and suboptimum differential detection receivers have been expressed in [36] in the form of an infinite series summation of the confluent hypergeometric functions. The BEP performance of the suboptimum receiver is also obtained in [37] as an infinite multi-level summation. Though exact expressions have been obtained in the literature, we use this as an example to demonstrate application of our new expression which results in alternative BEP expressions that involve only elementary functions.

The received signal over Lth path at the kth symbol interval is given by

$$\mathbf{r}(k) = \sqrt{E_b} e^{j\phi(k)} \mathbf{c}(k) + \mathbf{n}(k), \tag{5.39}$$

where E_b is the energy per transmitted bit, and $\phi(k)$ is the data-modulated phase. The complex fading gain $\mathbf{c}(k)$ is given by

$$\mathbf{c}(k) = de^{j2\pi f_d(k+1)T}[1, ..., 1]^T + \mathbf{b}(k), \tag{5.40}$$

where $de^{j2\pi f_d(k+1)T}$ is the LOS component in each path with Doppler shift f_d and $\mathbf{b}(k)$ is the scatter component. The correlation function of the scatter component is given by

$$\mathrm{E}[b_l(k)b_i^*(k-j)] = 2\sigma^2 r(j)\delta_{li}, \tag{5.41}$$

where $r(j)$ is the correlation coefficient. We define $\rho = r(1)$. $\mathbf{n}(k)$ is the complex AWGN noise, whose correlation function is given by

$$\mathrm{E}[n_l(k)n_i^*(k-j)] = N_0\delta_{li}\delta_j. \tag{5.42}$$

The K factor of the Rician distribution is given by $K = |d|^2/2\sigma^2$. The SNR at each path is defined as

$$\gamma_c = \frac{E_b(|d|^2 + 2\sigma^2)}{N_0} = \frac{2E_b\sigma^2(K+1)}{N_0}. \tag{5.43}$$

5.2.1 Suboptimum Receiver

For the suboptimum receiver which has no knowledge of the Doppler shift in the LOS component, the decision rule is given by

$$\text{Re}\left[\mathbf{r}(k-1)^H\mathbf{r}(k)\right] \underset{\text{bit } 1}{\overset{\text{bit } 0}{\gtrless}} 0. \tag{5.44}$$

Assuming that bit 0 is transmitted, i.e. $\Delta\phi(k) = 0$, and the reference phase $\phi(k-1) = 0$, hence, $\phi(k) = 0$, the BEP is given by

$$P_b = P(\text{Re}\left[\mathbf{r}(k-1)^H\mathbf{r}(k)\right] < 0), \tag{5.45}$$

which can also be expressed in quadratic form as

$$P_b = P(\|\mathbf{x}_0\|^2 < \|\mathbf{x}_1\|^2), \tag{5.46}$$

where

$$\begin{aligned} \mathbf{x}_0 &= \mathbf{r}(k) + \mathbf{r}(k-1), \\ \mathbf{x}_1 &= \mathbf{r}(k) - \mathbf{r}(k-1). \end{aligned} \tag{5.47}$$

The elements of $\mathbf{x}_0$ are i.i.d. complex Gaussian random variables with mean and variance

$$\begin{aligned} m_0 &= \sqrt{E_b}d[e^{j2\pi f_d(k+1)T} + e^{j2\pi f_d kT}], \\ 2\sigma_0^2 &= 4E_b\sigma^2(1+\rho) + 2N_0. \end{aligned} \tag{5.48}$$

Hence,

$$s_0^2 = 2LE_b|d|^2[1 + \cos(2\pi f_d T)]. \tag{5.49}$$

Similarly, the elements of $\mathbf{x}_1$ are i.i.d. complex Gaussian random variables with mean and variance

$$\begin{aligned} m_1 &= \sqrt{E_b} d[e^{j2\pi f_d (k+1)T} - e^{j2\pi f_d kT}], \\ 2\sigma_1^2 &= 4E_b\sigma^2(1-\rho) + 2N_0, \end{aligned} \tag{5.50}$$

and, hence,

$$a_1^2 = 2LE_b|d|^2[1-\cos(2\pi f_d T)]. \tag{5.51}$$

It is easy to show that $\mathbf{x}_0$ and $\mathbf{x}_1$ are independent. Thus, $\|\mathbf{x}_0\|^2$ and $\|\mathbf{x}_1\|^2$ are two independent noncentral Chi-square distributed random variables. Therefore, (5.46) can be expressed as (5.20), where (5.17) are simplified to

$$\begin{aligned} A_0 &= \frac{LK\gamma_c[1+\cos(2\pi f_d T)]}{K+1+(1+\rho)\gamma_c}, \\ A_1 &= \frac{LK\gamma_c[1-\cos(2\pi f_d T)]}{K+1+(1-\rho)\gamma_c}, \\ S_0 &= \frac{2(K+1+\gamma_c)}{K+1+(1-\rho)\gamma_c}, \\ S_1 &= \frac{2(K+1+\gamma_c)}{K+1+(1+\rho)\gamma_c}. \end{aligned} \tag{5.52}$$

Computation of (5.20) with (5.52) involving only elementary functions is simpler than computation using the Proakis' expression involving special functions.

In the case of $f_d = 0$, we have $A_1 = 0$. The BEP expression reduces to

$$\begin{aligned} P_b = &\exp\left(-\frac{LK\gamma_c}{1+K+\gamma_c}\right)\left[\frac{1+K+\gamma_c(1-\rho)}{2(1+K+\gamma_c)}\right]^L \\ &\cdot\sum_{j=0}^{L-1}(L-1+j)!\left[\frac{1+K+\gamma_c(1+\rho)}{2(1+K+\gamma_c)}\right]^j \sum_{l=0}^{j}\frac{\left\{\frac{LK\gamma_c[1+K+\gamma_c(1-\rho)]}{(1+K+\gamma_c)[1+K+\gamma_c(1+\rho)]}\right\}^l}{(j-l)!\;l!\;(L-1+l)!}, \end{aligned} \tag{5.53}$$

which is equivalent to the alternative BEP expressions in [48, eq. (9.393)] and [34, eq.(76)] derived using the Proakis' expression.

For the case of single diversity where $L = 1$, (5.53) reduces to the existing BEP expression in the literature [48, eq.(8.229)]

$$P_b = \frac{1+K+\gamma_c(1-\rho)}{2(1+K+\gamma_c)}\exp\left(-\frac{K\gamma_c}{1+K+\gamma_c}\right). \tag{5.54}$$

Letting $K = 0$, (5.53) reduces to the BEP over Rayleigh fading as

$$P_b = \left[\frac{1+\gamma_c(1-\rho)}{2(1+\gamma_c)}\right]^N \sum_{j=0}^{L-1} \binom{L-1+j}{j} \left[\frac{1+\gamma_c(1+\rho)}{2(1+\gamma_c)}\right]^j, \tag{5.55}$$

which is obtained in [33]. It is equivalent to the alternative form in [48, eq.(9.394)].

For the case of single diversity over Rayleigh fading, by letting $L = 1$ and $K = 0$, both (5.54) and (5.55) reduce to [48, eq.(8.230)]

$$P_b = \frac{1+\gamma_c(1-\rho)}{2(1+\gamma_c)}. \tag{5.56}$$

Therefore, by using the new expression for quadratic receivers, we may obtain more alternative performance expressions.

5.2.2 Optimum Receiver

For the optimum receiver which perfectly compensates the Doppler shift in the LOS component, the decision rule is given by

$$\mathrm{Re}\left[\mathbf{r}(k-1)^H \mathbf{r}(k) e^{-j2\pi f_d T}\right] \underset{\text{bit } 1}{\overset{\text{bit } 0}{\gtrless}} 0. \tag{5.57}$$

The BEP is given by

$$P_b = P(\mathrm{Re}\left[\mathbf{r}(k-1)^H \mathbf{r}(k) e^{-j2\pi f_d T}\right] < 0), \tag{5.58}$$

which can also be expressed in the same quadratic form as (5.46) where

$$\begin{aligned} \mathbf{x}_0 &= \mathbf{r}(k) + \mathbf{r}(k-1)e^{j2\pi f_d T}, \\ \mathbf{x}_1 &= \mathbf{r}(k) - \mathbf{r}(k-1)e^{j2\pi f_d T}. \end{aligned} \tag{5.59}$$

We can show that the elements of $\mathbf{x}_0$ are i.i.d. complex Gaussian random variables with mean and variance

$$\begin{aligned} m_0 &= 2\sqrt{E_b} d e^{j2\pi f_d (k+1)T}, \\ 2\sigma_0^2 &= 4E_b\sigma^2\left[1+\rho\cos(2\pi f_d T)\right] + 2N_0. \end{aligned} \tag{5.60}$$

Similarly, the elements of $\mathbf{x}_1$ are i.i.d. complex Gaussian random variables with mean and variance

$$\begin{aligned} m_1 &= 0, \\ 2\sigma_1^2 &= 4E_b\sigma^2\left[1-\rho\cos(2\pi f_d T)\right]+2N_0. \end{aligned} \tag{5.61}$$

The cross-covariance of x_{0l} and x_{1l} is given by

$$\mu_{01} = \mathrm{E}[(x_{0l}-m_0)(x_{1l}-m_1)^*] = j4E_b\sigma^2\rho\sin(2\pi f_d T), \tag{5.62}$$

$\mathbf{x}_0$ and $\mathbf{x}_1$ can be decorrelated by linear transformation, as in (5.27) with

$$\mu = j\frac{K+1+\gamma_c+\sqrt{(K+1+\gamma_c)^2-[\rho\gamma_c\sin(2\pi f_d T)]^2}}{\rho\gamma_c\sin(2\pi f_d T)}. \tag{5.63}$$

Hence, $\mathbf{y}_0$ and $\mathbf{y}_1$ are independent complex Gaussian distributed, with means and variances

$$\begin{aligned} m_0' &= \mu 2\sqrt{E_b}de^{j2\pi f_d(k+1)T}, \\ 2\sigma_0'^2 &= \frac{2N_0C_0}{K+1}, \\ m_1' &= 2\sqrt{E_b}de^{j2\pi f_d(k+1)T}, \\ 2\sigma_1'^2 &= \frac{2N_0C_1}{K+1}, \end{aligned} \tag{5.64}$$

where

$$\begin{aligned} C_0 &= (|\mu|^2+1)(K+1+\gamma_c)+(|\mu|^2-1)\rho\gamma_c\cos(2\pi f_d T)-2|\mu|\rho\gamma_c\sin(2\pi f_d T), \\ C_1 &= (|\mu|^2+1)(K+1+\gamma_c)-(|\mu|^2-1)\rho\gamma_c\cos(2\pi f_d T)-2|\mu|\rho\gamma_c\sin(2\pi f_d T). \end{aligned} \tag{5.65}$$

Therefore, the BEP of optimum BDPSK receiver can be expressed as (5.20), with

$$\begin{aligned} A_0 &= 2|\mu|^2LK\gamma_c/C_0, \\ A_1 &= 2LK\gamma_c/C_1, \\ S_0 &= 1+C_0/C_1, \\ S_1 &= 1+C_1/C_0. \end{aligned} \tag{5.66}$$

Computation of (5.20) with (5.66) involving only elementary functions is simpler than computation using the Proakis' expression involving special functions.

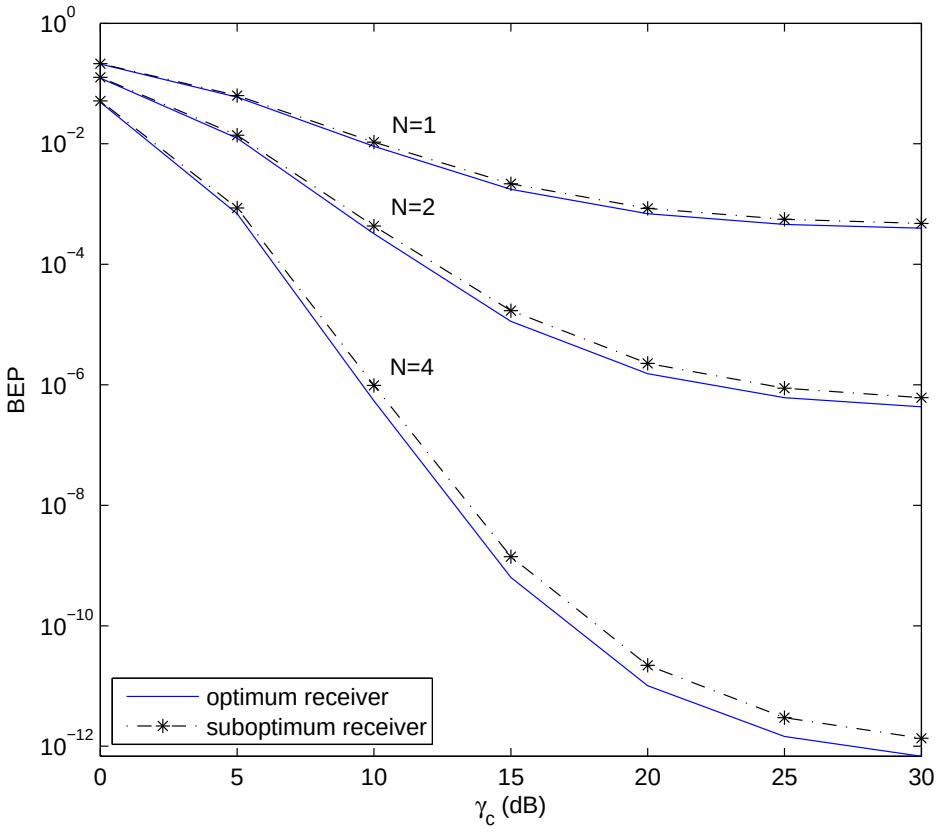

Figure 5.1: BEP performance comparison between optimum and suboptimum receivers over fast Rician fading with Doppler shift and diversity reception.

5.2.3 Numerical Results

The BEP performances of suboptimum and optimum receivers of DBPSK in eq. (5.20) with parameters in (5.52) and (5.66) are simpler than the equivalent expressions in [36, eq. (28), (40)] which involve the confluent hypergeometric function. Our expressions are also simpler than the Proakis' expression which involve the generalized Marcum Q-function and the modified Bessel function of the first kind.

Fig. 5.1 shows the BEP performances of the optimum and suboptimum receivers by numerical calculation using (5.20), (5.52) and (5.66) for $K = 5$, $f_dT = 0.03$ and $f_DT = 0.05$. The Jake's spectrum is assumed, where $\rho = J_0(2\pi f_D T)$. The numerical

results of (5.20) match well with those of Proakis' expression in (5.24) and [36, eq. (28)], therefore, only one curve is shown for each receiver. Though both (5.20) and [36, eq. (28)] involve infinite sequence summation, numerical calculations show that (5.20) converges faster than [36, eq. (28)], and takes less than half time to compute using MATLAB.

5.3 BEP of QDPSK over Fast Rician Fading with Doppler Shift and Diversity Reception

The exact BEP expression for QDPSK with suboptimum receiver in the presence of nonzero Doppler shift f_dT is obtained in [37]. The performance of the optimum receiver has not been found in the literature, though it can be obtained using the Proakis' expression in [8, Appendix B].

5.3.1 Suboptimum Receiver

The exact BEP of the Gray coded QDPSK suboptimum receiver is given by

$$P_b = \frac{1}{2}\left[P\left(\mathrm{Re}\left[\mathbf{r}(k-1)^H\mathbf{r}(k)e^{j\pi/4}\right]<0\right)+P\left(\mathrm{Re}\left[\mathbf{r}(k-1)^H\mathbf{r}(k)e^{-j\pi/4}\right]<0\right)\right]. \tag{5.67}$$

The first summation term can be expressed as

$$P\left(\mathrm{Re}\left[\mathbf{r}(k-1)^H\mathbf{r}(k)e^{j\pi/4}\right]<0\right)=P(\|\mathbf{x}_0\|^2<\|\mathbf{x}_1\|^2), \tag{5.68}$$

where

$$\begin{aligned}\mathbf{x}_0&=\mathbf{r}(k)+\mathbf{r}(k-1)e^{-j\pi/4},\\ \mathbf{x}_1&=\mathbf{r}(k)-\mathbf{r}(k-1)e^{-j\pi/4}.\end{aligned} \tag{5.69}$$

Similarly, the second summation term can be expressed as

$$P\left(\mathrm{Re}\left[\mathbf{r}(k-1)^H\mathbf{r}(k)e^{-j\pi/4}\right]<0\right)=P(\|\mathbf{x}_0\|^2<\|\mathbf{x}_1\|^2), \tag{5.70}$$

where

$$\begin{aligned}\mathbf{x}_0 &= \mathbf{r}(k) + \mathbf{r}(k-1)e^{j\pi/4},\\ \mathbf{x}_1 &= \mathbf{r}(k) - \mathbf{r}(k-1)e^{j\pi/4}.\end{aligned} \tag{5.71}$$

Denoting (5.20) as $f(A_0, A_1, S_0, S_1)$, (5.67) is given by

$$P_b = \frac{1}{2}\left[f(A_0, A_1, S_0, S_1) + f(A_0', A_1', S_0', S_1')\right], \tag{5.72}$$

where

$$\begin{aligned}A_0 &= 2LK\gamma_c\frac{[1+\cos(2\pi f_dT+\pi/4)]\,\mu^2 - 2\sin(2\pi f_dT+\pi/4)\mu + 1 - \cos(2\pi f_dT+\pi/4)}{[2\gamma_c(1+\rho/\sqrt{2})+K+1]\mu^2 - 2\sqrt{2}\gamma_c\rho\mu + 2\gamma_c(1-\rho/\sqrt{2})+K+1},\\ A_1 &= 2LK\gamma_c\frac{[1-\cos(2\pi f_dT+\pi/4)]\,\mu^2 - 2\sin(2\pi f_dT+\pi/4)\mu + 1 + \cos(2\pi f_dT+\pi/4)}{[2\gamma_c(1-\rho/\sqrt{2})+K+1]\mu^2 - 2\sqrt{2}\gamma_c\rho\mu + 2\gamma_c(1+\rho/\sqrt{2})+K+1},\\ S_0 &= 2\frac{(2\gamma_c+K+1)\mu^2 - 2\sqrt{2}\gamma_c\rho\mu + 2\gamma_c+K+1}{[2\gamma_c(1-\rho/\sqrt{2})+K+1]\mu^2 - 2\sqrt{2}\gamma_c\rho\mu + 2\gamma_c(1+\rho/\sqrt{2})+K+1},\\ S_1 &= 2\frac{(2\gamma_c+K+1)\mu^2 - 2\sqrt{2}\gamma_c\rho\mu + 2\gamma_c+K+1}{[2\gamma_c(1+\rho/\sqrt{2})+K+1]\mu^2 - 2\sqrt{2}\gamma_c\rho\mu + 2\gamma_c(1-\rho/\sqrt{2})+K+1},\end{aligned} \tag{5.73}$$

and

$$\begin{aligned}A_0' &= 2LK\gamma_c\frac{[1+\cos(2\pi f_dT-\pi/4)]\,\mu^2 + 2\sin(2\pi f_dT-\pi/4)\mu + 1 - \cos(2\pi f_dT-\pi/4)}{[2\gamma_c(1+\rho/\sqrt{2})+K+1]\mu^2 - 2\sqrt{2}\gamma_c\rho\mu + 2\gamma_c(1-\rho/\sqrt{2})+K+1},\\ A_1' &= 2LK\gamma_c\frac{[1-\cos(2\pi f_dT-\pi/4)]\,\mu^2 + 2\sin(2\pi f_dT-\pi/4)\mu + 1 + \cos(2\pi f_dT-\pi/4)}{[2\gamma_c(1-\rho/\sqrt{2})+K+1]\mu^2 - 2\sqrt{2}\gamma_c\rho\mu + 2\gamma_c(1+\rho/\sqrt{2})+K+1},\\ S_0' &= 2\frac{(2\gamma_c+K+1)\mu^2 - 2\sqrt{2}\gamma_c\rho\mu + 2\gamma_c+K+1}{[2\gamma_c(1-\rho/\sqrt{2})+K+1]\mu^2 - 2\sqrt{2}\gamma_c\rho\mu + 2\gamma_c(1+\rho/\sqrt{2})+K+1},\\ S_1' &= 2\frac{(2\gamma_c+K+1)\mu^2 - 2\sqrt{2}\gamma_c\rho\mu + 2\gamma_c+K+1}{[2\gamma_c(1+\rho/\sqrt{2})+K+1]\mu^2 - 2\sqrt{2}\gamma_c\rho\mu + 2\gamma_c(1-\rho/\sqrt{2})+K+1},\end{aligned} \tag{5.74}$$

where

$$\mu = \frac{2\gamma_c + K + 1 + \sqrt{(2\gamma_c+K+1)^2 - 2(\gamma_c\rho)^2}}{\sqrt{2}\gamma_c\rho}. \tag{5.75}$$

Computation of (5.20) with (5.73) and (5.74) involving only elementary functions is simpler than computation using the Proakis' expression involving special functions.

5.3.2 Optimum Receiver

The exact BEP of the Gray coded QDPSK suboptimum receiver is given by

$$P_b = \frac{1}{2}\left\{P\left(\mathrm{Re}\left[\mathbf{r}(k-1)^H\mathbf{r}(k)e^{j(-2\pi f_d T+\pi/4)}\right]<0\right) + P\left(\mathrm{Re}\left[\mathbf{r}(k-1)^H\mathbf{r}(k)e^{-j(2\pi f_d T+\pi/4)}\right]<0\right)\right\}. \tag{5.76}$$

The first summation term can be expressed as

$$P\left(\mathrm{Re}\left[\mathbf{r}(k-1)^H\mathbf{r}(k)e^{j(-2\pi f_d T+\pi/4)}\right]<0\right) = P(\|\mathbf{x}_0\|^2 < \|\mathbf{x}_1\|^2), \tag{5.77}$$

where

$$\begin{aligned}\mathbf{x}_0 &= \mathbf{r}(k) + \mathbf{r}(k-1)e^{j(2\pi f_d T-\pi/4)},\\ \mathbf{x}_1 &= \mathbf{r}(k) - \mathbf{r}(k-1)e^{j(2\pi f_d T-\pi/4)}.\end{aligned} \tag{5.78}$$

Similarly, the second summation term can be expressed as

$$P\left(\mathrm{Re}\left[\mathbf{r}(k-1)^H\mathbf{r}(k)e^{-j(2\pi f_d T+\pi/4)}\right]<0\right) = P(\|\mathbf{x}_0'\|^2 < \|\mathbf{x}_1'\|^2), \tag{5.79}$$

where

$$\begin{aligned}\mathbf{x}_0 &= \mathbf{r}(k) + \mathbf{r}(k-1)e^{j(2\pi f_d T+\pi/4)},\\ \mathbf{x}_1 &= \mathbf{r}(k) - \mathbf{r}(k-1)e^{j(2\pi f_d T+\pi/4)}.\end{aligned} \tag{5.80}$$

Following the approach in 5.1.2, (5.76) is given by

$$P_b = \frac{1}{2}\left[f(A_0, A_1, S_0, S_1) + f(A_0', A_1', S_0', S_1')\right], \tag{5.81}$$

with

$$\begin{aligned}A_0 &= 2LK\gamma_c\frac{(1+\frac{\sqrt{2}}{2})\mu^2 - \sqrt{2}\mu + 1 - \frac{\sqrt{2}}{2}}{C_0},\\ A_1 &= 2LK\gamma_c\frac{(1-\frac{\sqrt{2}}{2})\mu^2 + \sqrt{2}\mu + 1 + \frac{\sqrt{2}}{2}}{C_1},\\ S_0 &= 1 + C_0/C_1,\\ S_1 &= 1 + C_1/C_0,\end{aligned} \tag{5.82}$$

where

$$C_0 = [2\gamma_c(1+\rho\cos(\pi/4-2\pi f_dT))+K+1]\mu^2 - 4\gamma_c\rho\mu\sin(2\pi f_dT+\pi/4) \quad (5.83)$$

$$+ 2\gamma_c(1-\rho\cos(\pi/4-2\pi f_dT))+K+1, \quad (5.84)$$

$$C_1 = [2\gamma_c(1-\rho\cos(\pi/4-2\pi f_dT))+K+1]\mu^2 - 4\gamma_c\rho\mu\sin(2\pi f_dT+\pi/4) \quad (5.85)$$

$$+ 2\gamma_c(1+\rho\cos(\pi/4-2\pi f_dT))+K+1, \quad (5.86)$$

$$\mu = \frac{2\gamma_c+K+1+\sqrt{(2\gamma_c+K+1)^2-[2\gamma_c\rho\sin(\pi/4-2\pi f_dT)]^2}}{2\gamma_c\rho\sin(\pi/4-2\pi f_dT)}, \quad (5.87)$$

and

$$\begin{aligned} A_0' &= 2LK\gamma_c\frac{(1+\frac{\sqrt{2}}{2})\mu'^2+\sqrt{2}\mu'+1-\frac{\sqrt{2}}{2}}{C_0'}, \\ A_1' &= 2LK\gamma_c\frac{(1-\frac{\sqrt{2}}{2})\mu'^2-\sqrt{2}\mu'+1+\frac{\sqrt{2}}{2}}{C_1'}, \\ S_0' &= 1+C_0'/C_1', \\ S_1' &= 1+C_1'/C_0', \end{aligned} \quad (5.88)$$

where

$$C_0' = [2\gamma_c(1+\rho\cos(\pi/4+2\pi f_dT))+K+1]\mu'^2 + 4\gamma_c\rho\mu'\sin(2\pi f_dT+\pi/4) \quad (5.89)$$

$$+ 2\gamma_c(1-\rho\cos(\pi/4+2\pi f_dT))+K+1, \quad (5.90)$$

$$C_1' = [2\gamma_c(1-\rho\cos(\pi/4+2\pi f_dT))+K+1]\mu'^2 + 4\gamma_c\rho\mu'\sin(2\pi f_dT+\pi/4) \quad (5.91)$$

$$+ 2\gamma_c(1+\rho\cos(\pi/4+2\pi f_dT))+K+1, \quad (5.92)$$

$$\mu' = -\frac{2\gamma_c+K+1+\sqrt{(2\gamma_c+K+1)^2-[2\gamma_c\rho\sin(\pi/4+2\pi f_dT)]^2}}{2\gamma_c\rho\sin(\pi/4+2\pi f_dT)}. \quad (5.93)$$

Computation of (5.20) with (5.82) and (5.88) involving only elementary functions is simpler than computation using the Proakis' expression involving special functions.

5.3.3 Numerical Results

The BEP performances of suboptimum and optimum receivers of DBPSK in eq. (5.20) with parameters in (5.73), (5.74), (5.82) and (5.88) involve only elementary functions. Therefore, they are simpler than the Proakis' expression which involve

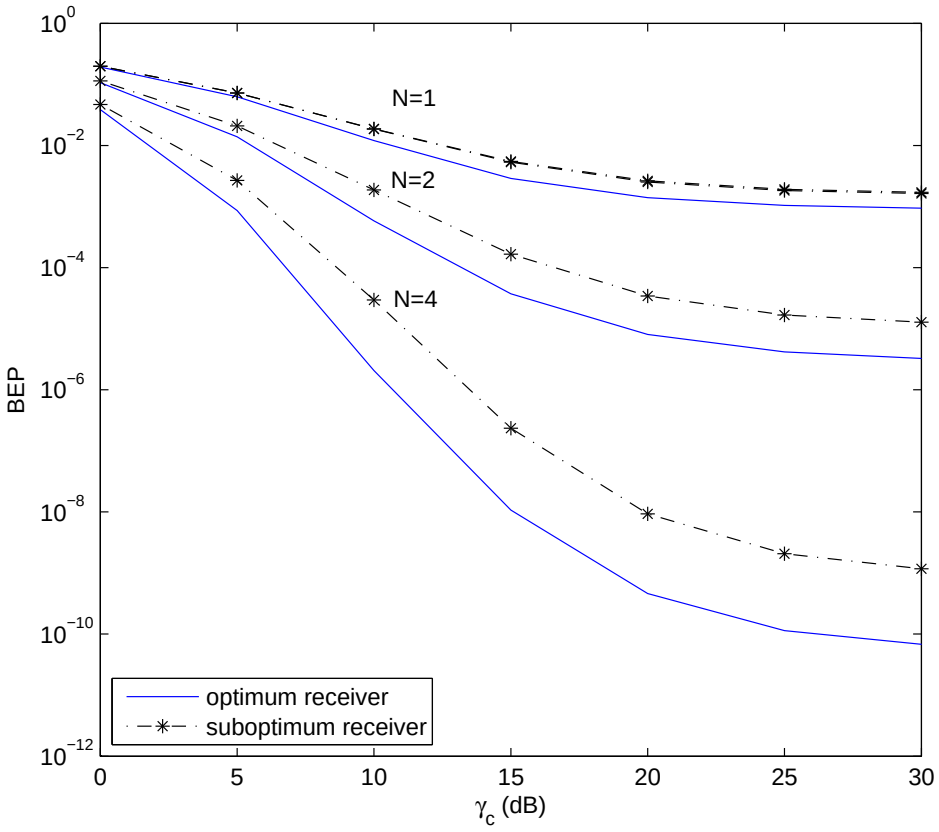

Figure 5.2: BEP performance comparison between QDPSK optimum and suboptimum receivers over fast Rician fading with Doppler shift and diversity reception.

the generalized Marcum Q-function and the modified Bessel function of the first kind.

Numerical results for QDPSK with $K = 5$, $f_dT = 0.03$, $f_dT = 0.05$ are shown in Fig. 5.1. Our expression matches perfectly with the Proakis' expression numerically, therefore, only one curve for each receiver is shown here. The gap between optimum and suboptimum QDPSK receivers is much larger than that for BDPSK. It shows that QDPSK is more susceptible to Doppler shift.

5.4 Conclusions

In this chapter, we obtained an exact expression for the error probability of a general quadratic receiver. The expression is in the form of a series summation involving only rational functions and exponential functions. Our expression is simpler than the Proakis' expression which involves the generalized Marcum Q-function and the modified Bessel function of the first kind. We apply our expression and obtain exact BEP performances of suboptimum and optimum BDPSK and QDPSK receivers over fast Rician fading with Doppler shift. Numerical results show that QDPSK is more susceptible to Doppler shift than BDPSK.

Chapter 6

Outage Probability over Fading Channels

Automatic repeat request (ARQ) is widely applied in packet transmission to achieve high reliability by using an error detecting code together with packet retransmission. It is originally designed for the additive white Gaussian noise (AWGN) channel, where the channel is time invariant, based on average performance measures. The commonly used average reliability performance measure for ARQ schemes is (average) accepted packet error probability (AAPEP) [39, 40]. It is defined as the packet error probability among all accepted packets. For transmission over a multipath fading channel, a signal is perturbed by a time-varying multiplicative complex fading gain in addition to AWGN. AAPEP is computed by considering packets that experience all channel conditions and takes an average over the channel fading distribution. In the averaging process, instantaneous information is no longer preserved. For example, in high data rate communication, a single fade may last over the duration of a large number of consecutive bits and may cause the loss of these data. In a network scenario, it would result in poor upper layer performance [38]. However, the average performance may still be good if the instantaneous performance in good channel conditions outweighs that in poor channel conditions. Hence, average performance measures are not adequate in providing a satisfactory

quality of service (QoS) for small-scale time-varying fading.

References [41–43] use the PEO probability as the performance measure for log-normal shadowing channels. This PEO probability is the probability that the average packet error probability (instantaneous packet error probability averaged over the fading gain distribution) exceeds an APEP threshold. Thus, this PEO probability is calculated using the statistical distribution of the shadowing parameter. Hence, [41–43] address the system outage caused by the shadowing effect which occurs over a large number of measurement locations [44].

A more meaningful performance measure for high data rate packet transmission or bursty transmission with ARQ over time-varying fading is instantaneous accepted packet error outage (IAPEO) probability. We first define a maximum tolerable IAPEP threshold, above which all accepted packets are considered unreliable. The IAPEO probability is the probability that the IAPEP exceeds the IAPEP threshold. It is more meaningful than AAPEP, as it reflects, in the long term, how often reliable transmission fails.

In order to compute IAPEO, we need to start at the bit level. We proposed to use the instantaneous bit error outage (IBEO) probability as a long-term performance measure for high data rate symbol-by-symbol transmission over time-varying fading, whereas the short-term performance measure is the IBEP. We first define a maximum tolerable IBEP threshold, above which all the data transmitted are considered lost or unreliable. The IBEO probability is the probability that the IBEP exceeds the IBEP threshold. As data are usually transmitted in packets, we extend the outage concept to packet transmission and propose instantaneous packet error probability (IPEP) and the IPEO probability in a similar manner as short-term and long-term performance measures for packet transmission.

For a given modulation scheme, the IBEO probability is mathematically equivalent to the probability that the instantaneous SNR falls below an SNR threshold required for the system to operate [48, chap.1]. However, if the SNR

outage probability is used as a performance measure, the SNR threshold values for different modulation schemes should be different. The IBEO probability uses the same IBEP threshold regardless of modulation scheme used, and, therefore, is a fair performance measure. The IBEO probability is also mathematically equivalent to the capacity outage probability [49] defined as the probability that the transmission rate is above the error-free Shannon capacity [50]. In practice, even when a system transmits at a rate below the Shannon capacity using a capacity achieving code, it still makes decision errors and the error performance is not related to the capacity outage probability. We want to analyze the outage performance of a specific practical system. Therefore, the capacity outage probability is not useful in our analysis.

We consider receiver with imperfect CSI in Rayleigh fading channels. Closed-form expressions and bounds on the IBEO/IPEO probabilities are obtained as functions of the channel estimation mean square error (MSE). It turns out that the IBEO/IPEO performance with imperfect CSI differs significantly from that of perfect CSI, in that the outage performance deteriorates rapidly with MSE, when MSE is above a certain value, which is determined partly by the IBEP/IPEP threshold chosen. We show that the system must operate above a minimum SNR in order to satisfy a design requirement of maximum tolerable IBEO/IPEO probability. We then obtain the optimum energy allocation between pilots and data that minimizes the outage performance. It is shown that a small fraction of the total energy, must always be dedicated to pilots to perform channel estimation. At the same time, the optimum pilot energy never exceeds half the total energy.

This chapter is organized as follows. In Section 6.1, we first list the upper and lower bounds on the erfc function and the inverse erfc function to be used in the outage performance analysis. In Section 6.2, the system model and channel estimation method are described. In Section 6.3, the IBEO/IPEO probabilities are analyzed. In Section 6.4, the optimum energy allocation solution that minimizes the outage performance is obtained. Conclusions are made in Section 6.5.

6.1 The erfc Function and Inverse erfc Function

The complementary error function, i.e. erfc, and its inverse function, erfc^{-1}, are used in our outage performance analysis. As both functions are not in closed form, further analysis involving the two functions are not trivial. Therefore, we first derive in this section, bounds and approximations that can be used in the outage performance analysis.

The erfc function is usually defined as [8, eq.(2-1-95)]

$$\text{erfc}(x) = \frac{2}{\sqrt{\pi}} \int_x^\infty \exp(-t^2) dt, \tag{6.1}$$

or in the Craig's form as [15, eq.(10)]

$$\text{erfc}(x) = \frac{2}{\pi} \int_0^{\pi/2} \exp\left(-\frac{x^2}{\sin^2\theta}\right) d\theta. \tag{6.2}$$

It is related to the Gaussian Q-function as

$$\text{erfc}(x) = 2Q(\sqrt{2}x). \tag{6.3}$$

We summarized in Chapter 3 many closed-form bounds on the Gaussian Q-functions and derived new lower bounds. However, only a few of them are invertible. The simplest bound is the single-term Chernoff bound

$$\text{erfc}(x) < \exp(-x^2). \tag{6.4}$$

The two-term Chiani upper bound (3.21)

$$\text{erfc}(x) < \frac{1}{2}\exp\left(-x^2\right) + \frac{1}{2}\exp\left(-2x^2\right), \tag{6.5}$$

is tighter than the Chernoff bound. We obtained a single-term lower bound in (3.52)

$$\text{erfc}(x) > \frac{1}{2}\exp\left(-\frac{4}{\pi}x^2\right). \tag{6.6}$$

We obtained the tighter two-term lower bound in (3.52)

$$\text{erfc}(x) > \frac{1}{3}\exp\left(-\frac{2\sqrt{3}}{\pi}x^2\right) + \frac{1}{3}\exp\left(-\frac{4\sqrt{3}}{\pi}x^2\right). \tag{6.7}$$

The inverse erfc function is required in calculating the outage probabilities. However, the two expressions of the erfc function in (6.1) and (6.2) are both not invertible. The inverse erfc function can be computed numerically in MATLAB using the function erfcinv. Alternatively, invertible bounds on the erfc function can be used to obtain closed-form bounds on the inverse erfc function. The Chernoff bound in (6.4) gives us the widely used upper bound

$$\text{erfc}^{-1}(x) < \sqrt{-\ln x}. \tag{6.8}$$

Using the tighter upper bound in (6.5), we obtain a closed-form upper bound on $\text{erfc}^{-1}(x)$ as

$$\text{erfc}^{-1}(x) < \sqrt{\ln\left(\frac{\sqrt{8x+1}+1}{4x}\right)}. \tag{6.9}$$

It is much tighter than the upper bound in (6.8). Similarly, using the lower bound in (6.6), we obtain a closed-form lower bound

$$\text{erfc}^{-1}(x) > \sqrt{-\frac{\pi}{4}\ln(2x)}. \tag{6.10}$$

Using the tighter lower bound in (6.7), we obtain a tighter closed-form lower bound

$$\text{erfc}^{-1}(x) > \sqrt{\frac{\sqrt{3}\pi}{6}\ln\left(\frac{\sqrt{12x+1}+1}{6x}\right)}. \tag{6.11}$$

Figure 6.1 shows that the upper bound in (6.9) is much tighter than the upper bound in (6.8), and the lower bound in (6.11) is much tighter than the lower bound in (6.10).

6.2 System Description

We consider transmission using BPSK or QPSK signals over a single-input-single-output wireless channel corrupted by Rayleigh fading and AWGN. The binary message sequence is first broken up into groups of m information bits. Each group of m information bits is encoded by a binary (n, m)

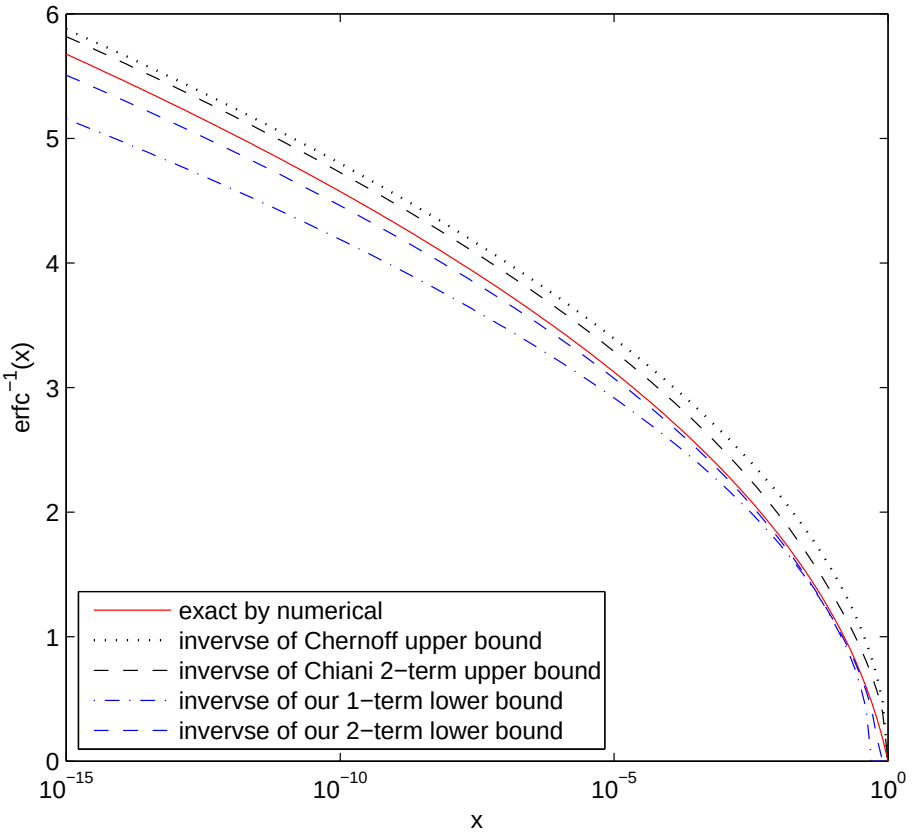

Figure 6.1: Upper and lower bounds on the inverse erfc function.

linear block code into n bits. Each group of n coded bits is prefixed by p pilot bits for channel estimation. The uncoded case is a special case of the general coded case by letting $n = m$. It is assumed that the p pilots bits are transmitted by BPSK modulation, while the n coded bits are modulated by either BPSK or QPSK.

The fading gain is assumed static over the duration of a packet. The received signal over the k-th symbol interval $[kT, (k+1)T)$, where T is the symbol duration, is given by

$$\begin{aligned} r_p(k) &= \sqrt{E_p}h + n(k), \qquad k = 1, ..., p, \\ r_d(k) &= \sqrt{E_d}e^{j\phi(k)}h + n(k), \quad k = p+1, ..., p + n/\log_2 M. \end{aligned} \tag{6.12}$$

Note that, as the symbol duration T is identical for BPSK and QPSK, the

transmission rate of QPSK is double that of BPSK. In (6.12), E_p and E_d are energy per transmitted pilot symbol and coded data symbol, respectively. M is the constellation size. We have $M = 2$ for BPSK and $M = 4$ for QPSK. For BPSK, we have

$$\phi(k) = \begin{cases} 0, & \text{bit } 0 \\ \pi, & \text{bit } 1 \end{cases} \tag{6.13}$$

and for Gray-coded QPSK,

$$\phi(k) = \begin{cases} 0, & \text{symbol 0 bits 00} \\ \frac{\pi}{2}, & \text{symbol 1 bits 01} \\ \pi, & \text{symbol 3 bits 11} \\ \frac{3\pi}{2}, & \text{symbol 2 bits 10} \end{cases} \tag{6.14}$$

The fading gain h is a complex Gaussian random variable with mean zero and variance $E[|h|^2] = 2\sigma^2$. The complex AWGN $\{n(k)\}_k$ are i.i.d. complex Gaussian random variables with mean zero and variance $E[|n(k)|^2] = N_0$. The noises $\{n(k)\}_k$ are independent of the fading gain h.

The effective SNR per information bit is defined as

$$\bar{\gamma} = \frac{2\sigma^2 E_b}{N_0}, \tag{6.15}$$

where the effective energy per information bit is given by

$$E_b = \frac{pE_p + n\frac{E_d}{\log_2 M}}{m}. \tag{6.16}$$

The increase in energy due to pilot insertion and coding redundancy is accounted for in E_b. As analysis later shows that the error outage performance in the presence of channel estimation error depends only on the normalized total pilot energy instead of the individual values of E_b or p, we define here the parameter ε as the fraction of total pilot energy normalized with respect to the total packet energy, i.e.

$$\varepsilon = \frac{pE_p}{pE_p + n\frac{E_d}{\log_2 M}}. \tag{6.17}$$

The minimum mean square error (MMSE) channel estimate $\hat{h}$ for one packet is given by [40]

$$\hat{h} = \sum_{i=1}^{p} w_o(i) r_p(i), \tag{6.18}$$

where we have

$$w_o(i) = \frac{2\sigma^2\sqrt{E_p}}{2\sigma^2 p E_p + N_0}, i = 1, ..., p \tag{6.19}$$

for blockwise static fading. The channel estimation MSE is given by

$$2V^2 = \frac{2\sigma^2 N_0}{2\sigma^2 p E_p + N_0} = 2\sigma^2 \frac{1}{\varepsilon m \bar{\gamma} + 1}. \tag{6.20}$$

The channel estimate $\hat{h}$ is a complex Gaussian random variable with mean zero and variance [76, eq.(2.48)]

$$2\hat{\sigma}^2 = 2(\sigma^2 - V^2) = \frac{(2\sigma^2)^2 p E_p}{2\sigma^2 p E_p + N_0} = 2\sigma^2 \frac{\varepsilon m \bar{\gamma}}{\varepsilon m \bar{\gamma} + 1}. \tag{6.21}$$

Hence, $x = |\hat{h}|^2$ is exponentially distributed with the PDF

$$p_x(x) = \frac{1}{2\hat{\sigma}^2} \exp\big(-\frac{x}{2\hat{\sigma}^2}\big) u(x), \tag{6.22}$$

where $u(x)$ is the unit step function, and $2\hat{\sigma}^2$ is given in (6.21).

In the special case of PCSI, we have

$$2V^2 = 0. \tag{6.23}$$

Substituting (6.23), (6.21) simplifies to

$$2\hat{\sigma}^2 = 2\sigma^2. \tag{6.24}$$

6.3 Instantaneous Error Outage Probability Analysis

Instantaneous error outage can be defined at bit level or packet level, depending on system design requirements.

6.3.1 Instantaneous Bit Error Outage Probability of BPSK and QPSK

We derive here the probability that the IBEP exceeds an IBEP threshold value. Assume that at the kth data symbol interval, the estimate of the channel gain h obtained by the MMSE channel estimator, is $\hat{h}$. Assume that the bit 0 is sent. Let e_b define the event that the detected bit contains an error. The IBEP conditioned on the channel estimate $\hat{h}$, i.e. $P(e_b|\hat{h})$, is given by [2, Appendix III]

$$\begin{aligned} P(e_b|\hat{h}) &= P\left(\mathrm{Re}[r_d(k)\hat{h}^* e^{-j\alpha}] < 0 \big| \phi(k) = 0, \hat{h}\right) \\ &= \frac{1}{2}\mathrm{erfc}\left(\sqrt{\frac{E_d \cos^2\alpha |\hat{h}|^2}{2E_d V^2 + N_0}}\right), \end{aligned} \tag{6.25}$$

where

$$\alpha = \begin{cases} 0, & \text{BPSK} \\ \pi/4, & \text{QPSK} \end{cases} \tag{6.26}$$

Assume that the IBEP threshold value is $P_{\text{IBEP}}^{\text{TH}}$. The instantaneous bit error outage (IBEO) probability, P_{IBEO}, is the probability that the IBEP exceeds $P_{\text{IBEP}}^{\text{TH}}$, i.e.

$$P_{\text{IBEO}} = P\left(P(e_b|\hat{h}) > P_{\text{IBEP}}^{\text{TH}}\right). \tag{6.27}$$

Substituting (6.25) into (6.27), P_{IBEO} can be simplified to

$$P_{\text{IBEO}} = P\left(x = |\hat{h}|^2 < \frac{\left[\mathrm{erfc}^{-1}(2P_{\text{IBEP}}^{\text{TH}})\right]^2}{c}\right) \tag{6.28}$$

where

$$c = \frac{E_d \cos^2\alpha}{2E_d V^2 + N_0}. \tag{6.29}$$

Here, the PDF of x is given in (6.22). The IBEO probability in (6.28) is in a form similar to the outage probability in diversity combining systems, which is defined as the probability that the combined instantaneous SNR at the receiver falls below a

certain SNR threshold [48, chap.1]. The latter is evaluated by integrating the SNR PDF over SNR values below the SNR threshold. Similarly, P_{IBEO} can be evaluated using the distribution of x in (6.22). Letting

$$b = \frac{1}{2\hat{\sigma}^2} = \frac{1}{2\sigma^2 - 2V^2}, \tag{6.30}$$

(6.28) simplifies to

$$P_{\text{IBEO}} = \int_{-\infty}^{\frac{\left[\text{erfc}^{-1}(2P_{\text{IBEP}}^{\text{TH}})\right]^2}{c}} p_x(x)dx = 1 - \exp(-y), \tag{6.31}$$

where

$$\begin{aligned} y &= \left[\text{erfc}^{-1}(2P_{\text{IBEP}}^{\text{TH}})\right]^2 \frac{b}{c}, \\ \frac{b}{c} &= \frac{2E_d V^2 + N_0}{2(\sigma^2 - V^2)E_d \cos^2\alpha}. \end{aligned} \tag{6.32}$$

Using the upper and lower bounds on the inverse erfc functions in (6.8), (6.9) and (6.11), (6.31) is upper bounded as

$$\begin{aligned} P_{\text{IBEO}} &\leq 1 - \left(\frac{\sqrt{16P_{\text{IBEP}}^{\text{TH}} + 1} + 1}{8P_{\text{IBEP}}^{\text{TH}}}\right)^{-b/c} \\ &\leq 1 - \left(2P_{\text{IBEP}}^{\text{TH}}\right)^{b/c} \end{aligned} \tag{6.33}$$

and lower bounded as

$$P_{\text{IBEO}} \geq 1 - \left(\frac{\sqrt{24P_{\text{IBEP}}^{\text{TH}} + 1} + 1}{12P_{\text{IBEP}}^{\text{TH}}}\right)^{-\frac{\sqrt{3}\pi}{6}\frac{b}{c}}. \tag{6.34}$$

We can show that (6.31) is a monotonically decreasing function of the channel estimation MSE $2V^2$. However, given a specific channel estimation method, e.g. MMSE, we cannot reduce MSE freely, as $2V^2$ and E_d are related if the total energy per packet is fixed. Substituting (6.17), (6.20) and (6.21), (6.32) becomes

$$\begin{aligned} y &= \frac{\left[\text{erfc}^{-1}(2P_{\text{IBEP}}^{\text{TH}})\right]^2}{\cos^2\alpha} \frac{(1-\varepsilon)m\log_2 M\bar{\gamma} + \varepsilon mn\bar{\gamma} + n}{(1-\varepsilon)\varepsilon m^2 \log_2 M\bar{\gamma}^2} \\ &= \begin{cases} \left[\text{erfc}^{-1}(2P_{\text{IBEP}}^{\text{TH}})\right]^2 \dfrac{(n-1)\varepsilon m\bar{\gamma} + m\bar{\gamma} + n}{(1-\varepsilon)\varepsilon m^2\bar{\gamma}^2}, & \text{BPSK} \\ \left[\text{erfc}^{-1}(2P_{\text{IBEP}}^{\text{TH}})\right]^2 \dfrac{(n-2)\varepsilon m\bar{\gamma} + 2m\bar{\gamma} + n}{(1-\varepsilon)\varepsilon m^2\bar{\gamma}^2}, & \text{QPSK} \end{cases} \end{aligned} \tag{6.35}$$

Hence, BPSK and QPSK with channel estimation have different IBEP and different IBEO probabilities.

For the special case of PCSI at the receiver, by letting $2V^2 = 0$ in (6.32), (6.31) reduces to

$$P_{\text{IBEO}} = 1 - \exp\left(- \left[\text{erfc}^{-1}(2P_{\text{IBEP}}^{\text{TH}})\right]^2 \frac{n}{(1-\varepsilon)m\bar{\gamma}} \right), \tag{6.36}$$

which is identical for BPSK and QPSK.

In a practical QoS specification, we may require that, in the long term, the fraction of all bits received that have IBEP greater than $P_{\text{IBEP}}^{\text{TH}}$ be no more than a threshold $P_{\text{IBEO}}^{\text{TH}}$. As the explicit expression of the IBEO probability is a function of the SNR, it is easy to show that the minimum SNR $\bar{\gamma}_b^{\text{TH}}$ that satisfies the IBEO threshold requirement, is given by

$$\bar{\gamma}_b^{\text{TH}} = \frac{\sqrt{[(n-1)\varepsilon + 1]^2 + 4dn(1-\varepsilon)\varepsilon} + (n-1)\varepsilon + 1}{2dm(1-\varepsilon)\varepsilon} \tag{6.37}$$

for BPSK, and

$$\bar{\gamma}_b^{\text{TH}} = \frac{\sqrt{[(n-2)\varepsilon + 2]^2 + 4dn(1-\varepsilon)\varepsilon} + (n-2)\varepsilon + 2}{2dm(1-\varepsilon)\varepsilon}, \tag{6.38}$$

for QPSK, where for both cases

$$d = -\frac{\ln(1 - P_{\text{IBEO}}^{\text{TH}})}{\left[\text{erfc}^{-1}(2P_{\text{IBEP}}^{\text{TH}})\right]^2} > 0. \tag{6.39}$$

For the special case of PCSI at the receiver with $2V^2 = 0$, (6.37) and (6.38) both reduce to

$$\bar{\gamma}_b^{\text{TH}} = \frac{n}{dm(1-\varepsilon)}, \tag{6.40}$$

which is identical for BPSK and QPSK.

6.3.2 Instantaneous Packet Error Outage Probability

Data are often transmitted, detected and retransmitted in the form of packets, instead of individual bits or symbols, e.g. in an ARQ scheme. Therefore, one may be more interested in the packet error performance. Thus, we extend the idea of IBEO probability to packet error performance, and propose the IPEO probability as a packet level QoS measure.

Uncoded Case

For uncoded transmissions, we have $n = m$. Let e_p define the event that the received packet contains one or more bit errors. The IPEP conditioned on the channel estimate $\hat{h}$ is given by

$$P(e_p|\hat{h}) = 1 - \left[1 - P(e_b|\hat{h})\right]^n, \tag{6.41}$$

where the IBEP $P(e_b|\hat{h})$ is given in (6.25). Similar to the IBEO probability , the IPEO probability represents the fraction of packets that has the IPEP exceeding an IPEP threshold $P_{\text{IPEP}}^{\text{TH}}$, i.e.

$$P_{\text{IPEO}} = P\left(P(e_p|\hat{h}) > P_{\text{IPEP}}^{\text{TH}}\right). \tag{6.42}$$

Substituting (6.41) into (6.42), P_{IPEO} can be shown equivalent to the IBEO probability $P(e_b|\hat{h}) > P_{\text{IBEP}}^{\text{TH}})$ with

$$P_{\text{IBEP}}^{\text{TH}} = 1 - \left(1 - P_{\text{IPEP}}^{\text{TH}}\right)^{1/n}. \tag{6.43}$$

Hence, the IPEO probability of BPSK or QPSK is given by (6.31) with (6.32) or (6.35) using $P_{\text{IBEP}}^{\text{TH}}$ in (6.43). Similarly, the minimum required SNR $\bar{\gamma}_p^{\text{TH}}$ that satisfies the IPEO requirement of $P_{\text{IPEO}} < P_{\text{IPEO}}^{\text{TH}}$ for BPSK and QPSK are given by (6.37) and (6.38) with (6.39), respectively, by using $P_{\text{IBEP}}^{\text{TH}}$ in (6.43) and replacing $P_{\text{IBEO}}^{\text{TH}}$ with $P_{\text{IPEO}}^{\text{TH}}$.

Error Detection Coded Case

We now consider the case of error-detection-coded packet transmissions. Let e_u define the event that the received packet contains an undetectable error pattern. The IPEP of a coded packet is defined as the conditional undetectable error probability $P(e_u|\hat{h})$. The IPEO probability is the probability that $P(e_u|\hat{h})$ exceeds an IPEP threshold. As the weight distributions for many codes are still unknown, it is difficult to compute the exact $P(e_u|\hat{h})$. However, we can use the following general upper bound for linear block codes [39, eq.(3.42)]

$$P(e_u|\hat{h}) \leq 2^{-(n-m)} P(e_p|\hat{h}). \tag{6.44}$$

Thus, the IPEO probability is upper bounded as

$$P_{\text{IPEO}} < P_{\text{IPEO}}^{\text{UB}} = P\left(P^{\text{UB}}(e_u|\hat{h}) > P_{\text{IPEP}}^{\text{TH}}\right). \tag{6.45}$$

Substituting (6.41) and (6.44) into (6.45), the IPEO upper bound is simplified to

$$P_{\text{IPEO}}^{\text{UB}} = P\left(P(e_b|\hat{h}) > P_{\text{IBEP}}^{\text{TH}}\right), \tag{6.46}$$

with

$$P_{\text{IBEP}}^{\text{TH}} = 1 - \left[1 - 2^{-(n-m)} P_{\text{IPEP}}^{\text{TH}}\right]^{1/n}, \tag{6.47}$$

which is equivalent to an IBEO probability. Therefore, the IPEO upper bound for BPSK and QPSK is given by (6.31) with (6.32) or (6.35) using $P_{\text{IBEP}}^{\text{TH}}$ in (6.47).

By setting the upper bound $P_{\text{IPEO}}^{\text{UB}} < P_{\text{IPEO}}^{\text{TH}}$, we can ensure that the exact IPEO performance satisfies the threshold requirement $P_{\text{IPEO}}^{\text{TH}}$, as

$$P_{\text{IPEO}} < P_{\text{IPEO}}^{\text{UB}} < P_{\text{IPEO}}^{\text{TH}}. \tag{6.48}$$

Thus, we can obtain an upper bound of the minimum required SNR $\bar{\gamma}_p^{\text{TH}}$, i.e. $\bar{\gamma}_p^{\text{TH,UB}}$, using results in Section 6.3.1. The $\bar{\gamma}_p^{\text{TH,UB}}$ for BPSK and QPSK are given by (6.37) and (6.38) with (6.39), respectively, by using $P_{\text{IBEP}}^{\text{TH}}$ in (6.47) and replacing $P_{\text{IBEO}}^{\text{TH}}$ with $P_{\text{IPEO}}^{\text{TH}}$.

Note that by letting $n = m$, the error-detection-coded transmission reduces to the uncoded transmission. The IPEP and IPEO expressions reduce to those of the uncoded transmission.

6.3.3 Numerical Results

It is shown in (6.35) and (6.36) that the IBEO probability depends only on the normalized total pilot energy ε, instead of the individual values of E_p or p. So, without loss of generality, we use a pilot length of $p = 5$ here. We analyze in this section the case of equal energy per transmitted bit where

$$E_p = \frac{E_d}{\log_2 M}, \tag{6.49}$$

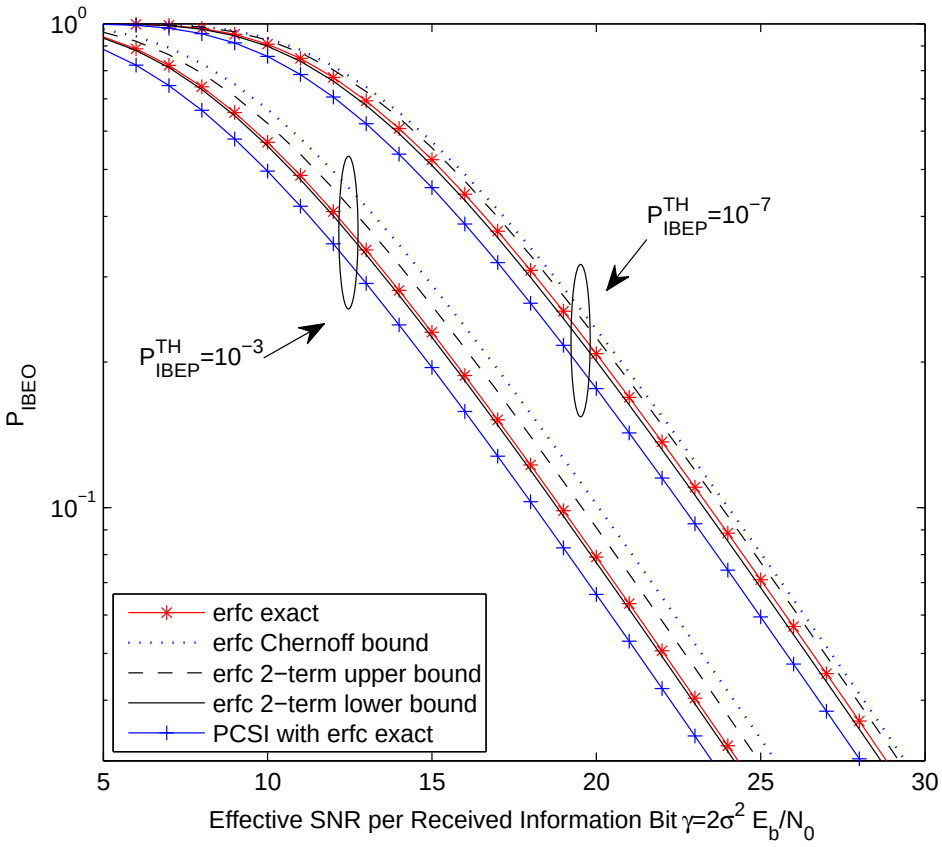

Figure 6.2: IBEO v.s. effective SNR $\bar{\gamma}$ for BPSK with $p = 5, m = 23, n = 28$.

and, hence,

$$\varepsilon_{eq} = \frac{p}{p+n}. \tag{6.50}$$

The IBEO probabilities of BPSK and QPSK with equal energy per transmitted bit are shown in Fig. 6.2 and Fig. 6.3, respectively. The upper bounds in (6.8) and (6.9) and the lower bound in (6.11) on the inverse erfc function are used to compute upper and lower bounds on the IBEO probability with imperfect CSI in (6.31) with (6.35) and the IBEO probability with PCSI in (6.36). The exact IBEO curves are computed numerically using the erfcinv function in MATLAB. The Chernoff bound leads to a simple IBEO probability upper bound expression, but the bound is quite

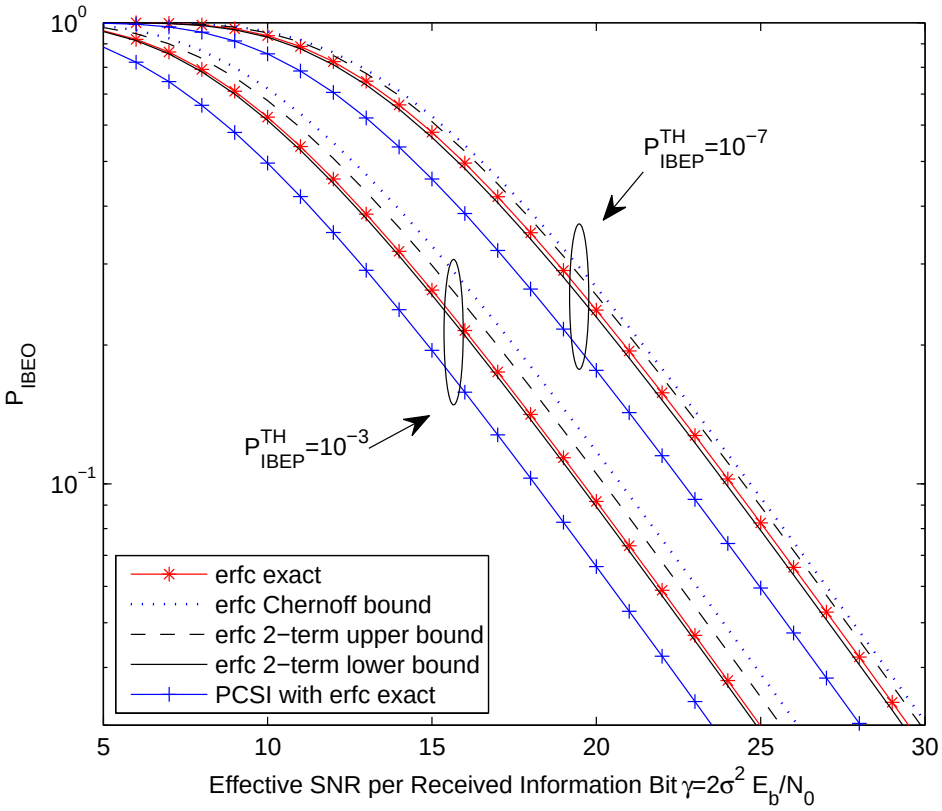

Figure 6.3: IBEO v.s. effective SNR $\bar{\gamma}$ for QPSK with $p = 5, m = 23, n = 28$.

loose for both BPSK and QPSK. The two-term Chiani exponential upper bound and our two-term exponential lower bound result in tighter closed-form upper and lower bounds on the IBEO probability. The upper and lower IBEO bounds differ less than 1dB and, therefore, serve as good indicators of the exact IBEO probability, when the exact inverse erfc function is not available. The IBEO performance loss due to imperfect CSI is about 1dB in SNR for BPSK, and about 1.5dB for QPSK. This shows that QPSK is more susceptible to channel estimation errors. The performance loss due to imperfect CSI is not affected by the IBEP threshold $P^{\text{TH}}_{\text{IBEP}}$.

The IBEO probabilities of BPSK and QPSK as a function of normalized channel estimation MSE are shown in Fig. 6.4 and Fig. 6.5, respectively. As expected, the upper and lower bounds are quite tight. When the MSE is above a critical value of about 10^{-2}, the IBEO performance saturates. When the MSE is below

the critical value, the IBEO performance improves fast with decreasing MSE. The MSE critical value corresponds to an SNR critical value of about 10dB in Fig. 6.2 and Fig. 6.3. The exact critical values, however, are affected by $P_{\mathrm{IBEP}}^{\mathrm{TH}}$. A smaller $P_{\mathrm{IBEP}}^{\mathrm{TH}}$ corresponds to a smaller MSE critical value, and a higher SNR critical value. As QPSK is more susceptible to channel estimation errors than BPSK, the IBEO probability of QPSK is higher than that of BPSK, given the same MSE.

Fig. 6.6 and Fig. 6.7 show the minimum SNR required $\bar{\gamma}_b^{\mathrm{TH}}$ as functions of the two system design parameters $P_{\mathrm{IBEP}}^{\mathrm{TH}}$ and $P_{\mathrm{IBEO}}^{\mathrm{TH}}$ for BPSK and QPSK, respectively. As the IBEP and the IBEO probability represent short-term and long-term reliability respectively, it is expected that a higher SNR is required to meet higher reliability requirements. Hence, the smaller the values of $P_{\mathrm{IBEP}}^{\mathrm{TH}}$ and $P_{\mathrm{IBEO}}^{\mathrm{TH}}$, the higher the required SNR to meet the requirements. QPSK requires a higher SNR than BPSK to achieve the same IBEO performance as it is more susceptible to channel estimation errors.

Fig. 6.8 and Fig. 6.9 show the maximum channel estimation MSE as functions of the two system design parameters $P_{\mathrm{IBEP}}^{\mathrm{TH}}$ and $P_{\mathrm{IBEO}}^{\mathrm{TH}}$ for BPSK and QPSK, respectively. The maximum allowed MSE deteriorates rapidly when $P_{\mathrm{IBEP}}^{\mathrm{TH}}$ or $P_{\mathrm{IBEO}}^{\mathrm{TH}}$ is large. Therefore, in order to keep the MSE below the above-mentioned MSE critical value, values of $P_{\mathrm{IBEP}}^{\mathrm{TH}}$ and $P_{\mathrm{IBEO}}^{\mathrm{TH}}$ should be properly chosen to be small. Again, as QPSK is more susceptible to channel estimation errors than BPSK, in order to achieve the same performance as BPSK, QPSK requires a smaller MSE.

Due to the equivalence of the IPEO probability to the IBEO probability, the IPEO performance and the effect of imperfect CSI on them is similar to the IBEO of symbol-by-symbol transmission, and therefore, is not repeated here.

6.4 Optimum Pilot Energy Allocation

It is well-known that the accuracy of channel estimation can be improved by using more energy on pilots. However, given fixed total transmission energy, an increase in pilot energy effectively reduces the energy available for data transmission. This,

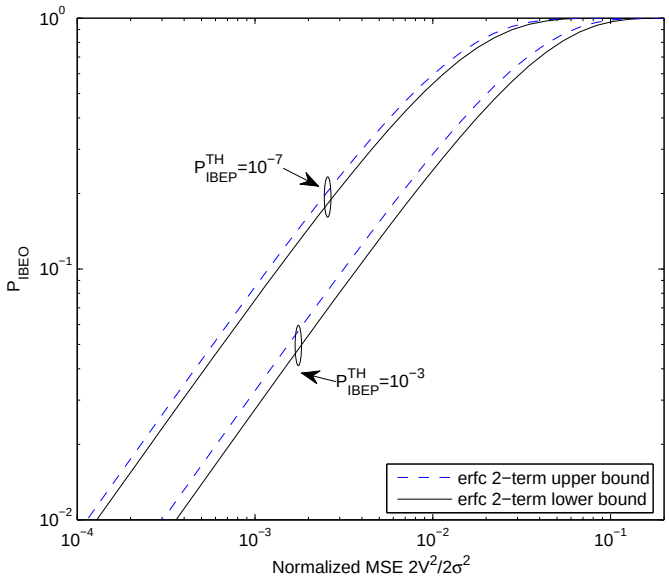

Figure 6.4: IBEO v.s. normalized MSE for BPSK with $p = 5, m = 23, n = 28$.

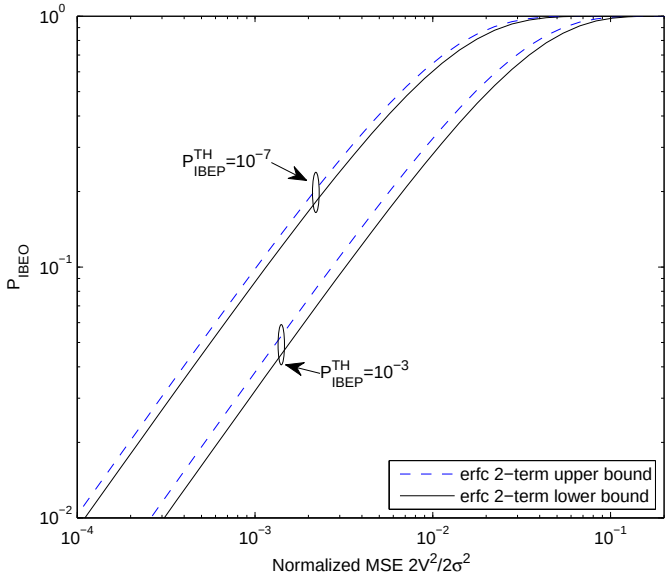

Figure 6.5: IBEO v.s. normalized MSE for QPSK with $p = 5, m = 23, n = 28$.

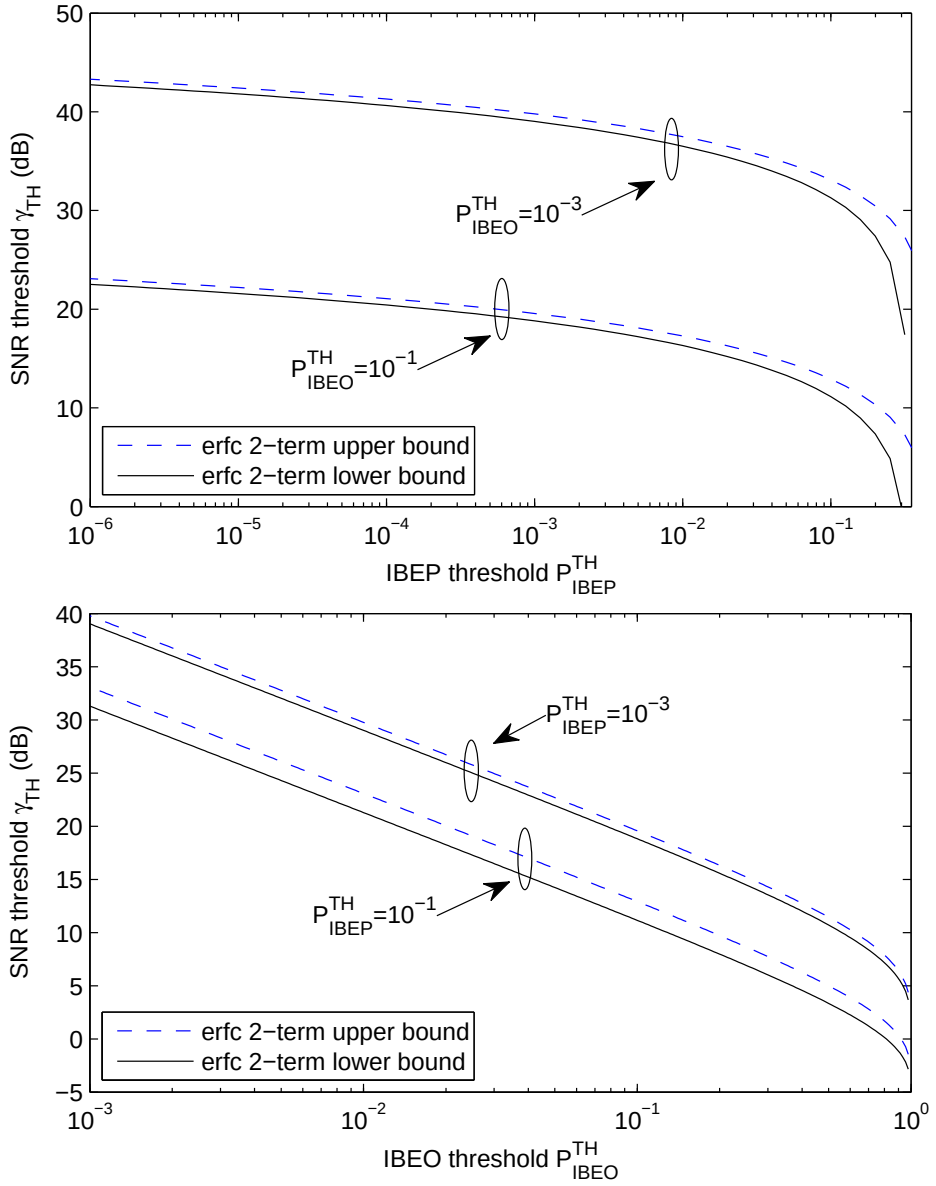

Figure 6.6: Minimum SNR $\bar{\gamma}_b^{TH}$ v.s. system design parameters $P^{\mathbf{TH}}_{\mathbf{IBEP}}$ and $P^{\mathbf{TH}}_{\mathbf{IBEO}}$ for BPSK with $p = 5, m = 23, n = 28$.

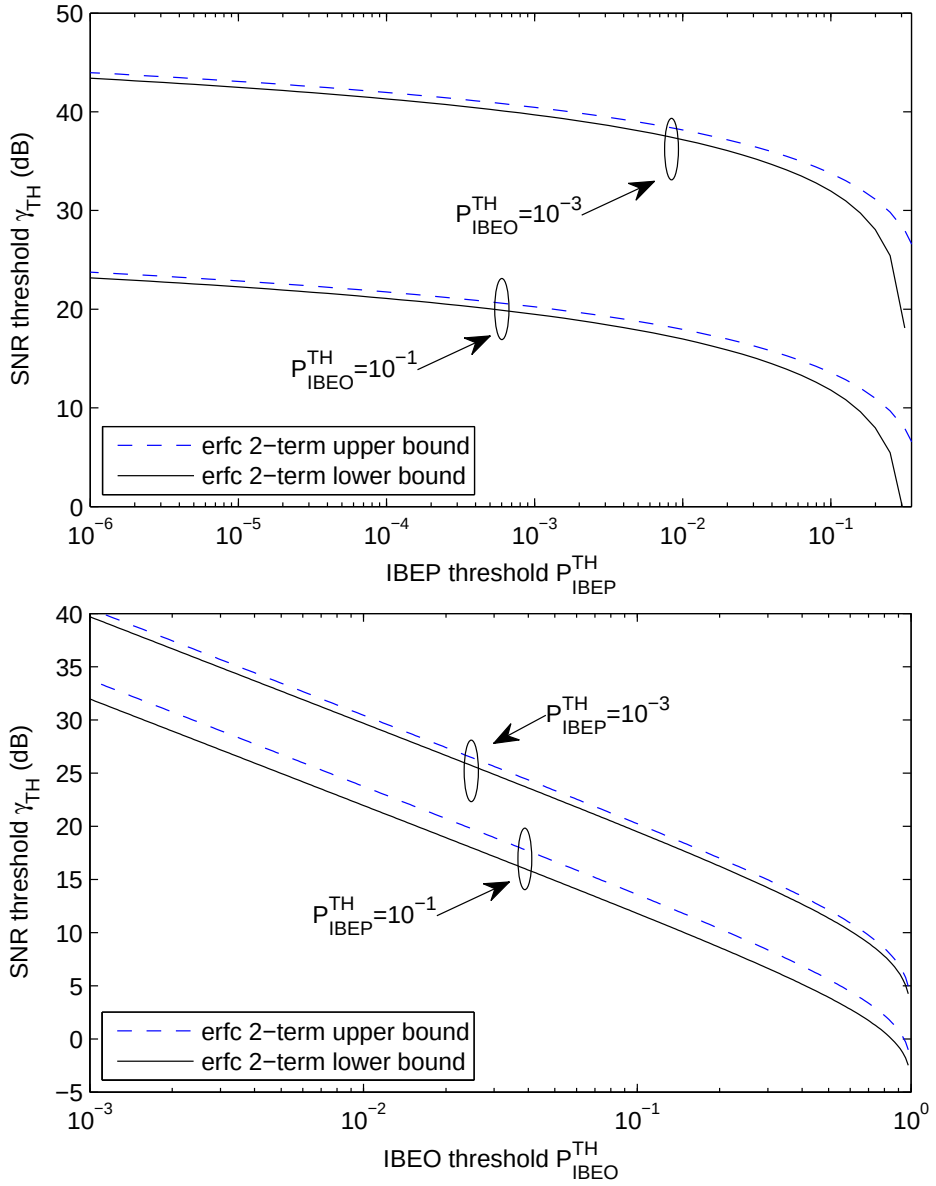

Figure 6.7: Minimum SNR $\bar{\gamma}_b^{TH}$ v.s. system design parameters $P^{\mathbf{TH}}_{\mathbf{IBEP}}$ and $P^{\mathbf{TH}}_{\mathbf{IBEO}}$ for QPSK with $p = 5, m = 23, n = 28$.

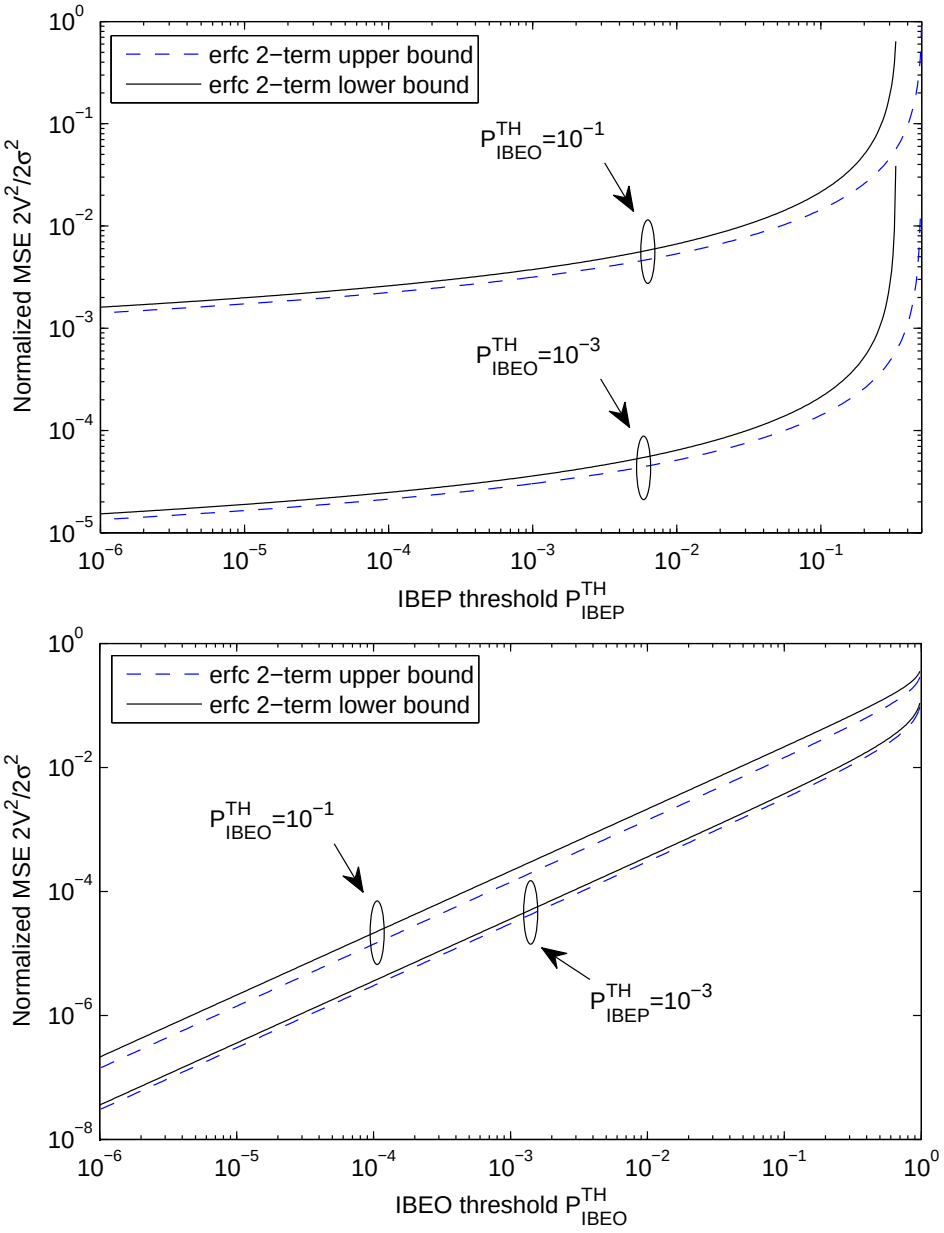

Figure 6.8: Maximum MSE allowed v.s. system design parameters $P^{\mathbf{TH}}_{\mathbf{IBEP}}$ and $P^{\mathbf{TH}}_{\mathbf{IBEO}}$ for BPSK with $p = 5, m = 23, n = 28$.

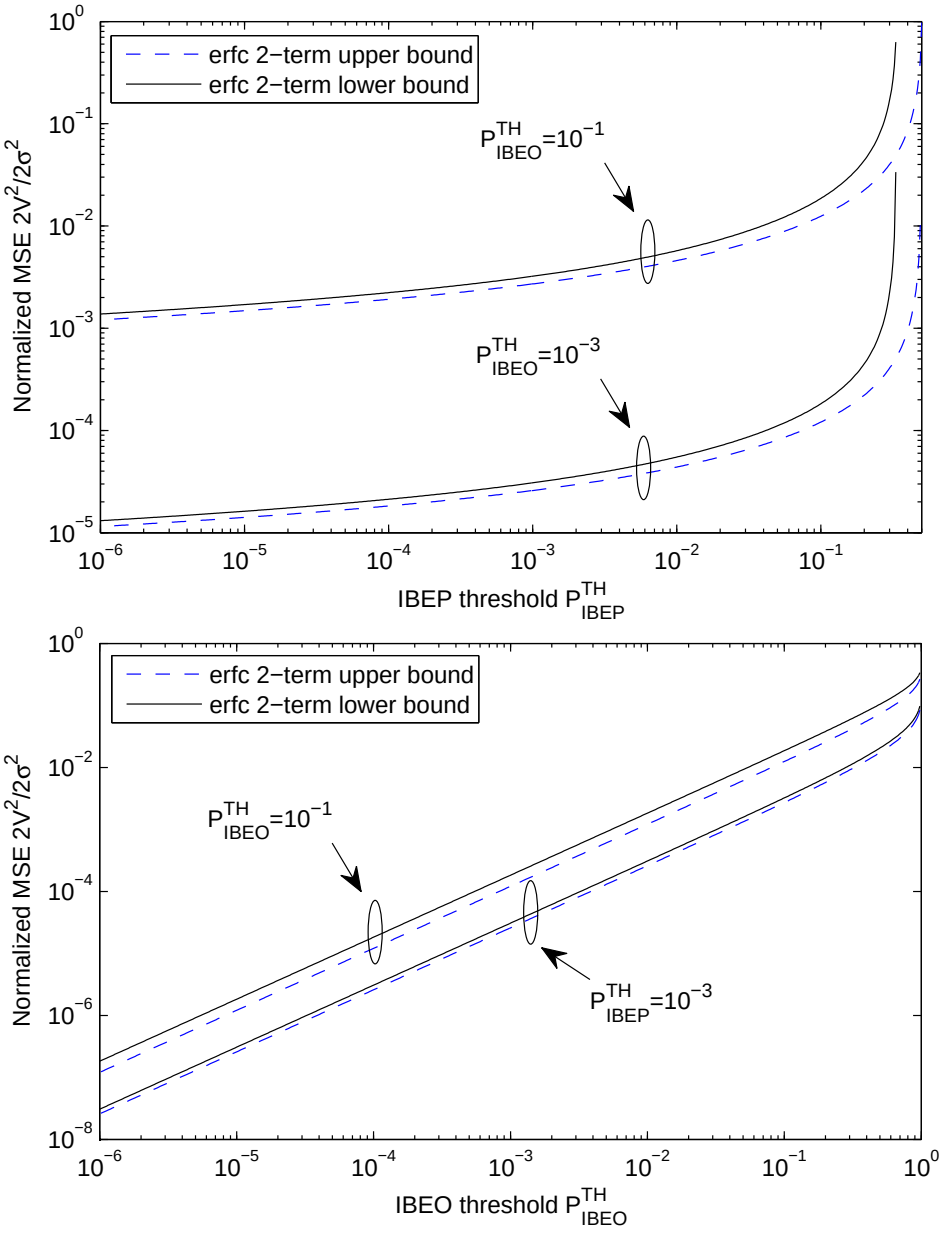

Figure 6.9: Maximum MSE allowed v.s. system design parameters $P^{\mathbf{TH}}_{\mathbf{IBEP}}$ and $P^{\mathbf{TH}}_{\mathbf{IBEO}}$ for QPSK with $p = 5, m = 23, n = 28$.

in turn, leads to degraded performance. Therefore, there should exist an optimum allocation of energy between pilot and data symbols such that the outage probability is minimized.

We first look into the minimization of the IBEO probability in (6.31), i.e.

$$\varepsilon_o = \arg \min_{0 \le \varepsilon \le 1} 1 - \exp(-y), \tag{6.51}$$

where y is given in (6.35). As $1 - \exp(-y)$ is a monotonically increasing function of y, minimizing P_{IBEO} is equivalent to minimizing y in (6.32), i.e.

$$\varepsilon_o = \arg \min_{0 \le \varepsilon \le 1} \left[\text{erfc}^{-1}(2P_{\text{IBEP}}^{\text{TH}})\right]^2 \frac{b}{c}. \tag{6.52}$$

As the coefficient $\left[\text{erfc}^{-1}(2P_{\text{IBEP}}^{\text{TH}})\right]^2$ is a positive constant, minimizing y is equivalent to minimizing b/c. Thus, the optimum energy allocation problem is simplified to the minimization of b/c, i.e.

$$\varepsilon_o = \arg \min_{0 \le \varepsilon \le 1} \frac{b}{c}. \tag{6.53}$$

The IBEO optimization problem does not depend on the IBEP threshold $P_{\text{IBEP}}^{\text{TH}}$. Therefore, the optimum solution applies to arbitrary $P_{\text{IBEP}}^{\text{TH}}$ values. It has been shown that the IPEO probability is equivalent to the IBEO probability with $P_{\text{IBEP}}^{\text{TH}}$ in (6.43) or (6.47). Thus, the optimum solution for IBEO probability also minimizes the IPEO probability. In addition, the optimization problem does not depend on the inverse erfc function. Hence, the same optimum solution applies regardless of the bounds on the inverse erfc function used.

6.4.1 BPSK

Using (6.35), the optimum energy allocation problem for BPSK in (6.53) simplifies to

$$\varepsilon_o = \arg \min_{0 \le \varepsilon \le 1} \frac{(n-1)\varepsilon m\bar{\gamma} + m\bar{\gamma} + n}{(1-\varepsilon)\varepsilon m^2\bar{\gamma}^2}. \tag{6.54}$$

By solving $\partial(b/c)/\partial\varepsilon = 0$, and hence,

$$(n-1)m\bar{\gamma}\varepsilon^2 + 2(m\bar{\gamma} + n)\varepsilon - (m\bar{\gamma} + n) = 0, \tag{6.55}$$

we obtain the optimum solution

$$\varepsilon_o = \frac{\sqrt{n(m\bar{\gamma}+1)(m\bar{\gamma}+n)} - (m\bar{\gamma}+n)}{(n-1)m\bar{\gamma}}. \tag{6.56}$$

Note that in (6.56), we have chosen the solution with $\varepsilon_o > 0$.

We next show that, for a given n value, the optimum value of ε_o satisfies the following inequalities for any m value:

$$\frac{\sqrt{n}-1}{n-1} \leq \varepsilon_o \leq \frac{1}{2}. \tag{6.57}$$

By showing that

$$\frac{\partial \varepsilon_o}{\partial \bar{\gamma}} = -\frac{n\left[\sqrt{n(m\bar{\gamma}+1)} - \sqrt{m\bar{\gamma}+n}\right]^2}{2(n-1)m\bar{\gamma}^2\sqrt{n(m\bar{\gamma}+1)(m\bar{\gamma}+n)}} \leq 0, \tag{6.58}$$

we prove that ε_o decreases monotonically with $\bar{\gamma}$. Therefore, ε_o is upper and lower bounded as [40]

$$\varepsilon_{\min} \leq \varepsilon_o \leq \varepsilon_{\max}, \tag{6.59}$$

where

$$\begin{aligned}
\varepsilon_{\min} &= \lim_{\bar{\gamma}\to 0} \varepsilon_o(\bar{\gamma}) = \lim_{\bar{\gamma}\to 0} \frac{\frac{\partial}{\partial\bar{\gamma}}\sqrt{n(m\bar{\gamma}+1)(m\bar{\gamma}+n)} - (m\bar{\gamma}+n)}{\frac{\partial}{\partial\bar{\gamma}}(n-1)m\bar{\gamma}} = \frac{1}{2}, \\
\varepsilon_{\max} &= \lim_{\bar{\gamma}\to \infty} \varepsilon_o(\bar{\gamma}) = \lim_{\bar{\gamma}\to \infty} \frac{\sqrt{n\left(m+1/\bar{\gamma}\right)\left(m+n/\bar{\gamma}\right)} - (m+n/\bar{\gamma})}{(n-1)m} = \frac{\sqrt{n}-1}{n-1}.
\end{aligned} \tag{6.60}$$

This shows that, at higher SNR values, less optimum pilot energy is required. However, a small fraction of the total energy, i.e. $(\sqrt{n}-1)/(n-1)$, must always be dedicated to pilots to perform channel estimation. On the other hand, the optimum pilot energy never exceeds half the total energy.

For a given SNR value $\bar{\gamma}$, ε_o is a monotonically decreasing function of the data length n. It can be proven by showing that

$$\frac{\partial \varepsilon_o}{\partial n} = -\frac{(m\bar{\gamma}+1)\left[\sqrt{n(m\bar{\gamma}+1)} - \sqrt{m\bar{\gamma}+n}\right]^2}{2\sqrt{n(m\bar{\gamma}+1)(m\bar{\gamma}+n)}(n-1)^2 m\bar{\gamma}} \leq 0. \tag{6.61}$$

6.4.2 QPSK

Using (6.35), the optimum energy allocation problem for QPSK simplifies to

$$\varepsilon_o = \arg \min_{0 \le \varepsilon \le 1} \frac{(n-2)\varepsilon m\bar{\gamma} + 2m\bar{\gamma} + n}{(1-\varepsilon)\varepsilon m^2\bar{\gamma}^2}. \tag{6.62}$$

By solving $\partial(b/c)/\partial\varepsilon = 0$, and hence,

$$(n-2)m\bar{\gamma}\varepsilon^2 + 2(2m\bar{\gamma} + n)\varepsilon - (2m\bar{\gamma} + n) = 0, \tag{6.63}$$

we obtain the optimum solution for QPSK

$$\varepsilon_o = \frac{\sqrt{n(m\bar{\gamma}+1)(2m\bar{\gamma}+n)} - (2m\bar{\gamma}+n)}{(n-2)m\bar{\gamma}}. \tag{6.64}$$

By showing that

$$\frac{\partial \varepsilon_o}{\partial \bar{\gamma}} = -\frac{n\left[\sqrt{n(m\bar{\gamma}+1)} - \sqrt{2m\bar{\gamma}+n}\right]^2}{2(n-2)m\bar{\gamma}^2\sqrt{n(m\bar{\gamma}+1)(2m\bar{\gamma}+n)}} \le 0, \tag{6.65}$$

we prove that ε_o decreases monotonically with $\bar{\gamma}$. Therefore, the upper and lower limits of ε_o can be found by

$$\begin{aligned}
\varepsilon_{\min} &= \lim_{\bar{\gamma}\to 0} \varepsilon_o(\bar{\gamma}) = \lim_{\bar{\gamma}\to 0} \frac{\frac{\partial}{\partial\bar{\gamma}}\sqrt{n(m\bar{\gamma}+1)(2m\bar{\gamma}+n)} - (2m\bar{\gamma}+n)}{\frac{\partial}{\partial\bar{\gamma}}(n-2)m\bar{\gamma}} = \frac{1}{2}, \\
\varepsilon_{\max} &= \lim_{\bar{\gamma}\to \infty} \varepsilon_o(\bar{\gamma}) = \lim_{\bar{\gamma}\to \infty} \frac{\sqrt{n\left(m+1/\bar{\gamma}\right)\left(2m+n/\bar{\gamma}\right)} - (2m+n/\bar{\gamma})}{(n-2)m} = \frac{\sqrt{2n}-2}{n-2}.
\end{aligned} \tag{6.66}$$

For a given SNR value $\bar{\gamma}$, by showing that

$$\frac{\partial \varepsilon_o}{\partial n} = -\frac{(m\bar{\gamma}+1)\left[\sqrt{n(m\bar{\gamma}+1)} - \sqrt{2m\bar{\gamma}+n}\right]^2}{\sqrt{n(m\bar{\gamma}+1)(2m\bar{\gamma}+n)}(n-2)^2 m\bar{\gamma}} \le 0, \tag{6.67}$$

we conclude that ε_o decreases monotonically with the data length n.

6.4.3 Numerical Results

Comparisons of the IBEO performance using equal bit energy allocation and optimum pilot energy allocation with BPSK and QPSK are shown in Fig. 6.10

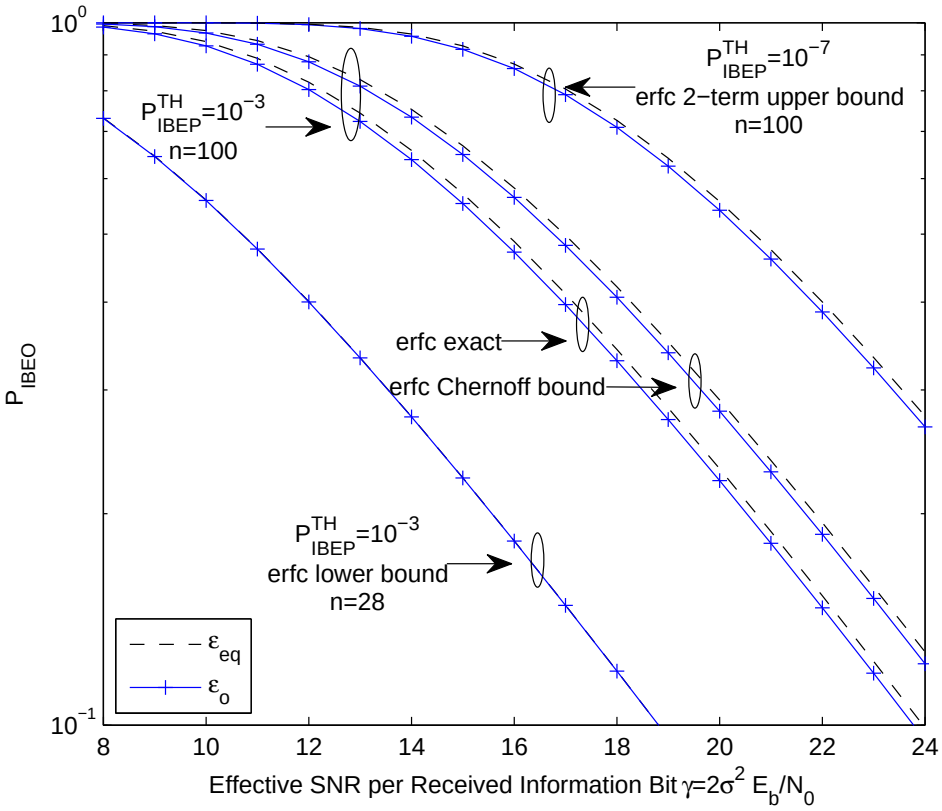

Figure 6.10: Optimum IBEO performance for BPSK with $p = 5, m = 23$.

and Fig. 6.11, respectively. Optimum pilot energy allocation clearly outperforms equal bit energy allocation. The gain in SNR is about 0.2dB for large n values. The improvement in performance is only significant when n is large. When n is close to m, the pilot energy based on equal bit energy allocation is close to that of optimum pilot energy allocation. Thus, the difference in performance is small between the two allocation methods. The amount of performance improvement is not affected by the value of $P_{\text{IBEP}}^{\text{TH}}$, or the inverse erfc function used. As QPSK is more susceptible to channel estimation errors, its performance improvement by optimum pilot energy allocation is more significant than that of BPSK.

The unique optimum pilot energy solution for BPSK and QPSK are shown in Fig. 6.12 and Fig. 6.13, respectively. The solution ε_o decreases with effective SNR $\bar{\gamma}$. Thus, a smaller fraction of energy is required on pilots for channel estimation

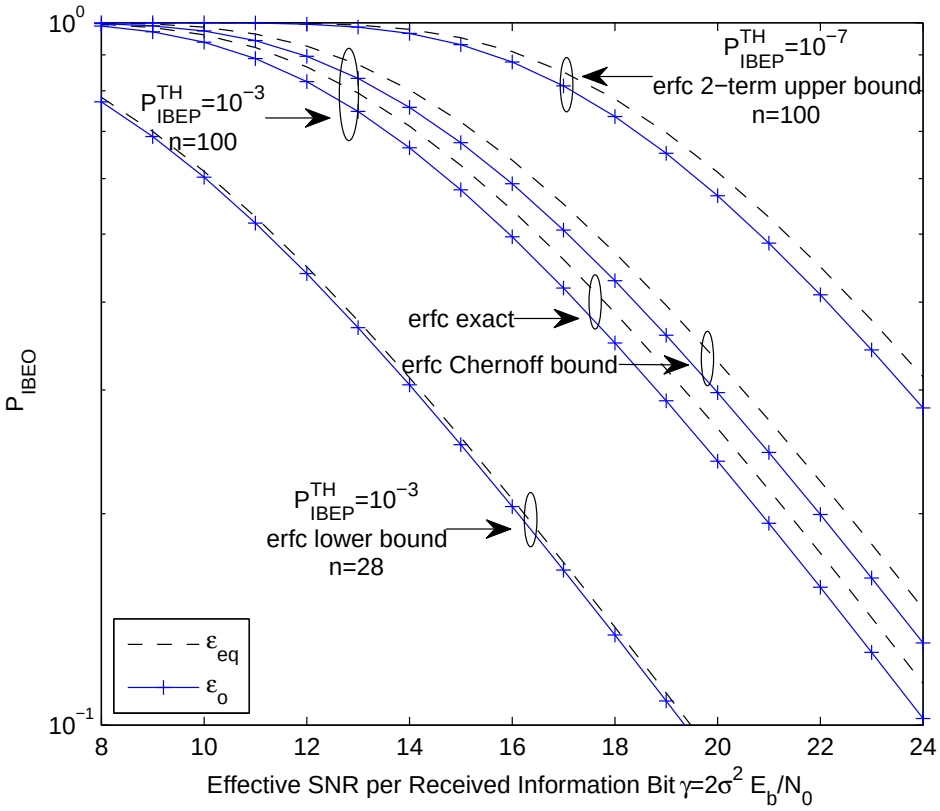

Figure 6.11: Optimum IBEO performance for QPSK with $p = 5, m = 23$.

when the signal condition is good. The solution ε_o is upper and lower bounded as in (6.59), (6.60) and (6.66). As QPSK is more susceptible to channel estimation errors, more pilot energy is required for optimum IBEO performance than BPSK.

Fig. 6.14 and Fig. 6.15 show that, for both BPSK and QPSK, when n increases, a smaller fraction of total energy is used on pilots. This is accompanied by a smaller bandwidth expansion of $p/(n/\log_2 M)$ caused by insertion of pilot symbols. However, the value of n is limited by the channel fade rate, as the channel gain is assumed static over the duration of $(p + n/\log_2 M)$ symbols.

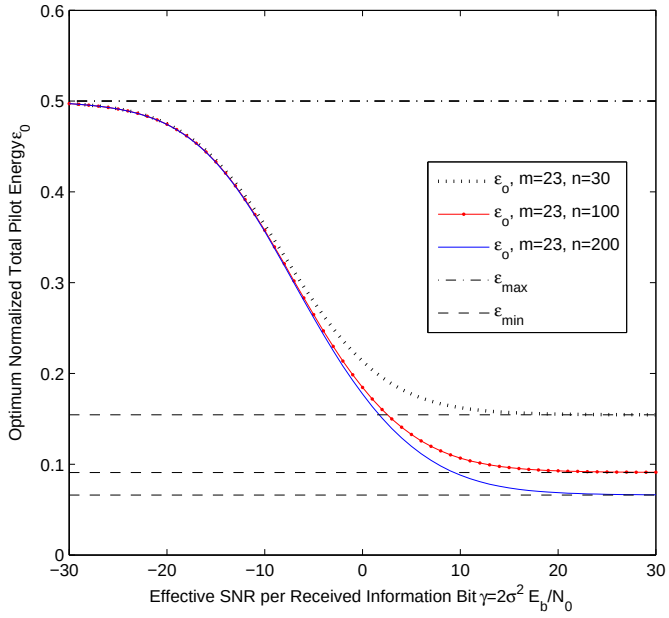

Figure 6.12: Optimum normalized total pilot energy ε_o v.s. effective SNR $\bar{\gamma}$ for BPSK with $p = 5$.

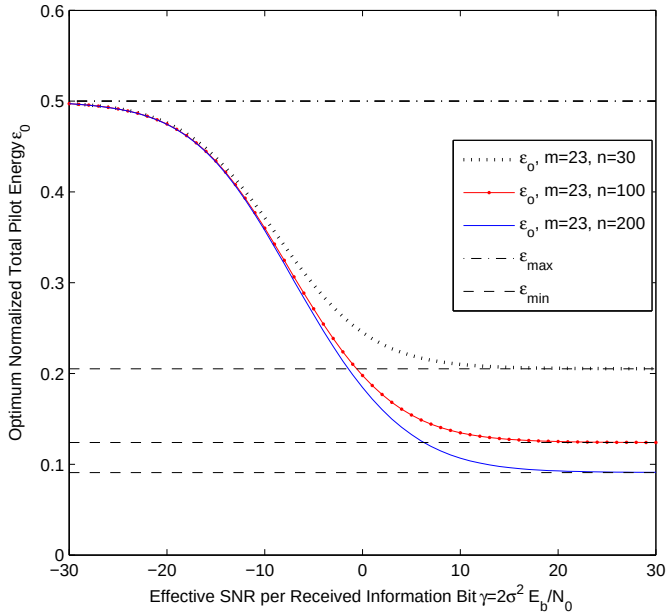

Figure 6.13: Optimum normalized total pilot energy ε_o v.s. effective SNR $\bar{\gamma}$ for QPSK with $p = 5$.

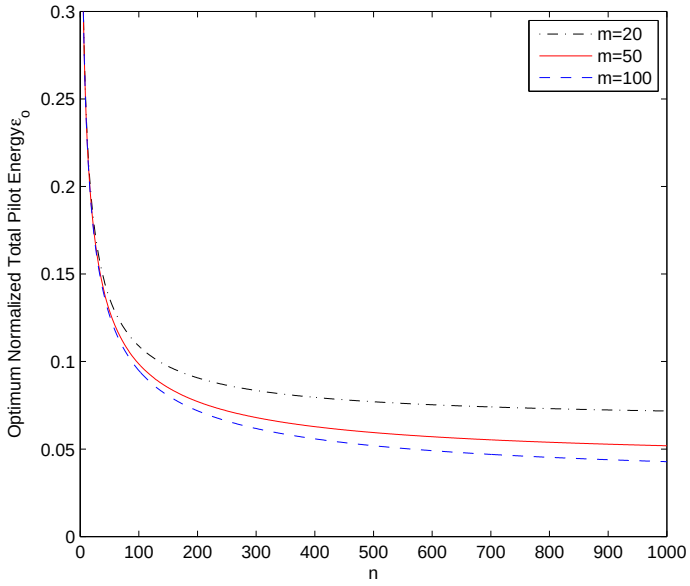

Figure 6.14: Optimum normalized total pilot energy ε_o v.s. data length n at $\bar{\gamma} = 10$dB for BPSK with $p = 5$.

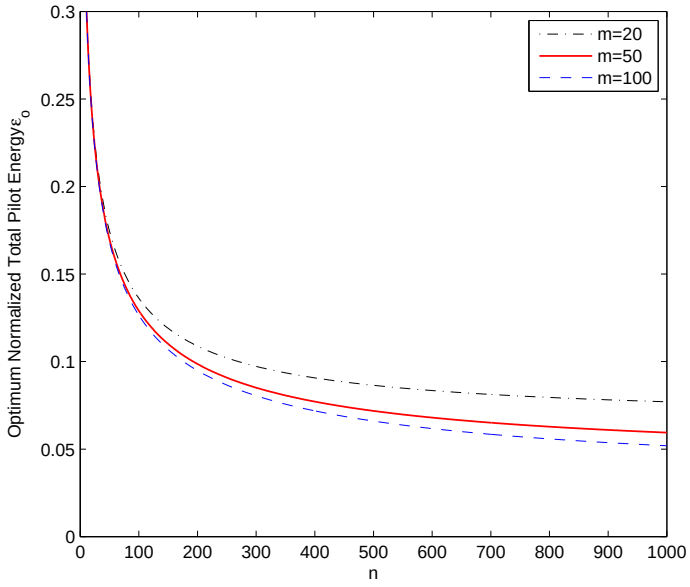

Figure 6.15: Optimum normalized total pilot energy ε_o v.s. data length n at $\bar{\gamma} = 10$dB for QPSK with $p = 5$.

6.5 Conclusions

In this chapter, we proposed to use IBEP/IPEP to represent the short-term reliability of symbol-by-symbol/packet transmission, and IBEO/IPEO probability to represent the long-term reliability of symbol-by-symbol/packet transmission, respectively. A closed-form expression and upper and lower bounds are obtained for the IBEO probability over Rayleigh fading channels with imperfect CSI. The IPEO probability is shown equivalent to the IBEO probability. It is shown that the IBEO/IPEO performance improves rapidly with MSE, when MSE drops below a certain value, which is determined partly by the IBEP/IPEP threshold chosen.

The optimum allocation of energy between pilot and coded bits that minimizes the IBEO/IPEO probability is derived. It is shown that the optimum allocation is not affected by the IBEP/IPEP threshold values.

Chapter 7

ARQ with Channel Gain Monitoring

As discussed in Chapter 6, ABEP, being an average metric, does not reflect the poor instantaneous quality of service (QoS) experienced by the user over such long fades, nor does it reflect how often such poor QoS occurs. We proposed in Chapter 6 to use the IBEO/IPEO probability as a performance measure for high data rate transmission over time-varying fading. It is defined as the probability that the IBEP/IPEP exceeds the IBEO/IPEO threshold. It reflects, in the long term, how often continuous transmission fails. Thus, IBEO/IPEO provides a new dimension in QoS than IBEP/IPEP.

We extend here the idea of IBEO from symbol-by-symbol transmission to packet transmission with ARQ schemes, and propose an instantaneous performance measure, the IAPEO probability. An IAPEO event is defined as the event that the IAPEP conditioned on a given fading gain, exceeds a maximum tolerable IAPEP threshold. The IAPEO probability is the probability that the IAPEP exceeds the IAPEP threshold, and is calculated using the channel fading statistics. We show that, for a pure ARQ, the system must operate above a minimum SNR, in order to satisfy a design requirement of a maximum tolerable IAPEO.

In order to overcome the shortcoming of the conventional ARQ, we next

propose an ARQ scheme by integrating channel gain monitoring with a conventional pure ARQ scheme, naming it ARQ-CGM. If the channel gain estimate is below a threshold, a retransmit request is send to the transmitter; otherwise, a packet proceeds to demodulation and cyclic redundancy check (CRC). A closed-form upper bound expression for the IAPEO is obtained as a function of a channel estimate threshold value. For any SNR, the channel estimate threshold value that ensures a maximum system design IAPEO threshold can be obtained. The IAPEO performance of ARQ-CGM is related to the conventional average performance measures, i.e. average throughput, goodput and AAPEP. It is shown that the AAPEP of ARQ-CGM improves over the conventional ARQ with a compromise in throughput and goodput.

When the channel gain threshold is set to be zero, ARQ-CGM reduces to the conventional ARQ. Therefore, the outage performance, AAPEP, throughput and goodput we obtain for ARQ-CGM also apply to the conventional ARQ by setting the channel gain threshold to zero.

This chapter is organized as follows. In Section 7.1, the IAPEO performance of the conventional ARQ is obtained. In Section 7.2, ARQ-CGM is proposed and its outage performance is obtained. The average performance measures of ARQ-CGM are obtained in Section 7.3. Numerical Results are obtained and analyzed in Section 7.4. Conclusions are made in Section 7.5.

7.1 Instantaneous Accepted Packet Error Outage of Conventional ARQ

The system model is the same as that in Section 6.2 and therefore, is not repeated here. Let e_a define the event that the receiver accepts a packet that contains an error pattern. Given a channel estimate $\hat{h}$, the IAPEP is the probability that the

receiver commits an error in accepting packets, and is given by [39, eq.(22.1)]

$$P(e_a|\hat{h}) = \frac{P(e_u|\hat{h})}{1 - P(e_p|\hat{h}) + P(e_u|\hat{h})}. \tag{7.1}$$

Substituting (6.41) and (6.44), we obtain an upper bound on IAPEP, as

$$P(e_a|\hat{h}) \leq P^{\mathrm{UB}}(e_a|\hat{h}) = \frac{1 - \left(1 - P(e_b|\hat{h})\right)^n}{1 + [2^{n-m} - 1]\left(1 - P(e_b|\hat{h})\right)^n}. \tag{7.2}$$

Assume that the maximum tolerable IAPEP threshold value is $P^{\mathrm{TH}}_{\mathrm{IAPEP}}$. The IAPEO probability, P_{IAPEO}, is the probability that the IAPEP exceeds $P^{\mathrm{TH}}_{\mathrm{IAPEP}}$, i.e.

$$P_{\mathrm{IAPEO}} = P\left(P(e_a|\hat{h}) > P^{\mathrm{TH}}_{\mathrm{IAPEP}}\right). \tag{7.3}$$

From (7.2), it is clear that P_{IAPEO} is upper bounded as

$$P_{\mathrm{IAPEO}} \leq P^{\mathrm{UB}}_{\mathrm{IAPEO}} = P\left(P^{\mathrm{UB}}(e_a|\hat{h}) > P^{\mathrm{TH}}_{\mathrm{IAPEP}}\right). \tag{7.4}$$

Substituting (7.2) into (7.4), $P^{\mathrm{UB}}_{\mathrm{IAPEO}}$ can be simplified to

$$P^{\mathrm{UB}}_{\mathrm{IAPEO}} = P\left(P(e_b|\hat{h}) > P^{\mathrm{TH}}_{\mathrm{IBEP}}\right), \tag{7.5}$$

where

$$P^{\mathrm{TH}}_{\mathrm{IBEP}} = 1 - \left[\frac{1 - P^{\mathrm{TH}}_{\mathrm{IAPEP}}}{1 + (2^{n-m} - 1)P^{\mathrm{TH}}_{\mathrm{IAPEP}}}\right]^{1/n}. \tag{7.6}$$

Hence, the upper bound on the IAPEO probability is equivalent to an IBEO probability, with $P^{\mathrm{TH}}_{\mathrm{IBEP}}$ in (7.6). Therefore, the IAPEO upper bound for BPSK and QPSK is given by (6.31) with (6.32) or (6.35) using $P^{\mathrm{TH}}_{\mathrm{IBEP}}$ in (7.6).

Upper bounds on the minimum required SNR, $\bar{\gamma}_p^{\mathrm{TH,UB}}$, for BPSK and QPSK that satisfy the IAPEO threshold of $P^{\mathrm{TH}}_{\mathrm{IAPEO}}$ are given by (6.37) and (6.38) with (6.39), respectively, by using $P^{\mathrm{TH}}_{\mathrm{IBEP}}$ in (7.6) and replacing $P^{\mathrm{TH}}_{\mathrm{IBEO}}$ with $P^{\mathrm{TH}}_{\mathrm{IAPEO}}$. Due to the equivalence of IAPEO probability to the IBEO probability, the IPEO/IAPEO performances and the effect of imperfect CSI on them are similar to the IBEO of symbol-by-symbol transmission.

Same as the IBEO performance in Fig. 6.2 and Fig. 6.3, the IAPEO performance decreases monotonically with the SNR. Therefore, the system must operate above a minimum SNR, in order to satisfy a design requirement of a maximum tolerable IAPEO.

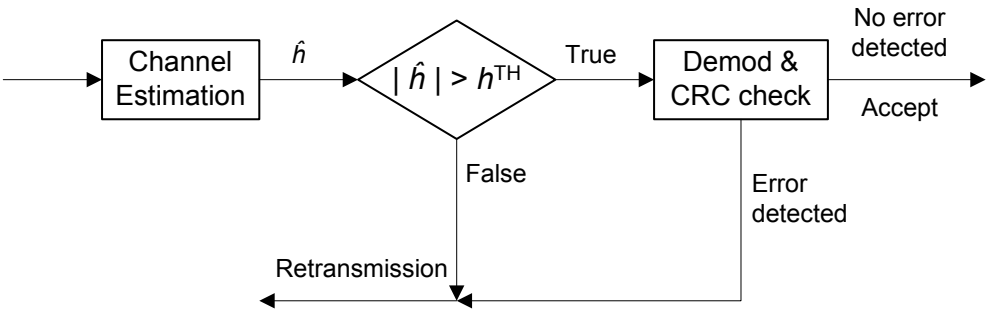

Figure 7.1: Receiver diagram of ARQ-CGM.

7.2 ARQ-CGM and Outage Performance

In conventional pure ARQ schemes, if the SNR is lower than the SNR required for desired outage performance of $P_{\text{IAPEO}}^{\text{TH}}$, the system cannot achieve the required $P_{\text{IAPEO}}^{\text{TH}}$. To cope with this shortcoming of conventional ARQ schemes, we propose in this section a new ARQ scheme by incorporating channel gain monitoring with a conventional pure ARQ scheme. We name it ARQ-CGM.

The receiver diagram of ARQ-CGM is shown in Fig. 7.1. Similar to conventional pure ARQ schemes, channel estimation is performed to obtain an estimate of the channel gain, which is necessary for coherent demodulation of BPSK/QPSK signals. The magnitude of the channel estimate $\hat{h}$ is checked against a channel estimate threshold $|h^{\text{TH}}|$. If $\hat{h}$ is greater than $|h^{\text{TH}}|$, the received signal proceeds to demodulation and CRC check. If $\hat{h}$ is less than $|h^{\text{TH}}|$, a retransmission request is sent to the transmitter. This scheme can apply to all three basic retransmission protocols, namely, SR-ARQ, SW-ARQ and GBN-ARQ. We name them SR-ARQ-CGM, SW-ARQ-CGM and GBN-ARQ-CGM. ARQ-CGM can also apply to other variants of retransmission protocols, such as opportunistic multi-hop ARQ in underwater networks [77, 78].

The IAPEP conditioned on the channel estimate $\hat{h}$ is the same as that of the conventional ARQ in (7.1) when $|\hat{h}| > |h^{\text{TH}}|$. When $|\hat{h}| < |h^{\text{TH}}|$, packets are not accepted, and hence, the IAPEP is zero. The IAPEO is thus defined

as the probability that the IAPEP exceeds the threshold $P_{\text{IAPEP}}^{\text{TH}}$, conditioned on $|h| > |h^{\text{TH}}|$, i.e.

$$P_{\text{IAPEO}}^{\text{CGM}} = P\left(P(e_a|\hat{h}) > P_{\text{IAPEP}}^{\text{TH}} \middle| |\hat{h}| > h^{\text{TH}}\right). \tag{7.7}$$

Using the upper bound (7.2) and substituting the IBEP expression in (6.25), we obtain an upper bound on the IAPEO probability as

$$P_{\text{IAPEO}}^{\text{CGM,UB}} = P\left(x = |\hat{h}|^2 < \frac{\left[\text{erfc}^{-1}(2P_{\text{IBEP}}^{\text{TH}})\right]^2}{c} \middle| |\hat{h}| > h^{\text{TH}}\right), \tag{7.8}$$

where c is given in (6.29) and $P_{\text{IBEP}}^{\text{TH}}$ is given in (7.6). The conditional probability can be evaluated by Bayes Theorem as

$$P_{\text{IAPEO}}^{\text{CGM,UB}} = \frac{P\left(x = |\hat{h}|^2 < \left[\text{erfc}^{-1}(2P_{\text{IBEP}}^{\text{TH}})\right]^2/c, |\hat{h}| > h^{\text{TH}}\right)}{P(|\hat{h}| > h^{\text{TH}})}. \tag{7.9}$$

Given the PDF of x in (6.22), (7.9) is simplified as

$$\begin{aligned} P_{\text{IAPEO}}^{\text{CGM,UB}} &= \frac{\displaystyle\int_{x=|h^{\text{TH}}|^2}^{\left[\text{erfc}^{-1}(2P_{\text{IBEP}}^{\text{TH}})\right]^2/c} p_x(x)dx}{\displaystyle\int_{x=|h^{\text{TH}}|^2}^{\infty} p_x(x)dx} \\ &= 1 - \exp\left(-y + b|h^{\text{TH}}|^2\right), \end{aligned} \tag{7.10}$$

where y and b are given in (6.32) and (6.30), respectively. Comparing with the IAPEO probability of conventional ARQ schemes, which is equivalent to the IBEO probability in (6.31), the IAPEO upper bound of ARQ-CGM in (7.10) only differs by the term $\exp\left(b|h^{\text{TH}}|^2\right)$. We can adjust the IAPEO performance of ARQ-CGM simply by changing the channel estimate threshold value h^{TH}. In other words, incorporation of channel gain monitoring allows us to have more control of the outage performance of accepted packets.

Assume that the maximum tolerable IAPEO probability is $P_{\text{IAPEO}}^{\text{TH}}$. By setting the upper bound $P_{\text{IAPEO}}^{\text{CGM,UB}} < P_{\text{IAPEO}}^{\text{TH}}$, we can ensure that the exact IAPEO performance satisfies the threshold requirement. Using the exact expression of the

IAPEO upper bound in (7.10), it is easy to show that the IAPEO requirement is satisfied when using the channel estimate threshold

$$|h^{\mathrm{TH}}| = \sqrt{\frac{1}{b}\ln(1-P_{\mathrm{IAPEO}}^{\mathrm{TH}}) + \frac{1}{c}\left[\mathrm{erfc}^{-1}(2P_{\mathrm{IBEP}}^{\mathrm{TH}})\right]^2}. \tag{7.11}$$

Applying the upper and lower bounds on the inverse erfc functions in (6.8), (6.9) and (6.11), $|h^{\mathrm{TH}}|$ is upper bounded as

$$\begin{aligned} |h^{\mathrm{TH}}| &< \sqrt{\frac{1}{b}\ln(1-P_{\mathrm{IAPEO}}^{\mathrm{TH}}) + \frac{1}{c}\ln\left(\frac{\sqrt{16P_{\mathrm{IBEP}}^{\mathrm{TH}}+1}+1}{8P_{\mathrm{IBEP}}^{\mathrm{TH}}}\right)} \\ &< \sqrt{\frac{1}{b}\ln(1-P_{\mathrm{IAPEO}}^{\mathrm{TH}}) - \frac{1}{c}\ln(2P_{\mathrm{IBEP}}^{\mathrm{TH}})}, \end{aligned} \tag{7.12}$$

and lower bounded as

$$|h^{\mathrm{TH}}| > \sqrt{\frac{1}{b}\ln(1-P_{\mathrm{IAPEO}}^{\mathrm{TH}}) + \frac{1}{c}\frac{\sqrt{3}\pi}{6}\ln\left(\frac{\sqrt{24P_{\mathrm{IBEP}}^{\mathrm{TH}}+1}+1}{12P_{\mathrm{IBEP}}^{\mathrm{TH}}}\right)}. \tag{7.13}$$

When the exact inverse erfc function is not available numerically, the upper bounds on $|h^{\mathrm{TH}}|$ should be used to ensure the maximum tolerable IAPEO.

In contrast to conventional ARQ schemes, given any SNR value, we can always find the threshold $|h^{\mathrm{TH}}|$ for ARQ-CGM such that the IAPEO threshold requirement is satisfied. If the required IAPEO threshold is greater than the IAPEO of conventional ARQ schemes in (6.31), $|h^{\mathrm{TH}}|$ is reduced to zero, and the ARQ-CGM scheme reduces to a conventional ARQ scheme.

7.3 Average Performance of ARQ-CGM

7.3.1 SR-ARQ-CGM

The average probability of a packet being correctly received and finally accepted by the receiver is given by $P(C_p, |\hat{h}| > h^{\mathrm{TH}})$. It can be evaluated by averaging the

instantaneous value, i.e. $P(C_p, |\hat{h}| > h^{\mathrm{TH}}|\hat{h})$ over the distribution of $x = |\hat{h}|^2$, i.e.

$$\begin{aligned} P(C_p, |\hat{h}| > h^{\mathrm{TH}}) &= \int_0^{\infty} P(C_p, |\hat{h}| > h^{\mathrm{TH}}|\hat{h}) b \exp(-bx) dx \\ &= \int_{|h^{\mathrm{TH}}|^2}^{\infty} \left[1 - \frac{1}{2}\mathrm{erfc}(\sqrt{cx})\right]^n b \exp(-bx) dx. \end{aligned} \tag{7.14}$$

Using the Chernoff bound on the erfc function in (6.4), a lower bound on (7.14) is obtained as

$$Z > \sum_{l=0}^{n} \left[1 - \frac{1}{2}\exp\left(-c|h^{\mathrm{TH}}|^2\right)\right]^{n-l} \exp\left[-(b+lc)|h^{\mathrm{TH}}|^2\right] \prod_{k=0}^{l-1} \frac{n-k}{2(b/c+k+1)}. \tag{7.15}$$

Applying the tighter upper bound on the erfc function in (6.5), a tighter lower bound on (7.14) is obtained as

$$Z > \sum_{k=0}^{n} \binom{n}{k} \left(-\frac{1}{4}\right)^k \sum_{t=0}^{k} \binom{k}{t} \frac{\exp\left\{-\left[(2k-t)c + b\right]|h^{\mathrm{TH}}|^2\right\}}{(2k-t)\frac{c}{b} + 1}. \tag{7.16}$$

Applying the tight lower bound on the erfc function in (6.7), a tight upper bound on (7.14) is obtained as

$$Z < \sum_{k=0}^{n} \binom{n}{k} \left(-\frac{1}{6}\right)^k \sum_{t=0}^{k} \binom{k}{t} \frac{\exp\left\{-\left[\frac{2\sqrt{3}}{\pi}(2k-t)c + b\right]|h^{\mathrm{TH}}|^2\right\}}{\frac{2\sqrt{3}}{\pi}(2k-t)\frac{c}{b} + 1}. \tag{7.17}$$

Alternatively, using an accurate approximation of the erfc function in [79, eq.(31)]

$$\mathrm{erfc}(x) \approx \frac{1}{6}\exp(-x^2) + \frac{1}{3}\exp(-\frac{4}{3}x^2), \tag{7.18}$$

we obtain a closer approximation of $P(C_p, |\hat{h}| > h^{\mathrm{TH}})$ as

$$Z \approx \sum_{k=0}^{n} \binom{n}{k} \left(-\frac{1}{6}\right)^k \sum_{t=0}^{k} \binom{k}{t} \frac{\exp\left\{-\left(\frac{4k-t}{3}c + b\right)|h^{\mathrm{TH}}|^2\right\}}{2^t\left(\frac{4k-t}{3}\frac{c}{b} + 1\right)}. \tag{7.19}$$

The probability of a packet passing the channel estimate threshold test while containing at least one error bit is

$$\begin{aligned} P(e_p, |\hat{h}| > h^{\mathrm{TH}}) &= \int_{|h^{\mathrm{TH}}|^2}^{\infty} \left\{1 - \left[1 - \frac{1}{2}\mathrm{erfc}(\sqrt{cx})\right]^n\right\} b \exp(-bx) dx \\ &= \exp(-b|h^{\mathrm{TH}}|^2) - P(C_p, |\hat{h}| > h^{\mathrm{TH}}). \end{aligned} \tag{7.20}$$

Using (6.44), the probability of a packet being accepted with undetectable error is upper bounded as

$$P(e_u, |\hat{h}| > h^{\mathrm{TH}}) \leq 2^{-(n-m)} P(e_p, |\hat{h}| > h^{\mathrm{TH}}). \tag{7.21}$$

Throughput is the rate of information bits accepted by the receiver, and includes packets that are accepted correctly and those accepted with undetectable error. Hence, we have

$$\eta_{sr} = \frac{m}{p + \frac{n}{\log_2 M}} \left[P(C_p, |\hat{h}| > h^{\mathrm{TH}}) + P(e_u, |\hat{h}| > h^{\mathrm{TH}}) \right]. \tag{7.22}$$

Substituting (7.20) and (7.21), we have

$$\eta_{sr} = \frac{m}{p + \frac{n}{\log_2 M}} \left\{ Z + 2^{-(n-m)} \left[\exp(-b|h^{\mathrm{TH}}|^2) - Z \right] \right\}. \tag{7.23}$$

Goodput is the rate of information bits accepted by the receiver correctly, i.e.

$$\eta_{sr}^{g} = \frac{m}{p + \frac{n}{\log_2 M}} P(C_p, |\hat{h}| > h^{\mathrm{TH}}) = \frac{m}{p + \frac{n}{\log_2 M}} Z. \tag{7.24}$$

The AAPEP, which shows the average reliability of ARQ-CGM, is given by

$$P(e_a) = 1 - \frac{\eta_{sr}^{g}}{\eta_{sr}} = \frac{\exp(-b|h^{\mathrm{TH}}|^2) - Z}{\exp(-b|h^{\mathrm{TH}}|^2) + (2^{n-m} - 1)Z}. \tag{7.25}$$

The AAPEP only depends on the channel error statistics and choice of the error detecting code and is independent of the retransmission protocol. Therefore, SR-ARQ-CGM, SW-ARQ-CGM and GBN-ARQ-CGM have the same AAPEP.

When h^{TH} is zero, ARQ-CGM reduces to the conventional ARQ. Therefore, the throughput, goodput and AAPEP of conventional SR-ARQ are given by (7.23), (7.24) and (7.25), respectively, by letting $|h^{\mathrm{TH}}| = 0$.

7.3.2 SW-ARQ-CGM

For throughput of SW-ARQ-CGM, we must consider the idle time spent in waiting for an acknowledgement for each transmitted packet. Let D be the idle time from the end of transmission of one packet to the beginning of transmission of the next.

Let τ be the signaling rate of the transmitter in bits per second. The round-trip delay time is defined as the time interval between between the transmission of a packet and the reception of its acknowledgement. In one round-trip delay time, the transmitter can transmit a total of $1+D\tau/(p+n/\log_2 M)$ packets if it does not stay idle. By evaluating the average number of packets that the transmitter could have transmitted during the interval from the beginning of transmission of one packet to the reception of a positive acknowledgement for that packet, the throughput of SW-ARQ-CGM follows [39, eq.(22.6)] as

$$\eta_{sw} = \frac{m\left[P(C_p, |\hat{h}| > h^{\mathrm{TH}}) + P(e_u, |\hat{h}| > h^{\mathrm{TH}})\right]}{p + \frac{n}{\log_2 M} + D\tau} \tag{7.26}$$

$$= \frac{m\left\{Z + 2^{-(n-m)}\left[\exp(-b|h^{\mathrm{TH}}|^2) - Z\right]\right\}}{p + \frac{n}{\log_2 M} + D\tau}. \tag{7.27}$$

Making use of the AAPEP of SW-ARQ-CGM, which is the same as that of SR-ARQ-CGM in (7.25), the goodput of SW-ARQ-CGM can be derived as

$$\eta_{sw}^{g} = \frac{mZ}{p + \frac{n}{\log_2 M} + D\tau}. \tag{7.28}$$

7.3.3 GBN-ARQ-CGM

In GBN-ARQ-CGM, when the transmitter receives a retransmission request, it resends that packet and the $N-1$ packets that were transmitted earlier. The parameter N depends on the transmission rate τ and the round-trip delay $D + (p + n/\log_2 M)/\tau$ and is given by $N = 1 + D\tau/(p + n/\log_2 M)$. Therefore, the throughput of GBN-ARQ-CGM is given by [39, eq.(22.5)]

$$\eta_{gbn} = \frac{mP}{p + \frac{n}{\log_2 M} + D\tau(1-P)}, \tag{7.29}$$

where $P = P(C_p, |\hat{h}| > h^{\mathrm{TH}}) + P(e_u, |\hat{h}| > h^{\mathrm{TH}})$. Hence, we obtain

$$\eta_{gbn} = \frac{m\left\{Z + 2^{-(n-m)}\left[\exp(-b|h^{\mathrm{TH}}|^2) - Z\right]\right\}}{p + \frac{n}{\log_2 M} + D\tau\left\{1 - Z - 2^{-(n-m)}\left[\exp(-b|h^{\mathrm{TH}}|^2) - Z\right]\right\}} \tag{7.30}$$

Making use of the AAPEP of GBN-ARQ-CGM, which is the same as that of SR-ARQ-CGM in (7.25), the goodput of SW-ARQ-CGM can be derived as

$$\eta_{gbn}^{g} = \frac{mZ}{p + \frac{n}{\log_2 M} + D\tau \left\{1 - Z - 2^{-(n-m)} \left[\exp(-b|h^{\mathrm{TH}}|^2) - Z\right]\right\}}. \tag{7.31}$$

7.4 Numerical Results

The performance bounds obtained for conventional ARQ in Section 7.1 and those for ARQ-CGM in Section 7.2 and 7.3 depend on the values of m and n and are not influenced by the specific code structure. Without loss of generality, a (28,23) linear block code is adopted in this section. Analysis in the last two sections show that the performance of the conventional ARQ and ARQ-CGM depend only on the normalized total pilot energy ε, instead of the individual value of E_p or p. Therefore, without loss of generality, we use a pilot length of $p = 5$ here. We consider here only the equal bit energy allocation case, i.e. $E_p = E_d/\log_2 M$.

For the conventional ARQ, in order to satisfy the maximum tolerable IAPEO threshold $P_{\mathrm{IAPEO}}^{\mathrm{TH}}$, the SNR must be above the minimum SNR, $\bar{\gamma}^{\mathrm{TH}}$, given in (6.37) and (6.38) for BPSK and QPSK, respectively. ARQ-CGM, however, is able to achieve $P_{\mathrm{IAPEO}}^{\mathrm{TH}}$ at any SNR value by setting the right channel estimate threshold h^{TH}, as shown in Fig. 7.2 and Fig. 7.3. The exact numerical inverse erfc function is used here. One may want to set the channel estimate threshold to be greater than $|h^{\mathrm{TH}}|$ to obtain a lower IAPEO. This, however, will lead to a lower throughput and goodput due to more retransmissions, and, hence, is not advised. The IAPEO curves of the two schemes start to merge at $\bar{\gamma}^{\mathrm{TH}}$, when $|h^{\mathrm{TH}}|$ reduces to 0 and ARQ-CGM reduces to the conventional ARQ.

The channel estimate threshold $|h^{\mathrm{TH}}|$ for BPSK and QPSK are shown in Fig. 7.4 and Fig. 7.5, respectively. The figures show that the bounds on $|h^{\mathrm{TH}}|$ in (7.12) and (7.13) are quite tight. The value of $|h^{\mathrm{TH}}|$ is dominated by $P_{\mathrm{IAPEP}}^{\mathrm{TH}}$ at low SNR, and dominated by $P_{\mathrm{IAPEO}}^{\mathrm{TH}}$ at high SNR. As the IAPEO performance of QPSK is worse than that of BPSK, the required $|h^{\mathrm{TH}}|$ to satisfy for QPSK is larger than that

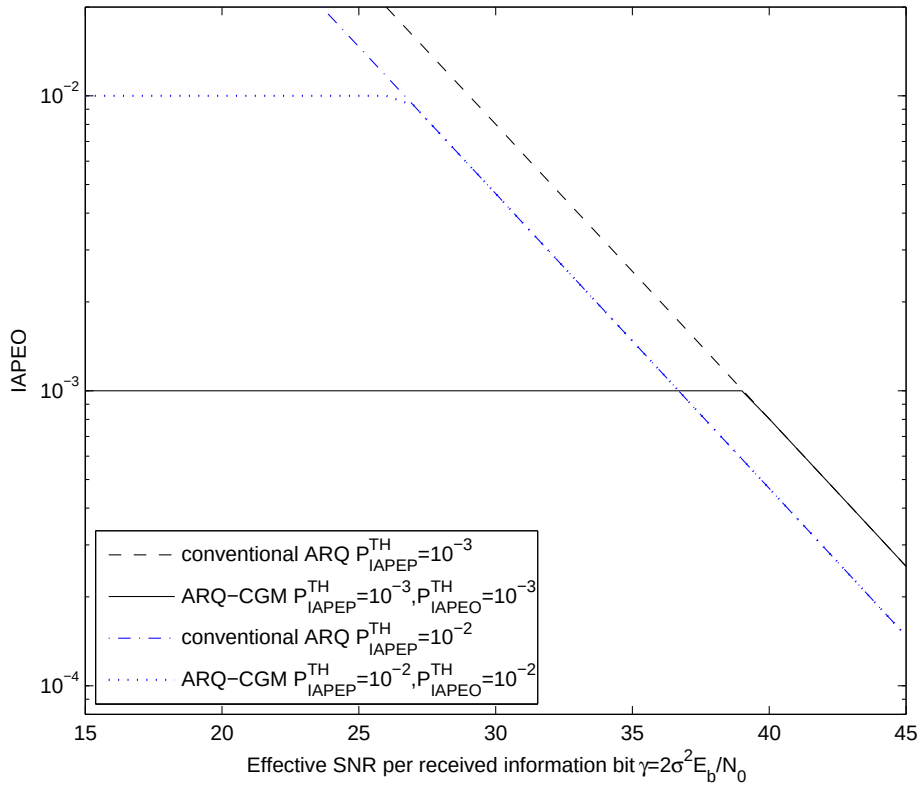

Figure 7.2: IAPEO probability v.s. effective SNR $\bar{\gamma}$ for BPSK with $p = 5, m = 23, n = 28, \varepsilon = \varepsilon_{eq}$.

of BPSK.

The goodput of SR-ARQ-CGM with BPSK using the bounds and approximation in (7.15)–(7.19) are compared in Fig. 7.6. We observe that the bounds are very tight. The following numerical results are obtained using the approximation in (7.19).

The AAPEP of ARQ-CGM is lower than that of conventional ARQ, as shown in Fig. 7.7. In other words, the average reliability of ARQ is also improved by channel gain monitoring. As expected, the improvement in reliability comes with the tradeoff of lower throughput and goodput, as shown in Fig 7.8 and Fig. 7.9, respectively. It is a result of more retransmissions caused by channel gain monitoring.

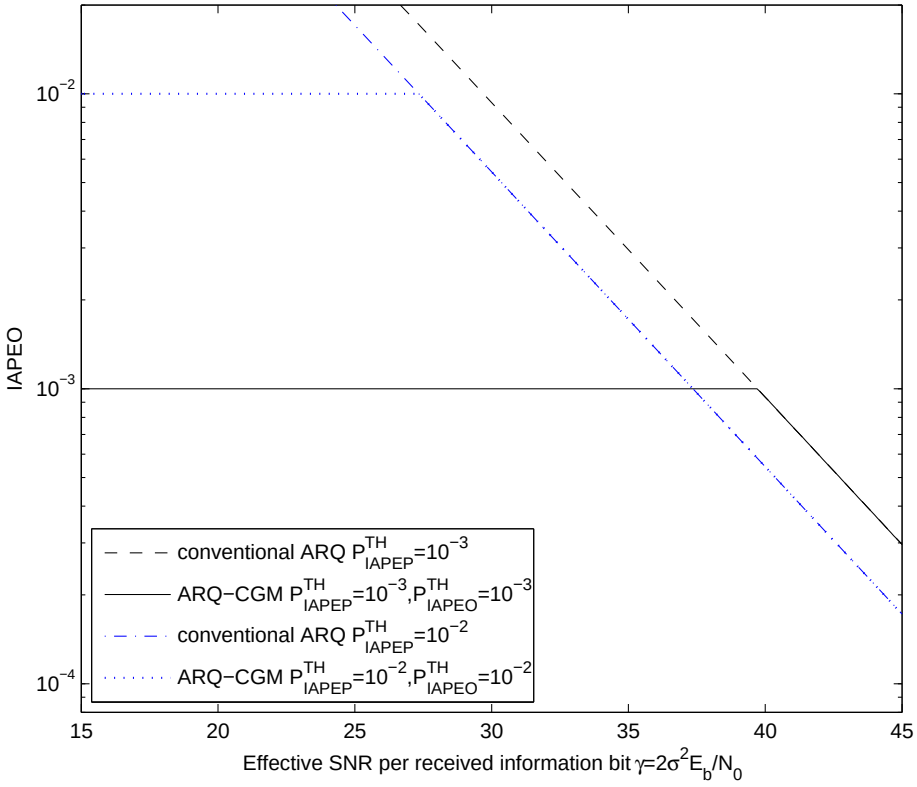

Figure 7.3: IAPEO probability v.s. effective SNR $\bar{\gamma}$ for QPSK with $p = 5, m = 23, n = 28, \varepsilon = \varepsilon_{eq}$.

The throughput and goodput of ARQ-CGM with BPSK and QPSK are compared in Fig. 7.10 and Fig. 7.11, respectively. Theoretically, the transmission rate of QPSK is double that of BPSK. Due to the pilot overhead and the fact that QPSK is more susceptible to imperfect CSI, the throughput and goodput of ARQ-CGM with QPSK is less than double those of BPSK.

7.5 Conclusions

The probability of IAPEO is proposed as a performance measure for ARQ schemes over wireless channels. We obtain a closed-form upper bound expression for IAPEO of a pure ARQ over Rayleigh fading. We show that, in order to satisfy a system

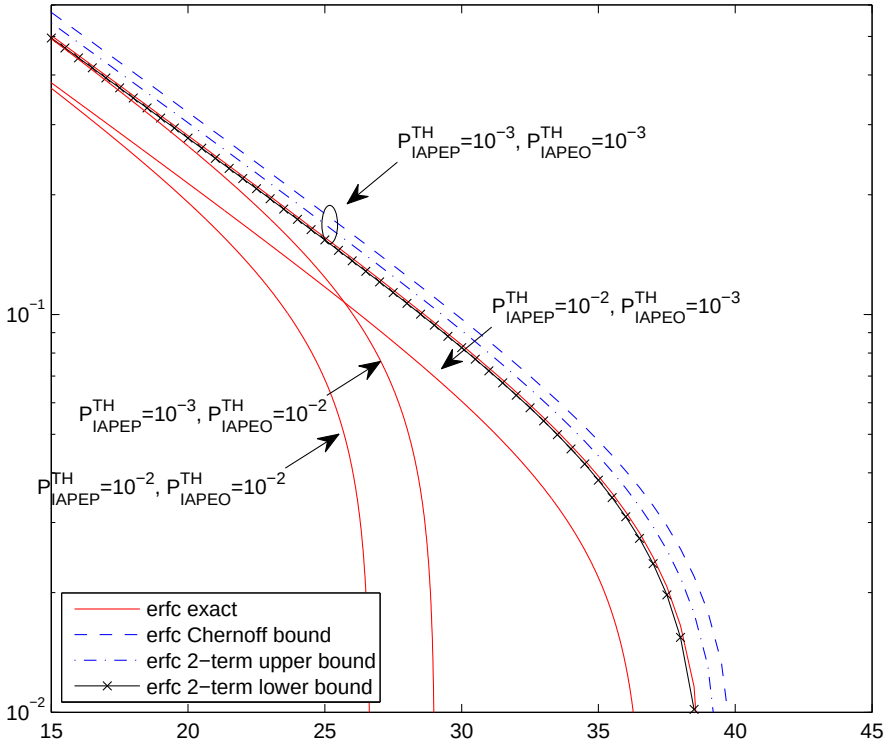

Figure 7.4: Channel estimate threshold $|h^{\mathbf{TH}}|$ v.s. effective SNR $\bar{\gamma}$ for BPSK with $p = 5, m = 23, n = 28, \varepsilon = \varepsilon_{eq}$.

design requirement of maximum tolerable IAPEO, the system must operate above a minimum SNR value. To overcome this shortcoming, we propose ARQ-CGM, such that the IAPEO requirement can be satisfied at any SNR value with the right channel gain threshold. The IAPEO performance of ARQ-CGM with selective repeat retransmission protocol is related to the conventional performance measures, i.e. AAPEP, throughput and goodput. It is shown that its average reliability is higher than the conventional ARQ, at the cost of lower throughput and goodput.

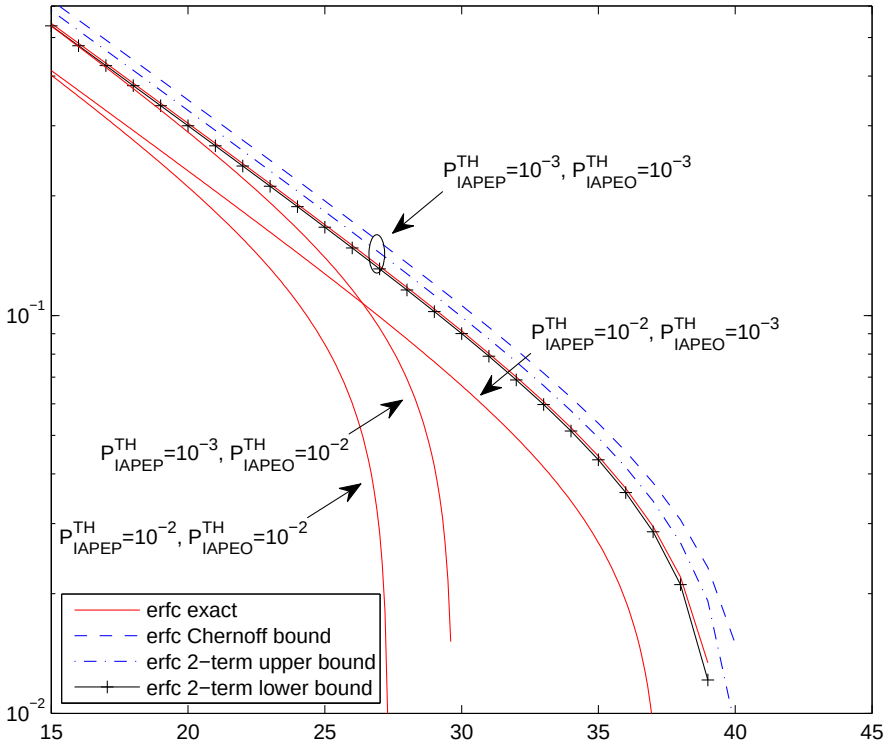

Figure 7.5: Channel estimate threshold $|h^{\mathbf{TH}}|$ v.s. effective SNR $\bar{\gamma}$ for QPSK with $p = 5, m = 23, n = 28, \varepsilon = \varepsilon_{eq}$.

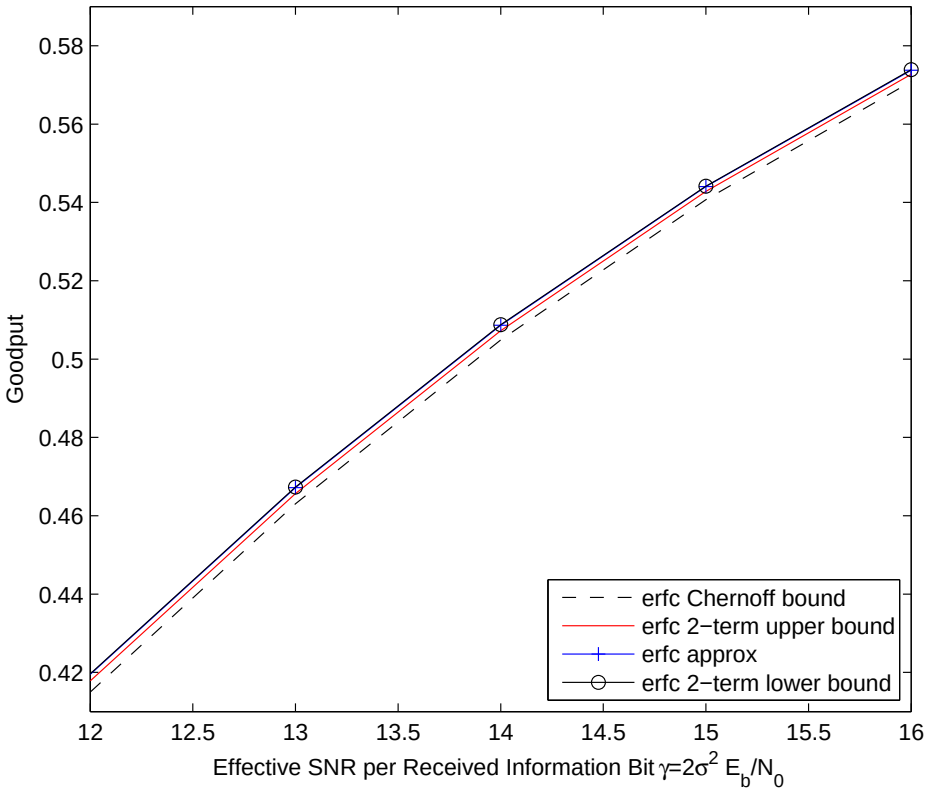

Figure 7.6: Comparison of bounds and approximation of goodput with BPSK, $p = 5, m = 23, n = 28, P^{\mathbf{TH}}_{\mathbf{IAPEP}} = 10^{-3}$ **and** $P^{\mathbf{TH}}_{\mathbf{IAPEO}} = 10^{-2}$**.**

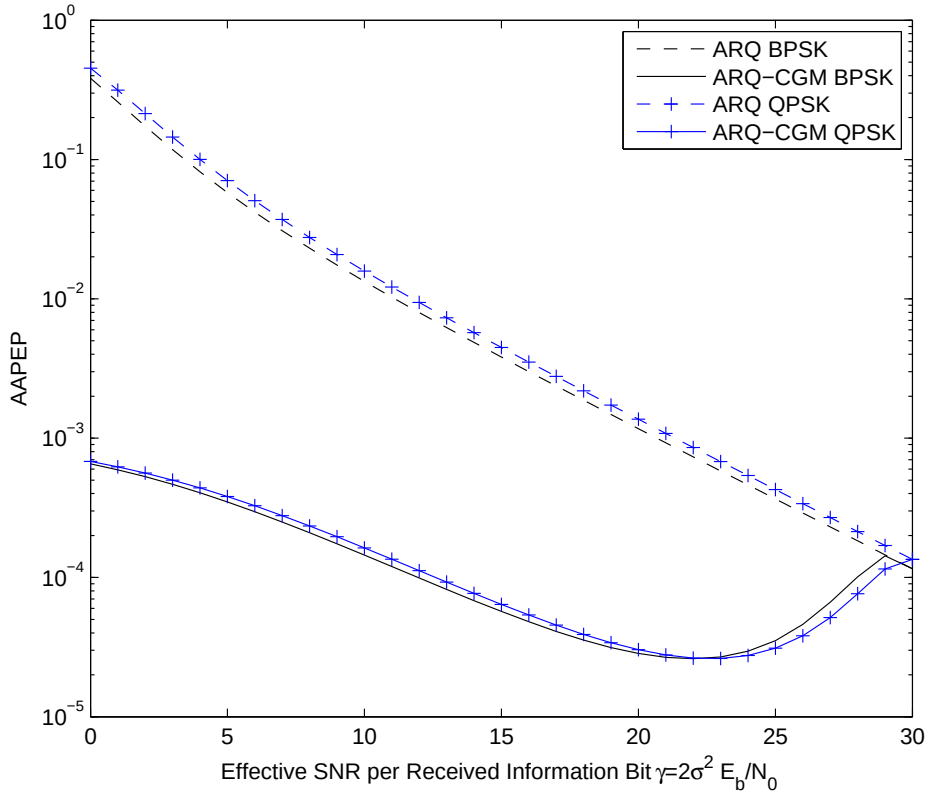

Figure 7.7: AAPEP of ARQ-CGM with BPSK and QPSK, $p = 5, m = 23, n = 28, P^{\mathbf{TH}}_{\mathbf{IAPEP}} = 10^{-3}$ **and** $P^{\mathbf{TH}}_{\mathbf{IAPEO}} = 10^{-2}$**.**

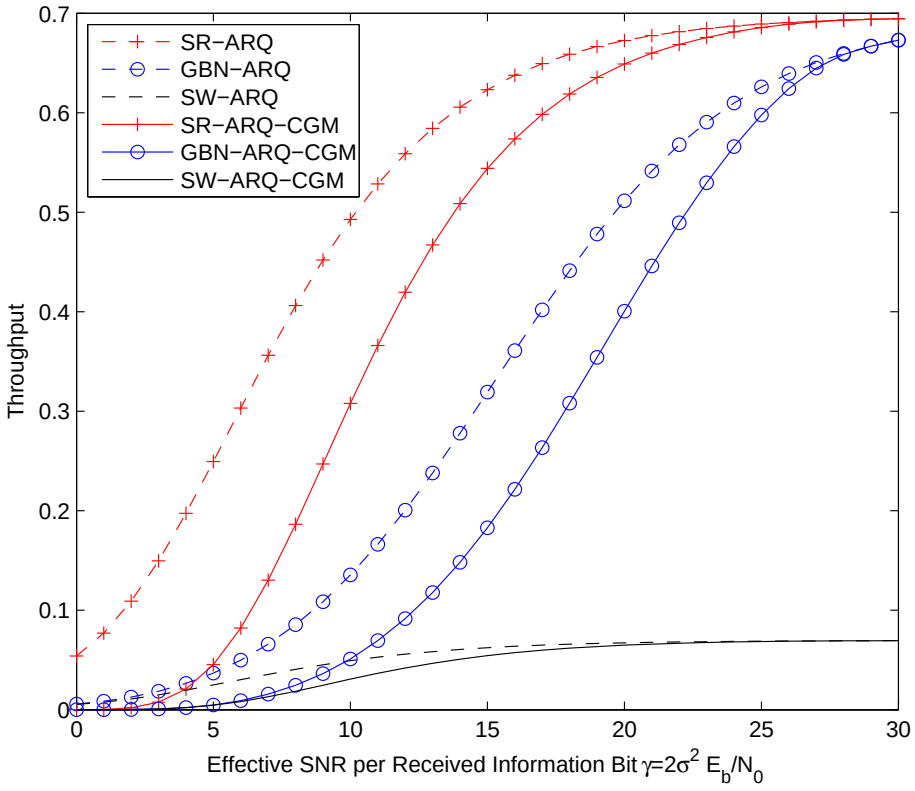

Figure 7.8: Throughput of ARQ-CGM with BPSK, $p = 5, m = 23, n = 28, P_{\mathbf{IAPEP}}^{\mathbf{TH}} = 10^{-3}$ **and** $P_{\mathbf{IAPEO}}^{\mathbf{TH}} = 10^{-2}$**.**

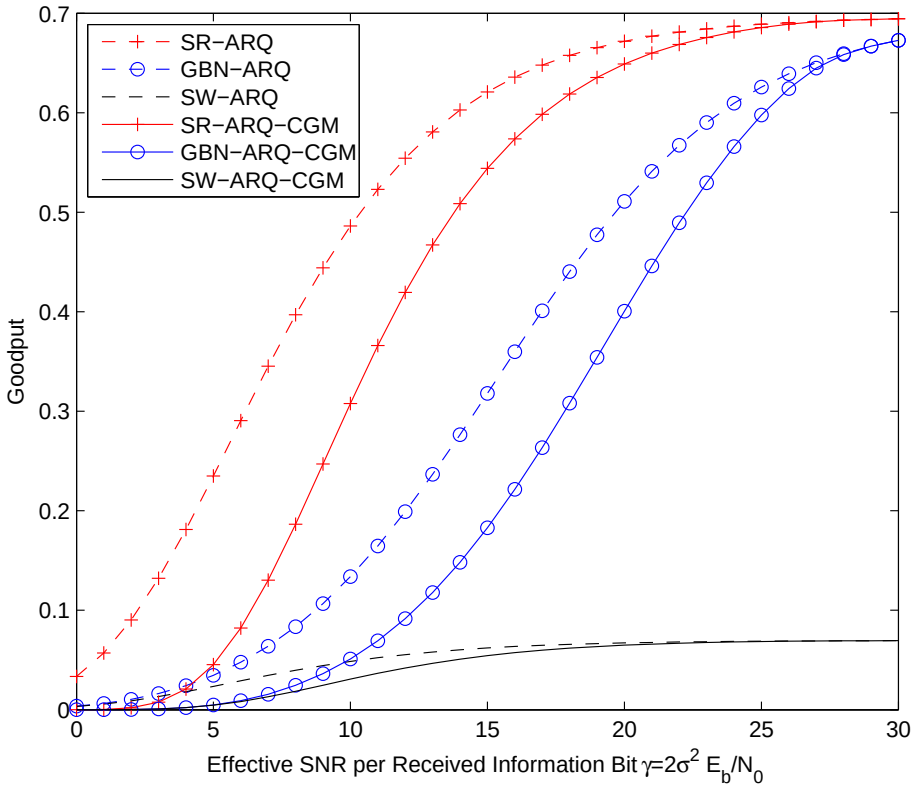

Figure 7.9: Goodput of ARQ-CGM with BPSK, $p = 5, m = 23, n = 28, P_{\mathbf{IAPEP}}^{\mathbf{TH}} = 10^{-3}$ **and** $P_{\mathbf{IAPEO}}^{\mathbf{TH}} = 10^{-2}$**.**

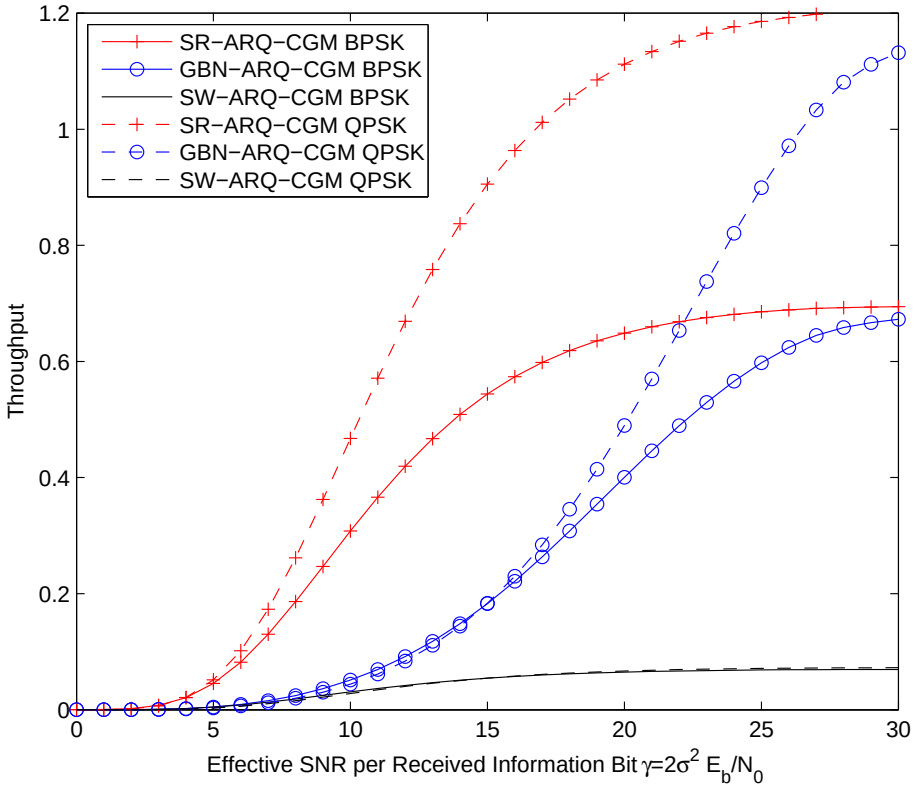

Figure 7.10: Throughput of ARQ-CGM with QPSK, $p = 5, m = 23, n = 28, P_{\mathbf{IAPEP}}^{\mathbf{TH}} = 10^{-3}$ **and** $P_{\mathbf{IAPEO}}^{\mathbf{TH}} = 10^{-2}$**.**

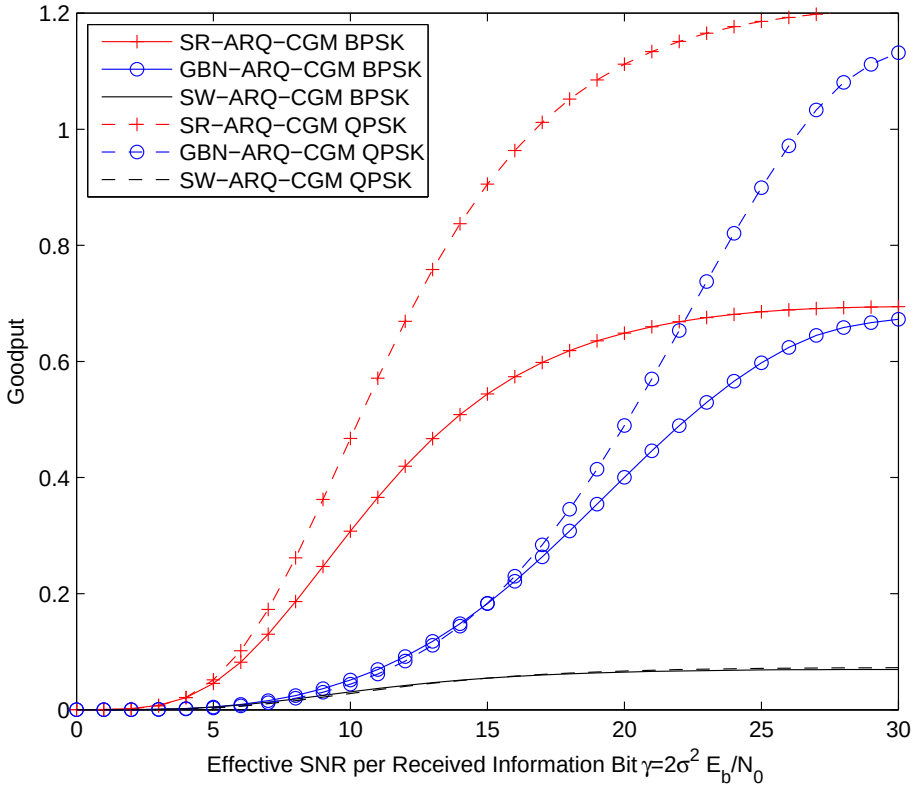

Figure 7.11: Goodput of ARQ-CGM with QPSK, $p = 5, m = 23, n = 28, P_{\mathbf{IAPEP}}^{\mathbf{TH}} = 10^{-3}$ **and** $P_{\mathbf{IAPEO}}^{\mathbf{TH}} = 10^{-2}$**.**

Chapter 8

Summary of Contributions and Future Work

8.1 Summary of Contributions

In order to design a robust receiver for fading channels, we applied the joint data sequence detection and blind channel estimation approach and assume that the receiver has no knowledge of the channel statistics and does not extract CSI. We have used this approach to obtain robust receivers for the phase noncoherent AWGN channel and an arbitrary flat fading channel. We can apply this approach to other channels to derive robust receivers. The receivers are sequence detectors. If the receiver objective is to detect the data sequence only, explicit extraction of the CSI is not needed. However, if the CSI is required, e.g. for CSI feedback to the transmitter [80], it can be computed using the data sequence decision. Sequence detectors, in general, have the implementation problem of exponential computational complexity. The trellis search algorithm is a powerful algorithm to reduce the exponential complexity to linear complexity.

For performance analysis, we started on the physical layer with coherent receivers. As the performance of coherent receivers are in the form of integrals of exponential functions (including the Gaussian Q-function), we proposed to use

the Jensen's inequality. We obtained three families of exponential bounds that have simple forms. Our bounds can be averaged over fading and they are much tighter than existing bounds with the same forms that can be averaged over the same fading channel. The tightness of the bounds can be improved by increasing the number of exponential terms. Moreover, coefficients of the bounds can be adjusted to tighten the bounds. We conclude that the Jensen's inequality is a very powerful tool in performance analysis.

Following coherent receivers, we then studied the performance of differential and noncoherent receivers whose decision metrics are in quadratic forms. By expressing the noncentral Chi-square distribution as a Poisson-weighted mixture of central Chi-square distributions, we obtained an exact expression of the error performance of quadratic receivers. This expression is in the form of a series summation involving only elementary functions. It can be truncated for numerical calculation. The BEP performances of optimum and suboptimum BDPSK and QDPSK receivers over fast Rician fading with Doppler shift were obtained using the general expression. Our general expression is more efficient than existing expressions in the literature in numerical computation. However, the limitation of our expression is that it is only applicable to Rician type signals. So is the Proakis' expression. The Simon's expression is obtained by averaging AWGN performance over arbitrary fading. Therefore, it is applicable to any fading channel.

Having analyzed the average performances of coherent receivers and differential/noncoherent receivers at the physical layer, we moved up to the data link layer. The issue that is been long neglected is that the performance measure for the physical layer at the data link layer or higher layers is the two Markov model which is entirely different from the ABEP/ASEP performance measures at the physical layer. Conventional higher layer performance analysis results do not show how higher layer performance are affected by the performance measures at the physical layer. We need to build a link between the performance measures of the two layers. Our first step was to propose the IBEP/IPEP/IAPEP and the IBEO/IPEO/IAPEO probability

as short-term and long-term reliability performance measures, respectively. A closed-form expression and bounds were obtained for the IBEO/IPEO/IAPEO probability over Rayleigh fading channels with imperfect CSI. We showed that the IBEO/IPEO/IAPEO performance improves rapidly with channel estimation MSE, when MSE drops below a certain value. The optimum allocation of energy between pilot and coded bits that minimizes the IBEO/IPEO/IAPEO probability was obtained. It was shown that the optimum allocation is not affected by the IBEP/IPEP/IAPEP threshold values. In order to achieve system design IAPEO performance at any SNR value, ARQ with channel gain monitoring was proposed. Its IAPEO, AAPEP, throughput and goodput were derived. It was shown that its average reliability is higher than the conventional ARQ, at the cost of lower throughput and goodput.

8.2 Future Work

In the average performance analysis for coherent receivers, the Jensen's inequality can be applied to lower bound integrals of exponential functions. We will look for more applications where this lower-bounding method can be applied. In addition, a convex function can be upper-bounded by its approximate using the Cotes trapezoidal rule [21]. This provides a method to upper-bound the Gaussian Q-function and other integrals of exponential functions.

For the average performance analysis for quadratic receivers, the expression we obtained is a general expression and can always applicable. There are many applications. For example, the energy detector used for spectrum sensing in cognitive radio is a quadratic receiver [81]. We can generalize the expression the case where the decision metrics have different cardinality. For example, in the outage performance analysis of multiuser detection in cellular communication, the decision metric for interferences has more components than decision metric for the signal. The Proakis' expression and the Simon's expression are not applicable to this scenario. Moreover, the expression we obtained involves infinite series. We can look for approximate or

upper/lower bounds based on the new form. We will look into the conditions when each approximation or bound may be applied.

We now move on to the data link layer. Conventionally, data link layer and upper layer protocols work and are analyzed based on the discrete-time two-state Markov-chain model. This model assumes that the channel condition or link reliability is either good or bad. The transition probabilities between the states are specified. The commonly used average performance measures in the physical layer, e.g. ABEP and ASEP, do not fit into this model directly [82]. We proposed to use IBEP/IPEP/IAPEP and IBEO/IPEO/IAPEO probability to represent short-term and long-term reliability. We will investigate how our IBEP/IBEO model can map to the Markov-chain model, such that existing protocol performance results based the Markov-chain model can be easily converted to the performance over fading. We will also look into cross-layer protocol design that uses or is based on the outage performance as the performance measure.

The outage probabilities we proposed are for fading channels. When the shadowing effect is taken into consideration, the same outage probabilities can be used, by averaging the fading gain over the fading distribution and the shadowing distribution. Therefore, the outage probabilities reflect the effects of both fading and shadowing. Alternatively, we may propose two sets of outage probabilities, one at the multipath fading level and one at the shadowing level. Thus, each set of outage probabilities only reflects the effect caused by multipath fading or shadowing. When the shadowing effect is considered, the mapping of the outage probabilities into the Markov chain model is more involved.

Bibliography

[1] P. Y. Kam and C. H. Teh, "Reception of PSK signals over fading channels via quadrature amplitude estimation," *IEEE Trans. Commun.*, vol. COM-31, no. 8, pp. 1024–1027, Aug. 1983.

[2] P. Y. Kam, "Optimal detection of digital data over the nonselective Rayleigh fading channel with diversity reception," *IEEE Trans. Commun.*, vol. 39, no. 2, pp. 214–219, Aug. 1991.

[3] R. Haeb and H. Meyr, "A systematic approach to carrier recovery and detection of digitally phase modulated signals on fading channels," *IEEE Trans. Commun.*, vol. 37, no. 7, pp. 748–754, Jul. 1989.

[4] J. K. Cavers, "An analysis of pilot symbol assisted modulation for Rayleigh fading channels," *IEEE Trans. Veh. Technol.*, vol. 40, no. 4, pp. 686–693, Nov. 1991.

[5] D. Divsalar and M. K. Simon, "Maximum-likelihood differential detection of uncoded and trellis coded amplitude phase modulation over AWGN and fading channels – metrics and performance," *IEEE Trans. Commun.*, vol. 42, no. 1, pp. 76–89, Jan. 1994.

[6] G. Colavolpe and R. Raheli, "Noncoherent sequence detection in frequency nonselective slowly fading channels," *IEEE J. Select. Areas. Commun.*, vol. 18, no. 11, pp. 2302–2311, Nov. 2000.

[7] A. Annamalai and C. Tellambura, "Error rates for Nakagami-m fading multichannel reception of binary and M-ary signals," *IEEE Trans. Commun.*, vol. 49, no. 1, pp. 58–68, Jan. 2001.

[8] J. G. Proakis, *Digital Communications*, 3rd ed. New York: McGraw-Hill, 1995.

[9] M. K. Simon and M.-S. Alouini, "A unified approach to the probability of error for noncoherent and differentially coherent modulations over generalized fading channels," *IEEE Trans. Commun.*, vol. 46, no. 12, pp. 1625–1638, Dec. 1998.

[10] H. M. Chaskar, T. V. Lakshman, and U. Madhow, "TCP over wireless with link level error control: analysis and design methodology," *IEEE/ACM Trans. Netw.*, vol. 7, no. 5, pp. 605–615, Oct. 1999.

[11] M. Gao and M. Wu, "On the delay performance of selective-repeat ARQ for underwater acoustic channels," in *Proc. Wireless VITAE*, Aalborg, Denmark, May 2009, pp. 727–731.

[12] P. Ho and D. Fung, "Error performance of multiple-symbol differential detection of PSK signals transmitted over correlated Rayleigh-fading channels," *IEEE Trans. Commun.*, vol. 40, no. 10, pp. 1566–1569, Oct. 1992.

[13] B. Bhukania and P. Schniter, "On the robustness of decision-feedback detection of DPSK and differential unitary space-time modulation in Rayleigh-fading channels," *IEEE Trans. Wireless Commun.*, vol. 3, no. 5, pp. 1481–1489, Sep. 2004.

[14] P. Y. Kam, "Maximum-likelihood digital data sequence estimation over the Gaussian channel with unknown carrier phase," *IEEE Trans. Commun.*, vol. COM-35, no. 7, pp. 764–767, Jul. 1987.

[15] Y. W. Craig, "A new, simple and exact result for calculating the probability of error for two-dimentional signal constellations," in *IEEE MILCOM Conf. Rec.*, Boston, MA, 1991, pp. 25.5.1–25.5.5.

[16] P. Borjesson and C.-E. Sundberg, "Simple approximations of the error function Q(x) for communications applications," *IEEE Trans. Commun.*, vol. 27, no. 3, pp. 639–643, Mar. 1979.

[17] N. C. Beaulieu, "A simple series for personal computer computation of the error function," *IEEE Trans. Commun.*, vol. 37, no. 9, pp. 989–991, Sep. 1989.

[18] J. S. Dyer and S. A. Dyer, "Corrections to, and comments on, "Simple approximations of the error function Q(x) for communications applications"," *IEEE Commun. Lett.*, vol. 12, no. 4, p. 231, Apr. 2008.

[19] C. Tellambura and A. Annamalai, "Efficient computation of erfc(x) for large arguments," *IEEE Trans. Commun.*, vol. 48, no. 4, pp. 529–532, Apr. 2000.

[20] G. K. Karagiannidis and A. S. Lioumpas, "An improved approximation for the Gaussian Q-function," *IEEE Commun. Lett.*, vol. 11, no. 8, pp. 644–646, Aug. 2007.

[21] G. de Abreu, "Jensen-Cotes upper and lower bounds on the Gaussian Q-function and related functions," *IEEE Trans. Commun.*, vol. 57, no. 11, pp. 3328–3338, Nov. 2009.

[22] ——, "Super tight algebraic bounds on the Gaussian Q-function," in *Conf. Rec. of the Forty-Third Asilomar Conference on Signals, Systems and Computers 2009 (ACSSC'09)*, Pacific Grove, CA, Nov. 2009, pp. 948–951.

[23] J. M. Wozencraft and I. M. Jacobs, *Principles of Communication Engineering*. New York: Wiley, 1965.

[24] M. Chiani, D. Dardari, and M. K. Simon, "New exponential bounds and approximations for the computation of error probability in fading channels," *IEEE Trans. Commun.*, vol. 2, no. 4, pp. 840–845, Jul. 2003.

[25] N. Ekanayake, "Performance of M-ary PSK signals in slow Rayleigh fading channels," *Electronics Letters*, vol. 26, no. 10, pp. 618–619, May 1990.

[26] Y. G. Kim and N. C. Beulieu, "A note on error rates for Nakagami-m fading multichannel reception of binary and M-ary signals," *IEEE Trans. Commun.*, vol. 58, no. 9, p. 2471, Sep. 2010.

[27] H. Shin and J. H. Lee, "On the error probability of binary and M-ary signals in Nakagami-m fading channels," *IEEE Trans. Commun.*, vol. 52, no. 4, pp. 536–539, Apr. 2004.

[28] G. P. Efthymoglou, T. Piboongungon, and V. A. Aalo, "Error rates of M-ary signals with multichannel reception in Nakagami-m fading channels," *IEEE Commun. Lett.*, vol. 10, no. 2, pp. 100–102, Feb. 2006.

[29] J. Sun and I. S. Reed, "Performance of MDPSK, MPSK, and noncoherent MFSK in wireless Rician fading channels," *IEEE Commun. Lett.*, vol. 47, no. 6, pp. 813–816, Jun. 1999.

[30] T. T. Tjhung, C. Loo, and N. P. Secord, "BER performance of DQPSK in slow Rician fading," *Electronics Letters*, vol. 28, no. 18, pp. 1763–1765, Aug. 1992.

[31] M. Tanda, "Bit error rate of DQPSK signals in slow nakagami fading," *Electronics Letters*, vol. 29, no. 5, pp. 431–432, May 1993.

[32] C. Tellambura and V. K. Bhargava, "Unified error analysis of DQPSK in fading channels," *Electronics Letters*, vol. 30, no. 25, pp. 2110–2111, Dec. 1994.

[33] P. Y. Kam, "Bit error probabilities of MDPSK over the nonselective Rayleigh fading channel with diversity reception," *IEEE Trans. Commun.*, vol. 39, no. 2, pp. 220–224, Feb. 1991.

[34] Y. C. Chow, J. P. McGeehan, and A. R. Nix, "Simplified error bound analysis for M-DPSK in fading channels with diversity reception," *IEEE Proc. Commun.*, vol. 141, no. 5, pp. 341–350, Oct. 1994.

[35] J. F. Weng and S. H. Leung, "Analysis of DPSK with equal gain combining in Nakagami fading channels," *Electronics Letters*, vol. 33, no. 8, pp. 654–656, Apr. 1997.

[36] H. Fu and P. Y. Kam, "Effect of Doppler shift on performance of binary DPSK over fast Rician fading channels with diversity reception," in *Proc. ISITA'08*, Auckland, New Zealand, Dec. 2008.

[37] Y. Ma and T. J. Lim, "Bit error probability for MDPSK and NCFSK over arbitrary Rician fading channels," *IEEE J. Sel. Areas Commun.*, vol. 18, no. 11, pp. 2179–2189, Nov. 2000.

[38] E. J. Lee and V. W. S. Chan, "Diversity coherent and incoherent receivers for free-space optical communication in the presence and absence of interference," *IEEE/OSA J. Opt. Commun. Netw.*, vol. 1, no. 5, pp. 463–483, Oct. 2009.

[39] S. Lin and D. J. Costello, *Error Control Coding*. Englewood Cliffs, New Jersey: Prentice Hall, 2004.

[40] L. Cao, P. Y. Kam, and M. Tao, "Impact of imperfect channel state information on ARQ schemes over Rayleigh fading channels," in *Proc. IEEE Int. Conf. Communications (ICC'09)*, Dresden, Germany, Jun. 2009, pp. 1–5.

[41] P. Mary, M. Dohler, J.-M. Gorce, G. Villemaud, and M. Arndt, "M-ary symbol error outage over Nakagami-m fading channels in shadowing environments," *IEEE Trans. Commun.*, vol. 57, no. 10, pp. 2876–2879, Oct. 2009.

[42] P. Mary, M. Dohler, J.-M. Gorce, and G. Villemaud, "Symbol error outage for spatial multiplexing systems in Rayleigh fading channel and lognormal shadowing," in *Proc. Signal Processing Advances in Wireless Communications (SPAWC)*, Perugia, Italy, Jun. 2009, pp. 349–353.

[43] A. Conti, W. M. Gifford, M. Z. Win, and M. Chiani, "Optimized simple bounds for diversity systems," *IEEE Trans. Commun.*, vol. 57, no. 9, pp. 2674–2685, Sep. 2009.

[44] T. S. Rappaport, *Wireless Communications: Principles and Practice.* Upper Saddle River, NJ: Prentice Hall, 1996.

[45] V. Tarokh, N. Seshadri, and A. R. Calderbank, "Space-time codes for high data rate wireless communication: performance criterion and code construction," *IEEE Trans. Inf. Theory*, vol. 44, no. 2, pp. 744–765, Mar. 1998.

[46] V. Tarokh, H. Jafarkhani, and A. R. Calderbank, "Space-time block codes from orthogonal designs," *IEEE Trans. Inf. Theory*, vol. 45, no. 5, pp. 1456–1467, Jul. 1999.

[47] B. M. Hochwald, T. L. Marzetta, T. J. Richardson, W. Sweldens, and R. Urbanke, "Systematic design of unitary space-time constellations," *IEEE Trans. Inf. Theory*, vol. 46, no. 6, pp. 1962–1973, Sep. 2000.

[48] M. K. Simon and M.-S. Alouini, *Digital Communication over Fading Channels: A Unified Approach to Performance Analysis*, 2nd ed. Hoboken, New Jersey, USA: John Wiley, 2005.

[49] Y. X. Y. Zhu and P. Y. Kam, "Outage probability of Rician fading relay channels," *IEEE Trans. Veh. Technol.*, vol. 57, no. 4, pp. 2648–2652, Jul. 2008.

[50] C. E. Shannon, "Communication in the presence of noise," *Proc. Institute of Radio Engineers*, vol. 37, no. 1, pp. 10–21, Jan. 1949.

[51] R. K. Kwan and O. Shimbo, "The effect of fading on the performance of a multihop PCM radio system," *IEEE Trans. Commun.*, vol. COM-18, no. 6, pp. 804–810, Dec. 1970.

[52] Y. Miyagaki, N. Morinaga, and T. Namekawa, "Error probability characteristics for CPSK signal through m-distributed fading channel," *IEEE Trans. Commun.*, vol. COM-26, no. 1, pp. 88–100, Jan. 1978.

[53] D. Warrier and U. Madhow, "Spectrally efficient noncoherent communication," *IEEE Trans. Inf. Theory*, vol. 48, no. 3, pp. 651–668, Mar. 2002.

[54] M. K. Simon and M.-S. Alouini, "Multiple symbol differential detection with diversity reception," *IEEE Trans. Commun.*, vol. 49, no. 8, pp. 1312–1319, Aug. 2001.

[55] D. J. Ryan, I. V. L. Clarkson, and I. B. Collings, "Blind detection of PAM and QAM in fading channels," *IEEE Trans. Inf. Theory*, vol. 52, no. 3, pp. 1197–1206, Mar. 2006.

[56] L. Lampe, V. P. R. Schober, and C. Windpassinger, "Multiple-symbol differential sphere decoding," *IEEE Trans. Commun.*, vol. 53, no. 12, pp. 1981–1985, Dec. 2005.

[57] V. Pauli and L. Lampe, "On the complexity of sphere decoding for MSDD," in *Proc. IEEE Int. Symp. Information Theory*, Seattle, WA, Jul. 2006, pp. 932–936.

[58] D. J. Ryan, I. B. Collings, and I. V. L. Clarkson, "GLRT-optimal noncoherent lattice decoding," *IEEE Trans. Signal Process.*, vol. 55, no. 7, pp. 3773–3786, Jul. 2007.

[59] V. Pauli, L. Lampe, R. Schober, and K. Fukuda, "Multiple-symbol differential detection based on combinatorial geometry," *IEEE Trans. Commun.*, vol. 56, no. 10, pp. 1596–1600, Oct. 2008.

[60] C. D. Meyer, *Matrix Analysis and Applied Linear Algebra*. Philadelphia: SIAM, 2000.

[61] T. Eng and L. B. Milstein, "Coherent DS-CDMA performance in Nakagami multipath fading," *IEEE Trans. Commun.*, vol. 43, no. 2/3/4, pp. 1134–1143, Feb/Mar/Apr 1995.

[62] B. Vucetic and J. Yuan, *Space-time Coding*. Hoboken, NJ: Wiley, 2003.

[63] G. L. Stuber, *Principles of Mobile Communication*, 2nd ed. New York: Kluwer Academic, 2001.

[64] I. Motedayen-Aval and A. Anastasopoulos, "Polynomial-complexity noncoherent symbol-by-symbol detection with application to adaptive iterative decoding of turbo-like codes," *IEEE Trans. Commun.*, vol. 51, no. 2, pp. 197–207, Feb. 2003.

[65] ——, "Polynomial-complexity ML sequence and symbol-by-symbol detection in fading channels," in *Proc. IEEE Int. Conf. Communications*, Anchorage, AK, May 2003, pp. 2718–2722.

[66] R. G. McKilliam, D. J. Ryan, I. V. L. Clarkson, and I. B. Collings, "An improved algorithm for optimal noncoherent QAM detection," in *Proc. AusCTW*, Christchurch, New Zealand, Jan. 2008, pp. 64–68.

[67] P. Y. Kam and P. Sinha, "A Viterbi-type algorithm for efficient estimation of M-PSK sequences over the Gaussian channel with unknown carrier phase," *IEEE Trans. Commun.*, vol. 43, no. 9, pp. 2429–2433, Sep. 1995.

[68] M. V. Eyuboğlu and S. U. H. Qureshi, "Reduced-state sequence estimation with set partitioning and decision feedback," *IEEE Trans. Commun.*, vol. 36, no. 1, pp. 13–20, Jan. 1988.

[69] A. P. R. Raheli and C.-K. Tzou, "Per-survivor processing: a general approach to MLSE in uncertain environments," *IEEE Trans. Commun.*, vol. 43, no. 2/3/4, pp. 354–364, 1995.

[70] I. S. Gradshteyn and I. M. Ryzhik, *Table of Integrals, Series, and Products*, 7th ed. Oxford: Academic Press, 2007.

[71] M. K. Simon, "A simpler form of the Craig representation for the two-dimensional joint Gaussian Q-function," *IEEE Commun. Lett.*, vol. 6, no. 2, pp. 49–51, Feb. 2002.

[72] R. F. Pawula, "A new formula for MDPSK symbol error probability," *IEEE Commun. Lett.*, vol. 2, no. 10, pp. 271–272, Oct. 1998.

[73] R. Li and P. Y. Kam, "Averages of the product of two Gaussian Q-functions over fading statistics and applications," *IEEE Commun. Lett.*, vol. 11, no. 1, pp. 58–60, Jan. 2007.

[74] N. C. Beaulieu, "A useful integral for wireless communication theory and its application to rectangular signaling constellation error rates," *IEEE Trans. Commun.*, vol. 54, no. 5, pp. 802–805, May 2006.

[75] R. K. Mallik, "Average of product of two Gaussian Q-functions and its application to performance analysis in Nakagami fading," *IEEE Trans. Commun.*, vol. 56, no. 8, pp. 1289–1299, Aug. 2008.

[76] S. Haykin, *Adaptive Filter Theory*, 4th ed. Upper Saddle River, NJ: Prentice Hall, 2002.

[77] H.-P. Tan, W. K. G. Seah, and L. Doyle, "A multi-hop ARQ protocol for underwater acoustic networks," in *Proc. OCEANS 2007*, Europe, Jun. 2007, pp. 1–6.

[78] H. Zhuang, H.-P. Tan, A. Valera, and Z. Bai, "Opportunistic ARQ with bidirectional overhearing for reliable multihop underwater networking," in *Proc. OCEANS 2010*, Sydney, May 2010, pp. 1–6.

[79] N. K. Y. Lee and H. Park, "Performance analysis of MIMO system with linear MMSE receiver," *IEEE Trans. Wireless Commun.*, vol. 7, no. 11, pp. 4474–4478, Nov. 2008.

[80] D. Samardzija and N. Mandayam, "Unquantized and uncoded channel state information feedback in multiple-antenna multiuser systems," *IEEE Trans. Commun.*, vol. 54, no. 7, pp. 1335–1345, Jul. 2006.

[81] S. Zheng, P.-Y. Kam, and Y.-C. Liang, "Bayesian spectrum sensing for digitally modulated primary signals in cognitive radio," in *Proc. IEEE Veh. Technol. Conf. (VTC 2011-Spring)*, Budapest, May 2011, pp. 1–5.

[82] D. Qiao, S. Choi, and K. G. Shin, "Goodput analysis and link adaption for ieee 802.11a wireless lans," *IEEE Trans. Mobile Comput.*, vol. 1, no. 4, pp. 278–292, 2002.

List of Publications

1. M. Wu, and P. Y. Kam, "ARQ with channel gain monitoring in the presence of imperfect receiver CSI," *IEEE Trans. Commun.* submitted for publication and in revision.

2. M. Wu and P. Y. Kam, "ARQ with packet-error-outage-probability QoS measure," in *Proc. IEEE Int. Conf. Commun. (ICC2011)*, Kyoto, Jun. 2011, pp. 1–5. (Best Paper Award)

3. M. Wu and P. Y. Kam, "New exponential lower bounds on the Gaussian Q-function via Jensen's inequality," in *Proc. IEEE Veh. Technol. Conf. (VTC 2011-Spring)*, Budapest, May 2011, pp. 1–5.

4. M. Wu and P. Y. Kam, "Performance analysis and computational complexity comparison of sequence detection receivers with no explicit channel estimation," *IEEE Trans. Veh. Technol.*, vol. 59, no. 5, pp. 2625–2631, Jun. 2010.

5. M. Wu and P. Y. Kam, "Instantaneous symbol error outage probability over fading channels with imperfect channel state information," in *Proc. IEEE Veh. Technol. Conf. (VTC 2010-Spring)*, Taipei, May 2010, pp. 1–5.

6. M. Wu and P. Y. Kam, "Sequence detection on fading channels without explicit channel estimation," in *Proc. Wireless VITAE*, Aalborg, Denmark, May 2009, pp. 370–374.